

Microwave Assisted Organic Transformations on Fly Ash And Volcanic Ash Supported Catalytic Materials

A Thesis

Submitted to

University of Kota, Kota

For the Award of the Degree of

Doctor of Philosophy

in Chemistry

(Faculty of Science)



Supervised by:
Prof. Ashu Rani

Submitted by:
Niharika Shringi

**Department of Pure and Applied Chemistry
University of Kota, Kota**

2016



UNIVERSITY OF KOTA, KOTA

M.B.S. Marg, Kabir Circle, Rawatbhata Road, Kota (Raj.)

Prof. Ashu Rani

Department of Pure & Applied Chemistry
University of Kota, Kota

Residence

2-m-1, Rangbari Scheme
Kota-324005 (Raj.) India
Ph: +91-9352619059
e-mail: ashu.uok@gmail.com

Date :

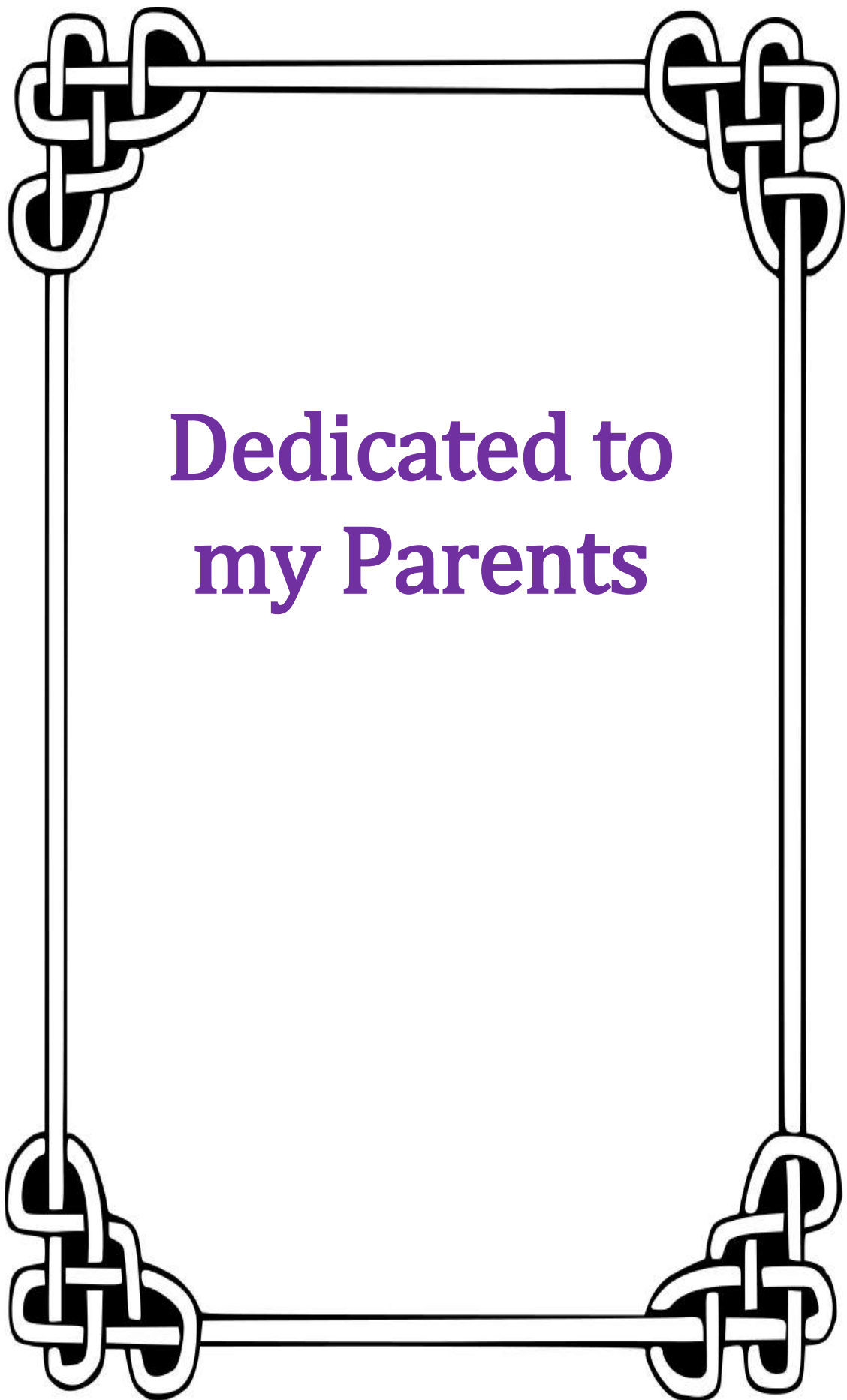
CERTIFICATE

It is to certify that the

- (i) Thesis entitled “**Microwave Assisted Organic Transformations on Fly Ash And Volcanic Ash Supported Catalytic Materials**” submitted by **Niharika Shringi** is an original piece of research work carried out by the candidate under my supervision.
- (ii) Literary presentation is satisfactory and the thesis is in a form suitable for publication.
- (iii) Work evidences the capacity of the candidate for critical examination and independent judgment.
- (iv) Candidate has put in at least 200 days of attendance every year.

A handwritten signature in black ink, appearing to read 'Ashu Rani', is written over a light blue grid background.

Prof. Ashu Rani



**Dedicated to
my Parents**

Acknowledgment

“Coming together is a beginning, staying together is progress, and working together is success”

-Henry Ford

These words are very true for the sincere efforts of people followed by adequate planning and dedication to achieve success in any field.

My thesis is the result of arduous research and culmination of the process that included constant assistance, support & guidance by my fellow researchers and academicians to whom I am deeply indebted. At the end of my thesis, it is a pleasant opportunity to express my thanks to all those who contributed in many ways to the success of this study and made it an unforgettable experience for me.

First of all endless thanks goes to Lord Almighty for all the blessings he has showered on me, provided me with essential insight and right approach towards fruitful topics related to my research, which has enabled me to write this last note in my research work.

*With deepest sense of gratitude, I am heartily thankful to my esteemed guide, **Prof. Ashu Rani** (Department of Pure & Applied Chemistry, University of Kota, Kota) for giving me opportunity to work under her guidance with an interesting and innovative research topic. Her invaluable help of constructive comments, suggestion and keen observation throughout the experimental and thesis works have contributed to the success of this research. Each meeting with her added invaluable aspects to the implementation and broadened my perspective. From her I have learned to think critically and independently, to select problems, solve them and to present their solutions. Without her valuable and sincere concerns this work could not be presented this time.*

I gratefully acknowledge Prof. M. S. Sharma, ex-Vice Chancellor and Prof. P.K. Dashora, Vice Chancellor for providing me laboratory facilities available in the university.

I am also cordially thankful to Dr. Neelu Chauhan, Dr. Bhavani Singh, Dr. Shewta Vyas, Dr. Sushil Kumar Sharma and Mr. Ankit Sharma faculty staff of Department of Pure & Applied Chemistry, University of Kota, Kota for their direct and indirect support during the whole research period. I express sincere thanks to Dr. Arun Kumar for his unforgettable help, valuable discussions and encouragement throughout the research period. I would also like to pay appreciation to Dr. Shweta Saxena and Dr. Bhartiya Sharma for encouraging and helpful support in various sections of this research.

I am indebted to my seniors, Dr. Chitralkha Khatri, Dr. Deepti Jain, Dr. Dimple Geol, Dr. Anita Sharma, Dr. Shefali Saxena, Dr. Renu Hada, Dr. Sakshi Kabra, Dr. Stuti Katara and Swarnima Agrawal for their motivation in my initial days and valuable suggestions in experimentation during my entire research period. This list is incomplete without acknowledging my senior, Dr. Khushboo Srivastava, for her unconditional support and friendly behaviour throughout this journey. I would also like to extend warm thanks to my lab mates Priyanka Rajoriya, Hariom Gaur, Kiran Parashar, Deepak Karsolia, Nidhi Gautam, Rajesh and Niranjana who extended their co-operation during the progress of this research work. With a particular mention, I would also like to thank Vinod Kumar and Avinash Srivastava for their valuable and timely cooperation during literature survey.

I am extremely thankful to Fly Ash Mission, Department of Science and Technology, New Delhi for providing financial support as Senior Research Fellow (SRF) under the project FAU/DST/600(56)/C/2013-14 and availing high-tech instrumentation facilities for research work in my department. I also

pay gratitude to Dr. D.D. Phase and Er. V.K. Ahire for SEM-EDX analysis, Dr. Mukul Gupta for XRD, Dr. T. Shripathi and Dr. Uday Deshpande for UV-Vis DRS analysis at UGC DAE-CSR Lab, Indore.

I am also thankful to Mr. Rawat and Mr. Chauhan, Indica Chem. Ind. Pvt. Ltd., Kotdwar (Uttarakhand) for providing me samples of volcanic ash.

My special thanks to technical and non-technical the staff of laboratory assistants, accounts and administrative divisions of University for their favorable help.

*At this moment of accomplishment, I have no words to express my indebt gratitude to beloved mother **Mrs. Aruna Shringi** and father **Mr. Kripa Shankar Shringi**, younger sister **Nidhi Shringi** and brother **Amol Shringi** for their immense support and motivation throughout my light and dark times. I am cordially grateful to them to keep faith on skills and potentials during the entire research journey. Their fighting spirit towards ups and downs of entire process brought this process of studies to culminate successfully.*



Niharika Shringi

Contents

Chapters	Page no.
Chapter 1:- Introduction	1-40
Abstract	1
1.1 Introduction	2
1.2 Microwave theory	2
1.3 Microwave equipments	8
1.4 Heterogeneous catalysts and their role in microwave assisted organic synthesis	10
1.5 Microwave assisted synthesis of materials and their Applications	24
1.6 Fly ash as a heterogeneous catalyst	27
1.7 Perlite as a heterogeneous catalyst	30
1.8 Scope of the present work	32
1.9 References	33
Chapter 2: Microwave assisted acid activation of fly ash: A green process for enhancing its physico-chemical attributes for esterification under dielectric heating	41-69
Abstract	41
2.1 Introduction	42
2.2 Experimental details	44
2.3 Results and discussions	51
2.4 Comparative study of MSF-40 catalyst with other catalyst prepared under conventional heating	57
2.5 Catalytic activity	60
2.6 Mechanistic aspects	65
2.7 Regeneration and reusability of catalyst	66
2.8 Product identification	68
2.9 Conclusion	68
2.10 References	68

Chapter 3: Fly ash supported sulfated tin as a green and highly efficient solid acid catalyst for solvent-free, one pot synthesis of 14-aryl-14*H*-dibenzo[*a,j*] xanthenes under Microwave assisted conditions **70-102**

Abstract	70
3.1 Introduction	71
3.2 Experimental details	73
3.3 Results and discussions	77
3.4 Catalytic activity	86
3.5 Mechanistic aspects	93
3.6 Regeneration and reusability of catalyst	96
3.7 Identification of products	98
3.8 Conclusion	98
3.9 References	99

Chapter 4: Microwave assisted single step synthesis of coumarin derivatives via Pechmann condensation reaction using fly ash supported niobia as a solid acid catalyst **103-134**

Abstract	103
4.1 Introduction	104
4.2 Experimental details	106
4.3 Results and discussions	109
4.4 Catalytic activity	119
4.5 Mechanistic aspects	125
4.6 Regeneration and reusability of catalyst	129
4.7 Product identification	131
4.8 Conclusion	131
4.9 References	132

Chapter 5: Synthesis and characterization of chemically activated perlite supported tungsten oxide solid acid catalyst

for microwave assisted synthesis of ethyl levulinate used as fuel additive	135-167
Abstract	135
5.1 Introduction	136
5.2 Experimental details	137
5.3 Results and discussions	140
5.4 Catalytic activity	154
5.5 Mechanistic aspects	159
5.6 Regeneration and reusability of catalyst	163
5.7 Product identification	164
5.8 Conclusion	164
5.9 References	165

Annexure I-IV

Publications



Chapter-1

Introduction

ABSTRACT

This chapter presents a comprehensive review on basic principles of microwave chemistry and its valuable contribution in organic synthesis. It also gives a critical overview of the types of heterogeneous acid catalyzed microwave assisted organic transformations and also briefly describes the microwave assisted synthesis of support materials, pure and supported nanoparticles. Historical developments and recent trends in field of microwave assisted organic transformations catalyzed by heterogeneous catalysts are discussed briefly.

1.1 Introduction

‘Time is precious’ this quote is indeed also true for Science. Particularly, in synthetic chemistry large numbers of time consuming trials are required either for synthesis of new organic materials or optimizing existing synthesis routes in respect to selectivity, yield, reaction time, temperature and product quality and sustainability. To cut-off trial time, improve experimental efficiency and scientific creativity, development of new non-conventional techniques is still a trust area for researchers. In this context, the high speed microwave (MW) heating technique, termed as ‘**Bunsen burner of the 21st century**’ has been on the forefront attention due to its diverse revolutionary contributions in solid-state chemistry [1], nanotechnology [2], organic synthesis [3], peptide synthesis [4], polymer chemistry [5], material sciences [6], nanomaterials [7] and biochemical processes [8] etc. Microwaves are widely used in communication, remote sensing, food processing, navigation and electron paramagnetic resonance spectroscopy, but it has also made a well established position in commercial and domestic heating purposes [9]. In recent years, use of MW heating over conventional heating has turned to a safer more focused alternative due to advantageous features like short reaction time, rapid and instantaneous heating (in-core heating), high yields with better selectivity and emerged as a promising tool to address environmental concerning challenges following the green protocols [10].

1.2 Microwave theory

The term ‘**microwaves**’ is used for the electromagnetic radiations lying in between infrared and radio waves with wavelengths and measured in centimeters from 1 m to 0.1 cm or in the frequency range of 0.3 to 300 Hz. All ‘kitchen’ microwave ovens and commercially available microwave reactors operates at frequency of 2.45 GHz (corresponding to a wavelength of 12.25 cm) to avoid interference with telecommunication, wireless networks and cellular phone frequencies, this frequency is perfect to produce low-cost magnetron used in domestic microwave ovens, 12.25 cm wavelength is smaller than cooking chamber and possess typical penetrating depth of few centimeters in food materials. However, this frequency is not optimized for water heating as it has

resonance frequency of 18 GHz and maximum MW energy to heat conversion occurring in this region [11]. The energy of MW photon is 1.0×10^{-5} eV (or about $0.037 \text{ kcal mol}^{-1}$) at 2.45 GHz frequency which is very low compared to the energy required to cleave a bond ($80\text{-}120 \text{ kcal mol}^{-1}$) [12] and yet lower than the energy required for Brownian motion. Thus, MW chemistry only provides efficient heating of materials and cannot induce chemical reactions and only affects molecular rotations [11].

1.2.1 Dielectric heating

MW enhanced chemistry is based on the efficient heating of materials by 'MW dielectric heating' i.e. a phenomenon dependent on the ability of a specific material (solvent or reagent) having permanent or induced dipole moment to absorb microwave chemistry and convert into heat [13]. It is necessary to understand that electric component of MW irradiation causes heating by three mechanisms: dipolar polarization (DP), ionic conduction and interfacial conduction as shown in **Figure 1.1**. MW irradiation of sample causes alignment of dipoles with applied electric field and as the field oscillates; the dipoles also attempt to realign to align themselves with applied electric field. In this process, depending upon the orientation time and disorientation relative to the radiation frequency, different amount of energy is lost in the form of heat through molecular friction and dielectric loss [14]. If the radiation frequency is too high then dipole doesn't have enough time realign to interact or if it perfectly interacts the alternating applied electric field then no motion and dissipation of heat takes place [15]. The 2.45 GHz frequency lies in between two extremes to give sufficient time to dipole to align with the field but rapid fluctuations doesn't allow the dipole to interact which produces molecular friction and collisions that give rise to dielectric heating [11]. On the other hand, ionic conduction (IC) involves back and forth oscillation of dissolved ionic species under the influence of MW irradiation which collides with neighbouring molecules and evolves heat. Ability of providing instantaneous superheating of ionic substances, IC possesses better heat generation capacity and transfers energy more efficiently than DP [16]. The interfacial polarization is a combined phenomenon of IC and DP found in such a

heating system comprises conducting material scattered in a non-conducting material like dispersion of metal particles in sulfur [17]. The instantaneous and fast reaction rate is also an important feature of MW heating. Since the MW transfers energy in less than nano seconds (10^{-9} s) and reactant molecules with kinetic relaxation time of 10^{-5} seconds unable to get complete relaxation which results as non-equilibrium condition and high instantaneous temperatures (T_i) which is much greater than the bulk temperature (T_B) produced in conventionally heated reactions. This affects the kinetics of the system and boosts the reaction rate as well as product yields [12]. By incorporation of external cooling by compressed air with simultaneous irradiation of microwaves more heating can be supplied to the reaction mixture. In conventional MW synthesis, initial high power is supplied which increases T_B to the desired temperature and as the desired temperature is attained MW power is cut-off to maintain it. In such condition, thermal heating dominates and complete utilization of MW effect does not occur. Simultaneous cooling and MW heating maintains the desired temperature along with the supply of MW to promote T_i responsible for rate enhancement [18].

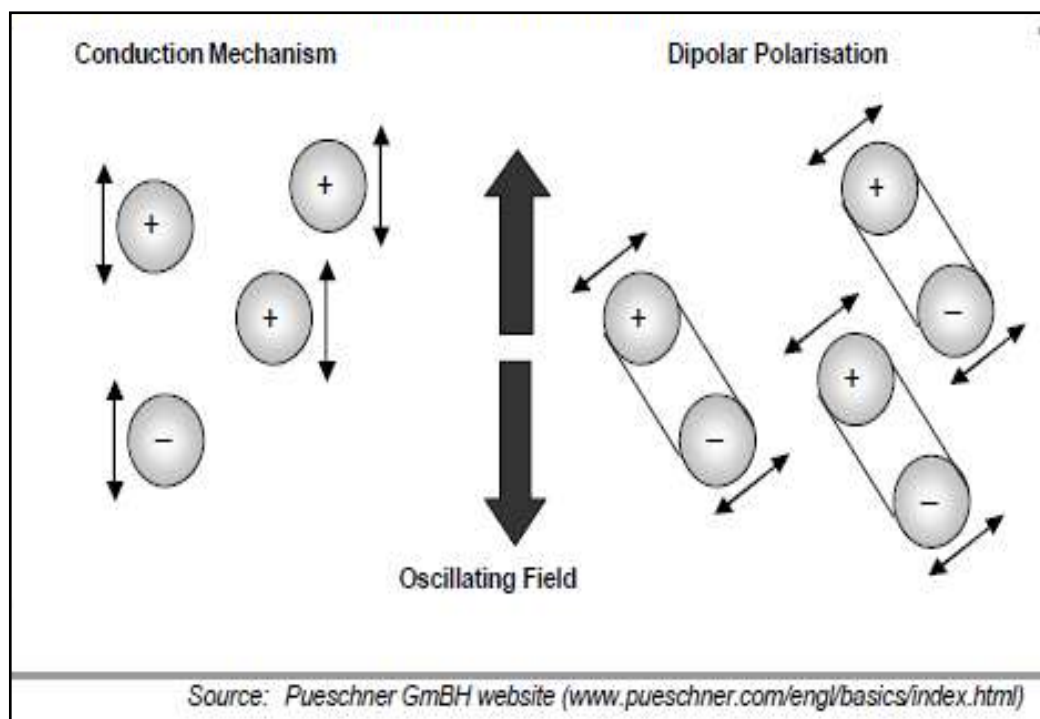


Figure 1.1: Heating mechanisms by microwave radiations [19]

The heating mechanisms of the material under MW irradiations mainly depend upon dielectric properties. Ability of a material to convert electromagnetic energy into heat at a given frequency is measured by dielectric tangent loss (Eqn. 1).

$$\tan \delta = \epsilon''/\epsilon' \quad \text{Eqn. (1)}$$

ϵ'' = dielectric loss, which represents the efficiency with which electromagnetic radiation is converted into heat

ϵ' = dielectric constant, ability to be polarized by the electric field.

A reaction medium with high loss factor value provides efficient absorption of MW and facilitates rapid heating. Organic solvents can be categorized as high ($\tan \delta > 0.5$), medium ($\tan \delta > 0.1 - 0.5$) and low ($\tan \delta < 0.1$). The dielectric loss (ϵ''), dielectric constant (ϵ') and loss factors ($\tan \delta$) for some of the organic solvents are summarized in **Table 1.1**.

Table 1.1: Loss factors ($\tan \delta$) of different solvents

Solvent	Dielectric loss (ϵ'')	Dielectric constant (ϵ')	$\tan \delta$	
Ethylene glycol	49.950	37.0	1.350	High MW absorbing solvents
Ethanol	22.866	24.3	0.941	
DMSO	37.125	45.0	0.825	
2-butanol	7.063	15.8	0.447	Medium MW absorbing solvents
Acetic acid	1.079	6.2	0.174	
Water	9.889	80.4	0.123	
Ethyl acetate	0.354	6.00	0.059	Low MW absorbing solvents
Toluene	0.096	2.4	0.040	
Hexane	0.038	1.9	0.020	

Ref.: [12] measured at room temperature and 2.45 GHz

1.2.2 Dielectric v/s conventional heating

In earlier days, chemical synthesis was carried out by convention heating sources such as oil bath, isomantle or hot plate. The mode of heat transfer is slow and inefficient as it depends upon the thermal conductivity of the various materials that must be penetrated. This results as a formation of temperature gradient in which temperature of reaction vessel becomes higher than that of reaction mixture which takes sufficient time and energy to allow container and materials to attain a thermal equilibrium. In contrast, MW heating involves in-core volumetric heating of materials by directly coupling with the molecules present in reaction mixture without heating the reaction vessel as shown in **Figure 1.2**. This causes as instantaneous and localized superheating of reaction mixture by either DP or IC depending upon the material being used in reaction [21]. Here, reaction vessels are made of MW transparent materials such as borosilicate glass, quartz or teflon to minimize wall effects during the reaction.

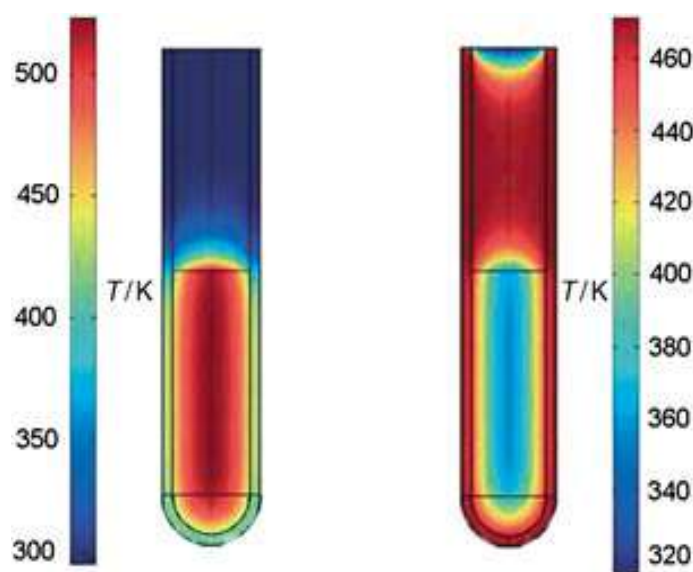


Figure 1.2: Temperature gradient of after 1 min of microwave heating (left) and oil bath (right) heating: difference in temperature profiles (finite element model). MW heating provides bulk heating by raising the temperature of whole volume (left) whereas in case of oil bath walls of the reaction tube is heated first [21].

1.2.3 Microwave effects

The drastic rate enhancement of chemical reaction under microwave irradiation is a combined effect of thermal (dielectric) and non-thermal or specific microwave effect. In thermal effects, dielectric heating uses peculiar ability of materials (liquids or solids) to convert electromagnetic energy into heat which is in contrast to classical heating having conduction and convection as heat transfer modes [22].

In MW heating, the magnitude of heat generation depends upon the dielectric properties of the molecules which signify that heating is selective and rapid. Another unique feature is ‘specific’ or non-thermal effect based on the Arrhenius law (Eqn. 2)

$$(k = A \exp (-\Delta G^{\#}/RT) \quad \text{Eqn. (2)}$$

k = rate constant; R = gas constant; T = Temperature

It involves direct interaction of alternating electric field with specific molecules in the reaction medium that induces orientation in dipoles or intermediates and thus, increase in collision frequency (A) and reduction in Gibb’s activation energy ($\Delta G^{\#}$) takes place. Considering the contribution of enthalpy ($\Delta H^{\#}$) and entropy to the value of $\Delta G^{\#}$ ($\Delta G^{\#} = \Delta H^{\#} - T\Delta S^{\#}$), it may be predicted that the magnitude of $-T\Delta S^{\#}$ increases with microwave induced heating due to dipolar polarization which is more uniform than convective heating [23]. Microwave effects are still a controversial subject and require a serious scientific rationalization for the observed effects on organic synthesis. According to the important observations reported by Kappe et. al these effects involve thermal phenomenon but not any specific effects [24]. Nevertheless, MW heating also possesses some novel characteristics such as superheating of solvents at atmospheric pressure, selective heating of polar species in a microwave transparent solvent, formation of ‘molecular radiators’ by direct coupling of MW with strong MW absorbing heterogeneous catalysts or specific reagents in less polar medium and elimination of wall effects by formation of inverted

temperature gradient as shown in **Section 1.3** which increases the reaction rates manifolds [22].

1.3 Microwave equipments

After the major breakthrough by Gedye et al. in 1986 [25,26] microwave ovens become an integral part in modern organic synthesis and has contributed in the development of pioneering works in synthetic chemistry. However, MW ovens are considered as ‘multimode’ instrument where due to random distribution of microwaves by MW resonator within the cavity produces areas of high and low microwave intensity. As a consequence, non-uniform heating of materials occurs. As MW ovens are open systems so temperature and pressure control is not possible that restricts its use in synthetic purpose because superheating of high volume organic solvents may cause fire or explosions [27]. Therefore, due to safety concerns, now these days for synthesis purposes use of dedicated instrument or synthesis systems are strongly recommended. According to the usage and reactor design two types of MW reactors are currently available: monomode and multimode reactor. At the beginning of the 21st century, development of MW reactors especially for the organic synthesis was developed by CEM (<http://www.cem.com>), Biotage (<http://www.biotage.com>) and Milstone (<http://www.milestonesrl.com>) companies. CEM and Biotage developed Biotage instruments based on ‘single-mode’ microwave resonator. In the reactor cavity, a continuous standing wave is generated with defined field strength regions subjecting the reaction vessel to high-energy density [23,28,29,30,31,32,33]. Modulation of the continuous standing wave by the system software controls the temperature levels, which are monitored by a calibrated infrared sensor. Monomode reactors with such design provide uniform heat distribution, precise control of temperature and pressure, ‘closed system’ (pressure up to 20 bars) and gives reproducible results. These characteristics allows organic reactions to be superheated (2-3 times the boiling point of the solvent) accelerating reaction rates, reduced side-product formation which results as cleaner reactions. In newer

developments in field of MW reactors to mitigate dielectric heating effects, use of SiC vessels and fibre optic (FO) sensors has gained popularity. SiC vessels are more corrosion resistant and better than glass even for concentrated acids or bases, chlorine, or HF gas. They also possess high MW absorptivity so absorbs MW energy readily and strongly [34]. Thus, the material can be heated quickly providing uniform temperature gradient. Use of internal FO and external IR sensor provides better facility to control the magnetron and the ramping of temperature [35]. In another type of reactors i.e. multimode reactors (conceptually similar to domestic oven), the MW enter the cavity is reflected by the walls loaded over the large cavity and several reaction vessels can be irradiated in one time in multi-vessel rotors (parallel synthesis). Taking in account the scalability of organic reactions and their safety concerns, Biotage developed a large synthesizer with synthesis capacity upto 300 g of material at a time whereas, CEM provided a multimode oven and a microwave system for flow-through synthesis and both readily provide multigram quantities of material [27]. Milestone offers multimode systems which are based on dual magnetron design which provides homogeneous and forward projected field that facilitates faster reaction rates with reproducible results. Another distinguished feature of this system is to support a comprehensive range of reaction vessels, allowing for either single reaction scale-up or multiple (simultaneous) reaction processing providing opportunities for parallel synthesis [27]. The multimode reactors are more energy efficient than monomode with increasing scale as the greater amount of material will absorb more MW energy which consumes proportionately lower power density than in a single mode instrument. [36]. In recent trends, to overcome scalability issues of microwave assisted organic synthesis, continuous-flow reactors are used available in both single and multimode cavities that allow the preparation of kilograms of materials by using microwave technology [37,38,39]. Herein, the reaction rate is increased by the rapid elevation of temperature and pressure, which can improve the productivity. Therefore, amalgamation of MW and flow system can be adapted to organic and inorganic materials syntheses.

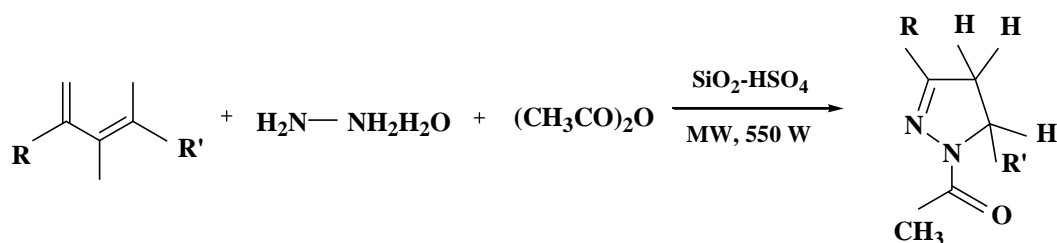
1.4 Heterogeneous catalysts and their role in microwave assisted organic synthesis

Catalytic technology has sound historical background of providing selective molecular transformations and has contributed to 90% of chemical manufacturing processes and to more than 20% of all industrial products [40]. Since the first report of microwave assisted organic synthesis [25,26], microwave irradiation has created 'green revolution' in all realms of synthetic chemistry. Applications including use of heterogeneous catalysis and non-traditional activation methods such as microwave irradiation has emerged prime tools to address environment concerning challenges in synthesis route within periphery of the green protocols. Combination of heterogeneous catalysis with microwave irradiation in organic synthesis offers several benefits: solid supports such as silica and alumina etc. are often very poor heat conductors and so they are very efficient microwave absorbents and acts as 'internal heating source'. Thus, they produce very strong microwave effect with significant temperature homogeneity, accelerated reaction rates and better conservation of final products compared to conventional heating methods [18]. Supported catalysts act a platform and medium to reactant molecules providing direct and selective heating to them which has also eliminated the solvent use and reaction occurs in '**dry or solvent-free media**'. The **microwave assisted organic synthesis in dry or solvent-free media (MASFOS)** has an indispensable part of organic synthesis chemistry due to better selectivity, small reaction time, less post work-up procedures [41]. Interaction of microwave with heterogeneous catalysts also causes generation of selectively heated thermal gradients known as 'hot spots'. These are thermal effects generated as the consequences inhomogeneity of the applied field, resulting in the temperature in certain zones within the sample being much greater than the macroscopic temperature. As described by Mingos in the decomposition of H_2S over $\gamma\text{-Al}_2\text{O}_3$ and $\text{MoS}_2\text{-}\gamma\text{-Al}_2\text{O}_3$ [42], the conversion rate was greatly influenced by generation of hot spots. However, excessive hot spot generation also had negative effect on coupling reaction as reported earlier [43].

Numerous inorganic and organic catalytic supports have been used for the development of solid acid catalysts and has catalyzed variety of microwave assisted organic transformations. These include silica, alumina, clay, activated carbon, zeolites, polymers, ion exchange resins, mesoporous materials and biomass derived alumino-silicates etc. Although extensive studies of heterogeneous catalyst catalyzed organic synthesis has been well precedent in the literature, fewer efforts have been done to throw some light on the microwave assisted organic transformations catalyzed by solid acids. The present chapter is an endeavour to summarize different types of solid acids currently in use and their role in organic transformations under dielectric heating and also accounts the synthesis of different supported catalysts prepared under microwave conditions.

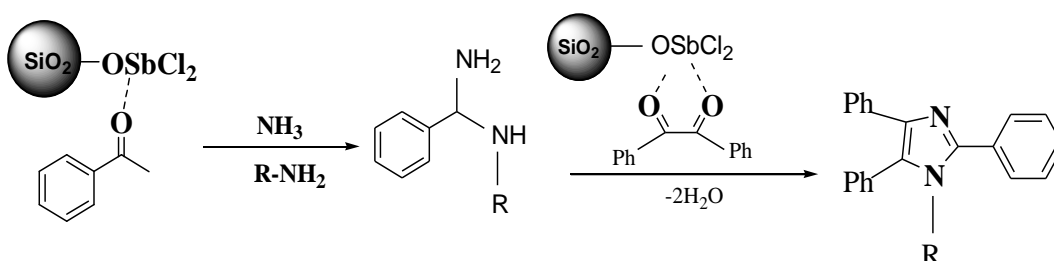
1.4.1 Silica supported solid acids

Silica also known as silox (from the Latin word “silex”) is a well established catalytic support material from many decades having heavily hydroxylated and easily functionalized mesoporous surface, high surface area and broad pore size distribution, low toxicity, cost effective and wide availability. 1-acetyl pyrazoline derivatives with important biological activities, such as epidermal growth factor receptor kinase-mediated, insecticidal and anti-inflammatory activities have been synthesized cyclization cum acetylation of aryl chalcones with hydrazine hydrate and acetic anhydride in the presence of **SiO₂-H₂SO₄** catalyst. Under MW irradiation of 4-6 min under solvent-free conditions 94% yield of N-acetyl pyrazoline was achieved [44] as shown in **Scheme 1.1**.



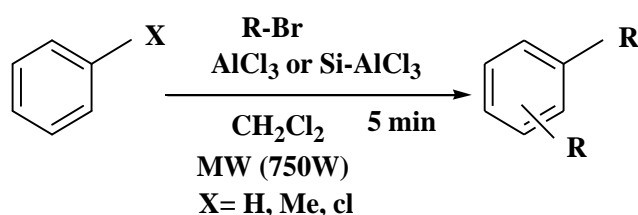
Scheme 1.1: Microwave assisted solvent-free cyclization cum acetylation of aryl chalcones with hydrazine hydrate and acetic anhydride in the presence of SiO₂-H₂SO₄ catalyst

Similarly, **silica supported sulfuric acid (SSA)** is used as an efficient catalyst for the preparation of quinolines from o-aminoarylketones and acetophenone via Friedländer condensation under microwave irradiation for 5 min and solvent-free conditions resulted as 91% yield [45]. **Nano silica supported phosphoric acid** has also efficiently catalyzed 14-aryl/alkyl-14*H*dibenzo[*a,j*]xanthenes and tetrahydrobenzo[*a*]xanthen-11-ones having important biological and pharmaceutical activities such as antibacterial and anti-inflammatory ones [46]. Microwave assisted synthesis of tri- and tetra-substituted imidazoles by cyclo-condensation of aldehyde, benzil, ammonium acetate and amine under solvent-free conditions is reported over Lewis acid **SbCl₃-SiO₂** catalyst. Compared to conventional procedure with hours of reaction time, reaction using 15 min of MW irradiation produced 95% yield and gave five reaction cycles with significant catalytic efficiency. The proposed mechanistic pathway for MW assisted synthesis of substituted imidazoles in the presence of SbCl₃/SiO₂ [47] as shown in **Scheme 1.2**



Scheme 1.2: Proposed mechanistic pathway for the formation of microwave assisted substituted imidazoles in the presence of SbCl₃/SiO₂.

Friedel-craft alkylation has been studied using MW chemistry and over solid-supported reagents. In this series, **silica supported AlCl₃** solid Lewis acid has been efficiently catalyzed MW assisted alkylation reaction (**Scheme 1.3**). As compared to classing heating, use of supported AlCl₃ MW irradiation superior yield was observed in this case [48].

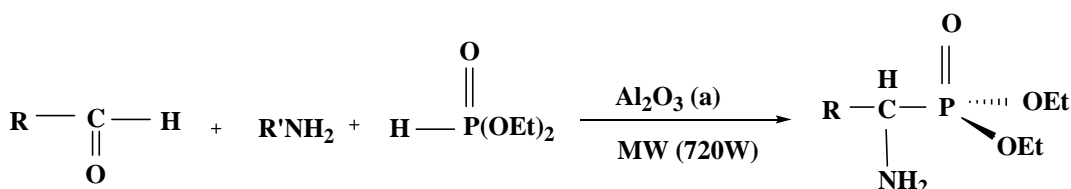


$\text{R} = \text{n-Pr, n-Bu, sec-Bu, 1-Pentyl, 3-Pentyl}$

Scheme 1.3: Microwave assisted Friedel-craft alkylation reaction

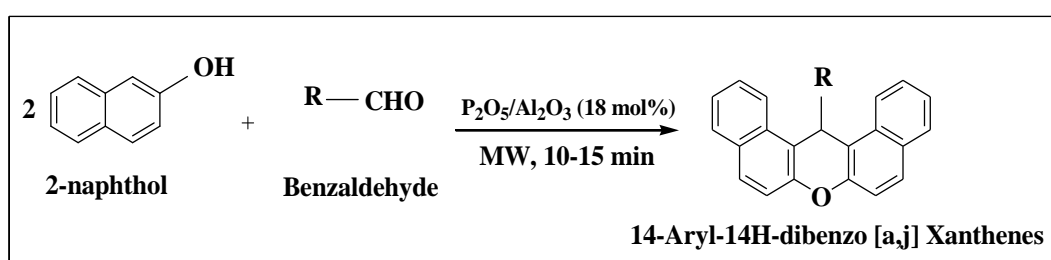
1.4.2 Alumina supported solid acids

Like silica, alumina is another material which has been widely used as catalytic support from many decades but in contrast to silica with natural origin alumina doesn't occur in nature. η - and γ - Al_2O_3 with high surface area and porosity has been used in heterogeneous catalysis [49]. In this context, acidic Al_2O_3 has successfully catalyzed solvent free synthesis of 1-aminoalkyl phosphonates under microwave irradiation with maximum 87% yield within 6 min [50] (**Scheme 1.4**). Quinoxalines were synthesized by condensation of benzene-1,2-diamine with both benzil and acyloin under microwave heating and gave better yield (96%) on acidic Al_2O_3 than the reaction over clay catalyst [51].



Scheme 1.4: Microwave assisted synthesis of 1-aminoalkyl phosphonates on acidic alumina using under solvent-free conditions

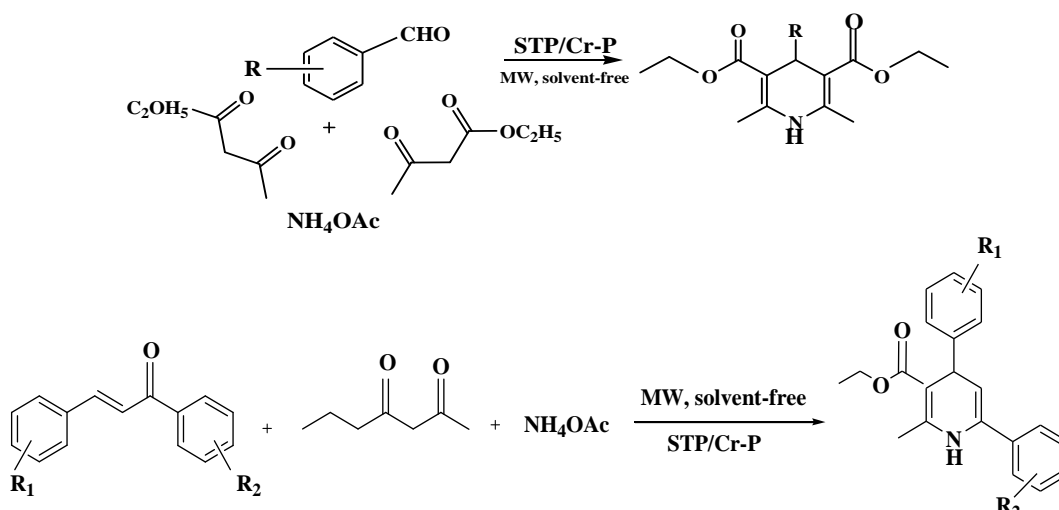
Benzoanthenes are important intermediates in organic synthesis due to their therapeutical and biological properties, pH-sensitivity fluorescent materials and in laser technology etc [52]. Al_2O_3 supported P_2O_3 an cost-effective, non-corrosive and eco-friendly catalyst has efficiently catalyzed microwave assisted synthesis of 14-aryl-14-*H*-dibenzo[*a,j*]xanthenes via. condensation of 2-naphthol and aldehydes (**Scheme 1.5**). Aldehydes with electron withdrawing groups produced better yield compare to electron donor groups.



Scheme 1.5: An efficient microwave assisted synthesis of 14-aryl-14-*H*-dibenzo[*a,j*]xanthenes over $\text{P}_2\text{O}_5/\text{Al}_2\text{O}_3$ catalyst

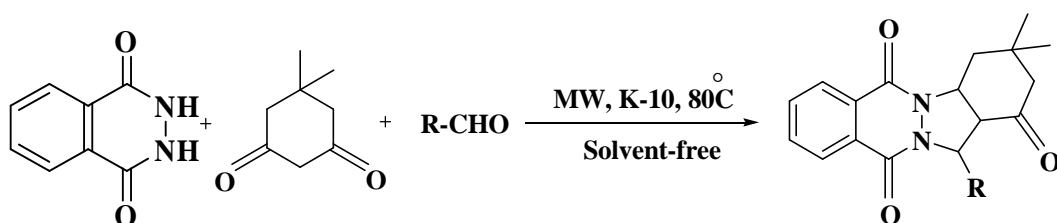
1.4.3 Clay supported solid acids

Clays are widespread, easily available and low-cost chemical natural aluminosilicates. In natural as well as numerous modified forms, clays are versatile materials that catalyze a variety of chemical reactions. Dihydropyridines (DHPs) are important class of bioactive molecules having applications as anticonvulsant, antianxiety and also used in synthesis of neuroprotectants and treatment of Alzheimer's disease [53]. **Silicotungstic acid nanoparticles dispersed on Cr-pillared clay (STA-Cr-P)** is used as an efficient solid acid catalyst for microwave assisted of 1,4-dihydropyridines (DHPs) by reaction of β -ketoester, benzaldehydes / chalcones and ethylacetoacetate under solvent-free conditions [54]. The synthesized STA-Cr-P catalyst achieved 75% yield in 5 min of reaction time whereas its parent clay was unable to catalyze the reaction (**Scheme 1.6**).



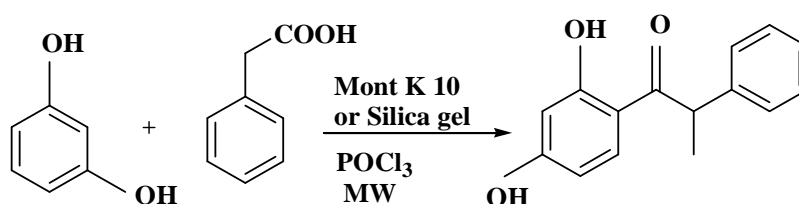
Scheme 1.6: STA/Cr-P catalyzed multicomponent condensation of arylaldehydes, ethylacetoacetate and ammonium acetate under microwave irradiation

An efficient, rapid and solvent-free synthesis of 2*H*-indazolo[2,1-*b*]phthalazine-triones has been accomplished by the reaction of phthalhydrazide, aldehydes and 5,5-dimethylcyclohexane-1,3-dione using Montmorillonite K-10 catalyst under MW irradiation conditions as given in **Scheme 1.7**. Under dielectric heating, 96% yield was achieved within 5 min using K-10 catalyst as compared to other catalysts like TiO₂, BF₃-SiO₂ and InF₃ etc. K-10 catalysts could be reused upto three reaction cycles without any noticeable loss of activity [55].



Scheme 1.7: Microwave assisted synthesis of 2*H*-Indazolo[2,1-*b*]phthalazine-triones catalyzed by K-10 under solvent-free condition

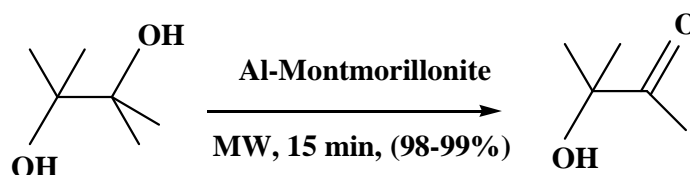
Friedel-craft acylation reaction has been extensively studied all over the world due to its wide applications in pharmaceuticals, cosmetics, plasticizers etc. **K-10 supported phosphoryl chloride (POCl₃-K-10)** efficiently catalyzed acylation reaction between resorcinol and phenylacetic acid under solvent-free microwave heating conditions and produced comparable results as **POCl₃-silica** [56] as displayed in **Scheme 1.8**.



Scheme 1.8: Friedel-craft acylation reaction of resorcinol and phenyl acetic acid over POCl₃-K-10 catalyst under microwave heating

Montmorillonite supported Al³⁺ has worked as an active solid acid catalyst for the esterification reaction of butanol and acetic acid [57] as well as Pinacol–pinacolone rearrangement of germinal alcohol under dielectric heating [58]. In Pinacol–pinacolone rearrangement, reaction time was drastically shortened to 15

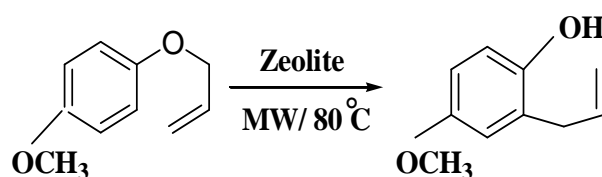
min from 15 h signifying the effect of in-core volumetric heating of MW (Scheme 1.9).



Scheme 1.9: Pinacol-pinacolone rearrangement of geminal alcohol under microwave irradiation

1.4.4 Zeolite supported solid acids

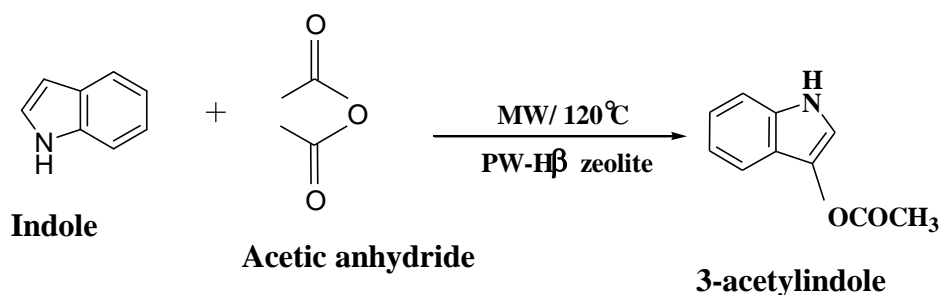
Zeolites are natural or artificial aluminosilicates with well-defined crystalline structures. With unique microporous nature, shape and size of pore system creates a steric effect on the reaction by controlling the accessibility of reactants and products. Thus, zeolites act as 'shape selective catalysts'. Their common catalytic applications are for shape selective applications such as bromination, acylation and chlorination etc. in liquid phase reactions, zeolites provide active sites located in rigid pores of aluminosilicate network facilitate checking of reactant molecules and promotes the formation of one isomer (usually most linear one) amongst other possible ones and can accelerate reaction rate either in catalytic or stoichiometric manner [59]. Under microwave heating, solvent free Claisen rearrangement of allyl 4-methoxyphenyl ether over H β zeolite at 80°C for 6 min to yield 63% yield [60] as shown in Scheme 1.10.



Scheme 1.10: Claisen rearrangement of allyl 4-methoxyphenyl ether over H β zeolite under MW irradiation

Modified zeolites have shown better catalytic performance compared to their parent H β zeolites. **Tungstophosphoric acid modified H β zeolite (PW-H β zeolite)** has efficiently catalyzed the microwave assisted Friedel-Craft acylation reaction of indole and acetic anhydride under solvent-free conditions

due presence of better active catalytic sites and lower amount of Lewis acid sites as determined by pyridine FTIR and ammonia TPD [61]. Microwave assisted synthesis at 200 W, 120°C for 8 min over PW-H β zeolites produced 100% conversion of indole and 82.9% selectivity to 3-acetylindole within 8 min as compared to its classing synthesis route with 3 h reaction time (**Scheme 1.11**).

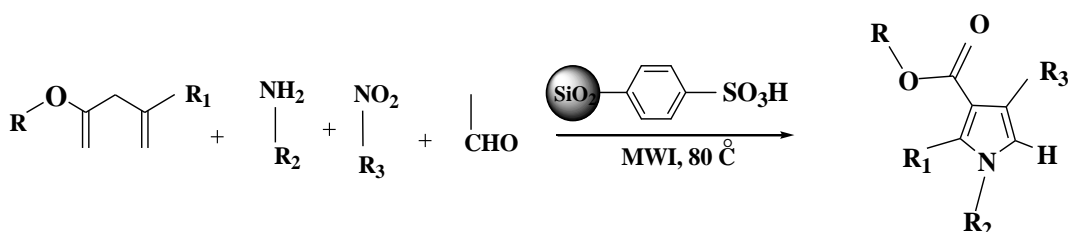


Scheme 1.11: Microwave assisted Friedel-craft acylation reaction of indole and acetic anhydride over PW-H β zeolite

Regioselective alkylation of naphthalene with alcohols has also been reported over **H-mordenite (HM) zeolite catalyst** under MW irradiation. During the reaction of 2-isopropyl naphthalene with isopropyl alcohol the conversion and selectivity of 43.5% and 66.4%, respectively were produced. Compared to conventional heating, in-core volumetric heating of MW resulted as high reaction rates and high selectivity for 2,6-dialkylnaphthalenes [62].

1.4.5 Polymer supported solid acids

Polymers especially spherical shaped has gained profound attention in heterogeneous catalysis due to their high surface area, uptake ability of different polarity and brittleness. In heterogeneous polymerizations, different synthesis methodologies such as precipitation, suspension, dispersion, membrane/micro channel emulsification and micro fluidic polymerizations have been used [63]. Using **p-Toluenesulfonic acid doped polystyrene (PS-PTSA)** with high stability, low price and tunable Lewis acidity has efficiently catalyzed one pot solvent-free microwave assisted cross-coupling-cyclization-oxidation to produce functionalized pyrrole from aldehyde, amine, active methylene, and nitroalkane. Compared to other catalysts such as FeCl₃-SiO₂, K-10 and InF₃, PS-PTSA was able to produce superior yield 93% within 56 min as shown in **Scheme 1.12** [64].

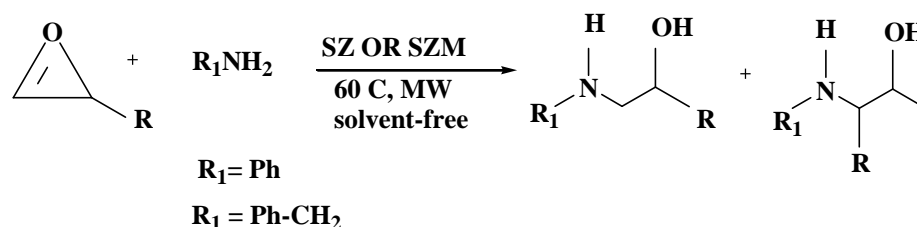


Scheme 1.12: Microwave assisted substituted pyrrole over PS-PTSA catalyst

Using **Polymer supported palladium (II) catalyst** rapid microwave Cross-Coupling reaction of aryl bromides with aryl boronic acids and sodium tetraphenylborate has been performed. The supported catalyst was prepared by ultrasonication of commercial Merrifield resin which improved its synthesis rate manifolds. The prepared catalyst efficiently catalyzed reaction upto five runs without losing its catalytic activity and produced better yields than its conventional counterparts [65].

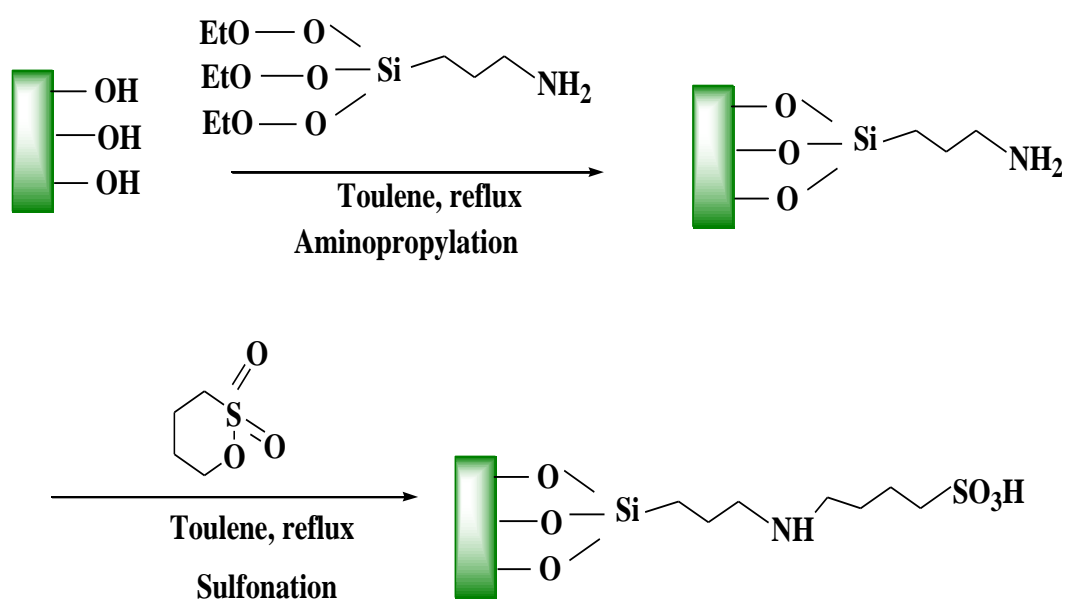
1.4.6 Mesoporous materials supported solid acids

Mesoporous materials has gained potential interest in the field of heterogeneous catalysis due to its fascinating characteristics such as high surface area, controllable pore size and narrow pore size distribution. Sulphated zirconia (SZ) firstly reported by 1979 by Hino and co-workers [66], has gained profound attention in solid acid catalysis due to high surface acidity. MCM-41 supported SZ has been used to catalyze regioselective nucleophilic opening of oxiranes with aniline and benzylamine to synthesize synthesis of β -amino alcohols under solvent-free microwave assisted conditions as displayed in **Scheme 1.13** [67]. The MCM-41 supported SZ catalyst gave remarkable yields enabling the regioselective synthesis of β -amino alcohols along with three reaction cycles without loss of catalytic efficiency.



Scheme 1.13: Microwave assisted synthesis of β -amino alcohols under solvent-free conditions over MCM-41 supported sulphated zirconia

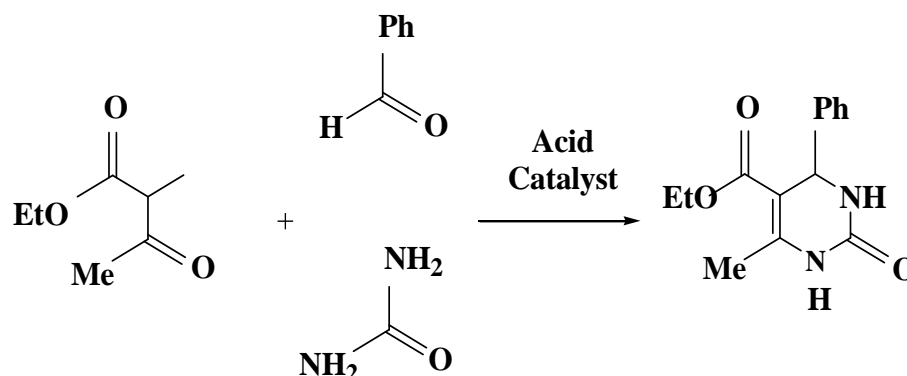
Covalently linked **sulfonic acid (SO_3H) modified MCM-41** mesoporous catalysts was prepared by amine functionalization followed by sulfonation as shown in **Scheme 1.14**. The prepared **SO_3H -MCM-41** was used as solid acid catalyst for Friedel-Crafts tert-butylation of hydroquinone enhanced by microwave heating. **SO_3H -MCM-41** gave excellent catalytic performance for the reaction by achieving remarkable 88.0% hydroquinone conversion and 93.1% selectivity (to 2-tert-butylhydroquinone (2-TBHQ) at 150°C after 8 min using nitrobenzene as a solvent. In addition, formation of small quantity of 2,6-di-tert-butylhydroquinone (2,6-DTBHQ, 4.0%) and other byproducts (2.9%) was also noticed. This result signified that the molecular sieving effect took place in the internal mesopores of the **SO_3H -MCM-41** turned the reaction towards the formation of only monosubstituted tert-butyl product [68].



Scheme 1.14: Functionalization of amine groups and anchoring of sulfonic acid functional groups on MCM-41 support

SBA-15 and VSB-5 supported FeCl_3 catalysts have been synthesized as an efficient, reusable and active Lewis acid by impregnation method. The catalytic performance of the prepared catalysts was evaluated by microwave-assisted Biginelli reaction using benzaldehyde, urea and ethyl acetoacetate under solvent-free conditions as given in **Scheme 1.15**. The prepared **$\text{FeCl}_3/\text{SBA-15}$** and

FeCl₃/VSB gave superior yields of 82 and 92% respectively at 180°C, 400W in 15 min than their parent support materials [69].



Scheme 1.15: Microwave assisted one pot solvent-free Biginelli reaction

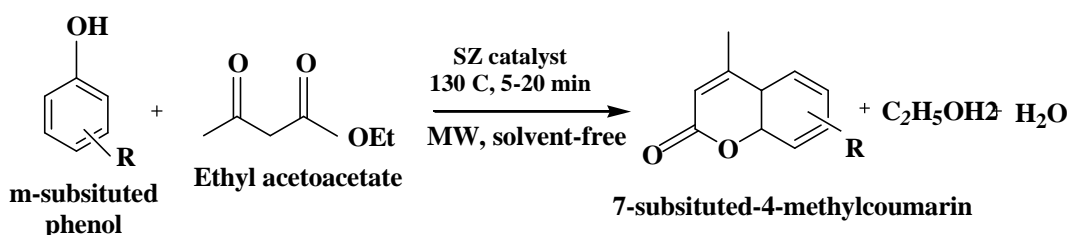
1.4.7 ZrO₂ supported solid acids

Over the past few decades, **zirconia (ZrO₂)** based acid catalysts have gained much popularity amongst other acid catalysts due to excellent catalytic performance for hydrocarbon conversions at mild conditions. Amongst zirconia promoted catalysts, **sulphated zirconia (SZ)** has been used widely for various organic transformations including multicomponent reactions, isomerization, alkylation, acetylation, esterification and some other industrial important reactions [70]. As investigated by Hino and Arata [71] SZ possesses 10⁴ times more acidity than sulphuric acid and has been considered as ‘superacid’ catalyst [72]. But the drawback of deactivation under both high temperature and in reducing atmosphere led to SO_x and H₂S formation respectively reducing its catalytic activity and stability. To overcome this limitation, researchers made SZ catalysts promoted by transition metals such as Fe, Mn, W, Mo, Cr and with noble metal Pt and developed types of superacid catalysts [73,74].

Nano-crystalline sulfated zirconia (SZ) has been efficiently used as solid acid catalyst for microwave assisted synthesis of coumarin derivatives under solvent-free conditions via Pechmann condensation reaction [75]. Using phenol derivatives like m-amino phenol, phloroglucinol, pyrogallol with ethyl acetoacetate over SZ catalyst, significant yields of 5,7-dihydroxy 4-methyl

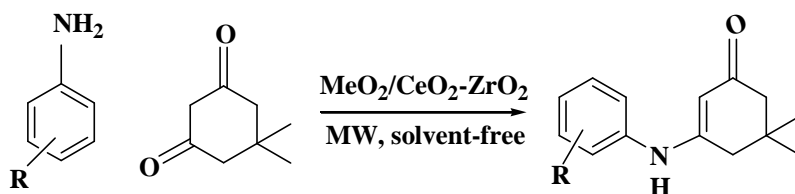
coumarin and 7,8-dihydroxy 4-methyl coumarins were achieved within 5-20 min at 130°C (**Scheme 1.16**).

The evaluation of catalytic activity of synthesized solid acid catalysts such as (5-20%) Mo(VI)/ZrO_2 and $\text{SO}_4^{2-}/\text{ZrO}_2$ by the microwave assisted synthesis of novel aromatic esters. The results established ZrO_2 based catalysts as efficient catalysts to produce aromatic esters in short duration of time [76].



Scheme 1.16: Microwave assisted 7-substituted-4-methylcoumarin synthesis under solvent-free conditions over nano-crystalline sulfated zirconia catalyst

In this series, $\text{MoO}_3/\text{CeO}_2\text{-ZrO}_2$ catalysts were prepared by simple co-precipitation to prepare $\text{CeO}_2\text{-ZrO}_2$ support followed by impregnation of MoO_3 . Amongst all, 20% $\text{MoO}_3/\text{CeO}_2\text{-ZrO}_2$ efficiently catalyzed the synthesis of β -enaminones by condensation of various anilines with dimedone under solvent-free conditions in microwave irradiations producing 95% yield within 3 min of reaction time [77] (**Scheme 1.17**).

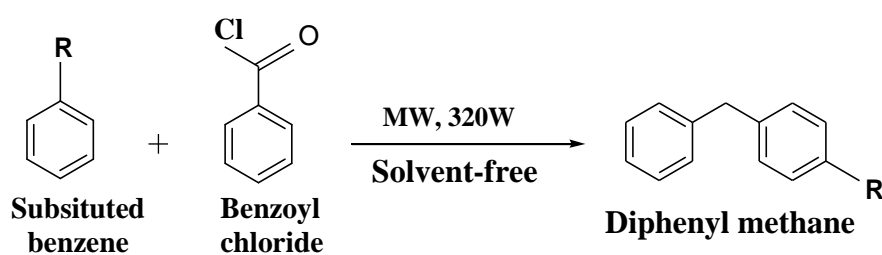


Scheme 1.17: Synthesis of β -enaminones by condensation of aniline with dimedone under solvent-free and microwave irradiation conditions over 20% $\text{MoO}_3/\text{CeO}_2\text{-ZrO}_2$

As precededent earlier, the world's fossil fuel reserves will be diminished by 2050 due to faster petroleum consumption (10^5 times) than the nature can create. To fulfill current energy requirements and to replace dependency on non-renewable sources has gained attention to search for renewable energy sources

have gained much attention. Production of biodiesel from various natural sources such as **edible oils** including soybean; canola; coconut; palm tree; rapeseed; rice bran; sunflower and cottonseed oils; **oils of non-edible crops** such as jatropha; castor; neem; karanja; rubber seed; used frying oils (waste cooking oil), animal fats; beef and sheep tallow; pongamia pinnata; maize; yellow grease; poultry fat; castor and algae and other **feedstock macro and microalgae** including cyanobacteria, wastewater treatment plant activated sludge, switch grass and other microbial communities is reported recently [78]. Using **tungstated zirconia (WO_3/ZrO_2)** solid acid catalyst, biodiesel is synthesized by in situ transesterification from dried biomass using microwave and sonication techniques. In situ transesterification combined the two steps (i.e. extraction of lipid and conversion to biodiesel) to a single step and minimized solvent requirement while the use of WO_3/ZrO_2 catalyst with ease of separation and effective reusability reduced the purification cost of biodiesel [79].

Microwave assisted benzoylation of benzene and its derivatives with benzoyl chloride to give diphenylmethane (substituted diphenylmethane) over **5% $\text{Bi}_2\text{O}_3/\text{ZrO}_2$, 3% and 5% $\text{Sb}_2\text{O}_3/\text{ZrO}_2$** under solvent-free conditions has been reported as shown in **Scheme 1.18**. Compared to catalytic activity of ZrO_2 , Sb and Bi promoted catalysts performed well due to better dispersion and presence of active surface sites [80].

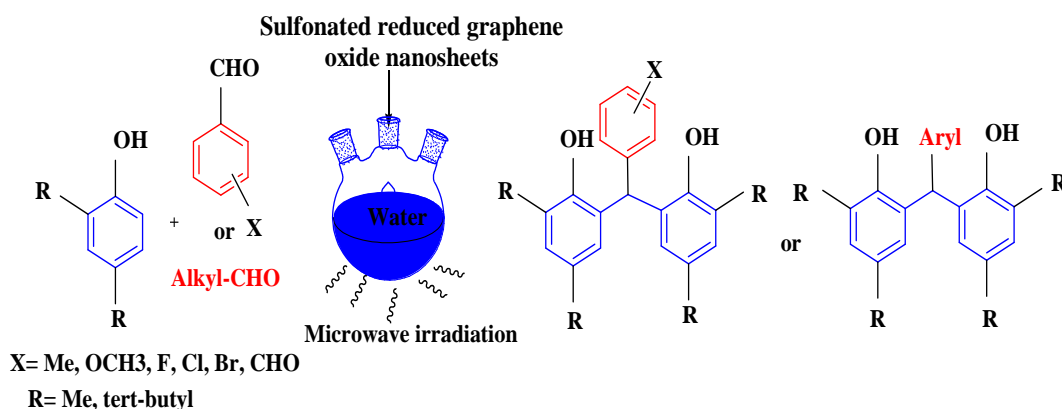


Scheme 1.18: Microwave assisted benzoylation reaction over $\text{Bi}_2\text{O}_3/\text{ZrO}_2$ and $\text{Sb}_2\text{O}_3/\text{ZrO}_2$ catalysts

1.4.8 Carbon supported solid acids

Carbon based solids are the next move toward more environmentally benign processes which are nontoxic and easy in separation and have a high acidic strength. SO_3H supported on reduced graphene oxide nanosheets has efficiently

catalyzed the synthesis of 6,6'-(aryl(alkyl)methylene)bis(2,4-dialkylphenol) derivatives from 2,4-dialkylphenols and aromatic and aliphatic aldehydes in aqueous media under microwave irradiation (**Scheme 1.19**). In addition, the catalyst could be recovered easily and reused several times without any considerable loss of its catalytic activity [81].



Scheme 1.19: Microwave assisted synthesis of synthesis of 6,6'-(aryl(alkyl)methylene)bis(2,4-dialkylphenol) derivatives over SO₃H supported on reduced graphene oxide nanosheets

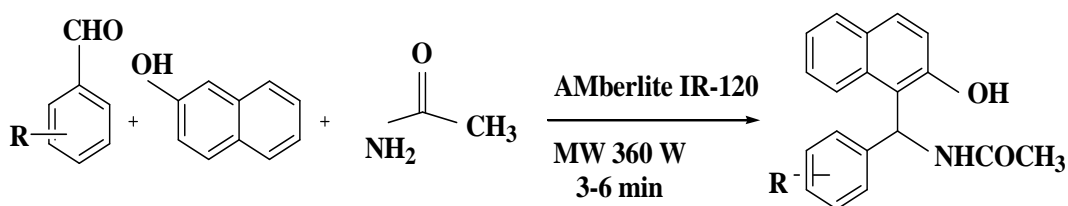
Derived from Lignin-rich residue, sulfonated char solid catalyst has been synthesized to catalyze microwave assisted hydrolysis of holocellulose (cellulose and hemicellulose) for production of sugars through liquification of holocellulose. Under microwave heating for 60 min at 393 K produced 82.5% yield of sugars comprising mono oligosaccharides and other units. The sulfonated char was recycled upto three reaction cycles maintaining equivalent efficiency as fresh run and showed better catalytic activity than dilute sulfuric acid in converting holocellulose into sugars under microwave irradiation [82].

1.4.9 Ion-exchange resins supported solid acids

Ion-exchange resins are insoluble macroporous polymers having capability to exchange specific ions with other ions within the polymer itself in a solution or reaction media. **Cation ion-exchange resin particles/PES hybrid catalytic membrane** has been used to catalyze esterification of acidified oil with methanol for biodiesel production under traditional heating method and microwave irradiation. Herein, biodiesel is produced from waste cooking oil containing lots of free fatty acids (FFAs) which cannot be directly used for biodiesel production

by alkaline-catalyzed transesterification due to soap formation. In previous years, esterification of FFAs in waste cooking oils used to take place by homogeneous strong acid-catalysts such as H_2SO_4 and HCl . But drawbacks like difficulty in separation from reaction mixture, corrosive nature and production of waste water promoted the use of supported homogeneous catalyst. Using optimized reaction conditions as reaction time 90 min, reaction temperature 60°C , methanol/acidified oil mass ratio 2.0:1, catalytic membrane loading 3 g and microwave power 240 W produced excellent FFA conversion upto 90%. Microwave assisted biodiesel production is a rapid, easy and green route which can also reduce its overall production cost [83].

1-aminomethyl-2-naphthols possessing depressor and bradycardia effects in humans and has been synthesized by the reaction of 2-naphthol, arylaldehyde and acetamide over **Amberlite IR-120** under microwave heating and solvent-free conditions [84]. Under microwave heating on replacing substituted benzaldehyde, 96-90% yields were achieved within 3-6 min without using any solvent as given in **Scheme 1.20**.



Scheme 1.20: Microwave assisted reaction of 2-naphthol, arylaldehyde and acetamide over Amberlite IR-120 under microwave heating and solvent-free conditions

1.10 Microwave assisted synthesis of materials and their applications

Microwaves have found a particular niche in all realms of synthetic chemistry especially in organic synthesis as heat source. In particular nanoparticles (NPs) synthesis, involvement of microwaves provides homogeneous in-core volumetric dielectric heating that leads to facilitates nucleation growth of NPs due to its rapid and more spatially uniform nucleation and growth of NPs. Following this phenomenon, new nanomaterials, catalysts as well as catalytic supports has been synthesized and given revolutionary results in their respective applications [7].

Pure metal oxide NPs with controlled sized and shapes, high area to volume ratio and large surface area has been extensively used in several areas of science and industry, especially catalysis due to high surface activity [85]. Colloidal Cu, Ag, Au, Pt NPs have been synthesized by ethanol/ethylene glycol/CMC driven metal ion reduction mechanism under dielectric heating possessed morphological features as nanospheres, naorods etc. [86]. Microwave assisted synthesized NPs such as Ru, ZnO (prepared by different synthetic routes) NPs have emerged as potential catalysts for various chemical applications as given in **Table 1.2**.

Mesoporous materials with uniform pores and high surface area has also been synthesized under microwave heating conditions with easier methodology and in very short time period compared to their classical preparation pathways. MCM-41, SBA-15 and SBA-16 have been synthesized under dielectric heating and shown remarkable high surface area and pore size [87,88].

Microwave heating is also helpful in synthesizing metal coated mesoporous materials as it also contributes into the uniform dispersion of metal species on supports. Different materials synthesized under dielectric heating and their applications are given in **Table 1.2**. In recent advancements, organically modified mesoporous silica with high inherent chemical reactivity has wide applications in separation technology and catalysis. These are synthesized under microwave heating due to advantageous properties with retention of original structural properties, homogeneous nucleation and reduced reaction time, production of smaller and more uniform particles [89]. Microwave heating technique has also become appealing tool in synthesis of organic biopolymers such as Aliphatic poly(ester)s and poly(ester) block copolymers such as Poly(ϵ -caprolactone) (PCL), Poly(ester)–poly(ethylene oxide) block copolymers including Polyurethanes (PUs), Poly alkyl carbonates (PACs), Polyamide, Grafted polymerization (ring opening polymerization) etc [90]. Although, use of microwave irradiation is in its infancy phase and lot of research is going on for its widespread full-fledged applications but still exceptional versatile advantageous characteristics and consistent modifications will give microwave chemistry a sustainable future.

Table 1.2: Microwave assisted synthesized materials with their applications

Type of material	Synthesis methodology	Conditions	Application	Ref.
Ru NPs	Using reducing agent and polymeric stabilizing agent (glucose and poly ethyl glycol)	Heated at 100°C, for 1 min ramp time and 20 sec hold time	Degradation of Congo red dye	[91]
ZnO Nano powder and ZnO hollow spheres	Precipitation and centrifugation, Solvothermal method under microwave assisted conditions	Final solution is irradiated for 5 min, Irradiation for 30 min at 200°C min	o-acylation alkyl or aryl alcohol with phenol, removal of Cr(IV) from water	[92], [93]
SBA-12 supported Au, Ag and Pd	Impregnation	time (usually 2-20 min) at 300-450W(maximum power output, 100–140 °C	oxidations of styrene and benzyl alcohol with H ₂ O ₂ under microwave irradiation	[94]
Fe-ISS, Fe-HMM Fe-MCM-41	Impregnation under microwave irradiation	200W at 15 min	microwave assisted oxidation and alkylation reaction	[95]
Silica coated CeO ₂ particles	Precipitation	Microwave irradiated for 2 min (maximum 500W) at 70°C	Degradation of methylene blue	[96]
TiO ₂ coated mesoporous	Impregnation under microwave	7 and 15 min under	Degradation of	[97]

carbon

irradiation

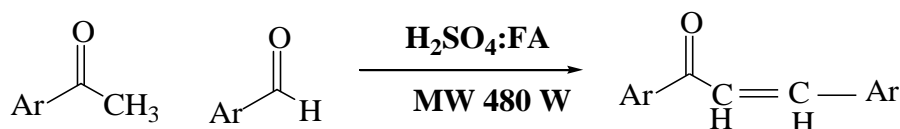
atmospheric
pressure

methylene blue

1.11 Fly ash as heterogeneous catalyst

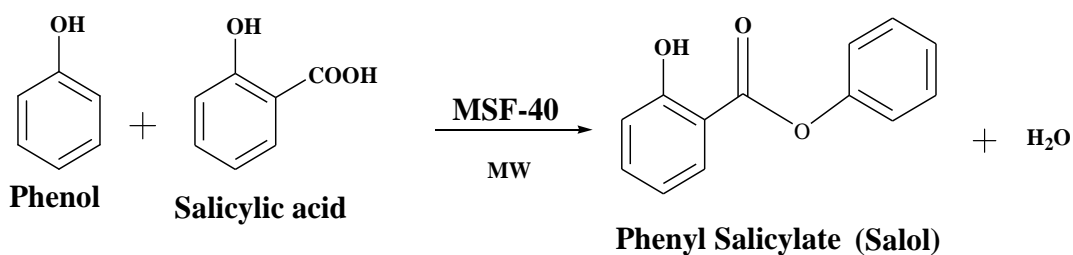
'Fly ash' (FA) is known as the lightweight fine particles of residual ash produced from combustion of pulverized coal in thermal power stations. To reduce pollution it is captured by electrostatic precipitators and bag houses before the flue gases reach the chimneys of power plants [98]. FA is a heterogeneous mixture of silica, alumina, ferric oxide, calcium oxide and other metal oxides, TiO_2 and Mn_2O_3 with crystallized phases of mulite, quartz and magnetite [99]. **American Society for testing Materials (ASTM C618)** [100] has categorized FA into types: C and F. Class-F, contains combined SiO_2 , Al_2O_3 , and Fe_2O_3 content of greater than 70% where as in case of Class C it is greater than 50%. Class-F type FA, with natural pozzolanic characteristics and lime binding capacity, has been widely used in cement manufacturing, building materials concrete and concrete-admixed products [101]. FA has also been used in adsorption of dyes and heavy metals [102,103], zeolites synthesis [104], air pollution [105] etc.

In recent years, FA has also been used in heterogeneous catalysis as a catalysts as well as catalytic support material under different reaction conditions. FA activated under microwave heating has actively and rapidly catalyzed the synthesis of array of naphthyl-substituted cyclohexanone, carboxylates, indazolones and nitro hydrozones in solvent-free conditions [106]. Microwave assisted synthesis of solvent-free chalcones via cross aldol condensation reaction has also been reported over **sulphuric acid activated fly ash ($\text{H}_2\text{SO}_4\text{:FA}$)** [107] as shown in **Scheme 1.21**.



Scheme 1.21: Microwave assisted synthesis of chalcones over $\text{H}_2\text{SO}_4\text{:FA}$ catalyst

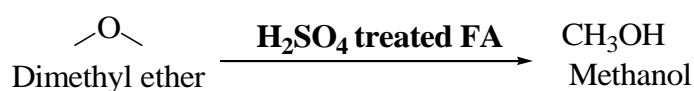
Mechanically activated FA has been transformed into an active solid acid catalyst by acid activation under microwave heating and has efficiently catalyzed microwave assisted esterification of salicylic acid and phenol as shown in **Scheme 1.22**. The catalyst was reused upto four reaction cycles maintaining catalytic activity as fresh run [108].



Scheme 1.22: Microwave-assisted solvent-free synthesis of salol over MSF catalyst

FA loaded *p*-toulene sulfonic acid (Fly ash: PTS) prepared by mixing has efficiently catalyzed aldol condensation of methyl ketones and substituted aldehydes under microwave irradiated conditions [109].

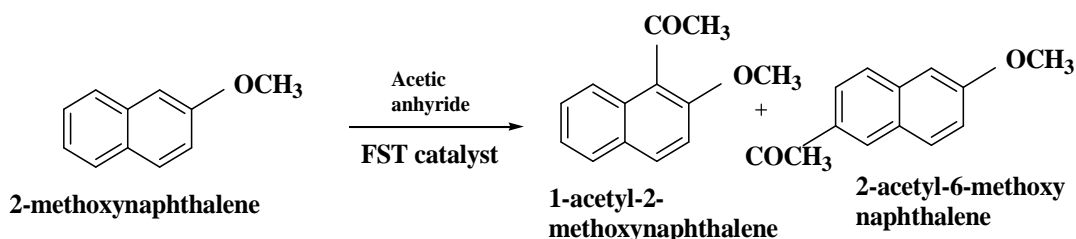
H₂SO₄ activated FA with active Brönsted acid sites has exhibited excellent catalytic activity for dehydration of methanol under vapour phase conditions for dimethyl ether (DME) production [110] (**Scheme 1.23**).



Scheme 1.23: Dehydration of dimethyl ether over H₂SO₄ activated FA catalyst under vapor phase conditions

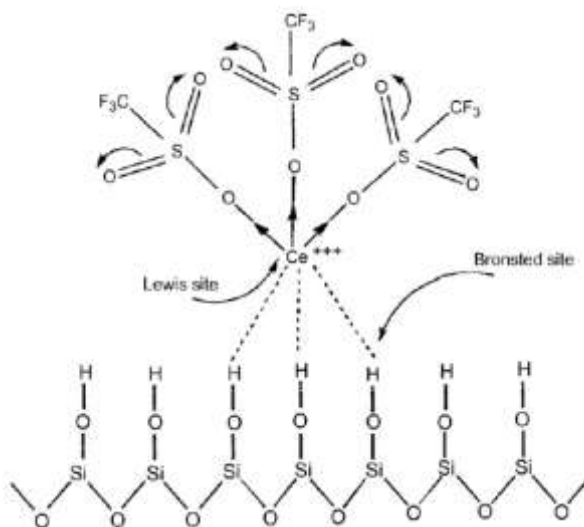
Recently, FA supported SO₄²⁻-SnO₂ nano catalyst has been used for the synthesis of serendipity product using substituted benzaldehyde, 3-amino-9-ethylcarbazole and dimedone in aqueous media [111]. Similarly, FA supported SO₄²⁻-Bi₂O₃ nano catalyst is found as promising catalyst for the synthesis of (6*H*-pyrido[3,2-*b*]carbazol-4-yl)aniline derivatives in water. [112]. Cobalt supported FA catalyst has been used for phenol degradation during waste water treatment [113].

FA supported scandium triflate (FST) as a Lewis acid catalyst has actively catalyzed solvent free single pot Friedel-Crafts acylation [114]. Over FST catalyst, gave remarkable acylation of 2-methoxynaphthalene (2-MN) using acetic anhydride as an acylating agent achieving 84% conversion and 73% selectivity of 2-acetyl-6-methoxynaphthalene (6-AMN) a precursor for anti-inflammatory drug (Scheme 1.24).



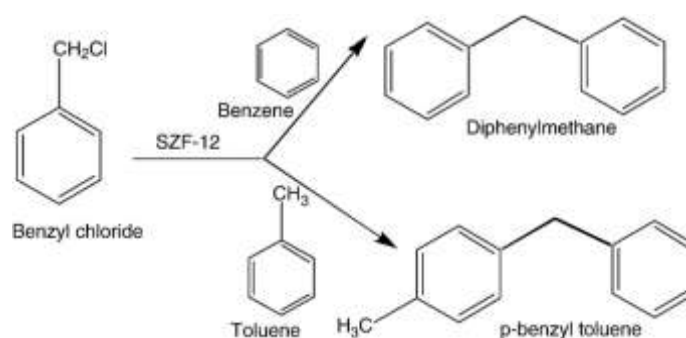
Scheme 1.24: Friedel-craft acylation of 2-methoxynaphthalene (2-MN) over FST catalyst

Similarly, **cerium triflate loaded FA (CFT)** has also been synthesized having thermally stable and very active Lewis acid sites as displayed in **Scheme 1.25**, CFT has efficiently catalyzed acylation of veratrole with acetic anhydride resulting 88% conversion to 3,4-dimethoxyacetophenone [115].



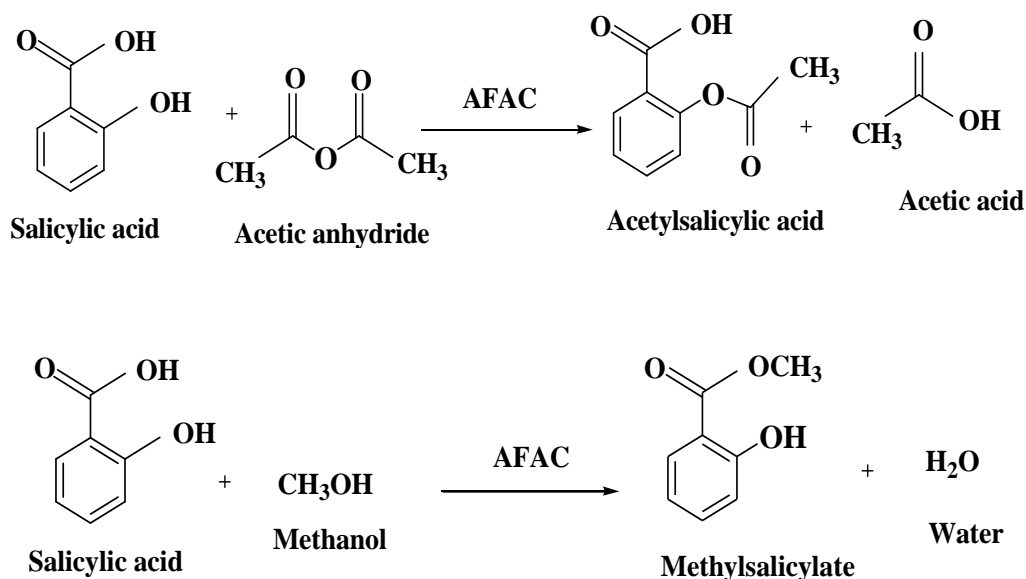
Scheme 1.25: Proposed structure of Lewis acid sites on CFT catalyst

Chemically activated FA supported sulphated zirconia with strong Brönsted and Lewis acid sites have actively catalyzed solvent-free benzoylation of benzene and its derivatives with benzoyl chloride [116] as given in **Scheme 1.26**.



Scheme 1.26: Benzylation of benzene and toluene with benzyl chloride over SZF-12 catalyst.

Nano-crystalline solid acid catalyst was prepared by acid refluxing of FA (AFAC). Prepared solid acid gave excellent yield of 97% with high purity of acetylsalicylic acid (aspirin) and a remarkable conversion 87% of salicylic acid to methyl salicylate (oil of wintergreen) [117] (**Scheme 1.27**).



Scheme 1.27: Solvent-free synthesis of acetylsalicylic acid and methyl salicylate over AFAC catalyst

1.12 Perlite as heterogeneous catalyst

Perlite is a siliceous, amorphous, volcanic lava glass comes into the category of igneous rocks. The perlite is produced by the flows related to thick accumulations of tuffs, lava flows and domes. It is available in gery, silver grey, dark brown and black colours. Chemically, perlite is a natural amorphous

alumino-silicate with metastable form [118] as natural, vitreous material containing 2-6% water [119]. Annual worldwide production of perlite is 700 million tones [120] Major producers are USA, Greece, China, Japan, Hungary and Turkey. The average chemical composition is silica (75%), with alumina (14.8%), K₂O (4.8%), Na₂O (2.9%), CaO (0.9%), MgO (0.1%), Fe₂O₃ (1.5%) and water (4.0%) [121]. During high temperature calcination, perlite gets expanded upto 10-20 times due to the vaporization of crystal water present in between perlite matrix generating bubbles in the softened structure [122]. The obtained perlite is known as ‘expanded perlite’ which gives magnificent insulation characteristics, low density and high porosity. The silicon atom present on the surface of perlite tends to retain their tetrahedral structure with oxygen atoms but at room temperature the coordination is accomplished by monovalent surface –OH groups [123]. Thus, various types of surface –OH groups as given in **Figure 1.3** have been identified on perlite surface which are mainly responsible for the adsorption capacity of perlite [124].

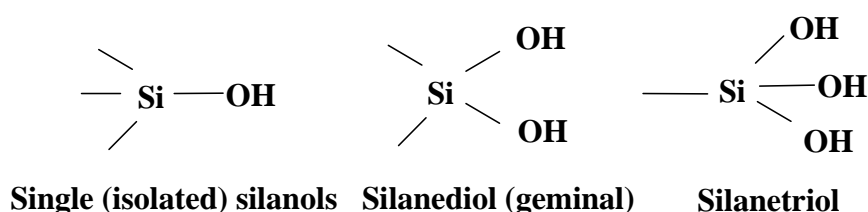


Figure 1.3: Types of arrays of hydroxyl groups present on surface of perlite

With all these expanded perlite has wide applications in the industry of building construction [125], precursor of geo-polymer formation [126], oil sorption [127], dye degradation [128], water purification [129], admixture to form thermal-insulating resilient PU foam composites [130] etc.

Recently, **perlite immobilized SO₃H solid acid (PeSA)** has been used as green heterogeneous catalyst for the heterocyclic multicomponent reaction which includes one pot synthesis of heterocyclic compounds such as 3,4-dihydropyrimidin-2-(1*H*)ones, 2,4,5-trisubstituted imidazoles coumarins and bis(indolyl)methanes. [131]. **SO₃H-Perlite** has also catalyzed the synthesis of 14-aryl 14*H*-dibenzo[*a,j*]xanthenes under microwave irradiated conditions and gave yield upto 82-96% with 4-10 min of short reaction time [132].

1.13 Scope of the present work

The present research work accounts for the development of novel, greener and cost-effective methodologies for the synthesis of fly ash and volcanic ash as an activated and supported solid acid catalyst to efficiently catalyze organic transformations under microwave assisted conditions. In heterogeneous catalysis, for homogeneous dispersion of metal moieties on support material synthesis methodology plays a vital role that directly affects its surface acidity and selectivity towards organic reaction. Mechanical and chemical modification techniques are used to improve textural, morphological and mineralogical characteristics of these solid wastes for homogeneous dispersion of metal oxide moieties. The resulted experimental results has been given with scientific illustrations to reveal changes occurred in phase, silica content and surface activity after mechanical and chemical activation in support materials.

The solid acid catalysts were prepared by microwave assisted acid activation and loading of metal i.e. sulfated tin ($\text{SO}_4^{2-}/\text{Sn}$), niobium (Nb) and tungsten (W) on solid waste supports. The physico-chemical features developed in these catalysts were analyzed by sophisticated analytical techniques such as XRD, FTIR, pyridine FTIR, UV-Vis DR, SEM-EDS and TGA.

Catalytic applications of the prepared catalysts were explored by microwave assisted organic reactions such as esterification and condensation reactions under solvent-free conditions. The obtained products by these reactions play important roles in the field of pharmaceuticals, cosmetics, laser dyes, agrochemical industries and bio-fuel additives. Microwave assisted conditions provided dielectric and in-core volumetric heating which results as shorter reaction times, better selectivity and yield of the product with minimizing side product formation. While the uses of supported acid catalysts in combination with microwaves act as a heat source and medium for the reactants, eliminates the use of solvents and promotes 'solvent-free' conditions. Catalysts could be easily regenerated by simple thermal activation and gave multiple numbers of reaction cycles without losing their catalytic activity.

1.14 References

- [1] M. Gharibeh, G.A. Tompsett, K.S. Yngvesson, W. C. Conner, *J. Phys. Chem. B* 113 (2009) 8930.
- [2] A.L. Washington, G.F. Strouse, *J. Am. Chem. Soc.* 130 (2008) 8916.
- [3] M.B. Gawande, S.N. Shelke, R. Zboril, R.S. Varma, *Acc. Chem. Res.* 47 (2014) 1338-1348.
- [4] B. Bacsá, S.B. ōsze, C.O. Kappe, *J. Org. Chem.* 75 (2010) 2103.
- [5] M. Bardts, N. Gonsior, H. Ritter, *Macromol. Chem. Phys.* 209 (2008) 25.
- [6] N.L. Campbell, R. Clowes, L.K. Ritchie, A.I. Cooper, *Chem. Mater.* 21 (2009) 204.
- [7] I. Bilecka, M. Niederberger, *Nanoscale* 2 (2010) 1358-1374.
- [8] J.R. Lill, *Microwave Assisted Proteomics*, RSC, Cambridge, 2009.
- [9] J. Anwar, U. Shafique, Waheed-uz-Zaman, R. Rehman, M. Salman, A. Dar, J.M. Anzano, U. Ashraf, S. Ashraf, *Arabian J. Chem.* 8 (2015) 100-104.
- [10] B. N. R. Baig, R.S. Varma, *Chem. Soc. Rev.* 41 (2012) 1559-1584.
- [11] C. Gabriel, S. Gabriel, E.H. Grant, B.S.J. Halstead, D.M.P. Mingos, *Chem. Soc. Rev.* 27 (1998) 213-223.
- [12] B.L. Hayes, *Aldrichimica Acta* 37 (2004) 66-77.
- [13] C.O. Kappe, D. Dallinger, S.S. Murphree, *Practical Microwave Synthesis for Organic Chemists*, Wiley-VCH: Weinheim, 2009.
- [14] C.O. Kappe, *Angew. Chem. Int. Ed.* 43 (2004) 6250 –6284.
- [15] B. Wathey, J. Tierney, P. Lidström, J. Westman, *Research focus* 7 (2002) 373-380.
- [16] N. Keiko, *J. Hom. Econ. Jpn.* 54 (2003) 351–356.
- [17] J. Anwar, U. Shafique, Waheed-uz-Zaman, R. Rehman, M. Salman, A. Dar, J.M. Anzano, U. Ashraf, S. Ashraf, *Arabian J. Chem.* 8 (2015) 100-104.
- [18] M. Gupta, S. Paul, R. Gupta, *Acta Chim. Slov.* 56 (2009) 749-764.

-
- [19] Pueschner GmbH website (www.pueschner.com/engl/basics/index.html).
 - [20] C. Oliver Kappe, *Chem. Soc. Rev.* 37 (2008) 1127–1139.
 - [21] J.-S. Schanche, *Mol. Diversity* 2003, 7, 293 – 300; Biotage AB (formally Personal Chemistry AB), www.personalchemistry.-com; www.biotage.com.
 - [22] A. de la Hoz, A'. Dr'az-Ortiz, A. Moreno, *Chem. Soc. Rev.* 34 (2005) 164-178.
 - [23] L. Perreux, A. Loupy, *Tetrahedron* 57 (2001) 9199-9233.
 - [24] V. Polshettiwar, R.S. Varma, *Chem. Soc. Rev.* 37 (2008) 1546-1557.
 - [25] R. Gedye, F. Smith, K. Westaway, H. Ali, L. Baldisera, L. Laberge and J. Rousell, *Tetrahedron Lett.* 27 (1986) 279–282.
 - [26] R. J. Giguere, T. L. Bray, S. M. Duncan and G. Majetich, *Tetrahedron Lett.* 27 (1986) 4945–4948.
 - [27] W.D. Shipe, S.E. Wolkenberg, C.W. Lindsley, *Drug Discovery Today: Technol.* 2 (2005) 155-161.
 - [28] P. Lidström, J. Tierney, B. Wathey, J. Westman, 57 (2001) *Tetrahedron* 9225-9283.
 - [29] M. Larhed, A. Hallberg, *Drug Discov. Today* 6 (2001) 406-416.
 - [30] A. Stadler, B.H. Yousefi, D. Dallinger, P. Walla, E. Van der Eycken, N. Kaval, C.O. Kappe, *Org. Proc. Res. Dev.* 7 (2003) 707–716.
 - [31] N.S. Wilson, C.R. Sarko, G.P. Roth, *Org. Proc. Res. Dev.* 8 (2004) 535–538.
 - [32] S.V. Ley, I.R. Baxendale, *Nat. Rev. Drug Discov.* 1 (2002) 573-586.
 - [33] C.O. Kappe, *Curr. Opin. Chem. Biol.* 6 (2002) 314-320.
 - [34] F. Meschke, G. Riebler, V. Hessel, J. Schurer, T. Baier, *Chem. Eng. Technol.* 28 (2005) 465-473.
 - [35] C.O. Kappe, *Chem. Soc. Rev.* 42 (2013) 4977-4990.
 - [36] J.D. Moseley, C. O. Kappe, *Green Chem.* 13 (2011) 794-806.

-
- [37] J. Wegner, S. Ceylan, A. Kirschninga, *Adv. Synth. Catal.* 354 (2012) 17-57.
 - [38] M.B. Gawande, S.N. Shelke, R. Zboril, R.S. Varma, *Acc. Chem. Res.* 47 (2014) 1338-1348.
 - [39] R. Morsch, M. Krull, C. Kayser, C. Boberski, R. Bierbaum, P.A. P. üschner, T.N. Glasnov, C. O. Kappe, *Green Process Synth.* 1 (2012) 281-290.
 - [40] G.A. Somorjai, H. Frei, J. Y. Park, *J. Am. Chem. Soc.* 131 (2009) 16589-16605.
 - [41] R.S. Verma, *Green Chem.* (1999) 43-54.
 - [42] X. Zhang, D.O. Hayward, D.M.P. Mingos, *Chem. Commun.* (1999) 975-976.
 - [43] Satoshi Horikoshi, Atsushi Osawa, Masahiko Abe, Nick Serpone, *J. Phys. Chem. C* 115 (2011) 23030-23035.
 - [44] G. Thirunarayanan, K.G. Sekar, *J. Taibah Uni. Sci.* 8 (2014) 124-136.
 - [45] M.A. Zolfigol, P. Salehi, M. Shiri, T. Faal Rastegar A. Ghaderi, *J. Iran. Chem. Soc.* 5 (2008) 490-497.
 - [46] A. Bamoniri, B.B. Fatemeh Mirjalilib, S. Nazemiana, *Current Chemistry Letters* 2 (2013) 27-34.
 - [47] J. Safari, S. Naseh, Z. Zarnegar, Z. Akbari, *J. Taibah Uni. Sci.* 8 (2014) 323-330.
 - [48] L.R. Zupp, V. L. Campanella, D.M. Rudzinski, F. Beland, R. Priefer, *Tetrahedron Lett.* 53 (2012) 5343-5346.
 - [49] S.N. Rashkeev, K. Sohlberg, M.V. Glazoff, J. Novak, S.J. Pennycock, S.T. Pantelides, *Phys. Rev.* 67 (2003) 1.
 - [50] B. Kaboudin, R. Nazari, *Tetrahedron Lett.* 42 (2001) 8211-8213.
 - [51] F. Mohsenzadeh, K. Aghapoor and H.R. Darabi, *J. Braz. Chem. Soc.* 18 (2007) 297-303.
 - [52] H. Naeimi, Z.S. Nazifi, *Appl. Catal. A: Gen.* 477 (2014) 132-140.

-
- [53] D.L. Comins, K. Higuchi, D.W. Young, *Dihydropyridine preparation and application in the synthesis of pyridine derivatives, Chapter 6, Advances in Heterocyclic Chemistry, Volume 110.*
 - [54] P. Kar, B.G. Mishra, *Chem. Eng. J.* 223 (2013) 647-656.
 - [55] M.V. Reddy, G.C. Sekhar Reddy, Y.T. Jeong, *Tetrahedron* 68 (2012) 6820-6828.
 - [56] N. Devi, *Res. J. Chem. Environ.* 10 (2006) 59-61.
 - [57] S. Ramesh, B.S. Jai Prakash, Y.S. Bhat, *Appl. Clay Sci.* 48 (2010) 159-163.
 - [58] E. Guitierrez, A. Loupy, G. Bram, E.R. Hitzky, *Tetrahedron Lett.* 30 (1989) 945.
 - [59] P. Gupta, S. Paul, *Catal. Today* 236 (2014) 153-170.
 - [60] D.K. Deodhar, A.S. Tipnis, S.D. Samant, *Ind. J. Chem.* 49B (2010) 1552-1555.
 - [61] G. Bai, T. Li, Y. Yang, H. Zhang, X. Lan, F. Li, J. Han, Z. Ma, Q. Chen, G. Chen, *Catal. Commun.* 29 (2012) 114-117.
 - [62] H. Yamashita, Y. Mitsukura, H. Kobashi, K. Hiroki, J. Sugiyama, K. Onishi, T. Sakamoto, *Appl. Catal. A: Gen.* 381 (2010) 145-149.
 - [63] M.T.Gokmen, F.E. Du Prez, *Prog. Polym. Sci.* 37 (2012) 365.
 - [64] V.V. Shinde, S.D. Lee, Y.S. Jeong, Y.T. Jeong, *Tetrahedron Lett.* 56 (2015) 859-865.
 - [65] L. Bai, Y. Zhang, J. Wang, *Complex. QSAR Comb. Sci.* 23 (2004) 875-882.
 - [66] M. Hino, S. Kobayashi, K. Arata, *J. Am. Chem. Soc.* 101 (1979) 6439-6441.
 - [67] G. Negrón-Silva, C.X. Hernández-Reyes, D. Angeles-Beltrán, L. Lomas-Romero, E. González-Zamora, *Molecules* 13 (2008) 977-985.
 - [68] E. Nga, S.N. Mohd Subaria, O. Marieb, R.R. Muktic, J. Juand, *Appl. Catal. A: Gen.* 450 (2013) 34-41.

-
- [69] B.J. Ahn, M.S. Gang, K. Chae, Y. Oh, J. Shin, W. Chang, *J. Indus. Eng. Chem.* 14 (2008) 401-405.
 - [70] M.K. Patil, A.N. Prasad, B.M. Reddy, *Curr. Org. Chem.* 15 (2011) 3961-3985.
 - [71] M. Hino, K. Arata, *J. Chem. Soc. Chem. Commun.* (1980) 851-852.
 - [72] R.J. Gillespie, *Acc. Chem. Res.* 1 (1968) 202-209.
 - [73] M. Hino, K. Arata, *J. Chem. Soc. Chem. Commun.* (1988) 1259-1260.
 - [74] M. Hino, K. Arata, *Chem. Lett.* (1989) 971.
 - [75] B. Tyagi, M.K. Mishra, R.V. Jasra, *J. Mol. Catal. A: Chem.* 286 (2008) 41-46.
 - [76] N. Thimmaraju, S.Z. Mohamed Shamsuddin, S.R. Pratap, K. Raja, *RSC Adv.* 5 (2015) 99517-99528.
 - [77] S.B. Rathod, M.K. Lande, B.R. Arbad, A.B. Gambhire, *Arabian J. Chem.* 7 (2014) 253-260.
 - [78] V.G. Gude, P. Patil, E. Martinez-Guerra, S. Deng, N. Nirmalakhandan, *Sustainable Chemical Processes* (2013) 1:5.
 - [79] A. Guldhe, B. Singh, I. Rawat, F. Bux, *Chem. Eng. Res. Des.* 92 (2014) 1503-1511.
 - [80] M. Basude, P. Sunkara, R. Sheelam and L. Paka, *J. Chem. Pharm. Res.* 4 (2012) 1136-1146.
 - [81] H. Naeimi, M. Golestanzadeh, *New J. Chem.* 39 (2015) 2697-2710.
 - [82] K. Wang, X. Xie, Z. Si, J. Jiang, J. Wang, *Adv. Mater. Sci. Eng.* (2015) 1-5.
 - [83] H. Zhang, J. Ding, Z. Zhao, *Bioresour. Technol.* 123 (2012) 72-77.
 - [84] M. Forouzani, H. Ghasemnejad-Bosra, *J. Saudi Chem. Soc.* (2011) DOI: 10.1016/arabj.2011.08.002.
 - [85] D. Astruc, Nano particles and Catalysis, *Wiley-VCH Verlag GmbH & Co. KGaA*, 2008.
 - [86] M. Baghbanzadeh, L. Carbone, P.D. Cozzoli, C.O. Kappe, *Angew. Chem. Int. Ed.* 50 (2011) 11312 -11359.

-
- [87] A.N. Ergün, Z.Ö. Kocabaş, M. Baysal, A. Yürüm, Y. Yürüm, *Chem. Eng. Commun.* 200:8, 1057-1070.
 - [88] C. Yuan, W. Hong-juan, X. Zhi-ning, *Trans. Nonferrous Met. Soc. China* 19 (2009) s656-664.
 - [89] G. Smeulder, V. Meynen, G. Van Baelen, M. Mertens, O.I. Lebedev, G. Van Tendeloo, B.U.W. Maes, P. Cool, *J. Mater. Chem.* 19 (2009) 3042-3048.
 - [90] A. Sosnika, Gustavo Gotelli, G.A. Abraham, *Prog. Polym. Sci.* 36 (2011) 1050–1078.
 - [91] S. Gupta, *J. Colloid. Interface Sci.* 411 (2013) 173-181.
 - [92] F.M. Moghaddam, H. Saeidian, *Mater. Sci. Eng., B* 139 (2007) 265-269.
 - [93] X. Zhao, L. Qi, *Nanotechnology* 23 (2012) 1-7.
 - [94] J. M. Campelo, T. D.Conesa, M. J. Gracia, M. J. Jurado, R. Luque, J.M. Marinas A. A. Romero, *Green Chem.* 10 (2008) 853–858.
 - [95] A. I. Carrillo, E. Serrano, R. Luque, J. G. Martínez, *Appl. Catal. A: Gen.* 453 (2013) 383-390.
 - [96] I.A. Siddiquey, T. Furusawa, Y. Hoshi, E. Ukaji, F. Kurayama, M. Sato, N. Suzuki, *Appl. Surf. Sci.* 255 (2008) 2419-2424.
 - [97] C. Pastravanu, M. Ignat, E. Popovici, V. Harabagiu, *J. Hazard. Mater.* 278 (2014) 382-390.
 - [98] S. Wang, H. Wu, *J. Hazard. Mater. B* 136 (2006) 482-501.
 - [99] I.G. Lodeiro, A. Palomo, A.F. Jimenez, *Cement Concr. Res.* 37 (2007) 175-183.
 - [100] M. Ahmaruzzaman, *Prog. Energy Combust. Sci.* 36 (2010) 327-363.
 - [101] R.S. Blissett, N.A. Rowson, *Fuel* 97 (2012) 1-23.
 - [102] M. Matheswaran, T. Karunanithi, *J. Hazard. Mater.* 145 (2007) 154-61.
 - [103] A.N. Ökte, D. Karamanis, D. Tuncel, *Catal. Today* 230 (2014) 205-213.
 - [104] V. Somerset, L. Petrik, E. Iwuoha, *J. Environ. Manage.* 87 (2008) 125-131.

- [105] Lu GQ, Do DD, *Fuel Process. Technol.* 27 (1991) 95-107.
- [106] V. Kanagarajan, M.R. Ezhilarasi, J. Thanusu, M. Gopalkrishanan, *Green Chem. Lett. Rev.* 4 (2011) 355-368.
- [107] G. Thirunarayanan, P. Mayavel, K. Thirumurthy, *Spectrochim. Acta Part A Mol. Biomol. Spectrosc.* 91 (2012) 18-22.
- [108] N. Shringi, K. Srivastava, A. Rani, *Chem Sci Rev Lett* 4 (2015) 561-570.
- [109] R. Sundararajan, R. Arulkumaran, D. Kamalakannan, R. Suresh, K. Ranganathan, S.P. Sakthinathan, G. Vanangamudi, *Int. J. Pharm. Chem. Sci.* 1 (2012) 1657.
- [110] D. Zeng, S. Liu, W. Gong, J. Qiu, H. Chen, G. Wang, *Fuel* 119 (2014) 202-206.
- [111] K. Thirumurthy, G. Thirunarayanan, *RSC Adv.* 5 (2015) 33595-33606.
- [112] K. Thirumurthy, G. Thirunarayanan, *Arabian J. Chem.* (2015) [http://dx.doi.org/ 10.1016/j.arabjc.2015.04.015](http://dx.doi.org/10.1016/j.arabjc.2015.04.015).
- [113] E. Satpura, S. Muhammad, H. Sun, H. Ming, M.O. Tadé, S. Wang, *Catal. Today* 190 (2012) 68.
- [114] A. Rani, C. Khatri, R. Hada, *Fuel Process. Technol.* 116 (2013) 366–373.
- [115] C. Khatri, M.K. Mishra, A. Rani, *Fuel* 89 (2010) 3853-3859.
- [116] C. Khatri, M.K. Mishra, A. Rani, *Fuel Process. Technol.* 91 (2010) 1288-1295.
- [117] C. Khatri, A. Rani, *Fuel* 87 (2008) 2886-2892.
- [118] M. Dagan, M. Alkan, *Fresenius Environ.* 13 (2004) 251-257.
- [119] M. Gürtürk, H.F. Oztop, A. Hepbash, *Energy Convers. Manag.* 75 (2013) 488-497.
- [120] S. Kabra, S. Katara, A. Rani, *Int. J. Innov. Res. Sci. Eng. Technol.* 2 (2013) 4319-4326.
- [121] M. Giannouri, T. Kalampalki, N. Todorova, T. Giannakopoulou, N. Boukos, D. Petrakis, T. Vaimakis, C. Trapalis, *Int. J. Photoenergy* (2013).

- [122] M. Taherishargh, I.V. Belvora, G.E. Murch, T. Boddu, *J. Hazard. Mater.* 152 (2008) 26.
- [123] M. Dokan, M. Alkan, Ümit Cakir, *J. Colloid Interface Sci.* 192 (1997) 114-118.
- [124] Seifpanahi Shabani, K., F.D. Ardejani, K. Badii, M.E. Olya, *Arabian J. Chem.* (2013) <http://dx.doi.org/10.1016/j.arabjc.2013.12.001>.
- [125] H. Aglan, M. Morsy, A. Allie, F. Douad, *Construction Building Mater.* 23 (2009) 138-145.
- [126] E.R. Vance, D.S. Perera, P. Imperia, D.J. Cassidy, J. Davis, J.T. Gourley, *J. Australian Ceramic Society* 45 (2009) 44-49.
- [127] D. Bastani, Safekordi, A. Alihosseini, V. Taghikhani, *Sep. Purif. Technol.* 52 (2006) 295-300.
- [128] A. Khani, M.R. Sohrabi, *Polish J. Chem. Technol.* 14 (2012) 69-76.
- [129] M. Długosz, J. Waś, K. Szczubiałka, M. Nowakowska, *J. Mater. Chem. A*, 2 (2014) 6931-6938.
- [130] T. Ting Li, Y.Chun Chuang, C.Hung Huang, C.Wen Lou, J. Horng Lin, *Fibers and Polymers* 16 (2015) 691-698.
- [131] E. Kolvari, N. Koukabi, M.M. Hosseini, *J. Mol. Catal. A: Chem.* 397 (2015) 68-75.
- [132] E. Mirhadi, A. Ramazani, M. Rouhani, S.W. Joo, *Chemija* 24 (2013) 320–324.



Chapter-2

*Microwave Assisted Acid Activation of
Fly Ash: A Green Process for Enhancing
Physico-Chemical Attributes for
Esterification under Dielectric Heating*

ABSTRACT

The present chapter investigates the structural, textural and morphological modifications of fly ash by mechanical and chemical activation with 5N H₂SO₄ under microwave heating. The physico-chemical attributes of activated samples were characterized by XRF, BET surface area analyzer, XRD, FTIR, pyridine FTIR and SEM-EDX techniques. Mechanical activation of fly ash by ball milling enhanced its degree of roughness and specific surface area (SSA) from 9 m²/g to 17 m²/g by breaking larger particles. As a green alternative to traditional heating, microwave irradiation provided in-core volumetric heating to milled fly ash samples during acid treatment to increase their surface area and acidity. The microwave exposure time was varied as 20 and 40 min to measure the effect of microwaves during acid treatment of milled fly ash. To evaluate the catalytic efficiency of the microwave assisted sulphuric acid activated fly ash (MSF) samples, solvent-free esterification for the synthesis of 'salol' under dielectric heating was performed which is commercially used as antiseptic and mild analgesic. The MSF-40 catalyst with 22 m²/g SSA and crystalline size of 14 nm produced highest 88% conversion of salicylic acid and 90% yield of salol, indicating the presence of sufficient amount of surface acidic site. The catalyst could be regenerated by simple microwave activation and reused upto four reaction cycles. Similar FTIR and pyridine FTIR spectra of fresh and regenerated MSF-40 indicate structural and acidic stability under experimental conditions.

2.1 Introduction

Approaches to address the environmental concerning challenges by application of non-traditional methods such as microwave (μW) irradiation and catalysis has emerged as major tools in green synthesis and engineering. The use of ' μW flash heating' in synthetic chemistry has emerged as an energy efficient heating source as it reduces processing time by several orders of magnitude by in-core volumetric heating, suppresses side reactions, improves yield, product purity and reproducibility compared to traditional processes [1]. Along with this, encouragement of heterogeneous catalysis in organic synthesis has facilitated greener, safer and non-corrosive route by reduction in waste and easy handling allows the design of continuous flow processes that are economically very attractive at the industrial scale compared to their homogeneous counterparts [2]. Involvement of μW irradiation with activated catalysts (AC) during reaction offer several advantages. AC not only provide active surface for the reaction but also acts as direct selective heating source by absorbing μW . The AC is also capable to serve as medium for reactions, promotes dry or solvent-free synthesis. Use of different phase catalyst other than reaction substrate provides easy recovery from reaction mixture and reusability of catalyst after simple activation [3].

Acid activation of inorganic materials such as silica, clays and activated carbon etc. with hot mineral acids under reflux condition is one of the widely used techniques to improve surface acidity thus catalytic efficiency of the material. In recent years, μW assisted acid treatment of clays has produced equivalent or better results compared to traditional refluxing methodologies. Among μW activation parameters, μW power plays a crucial role in specific surface area (SSA) enhancement and can affect the basic skeleton during acid treatment. Smectite clay treated with 2M HCl upto 500 W showed increased SSA but didn't change the component structure to any perceptible extent while the samples activated at 650 W showed partial destruction in structure as evident by XRD and also showed reduction in SSA [4,5]. Upto 600 W, Brazilian bentonite activated with H_2SO_4 (6N) didn't show any significant alternations and SSA also followed a proportional relationship. Activation above 800 W power gave more drastic

reduction and 1000 W showed complete destruction in structure while in SSA sharp declination was observed [6]. μ W assisted 4N H_2SO_4 treated Amazon flint kaolin served as an efficient solid acid catalyst for the biodiesel production with 96.4 % conversion rate for esterification confirming sufficient active catalytic sites compared to catalyst prepared under reflux conditions [7]. A second-order response surface model (RSM) with a central composite design was developed to study the variation in specific surface area of activated bentonite with μ W time, acid normality and μ W power. The obtained results revealed that increasing the time and acid normality improves the textural properties of bentonites, resulted as increased specific surface area ($142 \text{ m}^2/\text{g}$) with an acid normality of 5.2 N [8].

Fly ash (FA), an industrial solid waste has already been established as active solid support with increased active acid sites on FA surface. But conventional hydrothermal acid digestion and high temperature exposure for a longer time encouraged for finding a faster technique for FA supported catalyst preparation. μ W irradiation heating has been reported earlier in FA sintering [9]; zeolite synthesis [10] and curing of FA filled epoxy composites [11].

This chapter reports microwave assisted sulphuric acid (5N H_2SO_4) activated FA catalyst possessing stable Brönsted active sites catalyzing esterification reaction under microwave heating for solvent free synthesis of phenyl salicylate. The phenyl ester of salicylic acid or phenyl salicylate is used in medicine as internal antiseptic with name as 'salol'. Due to its pleasant taste and odour, it is used in perfumery, flavouring and sun tan preparations. It is also used an anodyne, analgesic and pain relieving agent [12]. Having ability to absorb UV light in the range of 290-325 nm, it finds its applications as ultraviolet radiation filters [13]. Previously, vapour phase synthesis of phenyl salicylate has been synthesized using sulphated zirconia and Mo(VI) ions modified zirconia catalysts [14] while its convective preparation has been reported over sulphated oxides of alumina, silica, zirconia and zeolites [15] catalysts. Recently, synthesis of salol over HNO_3 activated fly ash has been studied [16] But limitations such as longer reaction time to achieve better selectivity of the product, poisoning of catalytic active sites due moisture sensitive nature [17] and high preparation cost of

catalysts inspired to find new synthesis routes under green protocols. In the present work, microwave assisted synthesis of salol over MSF-40 catalyst of salol has been reported. Solid acid catalyst (MSF) has been synthesized by acid activation of fly ash under microwave heating. Microwave irradiation time was varied as 40 and 20 min to study its on activation of fly ash. MSF-40 catalyst gave remarkable 90% yield of ester and efficiently reused upto four reaction cycles without losing its catalytic efficiency.

2.2 Experimental details

2.2.1 Materials

2.2.2 Coal fly ash (Class F type with $\text{SiO}_2 + \text{Al}_2\text{O}_3 > 70\%$) was collected from Jamshedpur Thermal Power Station (Jamshedpur, Jharkhand, India). Concentrated sulphuric acid (98 %), salicylic acid and phenol were purchased from S. D. fine Chem. Ltd., India and were used as such.

2.2.3 Instrumentation details

Mechanical activation of fly ash was milled using **high energy planetary ball mill Retsch PM-100** having maximum rotation speed 650 RPM (**Figure 2.1a**). For sample milling, agate jar and 100 agate balls of 5 mm size are used maintaining ball to powder weight ratio (10:1).

CEM microwave furnace (Model- Phoenix) with temperature range to 100-1000°C is used for calcination of acid activated fly ash samples (**Figure 2.1b**).

The acid activation of milled FA and its catalytic evaluation by esterification reaction is carried out in **CEM Focused MicrowaveTM Synthesis System USA, Model-Discover** having a continuous microwave power delivery system with selectable power output from 0-300 watts (+/- 30 watts) programmable in 1-watt increments, self-adjusting, single mode microwave cavity with working frequency of 2.45 GHz and with manual and PC operated facility. Operating temperature range is 25-250°C while power limit is 0-300 Watt. Pressure is programmable from 0-300 psi (0-21 bar). The operating parameters can be controlled by **Synergy.exe software** that enables on-line control during the reaction run. The reaction temperature during the run can be monitored with

infrared sensor placed aligned just below the reaction vessel. The system is also facilitated by a **magnetic stir bar** and **built-in automatic magnetic stirrer** for continuous stirring of substrate materials inside the vessel. To control pressure under reaction conditions, **IntelliVent™ Pressure Control System** has installed as given in **Figure 2.3b&c**, uses a load cell connected to a 10ml vessel and sense the changes in the external deflection of the septa on top of the sealed pressure vessel. This captures and release mechanism helps to secure the reaction in the cavity. **Teflon spill cup** placed in the cavity protects detector from microwave exposure. **Air compressor** is used for providing cool air during ‘cooling time’ phase of the reaction run. The reaction run in CEM synthesis system is divided into three stages working either in open or closed vessel system:

- **Ramping time:** as CEM synthesis system starts, it is the time taken to attain given reaction parameters (time, temperature and pressure) by supply of maximum microwave power by microprocessor-controlled single-magnetron system.
- **Holding time:** after attaining the given reaction conditions, system enter into this phase. In this time period system maintains the reaction parameters by controlling the power supply.
- **Cooling time:** after completion of the given reaction time period, system transits into this stage to cool down reaction mixture within microwave cavity by lowering the given reaction temperature and pressure parameters below safer limits of 50°C and 15 psi respectively.

The preparation of the catalyst and its catalytic evaluation by organic reaction takes place using following modes:

❖ **Open vessel system**

This type of vessel system is used for the preparation of the catalyst under atmospheric pressure conditions using 80 ml round bottom flask with air condenser as shown in **Figure 2.2**. Before using this feature, in Synergy.exe software on menu bar go into the ‘option’ and mark ‘open vessel system’. On starting up, all three processing stages i.e. **ramping, holding and cooling time** are followed.

❖ Closed vessel system

Evaluation of catalytic activity of prepared catalysts is performed in closed vessel system of microwave synthesis system (**Figure 2.3a,b & c**) using **closed pyrex glass vials** (ca. 10 ml) with **teflon-coated septa** and **teflon stirring bar**. The reaction is carried out at desired temperature in solvent-free condition using **power maximum or Power_{max} (P_{max})** feature, responsible for maintaining temperature throughout the reaction by simultaneous μ W heating and cooling by compressed air. The pressure parameter during the reaction is controlled by **IntelliVent™ Pressure Control System** as described earlier. The reaction run is accomplished through the same stages of **ramping** (time taken to attain given time, temperature and pressure parameters), **holding** (maintaining and controlling reaction parameters during the run time) and **cooling time** (to cool down reaction mixture below safer limits).



(a)



(b)

Figure 2.1: (a) Planetary ball mill (b) CEM microwave furnace



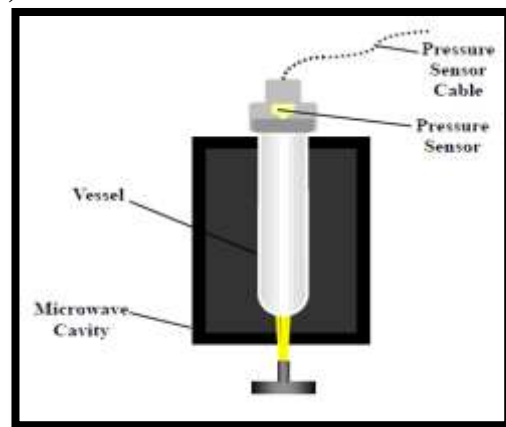
Figure 2.2: (a) CEM Discover with open vessel system (under atmospheric pressure conditions)



(a)



(b)



(c)

Figure 2.3: CEM Discover with (a) closed vessel system (b) its pressure IntelliVent™ system and (c) cross section view of IntelliVent™ pressure sensor

2.2.4 Preparation of catalyst

As received fly ash was washed with distilled water and carbon creamed up during washing was removed. The washed fly ash was dried at 100°C for 24 h and mechanically activated for 15 h using high energy planetary ball mill (Retsch PM-100, Germany) in an agate jar using agate balls of 5 mm size with rotation speed of 250 rpm and having ball to powder weight ratio (BPR) of 10:1. Fly ash gone through mechanical activation for 15 h (MFA-15) was chosen for further study and calcined at 800°C for 3 h to remove impurities of carbon, sulphur and others.

Acid activation of MFA-15 was carried out in an open vessel system of CEM microwave synthesis system. MFA-15 with 5N H_2SO_4 in a 1:2 molar ratio was filled in a round bottom flask and refluxed under microwave heating at 90 °C and 100 W for 20 and 40 min by following the same three ramping, holding and cooling stages to complete the reaction run as described earlier. Thus, obtained slurry was cooled, filtered and washed thoroughly with hot distilled water to achieve pH 7 and make it free from sulphate ions (tested by BaCl_2 solution). The activated samples were dried at 110 °C for 24 h followed by calcining at 450 °C for 1 h under static condition in CEM microwave furnace (Model-Phoenix). The prepared samples MSF-20 and MSF-40 are designated according to their microwave irradiation time. **Figure 2.4** represents the temperature and power monitoring profile for acid activation of MSF-40 catalyst. The steps of synthesis of acid activated fly ash catalysts are summarized in **Scheme 2.1**.

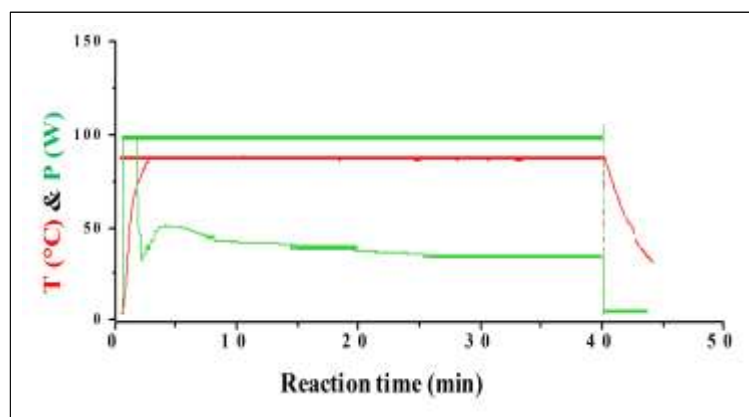
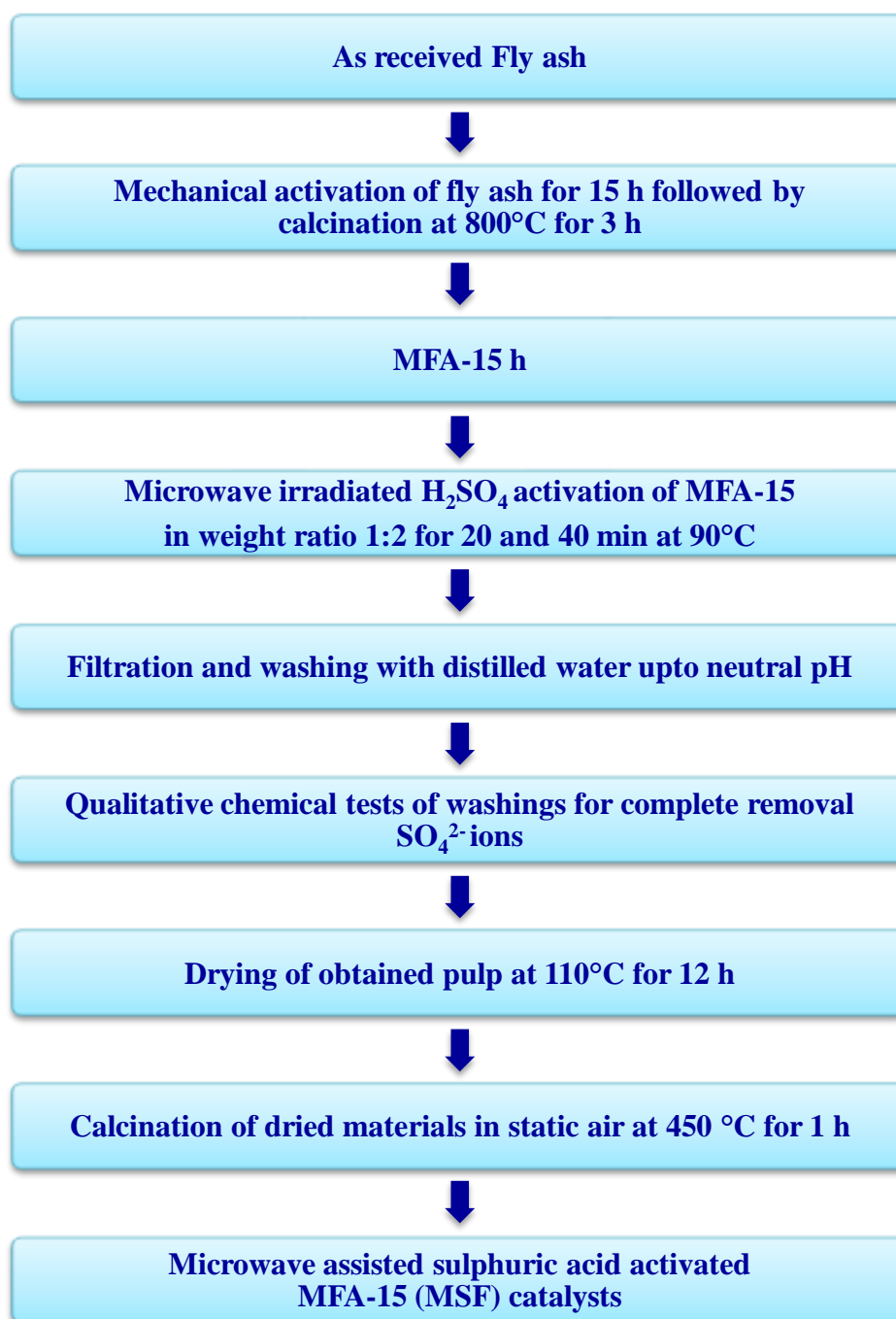


Figure 2.4: Temperature (T) and Power (P) profile of MSF-40 catalyst synthesis



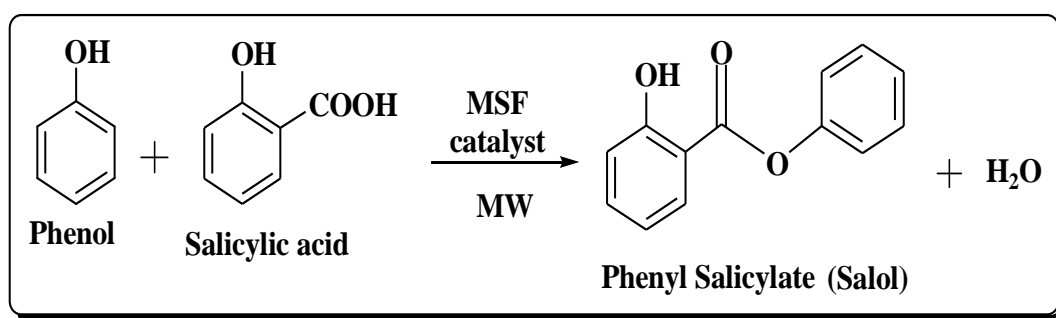
Scheme 2.1: Synthesis of microwave assisted sulphuric acid activated MFA-15 catalysts

2.2.5 Characterization Techniques

The physico-chemical and morphological attributes of FA, MFA-15 and MSF samples were analyzed by XRF, surface area analyzer, Powder XRD, FTIR spectrophotometer, pyridine FTIR, SEM and SEM-EDX as described in Annexure I.

2.2.6 Catalytic activity of MSF catalysts

The microwave assisted solvent-free esterification reaction using salicylic acid and phenol was carried by MSF catalyst as shown in **Scheme 2.2**.



Scheme 2.2: Microwave-assisted solvent-free synthesis of salol by esterification reaction over MSF catalyst

2.2.7 Microwave assisted solvent-free synthesis of salol

The catalytic performance of the prepared MSF catalyst was tested for microwave assisted solvent-free esterification for synthesis of salol. The reaction was performed in closed vessel system of CEM microwave synthesis system. In 10 ml Pyrex glass vial, phenol/salicylic acid with molar ratio of 2:1 and MSF catalyst (salicylic acid/MSF catalyst weight ratio = 5:1) were taken. Prior to the addition in reaction mixture the catalyst was activated at 450°C for 1 h in microwave furnace. Then Pyrex vial containing reaction mixture was placed in microwave cavity and IntelliVent placed was over it. The closed vessel based reaction was initiated at 120 °C; power 80 W with Pmax=ON; pressure (Pr) = 30 psi for 10 min following the same three stages ramping, holding and cooling stages as described earlier. After the reaction, acetone was added in the reaction mixture to dissolve the unreacted salicylic acid and filtered to separate out the

catalyst. The reaction conditions such as temperature, time, μ W power, reactant molar ratio and salicylic acid/MSF catalyst ratio were varied to obtain maximum conversion and product yield. The analysis of salicylic acid conversion and selectivity of the product ‘salol’ was carried out by Gas Chromatograph. The conversion of salicylic acid and yield of salol was calculated by using weight percent method as follows:

$$\text{Conversion (\%)} = \frac{(\text{Initial wt \%} - \text{Final wt \%})}{\text{Initial wt \%}} \times 100$$

$$\text{Yield (\%)} \text{ of salol obtained} = \frac{\text{g of salol obtained}}{\text{g of salol theoretically obtained}} \times 100$$

2.2.8 Catalyst regeneration

After initial run, the used catalyst was filtered, washed thoroughly with acetone and dried in oven at 110°C for 12 h followed by activation at 450°C for 1 h in microwave furnace. Thus, the regenerated catalyst was used in next reaction cycles under the same reaction conditions to analyze the stability of its acid sites.

2.3 Results and Discussion

Chemical composition of FA and MFA-15 was determined by XRF analysis as given in **Table 2.1** which shows small increase in silica content after milling. In case of other metal oxides, marginal decrement in Al_2O_3 and TiO_2 percentage is observed while CaO and Fe_2O_3 percentage showed marginal increment with longer milling time is observed [18].

The elemental composition of MSF catalysts determined by EDS analysis as given in **Table 2.2** shows that MSF-40 catalyst possessed higher amount of Si content as compared to MSF-20 while loss of other components was observed in both samples. This result confirms that acid treatment facilitates increase in Si content by leaching of the other components during acid activation [19].

Table 2.1: Chemical composition of FA and MFA-15

Chemical Components (%)	FA	MFA-15
SiO₂	62	64.27
Al₂O₃	29.7	28.2
Fe₂O₃	2.65	2.67
CaO	0.46	0.48
MgO	0.36	0.24
TiO₂	1.33	1.28
Na₂O	0.14	0.10
K₂O	0.79	0.13
Other elements	2.63	2.62
LOI	2.6	1.85

Table 2.2: Atomic % composition of MSF catalysts

Sample	O	Si	Al	Fe	Ca	K
	(%)	(%)	(%)	(%)	(%)	(%)
MSF-20	73.40	17.28	7.24	0.85	0.42	0.11
MSF-40	74.06	18.14	6.62	0.54	0.16	0.07

Changes in structural and textural properties of FA after mechanical activation for 15 h are summarized in **Table 2.3**. Mechanical treatment by high energy ball milling exerted high stress on FA particles led to breaking of bonds, generation and migration of chemical moieties in bulk thus resulted as increased specific surface area from 9 m²/g (FA) to 17 m²/g (MFA-15) along with marginal increment in silica percentage.

Table 2.3: Characterization of fly ash before and after mechanical as well as mechano-chemical activation

Sample	Specific surface area (m ² /g)	Crystalline size (nm)
FA	9	33
MFA-15	17	23
MSF-20	21	15
MSF-40	22	14

MSF catalysts prepared by acid activation under dielectric heating of microwaves showed manifold increase in surface area as compared to their parent material i.e. MFA-15 as represented in **Table 2.3**. MSF-40 catalyst possessed better surface area of 22 m²/g as compared to MSF-20 (21 m²/g) due to longer activation time. Increment in specific surface area from MFA-15 to MSF-40 was observed due to increased finely dispersed silica components by dissolution of mineral structure. However, further increase in μ W activation time didn't produce any significant results [8].

The structural features of RFA and MFA-15 were characterized by powder X-ray diffraction technique. XRD patterns as represented in **Figure 2.5 (a & b)** revealed characteristic peaks of crystalline phases of mulite ($3\text{Al}_2\text{O}_3 \cdot 2\text{SiO}_2$) at 16.4°, 25.8° and 26.2° while quartz (SiO_2) can be identified with strong peaks at 20.73°, 26.55°, 40.68° and 49.95°. Peaks at 35.56° and 35.62° are designated to iron oxide phases [20]. During high energy milling, high stress exerted on FA sample has caused reduction in crystallite size from 33 to 23 nm and increase in amorphous domains [21]. The intensity of quartz and mulite phases has reduced the most during the mechanical treatment.

Acid activation with 5N H_2SO_4 under dielectric heating for 20 and 40 min has increased amorphous content while crystalline size was reduced to 15 nm (MSF-20) and 14 nm (MSF-40) due to dissolution of some crystalline phases during acid treatment as illustrated in **Table 2.3**. The resemblance in XRD patterns of FA and MSF samples shown in **Figure 2.5 (c & d)** gives an evidence that dielectric heating at low (100 W) μ W power has not altered the basic skeleton of FA. Nevertheless, the surfacial structural changes were noticed due to partial destruction of alumino-silicate components evident by the increased silica content as shown in **Table 2.2**. Similar results were also reported in the literature signifying the effectiveness of μ W heating with low power supply [4,5].

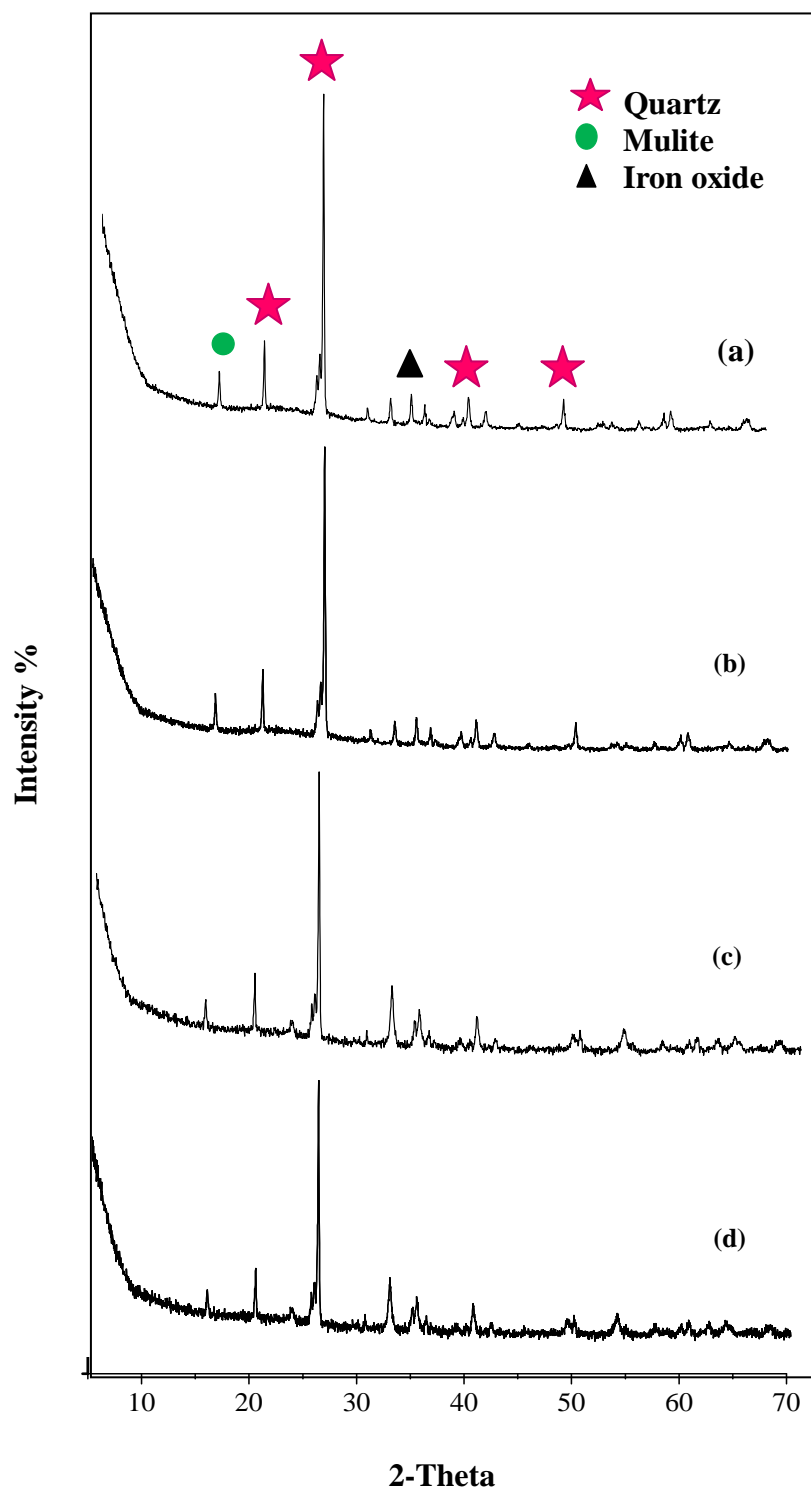


Figure 2.5: Powder XRD patterns of (a) Raw FA (b) MFA-15 (c) MSF-20 (d) MSF-40

The FTIR spectra of RFA and MFA-15 in **Figure 2.6a** shows a broad band with a maximum centered at $3500\text{-}3000\text{ cm}^{-1}$ attributed to surface silanol -OH groups due to physisorbed water. The peak at 1650 cm^{-1} attributed to the bending vibration ($\delta_{\text{O-H}}$) of coordinated water molecule. Mechanical activation for 15 h broke the quartz crystallites as evident by broadness in region of $1000\text{-}1200\text{ cm}^{-1}$ range corresponding to the valence asymmetric stretching vibrations of the silicate oxygen skeleton [22]. The whole exercise resulted as increased amorphous segments and formation of more of Si-OH groups.

FTIR spectra of MSF samples (**Figure 2.6b**) show noticeable increment in broadness at $3500\text{-}3000\text{ cm}^{-1}$ compared to RFA due to increased silanol groups and adsorbed water molecules on the surface. Instead of remaining isolated these surfacial hydroxyl groups shows extensive hydrogen bonding with their neighbouring hydroxyl groups resulting in broadness of band. The increased amorphous silica in milled and acid activated samples can be characterized by an intense band in the range of $1000\text{-}1300\text{ cm}^{-1}$ observed due to asymmetric Si-O-Si stretching which represents a higher shift from 1042 cm^{-1} (MFA-15) towards 1048 cm^{-1} (MSF-20) and 1061 cm^{-1} (MSF-40). The promotion in amorphous silica percentage (**Table 2.3**) in MSF catalysts enhanced surface area and increased population of surface hydroxyl groups are responsible for the improved surface reactivity of the samples.

The pyridine adsorbed FTIR spectra of MSF catalysts are shown in **Figure 2.7a & b**. The IR peaks at 1540 cm^{-1} and 1450 cm^{-1} in MSF catalysts confirms the presence of sufficient Brönsted and Lewis acidity due to formation of coordinated pyridine and hydrogen bonded pyridine respectively with surface -OH groups while band at 1490 cm^{-1} show the pyridine associated with all acidic sites [23]. The pyridine adsorbed spectrum of MSF-40 catalyst shows more intense peak at 1540 cm^{-1} and 1448 cm^{-1} confirming the presence of higher amount of acidic sites as compared to MSF-20. Microwave heating efficiently facilitates the surface acidity of the materials along with its textural and structural properties in less time under controlled heating [7]. A peak appeared at 1598 cm^{-1} in both catalysts corresponding to physisorbed pyridine [24].

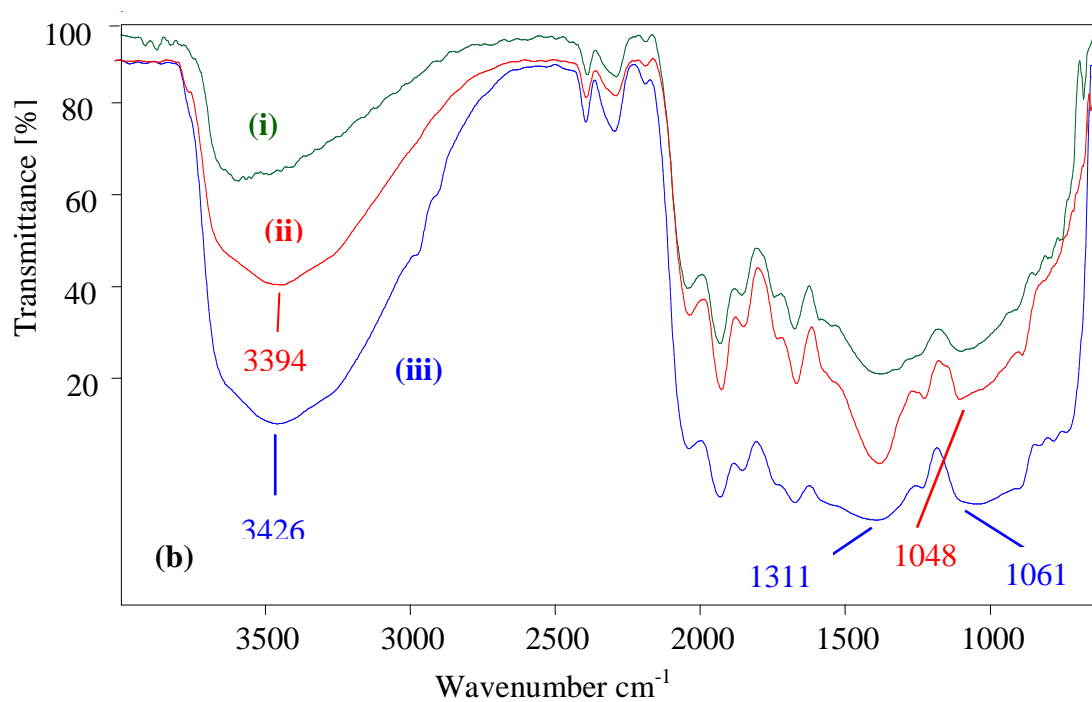
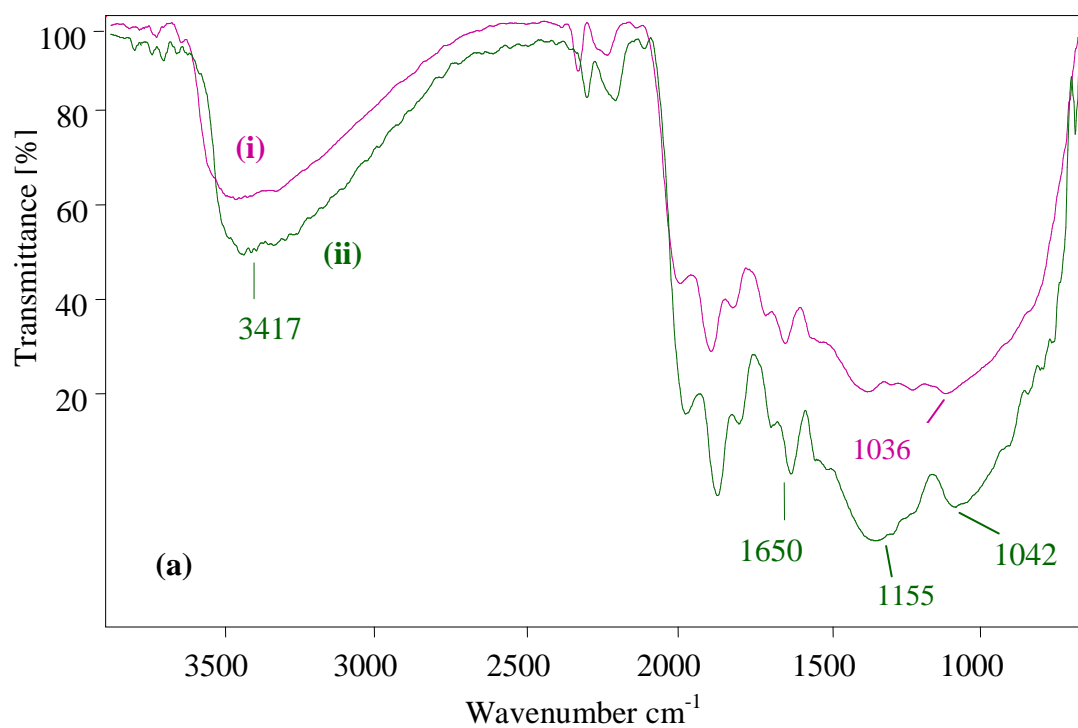


Figure 2.6: (a) FTIR spectra of (i) MFA-15 (ii) MSF-20 (iii) MSF-40

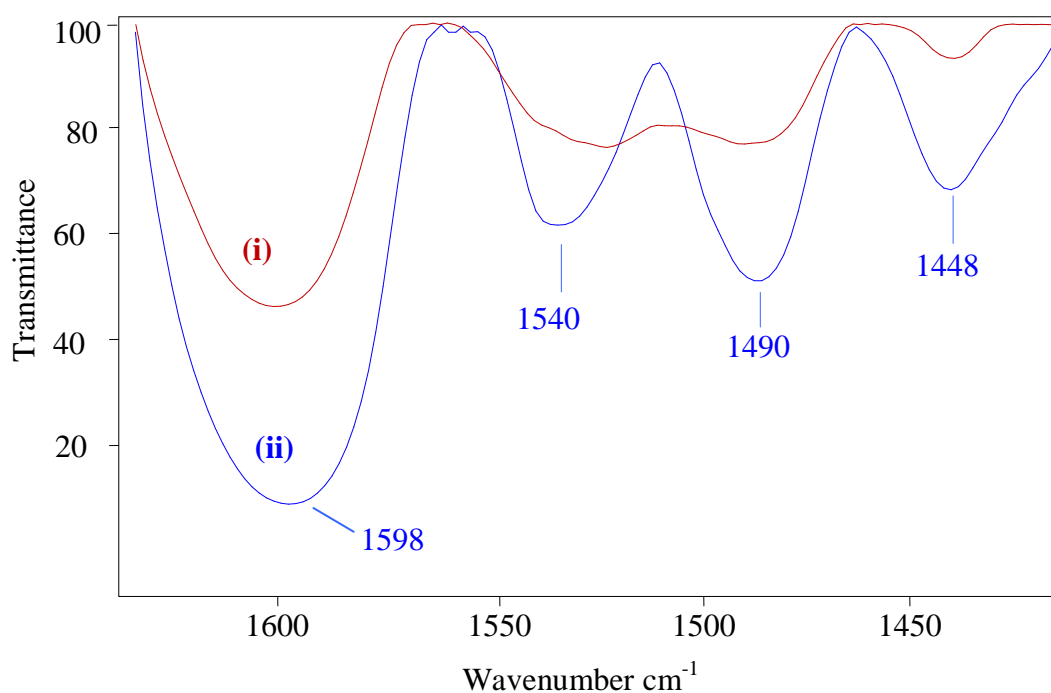


Figure 2.7: (a) Pyridine adsorbed FTIR spectra of (i) MSF-20 (ii) MSF-40

SEM micrographs of RFA in **Figure 2.8a** revealed its heterogeneous nature, comprising particles of different dimensions and shape, relatively smooth surface hollow cenospheres [25], whereas SEM image of MFA-15 (**Figure 2.8b**) shows that particles are broken down into irregular shaped particles with increased surface roughness. SEM images of MSF-40 revealed increased large gelatinous mass due to partial dissolution of alumino-silicate phases during acid treatment as shown in **Figure 2.8c**.

2.4 Comparative study of MSF-40 catalyst with other catalyst prepared under conventional heating

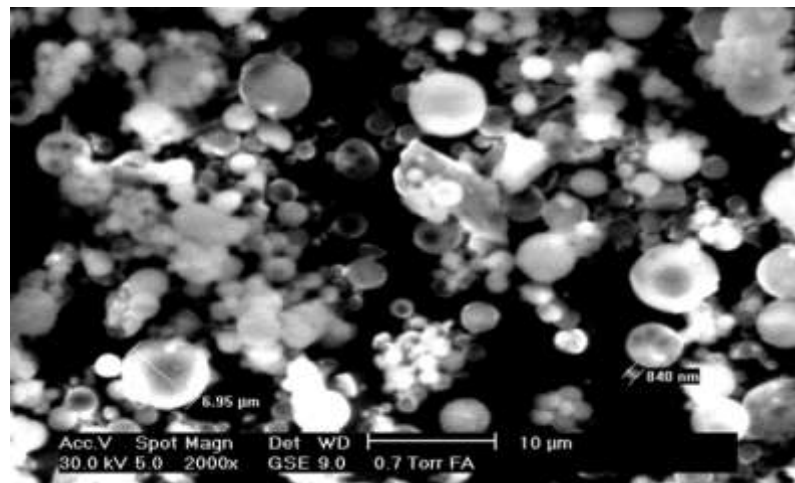
Comparative study of structural and textural attributes of treated fly ash samples prepared under conventional and dielectric heating conditions is given in **Table 2.4**.

Table 2.4: Comparative characterization of MSF-40 and other catalyst

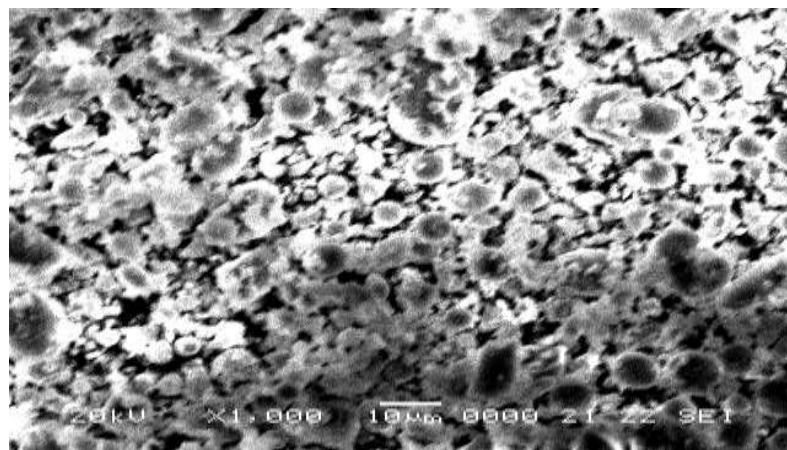
Catalyst	Preparation time	Concentration of H ₂ SO ₄	Surface area (m ² /g)	Crystalline size
MSF-40	40 min	5N	22	14
Other catalyst	5 days	5N	23	13

MSF-40: chemically activated fly ash under microwave heating for 40 min; Other catalyst (SAFA: H₂SO₄ treated fly ash under conventional heating source)

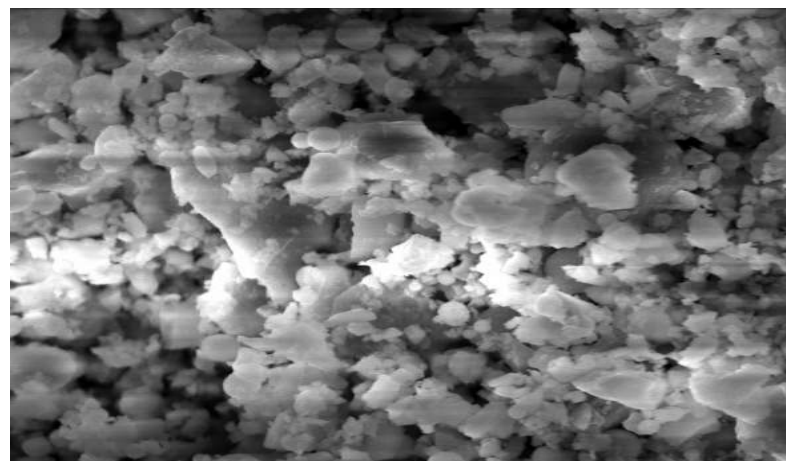
As compared to other catalyst (SAFA) [21] having 5 days refluxing preparation methodology, MSF-40 catalyst has prepared in very short time of 40 min under microwaves heating and has given almost similar results. Hence, these results presents strong evidence that microwave assisted heating can also generate analogous results as non-traditional heating source without disturbing its basic silicate skeleton.



(a)



(b)



(c)

Figure 2.8: SEM micrograph of (a) RFA (b) MFA-15 and (c) MSF-40

2.5 Catalytic activity of MSF catalysts

μ W assisted solvent-free synthesis of salol (phenyl salicylate) using phenol and salicylic acid (SA) was chosen as test reaction to check the catalytic activity of MSF catalysts. The reaction was also preceded uncatalyzed and using MFA-15 as catalyst conditions. The conversion of salicylic acid was poor in uncatalyzed condition (**Table 2.5**). Amongst all, MSF-40 catalyst gave the highest conversion (88%) of SA with 88% conversion and 90% yield of salol within 10 min due presence of sufficient amount of Brönsted acidic sites. On other hand, MSF-20 with 78% conversion and 82% yield of salol due having lesser population of acidic sites compared to MSF-40 catalyst. Hence, optimization of the esterification reaction parameters under microwave heating was carried out using MSF-40 catalyst to obtain maximum selectivity and yield of salol followed by its reusability evaluation.

Table 2.5: Catalytic activity of MFA-15, MSF catalysts and catalyst-free condition for esterification reaction under microwave irradiation

Catalyst	Conversion% SA	of Yield% of salol
-	Nil	Nil
MFA-15	25	16
MSF-20	78	82
MSF-40	88	90
SAFA	74	79

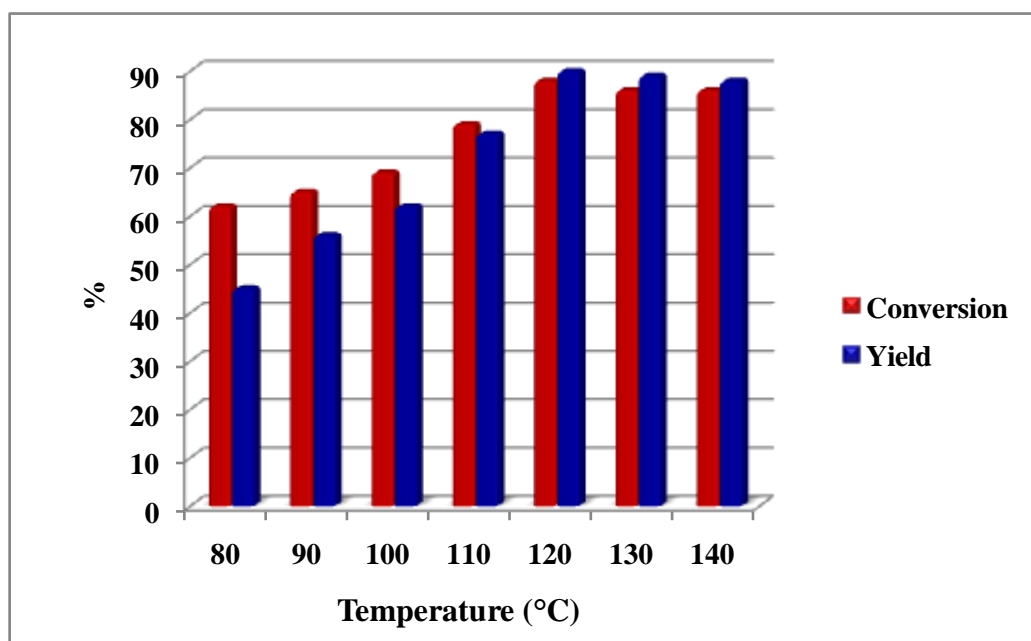
Reaction conditions under microwave irradiation: Temperature = 120°C; Time = 10 min; molar ratio (SA: Phenol) = 1:2; SA to MSF-40 catalyst ratio = 5:1, P = 80W; P_{max} = ON; Pr = 30 psi

Microwave assisted esterification reaction for salol synthesis was taken as test reaction to evaluate the catalytic performance of activated fly ash prepared under microwave (MSF-40) as well as conventional heating (SAFA) as shown in

Table 2.5 [22]. MSF-40 catalyst with more amounts of active catalytic sites gave better yield as compared to SAFA. These results confirms that microwave assisted acid activation facilitates homogeneous volumetric heating of the materials which results as better performance during course of the reaction to produce maximum yield with least amounts of by-products.

2.5.1 Effect of reaction temperature

Optimization of reaction temperature was carried out under temperature range from 70°C to 140°C to achieve maximum conversion% and yield% of phenyl salicylate. As illustrated in **Figure 2.9**, conversion % of SA and yield of salol has showed an increasing trend with rise in reaction temperature. Maximum conversion of SA 88% was obtained at 120°C with 98% selectivity and 90% yield of salol within 10 min by in-core volumetric heating of microwaves. The conversion of SA, selectivity and yield salol remained almost constant upto 140°C.

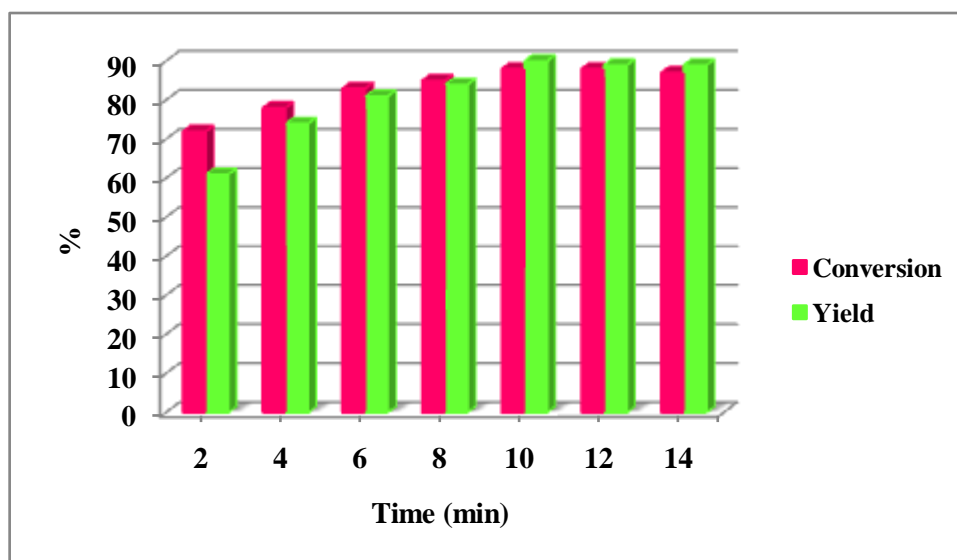


Reaction conditions: Temperature = 120°C; Time = 10 min; molar ratio (SA: Phenol) = 1:2; SA to MSF-40 catalyst ratio=5:1, P =80W; P_{max}= ON; Pr = 30 psi

Figure 2.9: Variation of conversion (%) of SA and yield (%) of salol over MSF-40 catalyst with temperature

2.5.2 Effect of reaction time

The effect of reaction time period on conversion of SA and yield of salol with maintaining rest of the reaction parameters same is represented in **Figure 2.10**. The conversion and yield parameters showed proportional relationship with increase in reaction time. The maximum conversion of SA was 88% with 90% yield within 10 min of reaction time was achieved and remained almost constant upto 14 min.

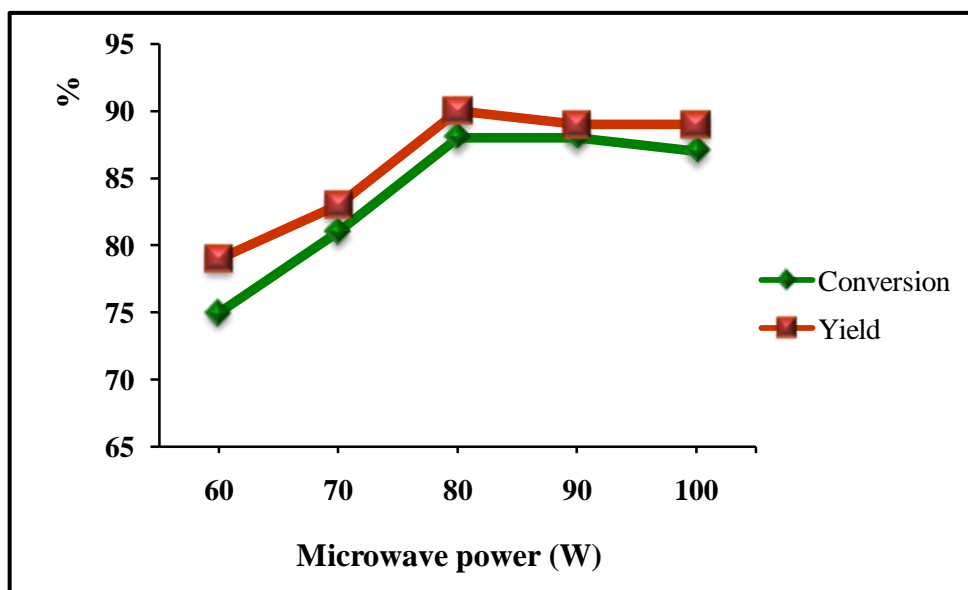


Reaction conditions: Temperature = 120°C; Time = 10 min; molar ratio (SA: Phenol) = 1:2; SA to MSF-40 catalyst ratio=5:1, P =80W; P_{max}= ON; Pr = 30 psi

Figure 2.10: Variation of conversion (%) of SA and yield (%) of salol over MSF-40 catalyst with time

2.5.3 Effect of microwave power

The influence of microwave power on the conversion% of SA and salol yield% was examined at different microwave power ranging from 60 to 100 W as illustrated in **Figure 2.11**. Maximum 88% conversion and 90% yield was obtained at 80W, after which the conversion & yield parameter remained constant till 100W. On further increasing power output conversion and yield parameters remained constant.



Reaction conditions: Temperature = 120°C; Time = 10 min; molar ratio (SA: Phenol) = 1:2; SA to MSF-40 catalyst ratio=5:1; Pr = 30 psi

Figure 2.11: Effect of microwave power on SA conversion% and yield% of salol

2.5.4 Effect of reactant molar ratio

The influence of molar ratio of SA and phenol on conversion and yield of salol was monitored at different molar ratios from 1:1 to 1:3 by increasing the amount of phenol only. However, using higher concentration studies with salicylic acid could not be conducted due to solubility restrictions [15]. As shown in **Table 2.6**, on increasing molar ratio of SA to phenol from 1:1 to 1:2, maximum conversion of SA (88%) and 90% yield of salol was obtained. The above results show that the yield of product increased with increasing the molar ratio of SA to phenol. This is mainly due to the reversible nature of the esterification reaction. With increase in molar ratio SA to phenol leads to a shift of equilibrium to the direction of salol ester production. However, further increasing molar ratio to 1:3, decrease in yield % of the salol was observed due to formation of diphenyl ether (by-product) formation at higher phenol content [12].

Table 2.6: Effect of molar ratio of SA/phenol on conversion (%) and yield (%) of salol over MSF-40 catalyst

Molar ratio (SA : phenol)	Conversion (%)	Yield (%)
1:1	35	42
1:1.5	64	72
1:2	88	90
1:3	79	82

Reaction conditions: Temperature = 120°C; Time = 10 min; SA/MSF-40 catalyst weight ratio=5:1; Power = 80W; P_{\max} = ON; Pr = 30 psi

2.5.5 Effect of SA to MSF-40 weight ratio

The effect of SA to MSF-40 weight ratio on conversion and yield was monitored by varying the amount of catalyst under optimized reaction conditions as shown in **Table 2.7**. Weight ratio of 5:1 gave maximum conversion of 88 % of SA and 90% yield of salol due to availability of sufficient amount of active catalytic sites. On further increase in the amount of catalyst no further change in conversion % was observed.

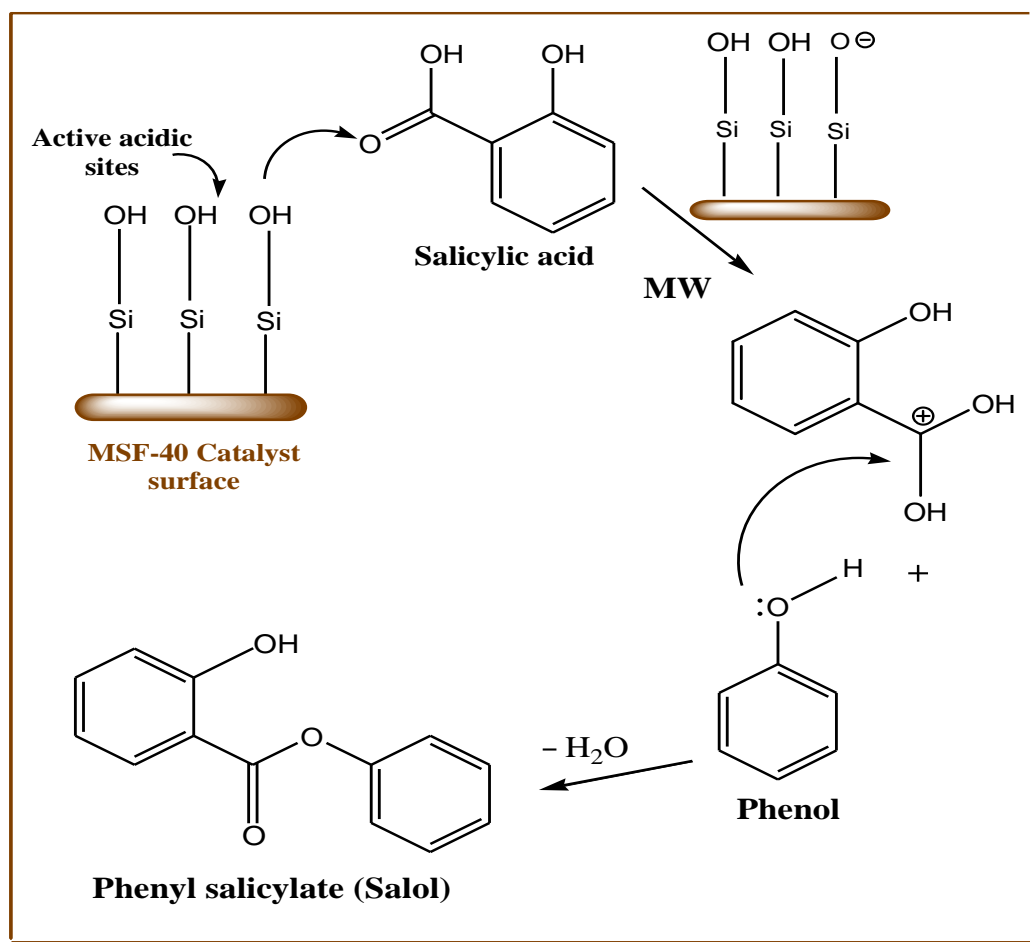
Table 2.7: Effect of SA to MSF-40 weight ratio on conversion (%) and yield (%) of SA to salol with MSF-40 catalyst

SA to MSF-40 weight ratio	Conversion (%)	Yield (%)
10:1	74	76
5:1	88	90
2:1	88	90

Reaction conditions: Temperature = 120°C; Time = 10 min; molar ratio (SA: Phenol) = 1:2; Power = 80W; P_{\max} = ON; Pr = 30 psi

2.6 Proposed mechanistic pathway of salol formation over acidic sites of MSF-40 catalyst

In proposed mechanism of salol synthesis, the salicylic acid gets adsorbed on acidic sites of MSF-40 catalyst and transforms into an electrophile by borrowing a proton from its surface hydroxyl groups. When phenol (dipolar species) interacts with the electric field component of microwave it starts oscillating and collide with neighbouring charged particles i.e. carbonium ion, results as intermolecular friction. This friction generates intense internal heat responsible for the formation of intermediate species which further leads to formation of salol with subsequent removal of water as a by-product as shown in Scheme 2.3.



Scheme 2.3: Proposed mechanistic pathway of microwave-assisted esterification of salicylic acid with phenol over MSF-40 catalyst

2.7 Regeneration and reusability of MSF-40 catalyst

The spent MSF-40 catalyst was washed, filtered and regenerated by simple microwave regeneration method by microwave calcining at 450°C for 1 h. Compared to the conversion and yield obtained in fresh run, the regenerated MSF-40 efficiently catalyzed esterification reaction upto four reaction cycles with SA conversion 88-84% and 86-81% yield of salol as shown in **Figure 2.12**, indicates that acidic sites are not lixiviated during regeneration. FTIR spectrum of fresh MSF-40 and regenerated catalyst after fourth reaction cycle (**Figure 2.13a**) shows resemblance in structural features and also signifies the stability of acidic sites during the reaction and even after regeneration. The pyridine FTIR spectrum of regenerated catalyst after fourth reaction run (**Figure 2.13b**) further confirms the sustainability of acidic sites developed through non-traditional acid activation method. The significant decrease in conversion was observed after fourth reaction cycle due to blockage of active sites of the catalyst by the deposition of carbonaceous material [26].

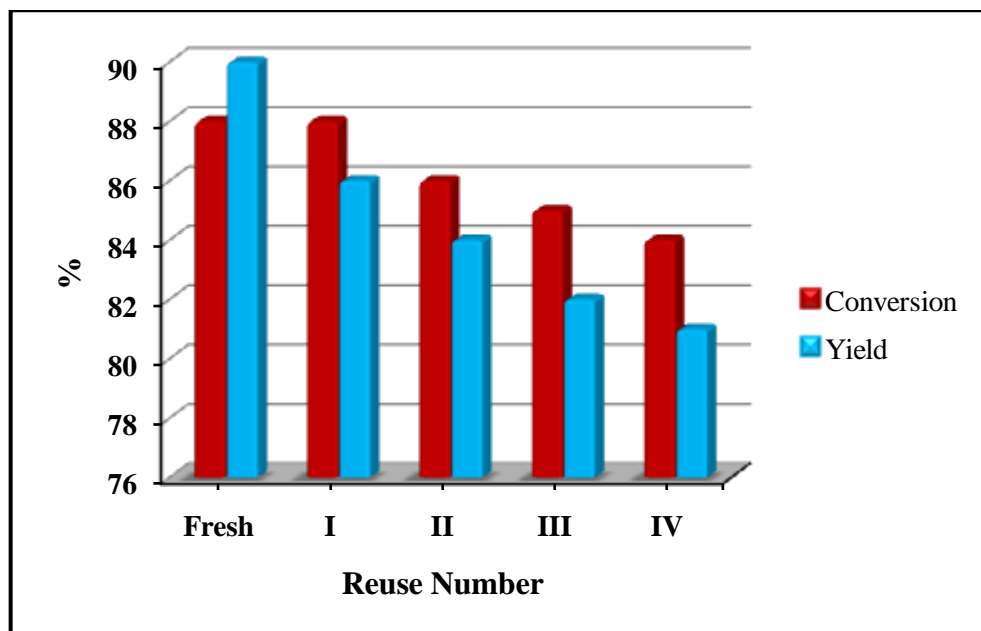


Figure 2.12: The reusability of MSF-40 catalyst for microwave assisted esterification reactions

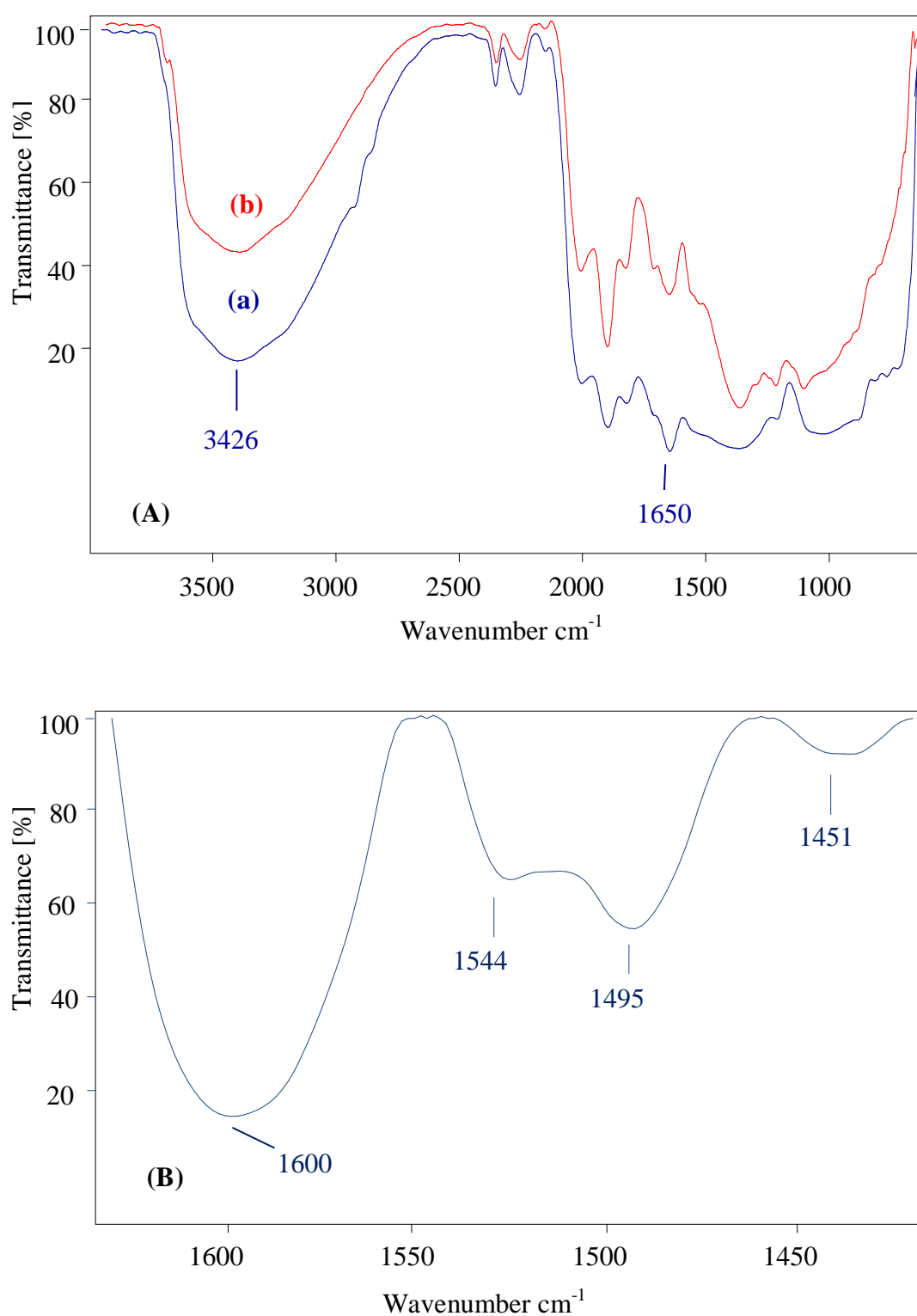


Figure 2.13: FTIR spectra of (A) (a) Fresh MSF-40 (b) regenerated MSF-40 catalyst and (B) pyridine FTIR of regenerated MSF-40 catalyst

2.8 Product identification

m.p. 41- 43 °C; **FTIR:** 3190 cm⁻¹, 1670 cm⁻¹, 1745 cm⁻¹, 1500 cm⁻¹, 1460 cm⁻¹, 1210 cm⁻¹

2.9 Conclusion

The present research work provides an energy efficient microwave methodology over traditional thermal refluxing for acid activation of FA under less processing time. Mechanical activation of FA increased surface area by breaking down larger particles while acid treatment under microwave heating further increased surface area, silica content and surface hydroxyl groups resulted as increased surface activity without alternating the basic skeleton of FA to any noticeable extent. Prepared MSF-40 catalyst gave 88% conversion of salicylic acid and 90% yield for solvent-free esterification reaction under dielectric heating. This investigation concludes that microwave in-core heating is a clean, fast and innovative source for improving the surfacial properties of FA and provides cost effective pathway for organic transformations with high conversion and better yield.

2.10 References

- [1] I. Bilecka, M. Niederberger, *Nanoscale* 2 (2010) 1358-1374.
- [2] K. Wilson, J.H. Clark, *Pure Appl. Chem.* 72 (2000) 1313-1319.
- [3] A. Dastan, A. Kulkarni, B. Török, *Green Chem.* 14 (2012) 17-37.
- [4] S. Korichi, A. Elias, A. Mefti, *Appl. Clay Sci.* 42 (2009) 432-438.
- [5] S. Korichi, A. Elias, A. Mefti, A. Bensmaili, *Appl. Clay Sci.* 59-60 (2012) 76-83.
- [6] E.L. Foletto, D.S. Paz, A. Gündel, *Appl. Clay Sci.* 83-84 (2013) 63-67.
- [7] A.N. Oliveira, L.R. Silva Costa, L.H. Oliveira Pires, L.A.S. Nascimento, R.S. Angélica, E.F. Costa Carlos, J.R. Zamian, G.N. Rocha Filho, *Fuel* 2013,103, 626-631.
- [8] S.R. Ljiljana, P.S. Petrović, M. Z. Vuković, B.T. Novaković, D.R. Stanisavljev, *Hem. Ind.* 65 (2011) 489–495.

-
- [9] S.Y. Chou, S.L. Lo, C.H. Hsieh, C.L. Chen, *J. Hazard. Mater.* 163 (2009) 357-362.
 - [10] X. Querol, A. Alastuey, A. López-Soler, F. Plana, J.M. Andrés, R. Juan, P. Ferrer, C.R. Ruiz, *Environ. Sci. Technol.* 31(1997) 2527-2533.
 - [11] T. Chaowasakoo, N. Sombatsompop, *Compos. Sci. Technol.* 67 (2007) 2282-2291.
 - [12] S.S.Z. Mohamed, N. Nagaraju, *J. Chem. Sci.* 122 (2010) 193-201.
 - [13] C.D. Hoyo, M.A. Vicente, V. Rives, *Clay Miner.* 33 (1998) 467-474.
 - [14] S.Z. Mohamed Shamshuddin, N. Nagaraju, *Catal. Commun.* 7 (2006) 593-599.
 - [15] G. Kuriakose, N. Nagaraju, *J. Mol. Catal. A: Chem.* 223 (2004) 155-159.
 - [16] S. Anita, A. Rani, *J. Nanosci. Tech.* 1 (2015) 4-8.
 - [17] B. M. Reddy, M.K. Patil, G.K. Reddy, B.T. Reddy, K.N. Rao *Appl. Catal. A: Gen.* 332 (2007) 183-191.
 - [18] J. Rao, P. Narayanaswami, S. Prasad, *Int. J. Eng. Sci. Technol.* 2 (2010) 284-299.
 - [19] F. Blanco, M.P. Garcia, J. Ayala *Fuel* 84 (2005) 89-96.
 - [20] S. Katara, S. Kabra, A. Sharma, R. Hada, A. Rani, *Inter. Res. J. Pure Appl. Chem.* 3 (2013) 299-307.
 - [21] A. Sharma, K. Srivastava, V. Devra, A. Rani, *Am. Chem. Sci. J.* 2012 (2) 177-187.
 - [22] G.A. Patil, S. Anandhan, *Inter. J. Energy Eng.* 2 (2012) 57-62.
 - [23] Y. Du, X. Du, M.S. George, *J. Phys. Chem. C* 111 (2007) 219-226.
 - [24] E.P. Parry, *J. Catal.* 2 (1963) 371-379.
 - [25] D. Jain, C. Khatri, A. Rani, *Fuel Process. Technol.* 91 (2010) 1015-1021.
 - [26] C. Khatri, A. Rani, *Fuel* 87 (2007) 2886-2892.



Chapter-3

*Fly ash supported Sulfated Tin as a
Green and Highly Efficient Solid Acid
Catalyst for Solvent-Free, One Pot
Synthesis of 14-aryl-14H-dibenzo[a,j]
xanthenes under Microwave
assisted conditions*

ABSTRACT

The present work describes the synthesis of fly ash supported sulfated tin catalyst for the synthesis of 14-aryl-14*H*-dibenzo[*a,j*]xanthenes via condensation reaction under microwave irradiation. STF catalysts with varying metal content (6, 10 and 16 wt.%) were synthesized by two step methodology which included chemical precipitation followed by 1N sulphuric acid impregnation. Prepared samples were characterized by N₂ adsorption-desorption, XRD, FTIR, UV-Vis DR and SEM-EDX techniques. Tetragonal phases of SnO₂, important for catalytic activity of the STF catalysts were confirmed by XRD patterns while the active sulfur groups were corroborated by the bands of S=O and S-O bonds appeared in FTIR spectra. With increase in tin content from 6 to 16 wt.%, Brönsted and Lewis acidic sites in prepared samples were also increased. Inductive effect of S=O bond on loaded Sn⁴⁺ species strengthened the Lewis acidity whereas adsorption of water molecules on these groups induced strong Brönsted acidity in STF catalysts. Catalytic performance of STF catalysts was evaluated by microwave assisted synthesis of 14-aryl-14*H*-dibenzo[*a,j*]xanthenes via condensation reaction. Synthesis of dibenzoxanthenes under in-core volumetric heating of microwaves has increased yield% in short reaction time. Thus, the activity and simple recyclability without losing catalytic activity has made STF catalyst a good alternative to literature methods.

3.1 Introduction

New environmental legislation and attention towards 'green and clean' technology have led to the development of environmentally benign catalysts. This involves the use of solid catalysts which are emerged as potential alternative to homogeneous liquid acids due to non-hazardous nature, enhanced selectivity, requirement in catalytic amounts, easy separation without any problem of waste disposal and easier post reaction work-up procedure [1]. In 1979, Hino and Arata first synthesized $\text{SO}_4^{2-}/\text{M}_x\text{O}_y$ type solid acid catalysts which possessed remarkable catalytic performances for organic reactions [2]. These catalysts have received much attention due to their advantageous attributes like high acid strength, stable in moisture, air and thermal conditions, less corrosive to reactors and containers and possessed remarkable catalytic performances over their homogeneous counterparts. Amongst sulfated metal oxides family, sulfated zirconia has been widely studied and possessed stronger acidity than $\text{SO}_4^{2-}/\text{Fe}_2\text{O}_3$, $\text{SO}_4^{2-}/\text{TiO}_2$, $\text{SO}_4^{2-}/\text{SiO}_2$ and $\text{SO}_4^{2-}/\text{HfO}_2$ [3]. Recently, it has been proved that sulfated tin oxide has higher acid strength and catalytic activity than that of sulfated ZrO_2 [4,5,6]. Thus, sulfated tin oxide (STO) ($\text{SO}_4^{2-}/\text{SnO}_2$) has become an interesting alternative to commercially available heterogeneous catalysts. STO catalyst has already been used for dehydration of xylose [7], acylation reaction [8], biodiesel production [9] and synthesis of pyrimidopyrimidines [10] and liquid phase selective dehydration of sorbitol to isosorbide [11] etc. Nevertheless, studies concerning the $\text{SO}_4^{2-}/\text{SnO}_2$ study are relatively limited due to difficulty in its preparation methodology. As the synthesized silica supported and pure SnO_2 remain as fine particles so to avoid the loss through filtration, ammonium acetate treatment is suggested to overcome the loss [12]. The acetate form is comparatively bigger in size than hydroxide form which can be separated easily through filtration. Tin oxide has been extensively used as solid acid or redox catalyst but low thermal stability and tendency to aggregate into large crystals at working temperature (approx. 400°C) limit its applications in field of catalysis [13]. Incorporation of tin on silica support provides better dispersion of tin species, high activity and resistance to deactivation [14]. While deposited active sulfate species bound to the surface of

metal oxide generates strong Lewis acidity by their inductive effect and also nurtures their Brönsted acidic sites by adsorbed water molecules [15]. Hence, for the development of solid acid catalyst with strong acidic strength, addition of sulfation becomes an imperative condition.

The synthesis of xanthene derivatives has received special attention due to their wide area of therapeutic and biological properties such as antibacterial, anti-cancer, anti-viral and activity. Along with these they are also used as photo-sensitizers in photodynamic therapy for the treatment of localized tumors, pH-sensitive fluorescent materials for visualization of bio-molecular scaffolds and as fluorescent dyes [16]. The many synthesis methods have been reported by numerous approaches including trapping of benzyne by phenol [17], reaction of 2-naphthol with formamide [18], cyclodehydrations [19] etc. However, use of excess reagents, prolonged reaction times, low yields, use of toxic solvents and harsh reaction conditions demands to find new alternative routes. Use of solid acid catalyst such as p-toluene sulfonic acid [20], silica sulfuric acid [21], amberlyst-15 [22] and Yb(OTf)₃ [23] etc. has been introduced for xanthenes synthesis via one pot condensation of β-naphthol and aryl aldehydes. These reported methods have improved the synthesis performance still some drawbacks viz. requirement of large amount of expensive reagents and catalysts, longer reaction times and tedious post work-ups, need of special apparatus etc are still remains area of research. Therefore, it is required to develop new eco-friendly synthesis pathway to mitigate these limitations along with improving product yield.

Recently, fly ash supported SO₄²⁻/SnO₂ catalyst has been developed by hydrothermal method for the synthesis of serendipity product via oxidation process [24]. In the present endeavor, fly ash (class-F type) was mechanically activated by milling for 15 h and used as catalytic support for the synthesis of fly ash supported sulfated tin catalyst. Structural changes in mechanically activated fly ash (MFA-15) after ball milling and loading of tin species on milled MFA-15 were investigated by XRD and FTIR. While textural properties were described by N₂ adsorption-desorption. Pyridine adsorbed FTIR spectra confirmed the presence of both type of acidic sites on all loaded samples and were conserved even on high

calcination temperature. Using similar methodology tin was also loaded on mechanically activated fly ash under microwave assisted conditions. But the prepared catalyst gave HgCl_2 test (test for determination of Sn^{4+} species) due less binding of tin moieties with active surface sites of fly ash. Although, presently many research papers has been published related to microwave assisted loading of metal oxides on different inorganic supports with efficient catalytic performances [25] but synthesis of fly ash supported metal oxide under this non-conventional heating was not feasible. Whereas, synthesized STF catalysts under conventional heating didn't give HgCl_2 test due to strong binding of tin moieties with fly ash surface. The catalytic performance of STF catalysts were evaluated under microwave assisted one pot, solvent-free synthesis of 14-aryl-14*H*-dibenzo[*a,j*]xanthenes under optimized conditions. Using activated fly ash as catalytic supports makes the whole process more economical and encourages the use of this anthropogenic solid waste in tin based catalysts also.

3.2 Experimental details

3.2.1 Materials and reagents

Fly ash (class-F) was collected from Tata Thermal Power Plant, Jamshedpur, India. Stannic chloride pentahydrate ($\text{SnCl}_4 \cdot 5\text{H}_2\text{O}$), ammonium acetate and ammonium hydroxide were purchased from Loba Chemie. 2-naphthol and benzaldehyde were supplied from S.D. fine chemicals, India.

3.2.2 Catalyst synthesis

The STF catalyst was synthesized in two steps using precipitation method followed by addition of sulfate groups through aqueous impregnation of 1N H_2SO_4 adopting procedure described as follows:

Fly ash was milled in high energy planetary ball mill (Retsch PM-100, Germany) in an agate jar using agate balls with ball to powder ratio (BPR) of 10:1 for 15 h at 250 RPM rotation speed. Mechanically activated fly ash (MFA-15) possessing $17 \text{ m}^2/\text{g}$ surface area was chosen as catalytic support material and calcined at 800°C for 3 h to remove carbon, sulphur and other impurities.

(i) Loading of tin on MFA-15 using precipitation method

The required amounts (1.06 g for 6 wt%, 1.771 g for 10 wt% and 2.834 g for 16 wt%) of stannic chloride pentahydrate were dissolved in double distilled water. The prepared solution was drop wise added into 6 g of MFA-15 in 100 ml beaker under constant stirring. Ammonium hydroxide (28%) was gradually added dropwise into the solution under stirring until final pH=8 was reached. The precipitated solution was kept on stirring for 24 h at 250 RPM and then filtered and washed thoroughly with 4% $\text{CH}_3\text{COONH}_4$ solution until all chloride ions were eliminated (silver nitrate test). The washed slurry was left in oven at 80°C for 24 h drying and calcined at 600°C for 3 h in muffle furnace. The resultant samples were designated as tin loaded MFA-15 (TF-15) and used further for sulfation.

(ii) Aqueous impregnation of TF samples by H_2SO_4 solution

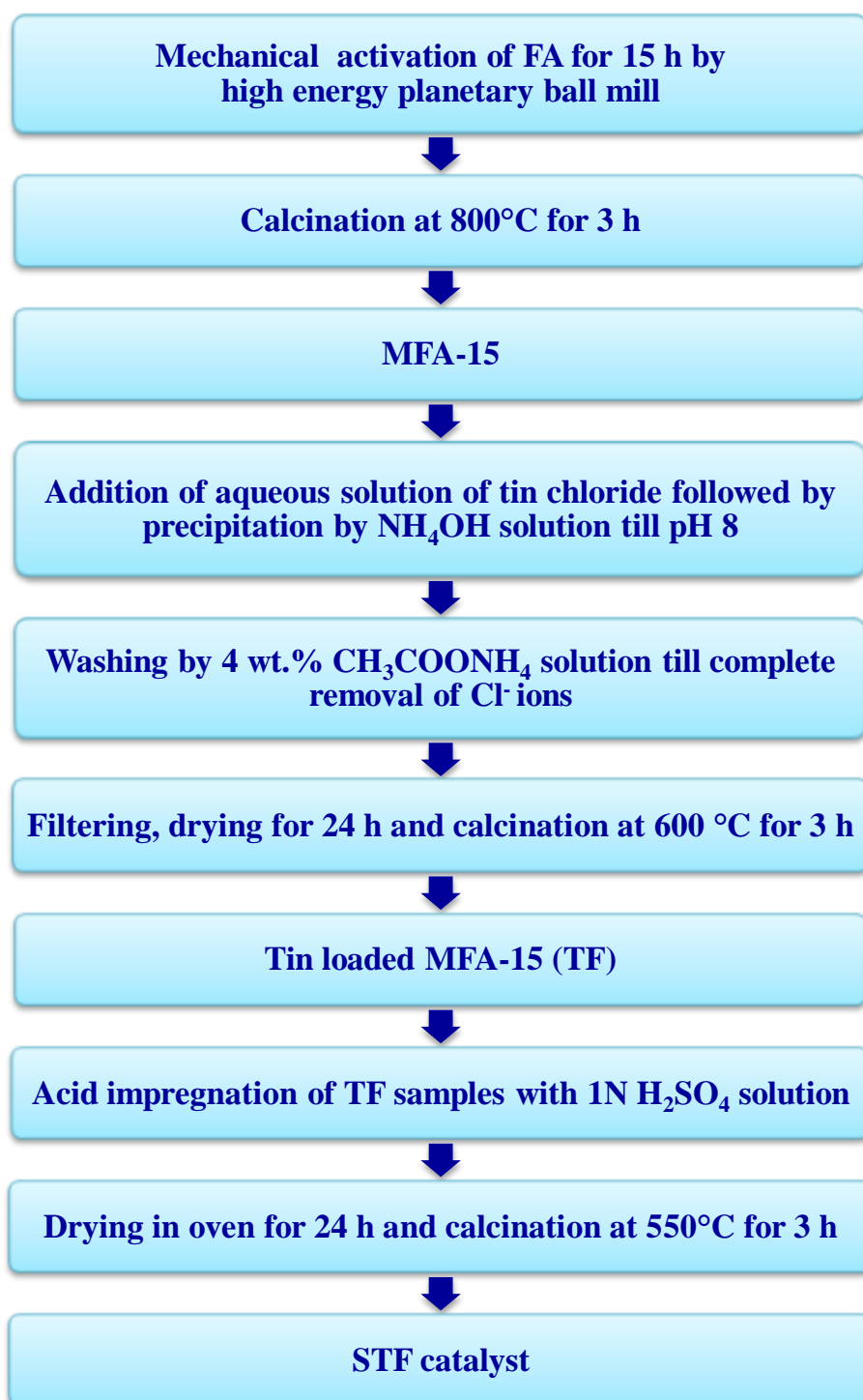
Fly ash supported sulfated tin samples were prepared by acid impregnation of prepared TF samples with appropriate amount of 1N H_2SO_4 solution (1g of TF powder per 15 ml of 1N H_2SO_4 solution) and kept under stirring at 280 RPM for 12 h. The obtained slurry was dried at 110°C for 24 h and calcined at 550°C for 3 h. The resultant samples were designated in the text as STF-6, STF-10 and STF-16 according to the wt% of the metal. The steps involved in the synthesis of fly ash supported sulfated tin are summarized in **Scheme 3.1**.

3.2.3 Catalyst characterization

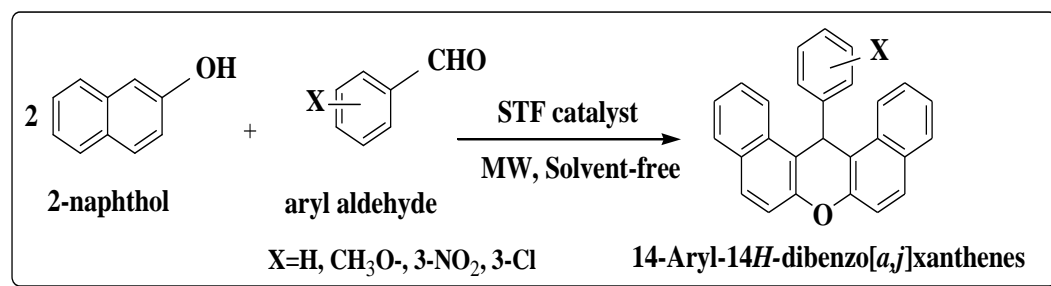
Physico-chemical, morphological, surfacial and textural properties of the synthesized STF catalysts were analyzed various techniques such as N_2 adsorption-desorption, X-ray diffraction, FTIR, pyridine FTIR, DR UV-Vis and SEM-EDS as illustrated in **Annexure I**.

3.2.4 Catalytic performance of STF catalysts

Evaluation of the catalytic activity of the prepared STF catalysts were performed by microwave assisted xanthenes synthesis as shown in **Scheme 3.2**.



Scheme 3.1: Synthesis of fly ash supported sulfated tin (STF) catalyst



Scheme 3.2: One pot solvent-free synthesis of 14-Aryl-14H-dibenzo[a,j] xanthene under microwave heating over STF catalysts

20 mmol of 2-naphthol and 10 mmol of benzaldehyde (benzaldehyde/STF catalyst weight ratio=5:1) were filled in 10 ml pyrex glass vial. 0.2 gm of STF-16 catalyst was added into the reaction mixture and before adding into reaction mixture, prepared STF catalyst was activated for 1 h at 400°C in muffle furnace. The reaction was carried out at 120°C, 60 psi pressure, 100W power with P_{\max} feature and medium stirring mode for 12 min in closed vessel system of CEM (model Discover) microwave synthesis system following all stages of ramping, holding and cooling as described in **Chapter 2**. After the completion of the reaction, the catalyst was filtered out and unreacted aldehyde was separated from product by washing with chloroform. To achieve maximum selectivity and yield of the 14-phenyl-14H-dibenzo[a,j] xanthene, reaction parameters viz. time, temperature, reactant molar ratio, catalyst to substrate ratio, power were optimized. The analysis of benzaldehyde conversion was carried out by Gas chromatograph. The conversion of benzaldehyde and yield of 14-phenyl-14H-dibenzo[a,j]xanthenes was calculated by using weight percent method as follows:

$$\text{Conversion (\%)} = \frac{(\text{Initial wt \%} - \text{Final wt \%})}{\text{Initial wt \%}}$$

$$\text{Yield (\%)} \text{ of salol obtained} = \frac{\text{g of xanthene obtained}}{\text{g of xanthene theoretically obtained}} \times 100$$

3.2.5 Catalyst regeneration

After extracted from fresh run, the obtained catalyst was washed thoroughly with acetone and dried in oven at 110°C for 12 h followed by activation at 400°C for 1 h in muffle furnace. Thus, the regenerated catalyst was ready to use for next reaction cycle under the same reaction conditions.

3.3 Results and discussion

The physico-chemical properties of MFA-15 and prepared STF catalysts are given in **Table 3.1**. Increase in tin and sulphur content from 6 to 16 wt.% blocked the small pores of the MFA-15 which led to progressive decrease in BET surface area with increase in Sn and S content.

Table 3.1 Physico-chemical properties of MFA-15 and STF catalysts

Sample	Sn content (wt.%)	S content (wt.%)	BET surface area (m ² /g)
MFA-15	0.0	0.07	17
STF-6	4.6	2.3	14
STF-10	8.1	3.6	12
STF-16	13.4	5.9	9

The X-ray diffractogram of MFA-15 shows crystalline phases of quartz, mulite, hematite and small amount of magnetite along with some amorphous content obtained due to breakage of large particles as indicated in **Figure 3.1 (a)**. After Sn loading, the sustainability of structural properties of fly ash as shown in **Figure 3.1 (b-d)** reveals the framework stability during catalyst preparation. The X-ray diffraction patterns of STF-6, STF-10 and STF-16 catalysts show a intense peak at $2\theta = 15^\circ$ corresponding to tin silicate (SnSiO_3) [26] component indicating towards incorporation of tin oxide species in the silica network of MFA-15. XRD patterns of all samples displayed characteristic peaks of SnO_2 tetragonal phase (ICDD, PDF file no. 41-1445) with cassiterite rutile structure at $2\theta = 26.6, 33.82$ and 51.8 [27] which is very important for the development of strong acidic sites in sulfated tin oxides [28]. XRD peaks at 25.2° and 42.82° corresponding to metastable orthorhombic phase of SnO_2 (JCPDS No. 29-1484) were also observed in all catalysts [29]. Metastable phase formed during transformation of distorted tetragonal phases into stable rutile tin oxide phase [30].

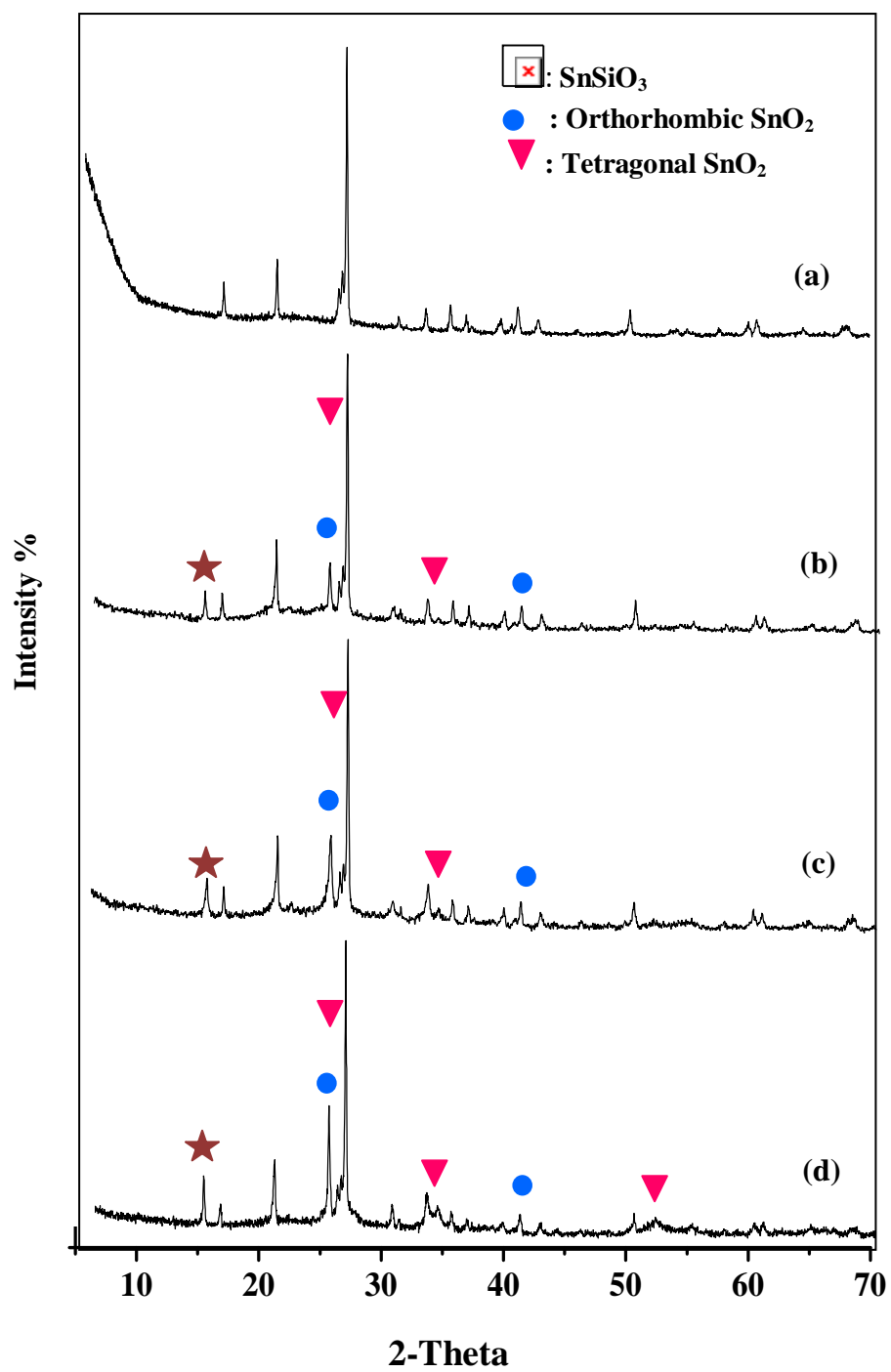


Figure 3.1: XRD patterns of (a) MFA-15 (b) STF-6 (c) STF-10 and (d) STF-16

The FTIR spectra of MFA-15, TF-16, STF-16 are shown in **Figure 3.2**. In the FTIR spectrum of MFA-15, appearance of a broad band between 3500-3000 cm^{-1} attributed to stretching vibrations of surface -OH groups of Si-OH and adsorbed water molecules on the surface while peak at 1650 cm^{-1} is assigned to bending mode ($\delta_{\text{O-H}}$) of water molecules. While broadening of band appeared in the range of 1000-1200 cm^{-1} is attributed to valence vibrations of the silicate oxygen skeleton characterized to the increased silica content due to 15 h milling [31]. FTIR spectrum of TF-16 has shown increased broadness and intensity of the band between 3500-3000 cm^{-1} denoted to the increment in amount of surface hydroxyl groups due to tin loading as displayed in **Figure 3.2(b)** [32]. The anchoring of tin species in MFA-15 was indicated by shifting of Si-O-Si stretching band at 1042 cm^{-1} to lower wave number 974 cm^{-1} for TF-16 [33]. Presence of dispersed SnO_2 clusters in MFA-15 silica network was evident by presence of its characteristic bands at 620 and 574 cm^{-1} [34].

After sulfation, the structural changes produced in TF samples are illustrated in **Figure 3.3 (a-c)**. Sulfate promoted tin loaded fly ash (STF-16) showed broader band at 3000-3500 cm^{-1} due to strong hydrogen bonding [35] and red shift in wave number corroborated to the addition of sulfate species and enhancement in acid strength by generation of S-OH groups [36] as shown in **Figure 3.2(a)**. As compared to STF-16, STF-10 and STF-6 displayed narrower broad band with lesser intensities due to lower Sn contents responsible for anchoring S-OH groups during acid impregnation. All STF catalysts showed increased intense bands highlights the presence of silanol groups in sufficient quantity after calcination at 550°C for 3 h signifies the stability of Brönsted acidic sites in prepared catalysts. The vibration band appeared at 1660 cm^{-1} is attributed to the bending mode of water molecules [35]. The decrease in intensity of the band at 620 cm^{-1} was also noticed as effect of sulfate addition due to stretching vibrations of S=O and the interaction of SnO_2 loaded MFA-15 resulted to a weaker bonding of Sn-O [37]. In all STF samples, new bands in the range of 1200-900 cm^{-1} region (**Figure 3.3**) are noticed after incorporation of SO_4^{2-} ions which are absent in TF-16 sample as shown in **Figure 3.2**. The bands at 1246 and 1144 cm^{-1} are ascribed to S-O asymmetric stretching vibrations corresponding to

the chelated sulfuric groups that are connected through bridge on the surface of Sn^{4+} cations [38]. The intense band at $1382\text{--}1391\text{ cm}^{-1}$ account for the asymmetric stretching vibration of $\text{S}=\text{O}$ at sulfate ion bonded to the tin oxide surface [39]. On hydration red shift in wave number to 1346 cm^{-1} of this band is observed here corresponding to decrease in bond order of $\text{S}=\text{O}$ covalent bond and an increase in partial charge of oxygen atom as also reported elsewhere [40] resulting as increase in acidic strength of catalysts. On increasing from STF-6, STF-10 to STF-16 the intensity of these peaks increased signifying strong interaction of SO_4^{2-} ions with tin loaded MFA-15 catalysts. The ionic structure of sulfate group bonded to surface in presence of adsorbed water molecules is also responsible for the Brönsted acidity of the catalyst [41]. Thus, the presence of these bands corroborates the strong interaction of SO_4^{2-} species with tin containing silica of MFA-15 support. The absence of band around 1400 cm^{-1} in all catalysts denotes the absence of polynuclear sulfates $\text{S}_2\text{O}_7^{2-}$ species on the catalytic surface [42].

FTIR spectroscopy using pyridine as a probe molecule is one of the most suitable analytical tool to distinguish Lewis and Brönsted acidic sites [43]. **Figure 3.4** represents the pyridine chemisorbed FTIR spectra of TF-16 and STF-16 catalyst in magnified range of $1700\text{--}1400\text{ cm}^{-1}$. Compared to STF-16, TF sample showed less intense bands of Lewis acidic site at 1440 and 1615 cm^{-1} along with bands at 1550 and 1655 cm^{-1} denoted to Brönsted acidic site as reported earlier also [44]. While sulfate promoted STF samples (**Figure 3.5**) possessed the intense bands of pyridinium ions (pyridine-Brönsted acid site complex) represented as the IR vibrations at 1553 and 1638 cm^{-1} whereas covalently bounded pyridine (pyridine-Lewis acid site complex) ascribed for the band at 1445 cm^{-1} [45]. Amongst STF samples, STF-16 catalyst with highest amount of Sn and S loading showed the most intense bands for both the acidic sites corroborating the presence of strong acidic sites. Thus, incorporation of sulfate ions in fly ash supported tin samples has induced strong Brönsted and Lewis acid sites required for development of highly active solid acid catalyst. More sulfate species coordinated to the structure of metal oxide induces strong Lewis acidity may due to the ability of the sulfur element to form surface sulfur complex having $\text{S}=\text{O}$ covalent bond that acts as electron-withdrawing species followed by the inductive effect. Thus,

the inductive effect of S=O makes the Lewis acid strength of Sn^{4+} stronger [46] and the Brönsted acidic sites are provided by protons generated by sulfate groups. Interchange of Lewis and Brönsted acidic centers is a significant concept which is also described in **Scheme 3.2**. During the adsorption of water vapour or hydration, availability of H_3O^+ and HSO_4^- converts Lewis acidic sites into Brönsted acidic sites with high protonic character [41]. Intensity of these peaks is observed to be the highest in STF-16 as compared to STF-6 and STF-10 catalyst. The increased tin content from 6 to 16 wt.% facilitated loading of more amount of SO_4^{2-} groups responsible for generation of Brönsted and Lewis acidic sites in better quantity. These results show similarity with earlier reported work, in which increasing zirconia content (6 to 12 wt.%) in fly ash supported sulphated zirconia catalyst produced more concentration of both Lewis and Brönsted acidic sites due to better loading of sulphate ions [35]. The intensive band at 1508 cm^{-1} results from the contributions from both Brönsted and Lewis acidic sites **Figure 3.4 & 3.5** [47].

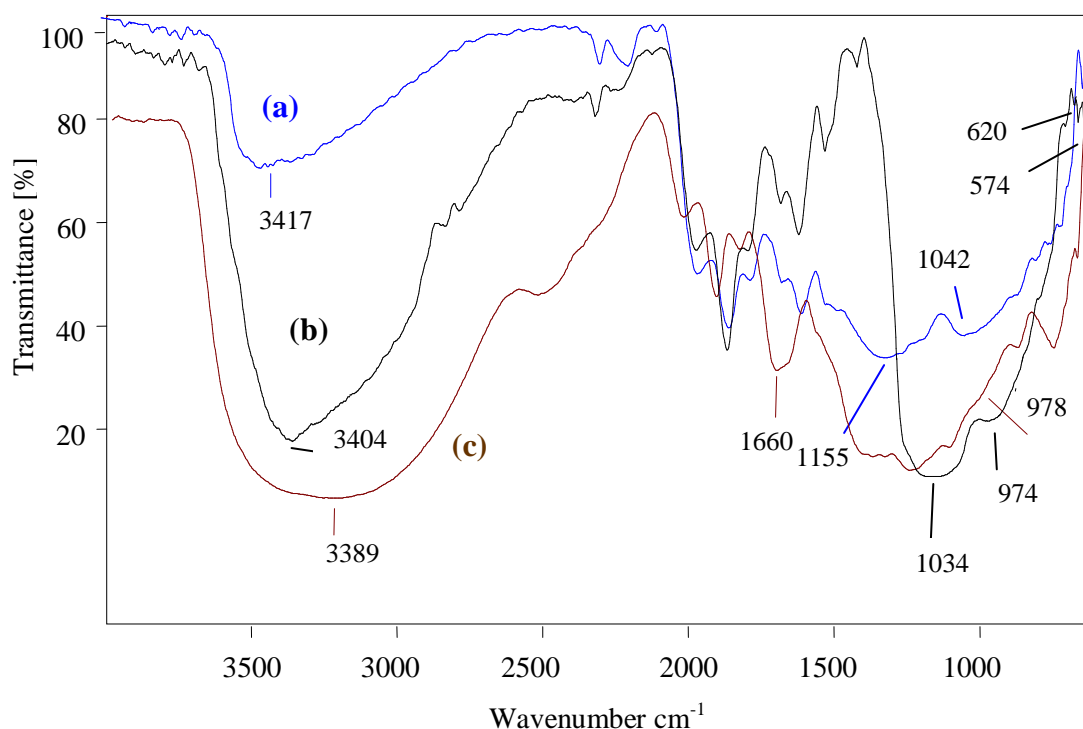


Figure 3.2: FTIR spectra of (i) MFA-15 (ii) TF-16 and (iii) STF-16

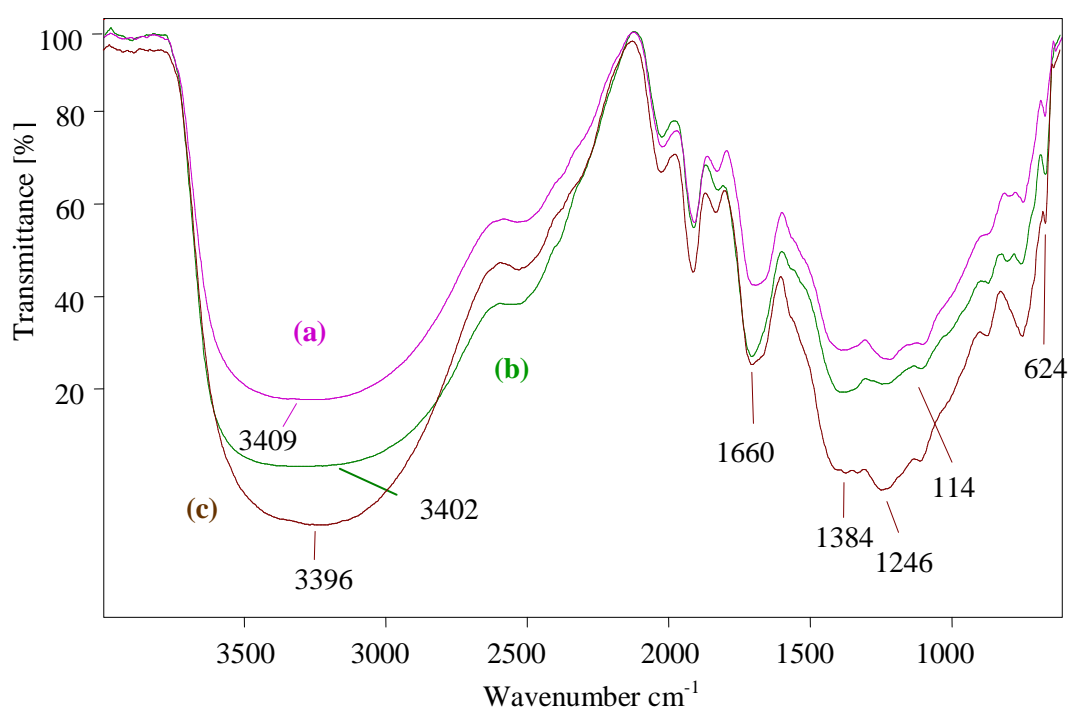


Figure 3.3: FTIR spectra of (a) STF-6 (b) STF-10 and (c) STF-16

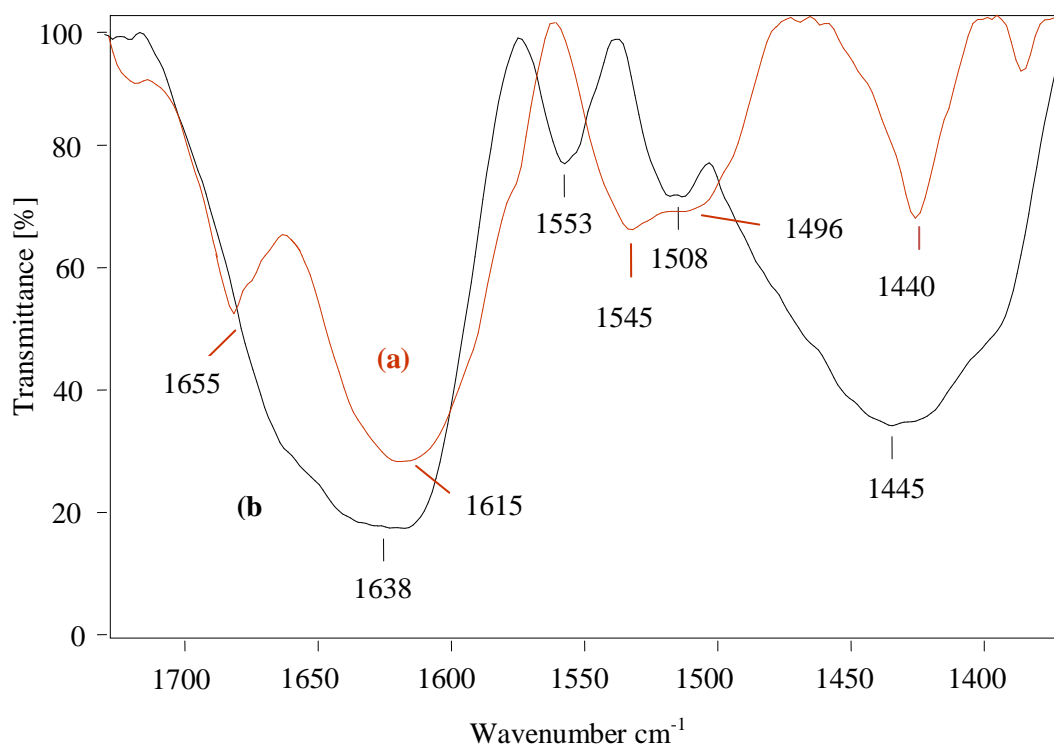


Figure 3.4: FTIR spectra of pyridine adsorbed (a) TF-16 and (b) STF-16

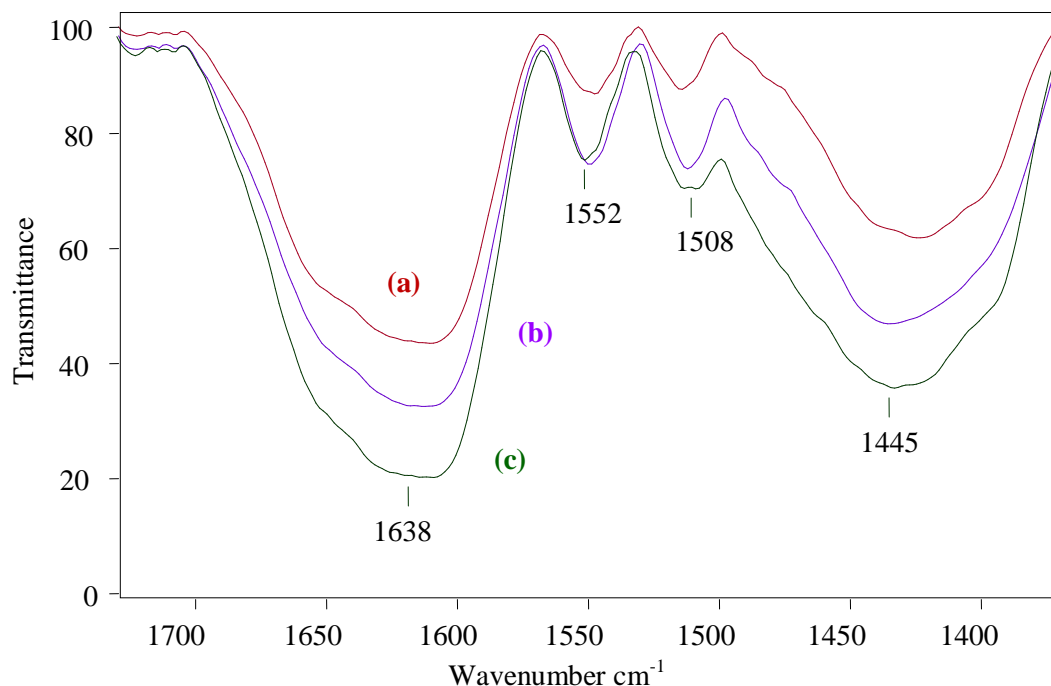


Figure 3.5: FTIR spectra of pyridine adsorbed (i) STF-6 (ii) STF-10 and (iii) STF-16

Diffuse reflectance UV–Vis spectroscopy is a very sensitive probe for the determination of type and coordination state of Sn species. It elucidates the incorporation of tin in MFA-15 structure as displayed in **Figure 3.6**. All STF samples exhibit electronic absorption bands in the range of 200–800 nm. Intense band with maximum intensity appeared at 210 nm ascribed to the isolated Sn^{4+} species in tetrahedral coordination and possessing ligand to metal charge transitions (LMCT) from O^{2-} to Sn^{4+} [48]. Increase in intensity of this band with increasing Sn content, signifies the successful deposition of tin species on silica framework of MFA-15. Electronic band at 270 nm displayed presence of some extra framework of Sn^{4+} species indicating towards the formation of small tin oxide agglomerates [49].

The surface morphologies of MFA-15 and STF-16 sample are displayed in **Figure 3.7**. Mechanical activation for 15 h has transformed smooth surface of fly ash particles into uneven, rough and irregular shaped due to break down of fine particles (**Figure 3.7 a**) [31]. SEM micrographs of STF-16 in **Figures 3.7b,c&d** show MFA-15 loaded SnO_2 species having flowery flakes like arrangement which has grown and dispersed all over the fly ash surface [24].

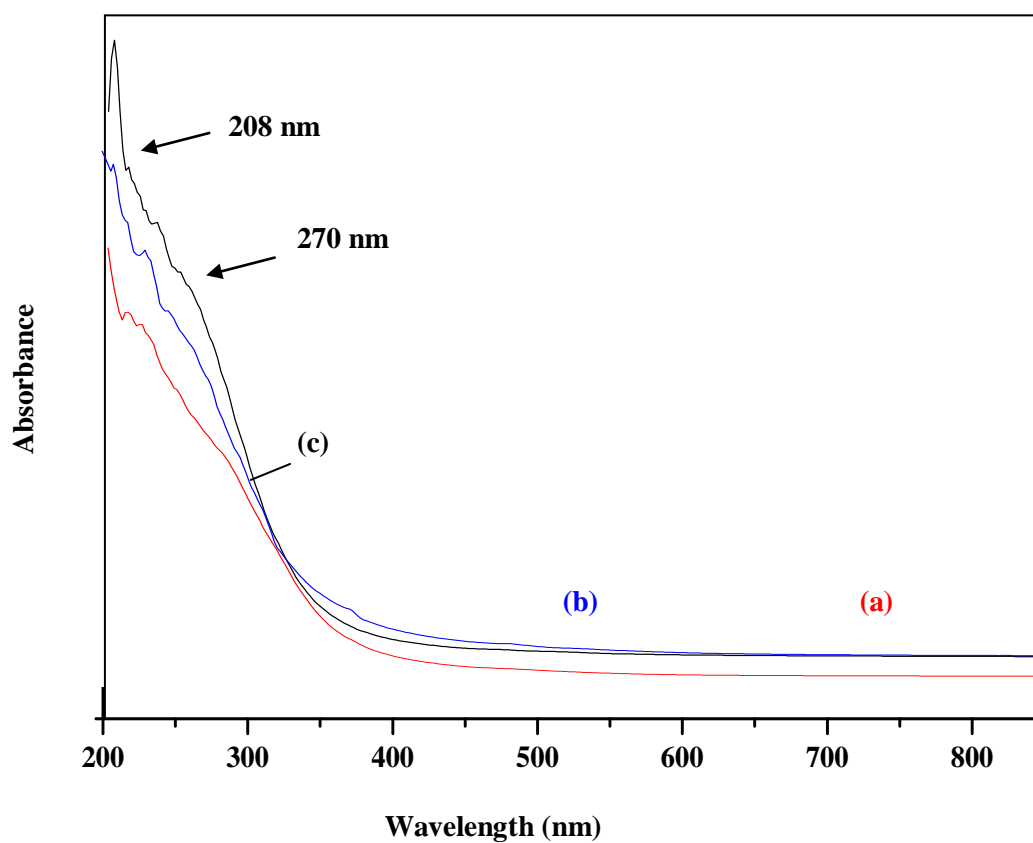
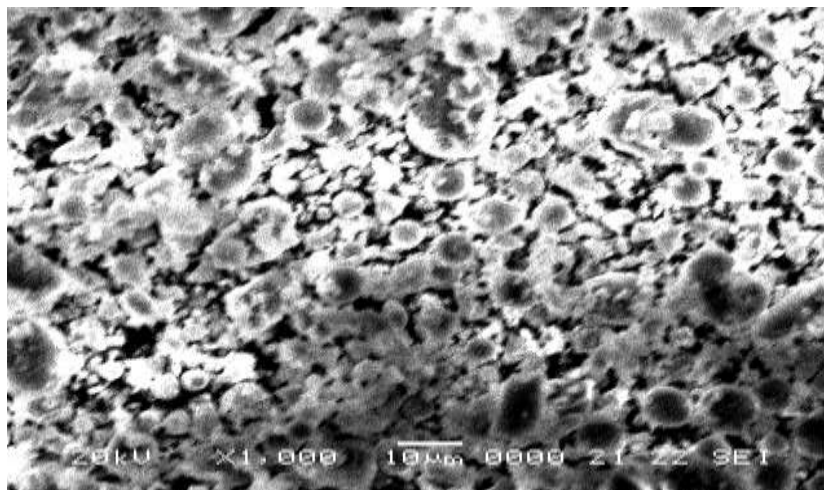
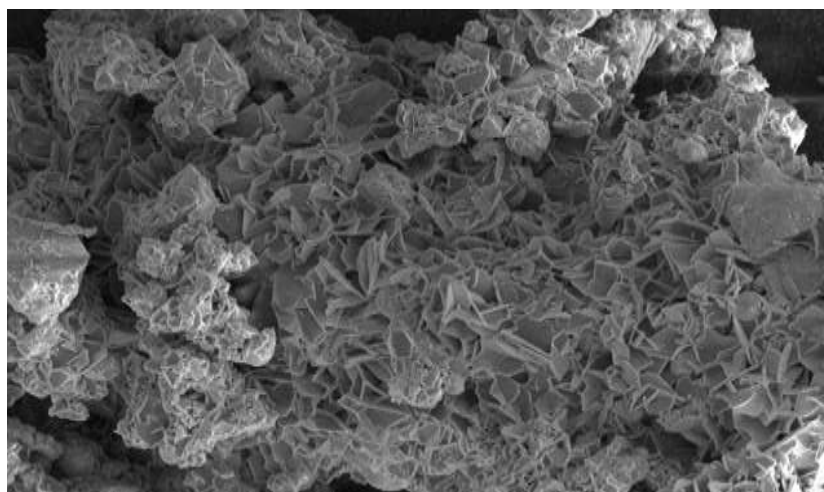


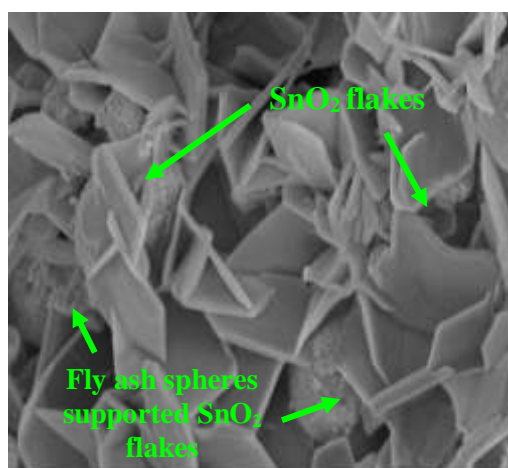
Figure 3.6: UV-VIS DR spectra of (a) STF-6 (b) STF-10 and (c) STF-16



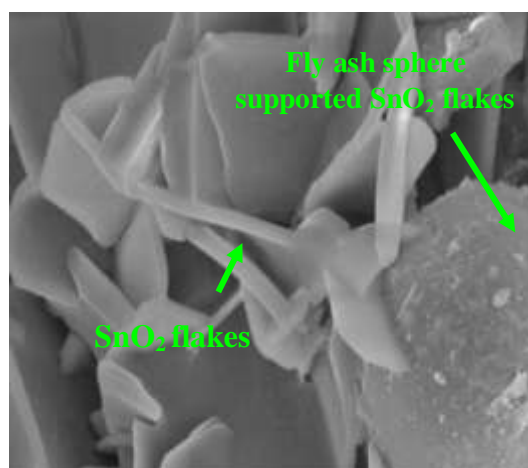
(a)



(b)



(c)



(d)

Figure 3.7: SEM micrographs of (a) MFA-15 and (b) STF-16 catalyst and (c&d) its magnified images

3.4 Catalytic performance of STF catalysts

The catalytic performance of the prepared catalysts were evaluated by microwave assisted 14-phenyl-14*H*-dibenzo[*a,j*]xanthenes synthesis at 120°C in 12 min using benzaldehyde and β -naphthol in molar ratio 1:2 and benzaldehyde to STF catalyst ratio 5:1, pressure (Pr) = 60 psi and 100 W power. No product formation was observed only in (μ W) heating and absence of catalyst. The reaction was also preceded using MFA-15 as catalyst but STF catalysts produced better conversion and selectivity results as shown in **Table 3.2**. Amongst STF catalysts, STF-16 gave the highest conversion of 95% and 90% yield due to presence of sufficient amount of Brönsted acidic sites compared to STF-6 and STF-10 catalysts.

Table 3.2: Catalytic activity of MFA-15, STF catalysts and catalyst-free condition for 14-phenyl-14*H*-dibenzo[*a,j*]xanthenes synthesis under microwave irradiation

Catalyst	Conversion% of benzaldehyde	Yield% of 14-phenyl-14 <i>H</i> -dibenzo[<i>a,j</i>]xanthenes
Only μ W	Nil	Nil
MFA-15	21	15
TF-16	64	48
STF-6	79	71
STF-10	88	82
STF-16	95	90

Reaction conditions under microwave irradiation: Temperature=120°C, Time=12 min, benzaldehyde/STF-16 ratio=5:1, benzaldehyde/ β -naphthol=1:2, Pr=60 psi, Power=100W and P_{max} = ON

As suggested by above results, STF-16 was considered as principal catalyst to optimize reaction parameters such as reaction time, temperature, power consumption, catalyst to substrate ratio and reactant molar ratio for obtaining maximum conversion and yield of 14-phenyl-14*H*-dibenzo[*a,j*]xanthenes under microwave assisted solvent-free conditions. The maximum efficiency of STF-16 was determined by its reusability evaluation.

3.4.1 Effect of reaction temperature

To evaluate the effect of reaction temperature on conversion and yield of the product, the reaction temperature was varied from 90°C to 140°C. On increasing temperature, increase in conversion and yield was noticed as illustrated in **Figure 3.8**. Maximum 95% conversion and 90% yield of xanthenes was obtained at 120°C whereas further rise in temperature, no appreciable change was noticed.

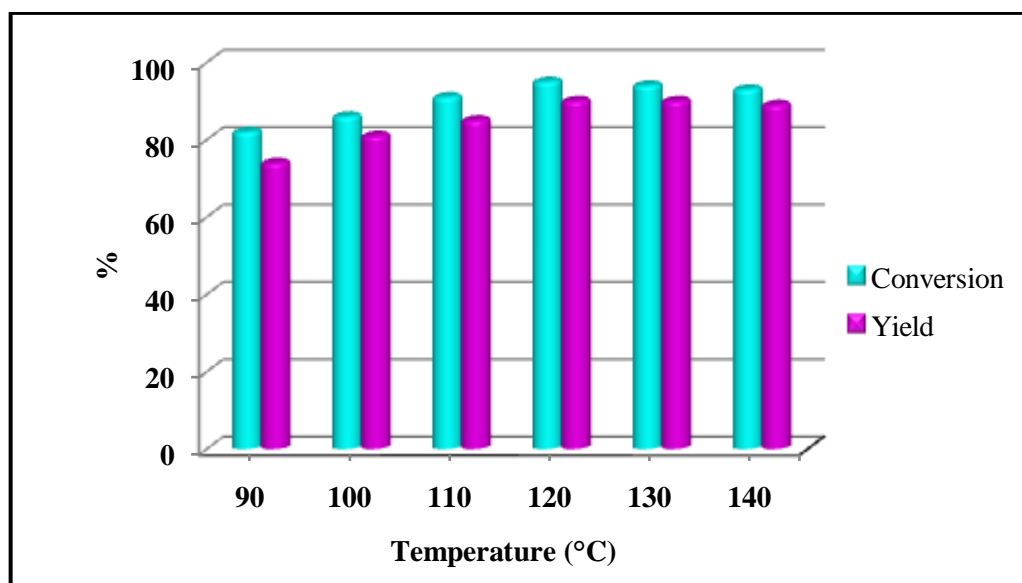


Figure 3.8: Variation of conversion% and yield% of 14-phenyl-14*H*-dibenzo[*a,j*]xanthenes over STF-16 catalyst with temperature

Reaction conditions: Time=12 min, benzaldehyde/STF-16 ratio=5:1, benzaldehyde/ β -naphthol=1:2, Pr=60 psi, Power=100W and P_{\max} = ON

3.4.2 Effect of reaction time

The experiments were carried out at varying reaction time period to determine the optimum reaction time (**Figure 3.9**). Under microwave irradiation, on increasing reaction time from 3 to 12 min, the conversion of benzaldehyde was increased upto 95% while yield of xanthenes was upto 90% respectively. With increase in time period, these parameters remained almost unaffected.

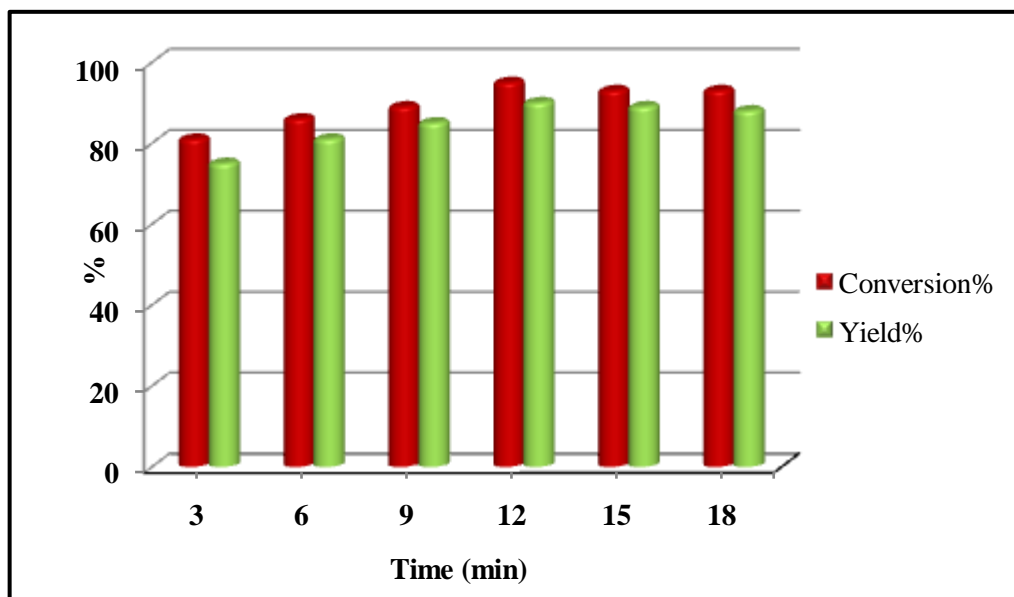


Figure 3.9: Variation of conversion% and yield% of 14-phenyl-14H-dibenzo[*a,j*]xanthenes over STF-16 catalyst with reaction time

Reaction conditions: Temperature=120°C, benzaldehyde/STF-16 ratio=5:1, benzaldehyde/ β -naphthol=1:2, Pr=60 psi, Power=100W and P_{\max} = ON

3.4.3 Effect of microwave power

The microwave power parameter was also examined in the range of 70W to 120W to achieve the highest product yield. A proportional relationship between microwave power and benzaldehyde conversion with yield was observed as illustrated in **Figure 3.10**. At 100W, maximum 95% benzaldehyde conversion and 90% yield of 14-phenyl-14H-dibenzo[*a,j*]xanthenes was achieved whereas its successors power didn't create much difference in these values.

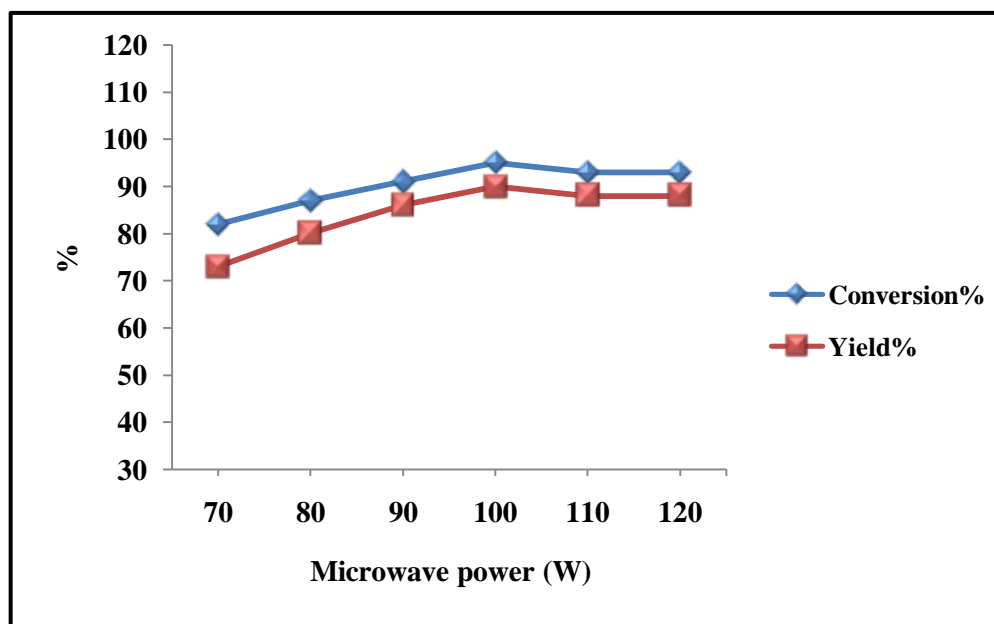


Figure 3.10: Variation of conversion% and yield% of 14-phenyl-14*H*-dibenzo[*a,j*]xanthenes over STF-16 catalyst with microwave power

Reaction conditions: Temperature=120°C, Time=12 min, benzaldehyde/STF-16 ratio=5:1, benzaldehyde/ β -naphthol=1:2, Pr=60 psi, and P_{\max} = ON

3.4.4 Effect of benzaldehyde and β -naphthol molar ratio

The effect of molar ratio of benzaldehyde and β -naphthol was studied at four different molar ratios viz. 1:1, 2:1, 1:2 and 1:3. The change in yield% at different molar ratios is shown in **Table 3.3**. Using molar ratio of 2:1 of benzaldehyde and β -naphthol, appreciable yield% was not observed due to lack of adequate quantity of β -naphthol required for better synthesis of xanthene product as described in **Scheme 3.4**. On increasing molar ratio of benzaldehyde and β -naphthol to 1:2, the yield raised to 90% due to presence of sufficient molar amount of reactants. Further increase in molar ratio to 1:3, the excess amount of β -naphthol restricted the stirring of the reaction mixture during the course of reaction under microwave heating and thus, impeded the reaction progress and led to decreased product yield.

Table 3.3: Effect of benzaldehyde to β -naphthol ratio on conversion% of benzaldehyde and yield% of 14-phenyl-14*H*-dibenzo[*a,j*] xanthenes

Benzaldehyde to β -naphthol molar ratio	Conversion% of benzaldehyde	Yield% of 14-phenyl-14 <i>H</i> -dibenzo[<i>a,j</i>]xanthenes
2:1	72	53
1:1	88	79
1:2	95	90
1:3	84	62

Reaction conditions: Temperature=120°C, Time=12 min, benzaldehyde/STF-16 ratio=5:1, benzaldehyde/ β -naphthol=1:2, Pr=60 psi, Power=100W and P_{max} = ON

3.4.5 Effect of benzaldehyde to STF-16 catalyst weight ratio

To determine the optimum amount of STF-16 catalyst, different experiments under microwave irradiation were conducted using different benzaldehyde to STF-16 catalyst weight ratios maintaining rest of the reaction conditions as earlier. On increasing weight ratio from 10:1 to 5:1, due to availability of better quantity of Brönsted sites increment in the benzaldehyde conversion to 95% and product yield with 90% was noticed (**Table 3.4**). The conversion% and yield% remained almost same on further rise in catalyst weight ratio to 2.5:1.

Table 3.4: Effect of benzaldehyde to STF-16 catalyst weight ratio on conversion% of benzaldehyde and yield% of 14-phenyl-14*H*-dibenzo [*a,j*] xanthenes

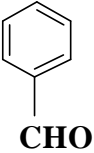
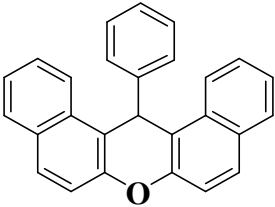
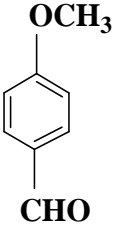
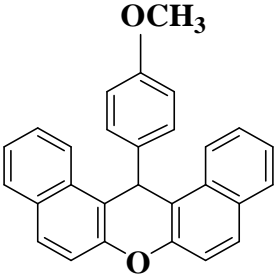
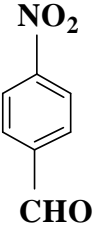
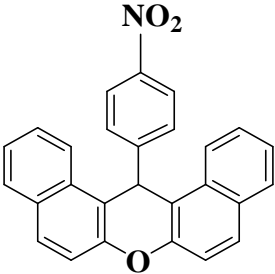
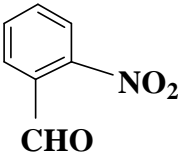
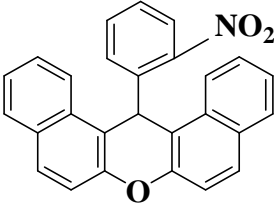
Benzaldehyde to STF-16 catalyst weight ratio	Conversion% of benzaldehyde	Yield% of 14-phenyl-14 <i>H</i> -dibenzo [<i>a,j</i>]xanthenes
10:1	85	77
5:1	95	90
2.5:1	95	90

Reaction conditions: Temperature=120°C, Time=12 min, benzaldehyde/ β -naphthol=1:2, Pr=60 psi, Power=100W and P_{max} = ON

3.4.6 Effect of substituted groups

To determine the effect of substituent on the yield% of the xanthenes, different functional groups containing benzaldehyde derivatives were used and the obtained yield% is displayed in Table 3.5.

Table 3.5: Synthesis of 14-aryl-14*H*-dibenzo[*a,j*]xanthenes derivatives under microwave heating conditions catalyzed by STF-16 catalyst

Entry	R-CHO	Product	Time (min)	Yield%
1			12	90
2			15	86
3			10	96
4			10	92

Effect of substituent groups attached on benzaldehyde skeleton on the yield of the product, 14-aryl-14*H*-dibenzo[*a,j*]xanthene has been illustrated in **Table 3.5**. Xanthene compounds bearing electron withdrawing groups (EWGs) gave better yield as compared to electron donating groups (EDGs). EWGs can activate the carbon atom of the carbonyl group for the nucleophilic attack on the α position of the β -naphthol whereas EDGs inactivate the carbonyl group via resonance resulted by non-bonded electron pair of the OCH₃ group (**Entry 2 Table 3.5**) and thus, decrease in rate of reaction and yield of the product is observed. Among EWGs, para substituted aryl aldehydes compound produced better yield compared to ortho substituted compounds due to steric effect between substituent at ortho position of the benzene ring and the xanthene ring. Thus, it can be concluded that aldehydes with EWGs reacted very well and produced excellent yields in shorter time than EDGs containing aldehydes which took longer reaction time.

3.4.7 Comparison with other reported catalyst

As depicted from **Table 3.6**, fly ash supported sulfated tin catalyst (STF-16) has given better yield of xanthene compound than some earlier reported commercial catalysts.

Table 3.6: Comparative study of catalytic potential of STF-16 catalyst with other reported catalysts for the synthesis of 14-phenyl-14*H*-dibenzo[*a,j*]xanthenes under microwave irradiation

Catalysts	Microwave power (W)	Time (min)	Yield%	Reference
Perlite-SO ₃ H nanoparticles*	700	8	86	[50]
P ₂ O ₅ /Al ₂ O ₃ **	900	12	85	[51]
STF-16***	100	12	90	Present work

* In microwave oven

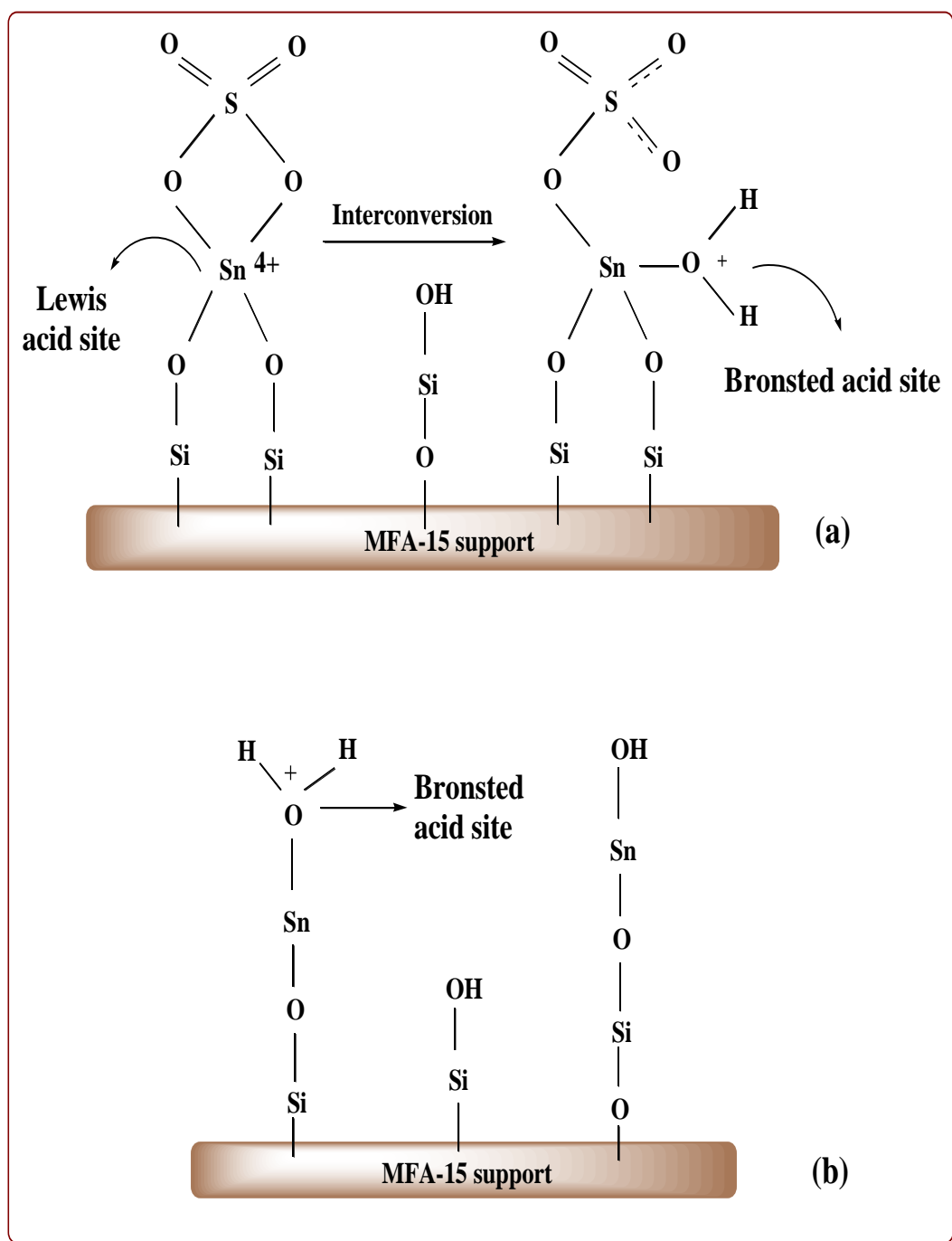
** In microwave laboratory system (micro-synth), model; Milestone

***In microwave synthesis system (CEM), model; Discover

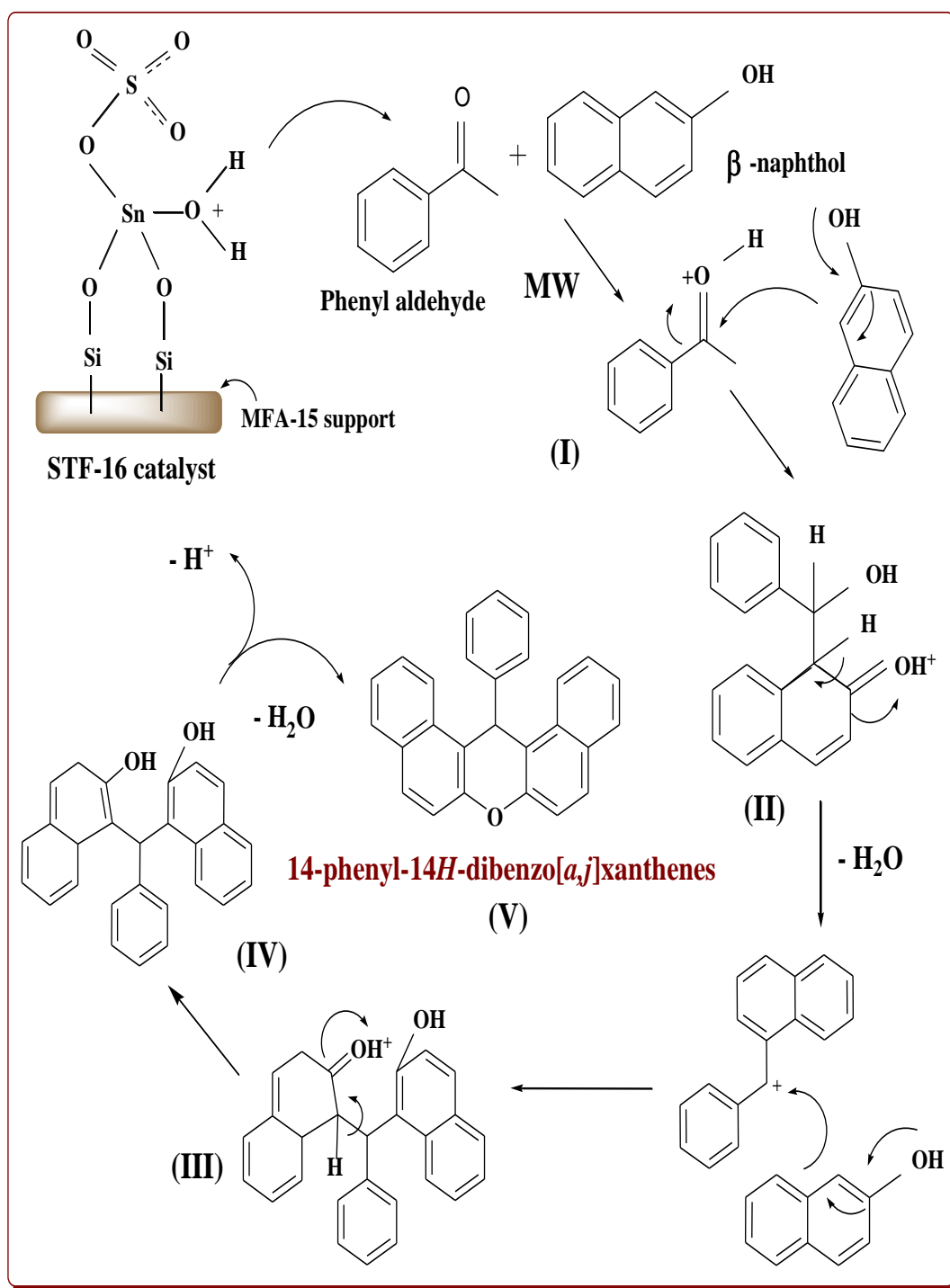
3.5 Mechanistic aspects

The proposed model structure of STF-16 catalyst is displayed in **Scheme 3.3 (a & b)**. Tin species are supported on MFA-15 surface by Si-O-Sn linkage. Sulfate species are bonded to tin atoms by bidentate chelating ligand as illustrated by FTIR spectra. Presence of Brönsted and Lewis acidic sites on STF-16 catalyst was confirmed by pyridine probed FTIR spectra described earlier in this chapter. The presence of surface sulfur complex with covalent S=O bond, produces inductive effect which generates strong Lewis acidity in STF catalysts. Adsorption of water molecules with surface sulfate groups behaves like ionic sulfate and generates Brönsted acidic sites [41]. However interconversion of Lewis to Brönsted acidic sites may occur during the reaction which is shown in **Scheme 3.3**. Other acidic sites on the surface are due to Si-OH or Si-Sn-OH groups.

In the synthesis of 14-phenyl-14*H*-dibenzo[*a,j*]xanthenes, the interaction of aryl aldehyde with the Brönsted acidic sites of STF-16 catalyst as shown in **Scheme 3.4**, generated the more electrophilic carbon center (microwave active species) of the activated aldehyde to form intermediate (I) which oscillates with electric field of the microwaves. The intermediate (I) interact with the first molecule of β -naphthol and produced intermolecular heat which helped in initial formation of carbonium ion (II). The formed carbonium ion reacts with the active methylene of second molecule of β -naphthol to produce oxonium species (III) which under goes intramolecular cyclodehydration reaction to afford 14-phenyl-14*H*-dibenzo[*a,j*]xanthenes as product and water as by product. Involvement of microwaves accelerated the intermediate formation by direct internal heating of reactant molecules and thus, speeded up rate of reaction product formation.



Scheme 3.3: Proposed model structure of MFA-15 supported sulfated tin catalyst (a) Generation of Brønsted and Lewis acid sites due to $\text{SO}_4^{2-}/\text{SnO}_2$ -MFA-15 (b) Generation of Brønsted site due to Si-Sn-OH



Scheme 3.4: Suggested reaction pathway for the one pot synthesis of 14-phenyl-14H-dibenzo[*a,j*]xanthenes under microwave assisted solvent-free conditions

3.6 Regeneration and reusability of STF-16 catalyst

The spent STF-16 catalyst removed from reaction cycles was filtered, washed and regenerated by calcining at 400°C for 1 h. After regeneration, STF-16 catalyst was efficiently used upto five reaction cycles with conversion and yield of 14-phenyl-14*H*-dibenzo[*a,j*]xanthenes upto 91-79% and 90-78% resp. as shown in **Figure 3.11**, indicating towards the sustainability of Brönsted acidic sites during regeneration. FTIR spectra of fresh STF-16 and regenerated catalyst of fifth reaction cycle as represented in **Figure 3.12**, illustrates the structural as well as acidic site stability during the reaction under microwave heating and after regeneration. Significant declination in yield% was noticed after fifth reaction cycle due to the physical adsorption of carbonaceous materials that blocked the active catalytic sites and hindered the contact of reactant molecules with catalytic sites. [52]. Similarity in the FTIR spectrum of fresh STF-16 and regenerated STF-16 catalyst (**Figure 3.12**) indicated the sustainability of sulphate and tin moieties with no change in chemical composition of surface structure. The stability, heterogeneity of STF-16 catalyst and probability of leaching of active sulphur and tin species was confirmed by Sheldon's hot filtration test [52] in which catalyst was taken off during midway through the reaction and then the progress of reaction is observed further in absence of the catalyst. The results showed that the extraction of STF-16 catalyst produce negative impact and reaction didn't proceed further. Hence, fly ash supported sulphated tin catalyst containing active sites are responsible for microwave assisted synthesis of 14-phenyl-14*H*-dibenzo[*a,j*]xanthenes and catalytic species are not leached out during the course of the reaction.

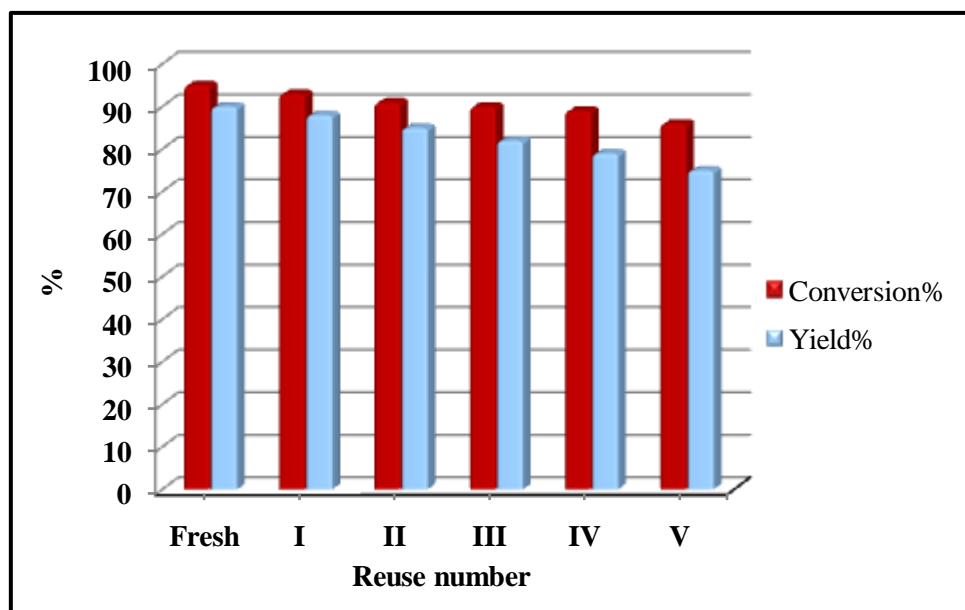


Figure 3.11: Reusability of STF-16 catalyst for microwave assisted 14-phenyl-14H-dibenzo[*a,j*]xanthenes

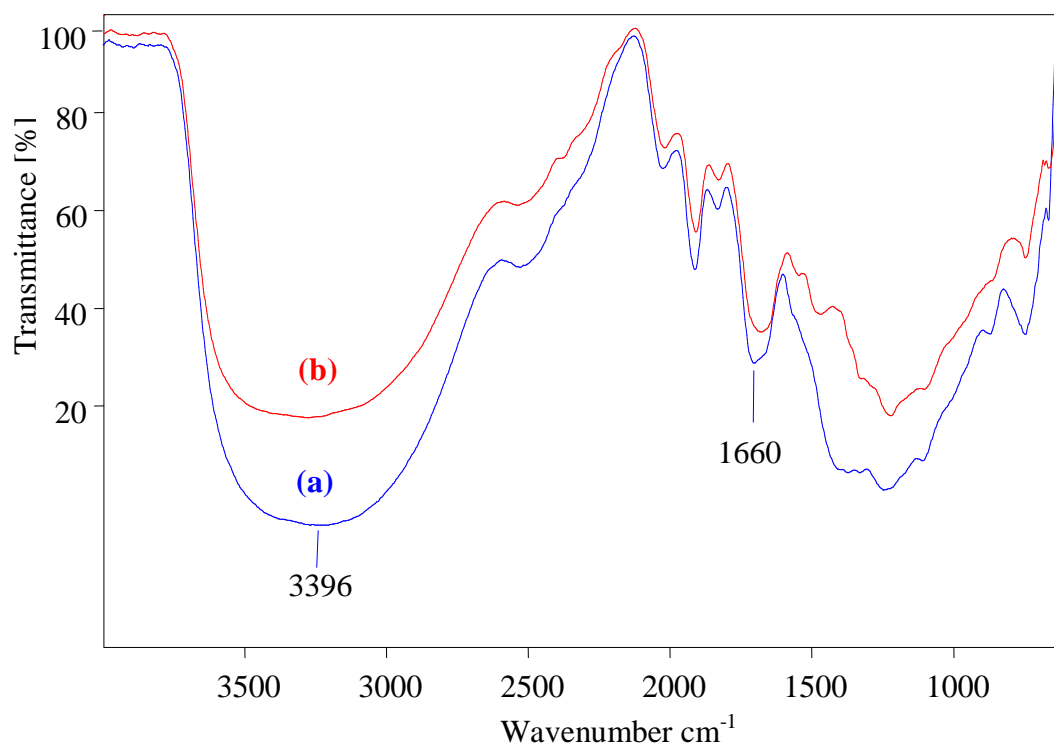


Figure 3.12: FTIR spectra of (a) Fresh STF-16 (b) regenerated STF-16 catalyst

3.7 Product identification

Product identification of selected dibenzoxanthenes is done by melting point analysis, ^1H NMR, ^{13}C NMR and FTIR techniques:

14-phenyl-14*H*-dibenzo[*a,j*]xanthenes: m.p.= 182–183°C; **FTIR (cm^{-1}):** 3059, 2894, 1630, 1590, 1515, 1255, 821; **^1H NMR (CDCl_3):** δ 6.46 (1H, s, CH), 6.92-7.02 (t, 1H, $J=7.6$, Ar), 7.14-7.18 (d, 2H, $J=7.5$ Hz), 7.40-7.45 (t, 2H, $J=7.5$ Hz), 7.49-7.53 (m, 4H, Ar), 7.57-7.60 (t, 2H, $J=7.2$, Ar), 7.82-7.85 (d, 2H, $J=8.0$, Ar), 8.38-8.42 (d, 2H, $J=8.8$, Ar); **^{13}C NMR (CDCl_3):** 148.79, 145.07, 131.42, 131.13, 128.93, 128.82, 128.55, 128.34, 126.46, 124.32, 122.76, 118.09, 117.39, 38.12

14-(4-Nitrophenyl)-14*H*-dibenzo[*a,j*]xanthene: m.p.= 308-309°C, **FTIR (cm^{-1}):** 3059, 2894, 1630, 1590, 1515, 1255, 821; **^1H NMR (CDCl_3):** δ 6.63 (s, 1H, CH), 7.44-7.48 (t, 2H, Ar), 7.52-7.55 (d, 2H, Ar), 7.60-7.65 (t, 2H, Ar), 7.69-7.72 (d, 2H, Ar), 7.83-7.88 (t, 4H, Ar), 8.00-8.02 (d, 2H, Ar), 8.28-8.33 (d, 2H, Ar); **^{13}C NMR (CDCl_3):** 152.08, 148.82, 146.24, 131.15, 129.14, 129.07, 128.90, 127.24, 124.65, 123.82, 122.07, 118.13, 115.84, 37.92

3.8 Conclusion

In the present study, an efficient, recyclable and cost effective solid acid catalyst is synthesized by loading of sulfated tin on 15 h mechanically activated fly ash. Mechanical activation improved the bulk and surface reactivity and facilitated surface area increment responsible for efficient loading of tin species on fly ash support. Loading of tin moieties on milled fly ash was done by chemical precipitation followed by sulphuric acid impregnation of MFA-15 supported tin species for deposition of active sulfur groups. The deposition of tin species in MFA-15 was confirmed by the presence of tetragonal phases in XRD patterns and Si-O-Sn bond in FTIR spectra whose intensity was increased with increasing metal content (6 to 16 wt.%). FTIR spectra also displayed the bands of S=O and S-O bonds, corroborating the deposition of sulphur on prepared STF catalysts. Sulfation of tin loaded samples enhanced the strength of Lewis acidity of Sn^{4+} due to inductive effect and Brönsted acidity due to surface -OH groups. The proposed model structure of the catalyst suggests interconversion of Lewis

acid sites to Brönsted acid sites. The catalyst STF-16, with tin (13.4 wt.%) and sulfur (5.9 wt.%) gave the highest yield of 14-phenyl-14*H*-dibenzo[*a,j*]xanthenes under microwave assisted conditions. The catalyst was easily regenerated by simple filtration, thermal activation and recycled upto five reaction cycles suggesting that acid sites were conserved efficiently. Sheldon's hot filtration test suggested that tin and active sulfur species were not lixiviated during the reaction run under dielectric heating. Fly ash supported sulfated tin catalysts are green and advantageous alternative of traditional homogeneous acids in terms of simple synthesis process, excellent catalytic activity, recyclability and reusability upto number of cycles.

3.9 References

- [1] K.N. Rao, K.M. Reddy, N. Lingaiah, I. Suryanarayana, P.S. Sai Prasad, *Appl. Catal. A: Gen.* 300 (2006) 139-146.
- [2] M. Hino, K. Arata, *Chem. Lett.* (1979) 1259-1260.
- [3] S.D. Jackson, J.S.J. Hargreaves, eds. *Metal oxide Catalysis* John Wiley & Sons 1 (2008).
- [4] H. Matsushashi, M. Hino, K. Arata, *Chem. Lett.* (1988) 1027.
- [5] H. Yu, H. Fang, H. Zhang, B. Li, F. Deng, *Catal. Commun.* 10 (2009) 920-924.
- [6] H. Matsushashi, M. Hino, K. Arata, K. Tanabe, H. Hattori, T. Ysmaguchi, T. Tanaka (Eds.), *Acid-Base Catalysis*, Kodansha, Tokoyo, (1989) 357.
- [7] T. Suzuki, T. yokoi, R. Otomo, J. N. Kono, T. Tatsumi, *Appl. Catal. A: Gen.* 408 (2011) 117-124.
- [8] H. Guo, P. Yan, X. Hao, Z. Wang, *J. Mater. Chem. Phys.* 112 (2008) 1065-1068.
- [9] M. J. De Silva and A. L. Cardoso, *J. Catalysts* (2013) 1-11.
- [10] R.L. Magar, P.B. Thorat, P.B. Thorat, V.V. Thorat, B.R. Patil, R.P. Pawar, *Chin. Chem. Lett.* 24 (2013) 1070–1074.

-
- [11] A.A. Dabbawala, D.K. Mishra, J.S. Hwang, *Catal. Commun.* 42 (2013) 1-5.
- [12] K. Nuithitikul, W. Prasitturattanachai, J. Limtrakul, *Inter. J. Chemical Reactor Eng.* 9 (2011) 1-21.
- [13] S.Y. Chen, H.D. Tsai, W.T. Chuang, J.J. Lee, C.Y. Tang, C.Y. Lin, S. Cheng, *J. Phys. Chem. C* 113 (2009) 15226–15238.
- [14] P. Salas, J.G. Hernandez, J.A. Montoya, J. Navarrete, J. Salmones, I. Schifter, J. Morales, *J. Mol. Catal. A: Chem.* 123 (1997) 149-154.
- [15] A.S.C. Brown, J.S.J. Hargreaves *Green Chem.* 1 (1999) 17-20.
- [16] H. Naeimi, Z.S. Nazifi, *Appl. Catal. A: Gen.* 477 (2014) 132-140.
- [17] D.W. Knight, P.B. Little, *J. Chem. Soc. Perkin Trans. I* (2001) 1771-1777.
- [18] J.V. Madhav, Y.T. Reddy, P.N. Reddy, M.N. Reddy, S. Kuarm, P.A. Crooks, B. Rajitha, *J. Mol. Catal. A: Chem.* 304 (2009) 85-87.
- [19] A. Bekaert, J. Andrieux, M. Plat, *Tetrahedron Lett.* 33 (1992) 2805.
- [20] A.R. Khosropour, M.M. Khodaei, H. Moghannian, *Synlett* (2005) 955-958.
- [21] H.R. Shaterian, M. Ghashang, A. Hassankhani, *Dyes Pigment* 76 (2008) 564-568.
- [22] S. Ko, C.F. Yao, *Tetrahedron Lett.* 47 (2006) 8827-8829.
- [23] W. Su, D. Yang, C. Jin, B. Zhang, *Tetrahedron Lett.* 49 (2008) 3391-3394.
- [24] K. Thirumurthy, G. Thirunarayanan, *RSC Adv.* 5 (2015) 33596-33606.
- [25] C. Yuan, W. Hong-Jaun, X. Zhi-ning, *Trans. Nonferrous Met. Soc. China* 19 (2009) s656-664.
- [26] J.L. Solis, V. Lantto, *Phys. Scr.* 69 (1996) 281.
- [27] M.K. Lam, Keat Teong Lee, A. R. Mohamed *Appl. Catal. B: Environ.* 93 (2009) 134–139.

-
- [28] D. Zhai, Y. Nie, Y. Yue, H. He, W. Hua, Z. Gao, *Catal. commun.* 12 (2011) 593-596.
- [29] Y. Li, Y.H. Zhao, Z.H. Zhang, W. Liu, V. Ortalan, Y.Z. Zhou, X.L. Ma, E.J. Lavernia, *J. Cryst. Growth* 310 (2008) 4226-4232.
- [30] Q. Zhang, P. Liu, C. Miao, Z. Chen, C.M. Lawrence Wub, C.H. Shek *RSC Adv.*, 2015, 5, 39285–39290.
- [31] N. Shringi, K. Srivastava, A. Rani, *Chem Sci Rev Lett* 4 (2015) 561-570.
- [32] F. Adam, J.N. Appaturia, Z.K.R. Thankappan, M.A.M. Nawi *Appl. Sur. Sci.* 264 (2013) 718– 726.
- [33] W. S. Cardoso, M. S. P. Francisco, A. M.S. Lucho, Y. Gushikem *Solid State Ionics* 167 (2004) 165–173.
- [34] H. Guo, P. Yan, X. Hao, Z. Wang, *Mater. Chem. Phys.* 112 (2008) 1065-1068.
- [35] C. Khatri, M.K. Modi, A. Rani, *Fuel Process. Technol.* 91(2010) 1288-95.
- [36] K.R.S. Devi, S. Jayshree, *Bull. Chem. React. Eng. Catalysis*, 7 (2013) 205-2147.
- [37] M.K. Lam, K.T. Lee, A.R. Mohamed, *Appl. Catal. B: Environ.* 93 (2009) 134-139.
- [38] Y. Gao, J. Wu, W. Zhang, Y. Tan, T. Tang, S. Wang, B. Tangn, J. Zhao *Ceram. Int.* 40 (2014) 8925–8929.
- [39] M. Nasouh Alaya, M.A. Rabah *Arabian J. Chem.* (2012) DOI: 10.1016/j.arabjc.2012.11.012.
- [40] E. Liu, A.J. Locke, R.L. Frost, W.N. Martens, *J. Mol. Catal. A: Chem.* 95 (2012) 353-354.
- [41] A.I. Ahmed, S.A. El-Hakam, A.S. Khder, W.S. Abo El-Yazeed, *J. Mol. Catal. A: Chem.* 366 (2013) 99-108.
- [42] G.D. Yadav, N.P. Ajgaonkar, A. Varma, *J. Catal.* 292 (2012) 99-110.

- [43] E.P. Parry, *J. Catal.* 2 (1963) 371-379.
- [44] A.S. Khder, E.A. El-Sharkawy, S.A. El-Hakam, A.I. Ahmed, *Catal. Commun.* 9 (2008) 769-777.
- [45] A.I. Ahmed, S.A. El-Hakam, M.A. Abd Elghany, W.S. Abo El-Yazeed, *Appl. Catal. A: Gen.* 407 (2011) 40-48.
- [46] S. Furuta, H. Matsushashi, K. Arata, *Appl. Catal. A: Gen.* 269 (2004) 184-191.
- [47] A.S. Khder, A.I.Ahmed, *Appl. Catal. A: Gen.* 354 (2009) 153–160.
- [48] Z.C. Liu, H.R. Chen, W.M. Huang, J.L. Gu, W.B. Bu, Z.L. Hua, J.L. Shi, *Microporous Mesoporous Mater.* 89 (2006) 270–275.
- [49] Z. Kang, X. Zhang, H. Liu, J. Qiu, K.L. Yeung *Chem. Eng. J.* 218 (2013) 425–432.
- [50] E. Mirhadi, A. Ramazani, M. Rouhani, S.W. Joo, *Chemija* 24 (2013) 320-324.
- [51] A. Zarei, A. R. Hajipour, L. Khazdooz, *Dyes and Pigments* 85 (2010) 133-138.
- [52] C. Khatri, D. Jain, A. Rani, *Fuel* 89 (2010) 3853–3859.



Chapter-4

*Microwave Assisted Single step
synthesis of Coumarin Derivatives via
Pechmann Condensation Reaction using
Fly Ash Supported Niobia as a Solid
Acid Catalyst*

ABSTRACT

Fly ash supported niobia (NBF) has been reported as solid acid catalyst for microwave assisted solvent-free synthesis of coumarins and its derivatives. Varying amounts of niobium wt.% loaded on 15 h milled low calcium fly ash were studied. The prepared NBF samples were characterized by XRD, FTIR, pyridine FTIR, UV-vis DR and SEM-EDX techniques. Characterization results showed that with increase in niobium content polymerized niobyl species with strong Lewis and Brönsted acid sites were stabilized on fly ash. NBF-10 sample with sufficient amount of Brönsted sites gave maximum 88% yield of coumarin under dielectric heating. Use of microwave active reactants such as resorcinol, ethyl acetoacetate and ethanol generated as side product augmented the reaction rate to produce maximum yield%. NBF-10 catalyst could be regenerated and reused upto maximum four reaction cycles and also passed hot filtration test indicated its structural stability during the course of reaction.

4.1 Introduction

Coumarins are the benzo-2-pyrone derivatives mainly occur in the plants of Rutaceae and Umbelliferae family which include carrot, parsley, cumin, and celery [1]. These are one of the most important compounds of natural products and in synthetic organic chemistry due to their ample of applications in perfumery, agrochemicals, as intermediates and additives in food and cosmetics [2]. In pharmaceuticals, Dicoumarol, a fermentation product of coumarin is a potent anticoagulant while other pharmaceutically important coumarins derivatives such as Gentisin a chemopreventive agent is used to treat breast and prostate cancers and novobiocin, coumermycin and chlorobiocin are DNA gyrase inhibitors [3]. Amongst coumarin derivatives, 7-hydroxy-4-methylcoumarins (β -methylumbelliferone) is used as efficient laser dye, standard for fluorometric determination of enzymatic activity, fluorescent brightener and as a starting material for the preparation of insecticide and fluorocoumarin [4].

Coumarins are mainly extracted from plant sources by different extraction methods such as maceration under sonication, infusion and supercritical fluid extraction [5]. However, requirements of sophisticated instruments based on separation process to get pure product and tedious and time consuming process has encouraged its synthetic production route to meet out the consumption demands. Various synthetic methods such as Pechmann condensation [6], Knoevenagel condensation [7], Perkin [8], Reformatsky [9], Wittig reaction [10] and Claisen rearrangement [11] have been widely used for coumarins synthesis. But most of these methods suffer from harsh reaction conditions like use of toxic reagents, longer reaction time, high temperature etc. However, Pechmann condensation is one of the most widely used method involving condensation of phenol derivatives with a β -ketoester [12]. Commonly Pechmann condensation is catalyzed by conc. H_2SO_4 [13], trifluoroacetic acid [14] and P_2O_5 etc [15]. Synthesis methods using transition metal catalysis [16], ionic liquid [17] and microwave irradiation [18] have also been reported in the literature. But these procedures also somewhere suffers limitations such as low thermal stability, lack of reproducibility and use of catalysts in stoichiometric amount creating environmental problems during disposal of post-reaction waste. To overcome

these drawbacks, use of heterogeneous catalysts as an environmentally benign alternative has been inculcated using non-conventional synthesis routes such as microwave assisted conditions.

Niobium oxide and its compounds have received an increasing attention in the field of catalysis with diverse functions such as promoter, support, redox materials and acid catalysts [19]. As the pure amorphous niobium oxide possesses low surface area and poor thermal stability [20]. Recently, more emphasis has been given on emphasis has been given on the development of supported catalysts with enhanced efficiency. The materials containing niobium (Nb) in form the of mixed oxides, niobia supported various oxides, Nb-containing layered materials etc. have been applied in different reactions such as dehydration of alcohols [21], condensation [22], esterification [23], hydrolysis [24], biodiesel production [25] and photocatalysis [26]. Dispersion of niobium oxide over inorganic supports produces different surface species and their catalytic activity depends upon the metal precursor, metal loading and synthesis procedure. Thus, at low niobium oxide loading (1 wt.%) on silica isolated NbO_4 units predominates while increasing Nb loading species of polymerized NbO_x or bulk Nb_2O_5 forms [27]. According with Tanabe's approach incorporation of Nb^{5+} into tetra coordinated silica network generates Lewis and Brönsted acid sites depending upon coordination environment of Nb and relative ratio of Nb to silica in the sample composition [28].

Here in, synthesis and characterization of mechanically activated fly ash supported niobia species and their catalytic activity for the solvent-free, one pot synthesis of 7-hydroxy-4-methylcoumarin under microwave heating has been investigated. Structural features in niobia loaded fly ash were determined by XRD and FTIR while morphological characters were illustrated by SEM micrographs. Dispersion of niobia states was analyzed by UV-vis DR spectra. Acidity measurements were performed by pyridine probed FTIR spectra. Leachability of Nb species was observed by Sheldon's hot filtration test. Regeneration and reuse of the prepared samples also reflected the stability and conservation of acid sites as well as bonding strength of introduced niobia species in mechanically activated fly ash.

4.2 Experimental details

4.2.1 Materials and reagents

Fly ash (class-F type) was collected from Tata Thermal Power Plant, Jamshedpur, India. Niobium oxalate hydrate ($C_{10}H_5NbO_{20}.xH_2O$) was purchased by Alfa Aesar. Ethyl acetoacetate, m-amino phenol, resorcinol, pyrogallol and phloroglucinol were supplied by S.D. fine chemicals, India.

4.2.2 Catalyst synthesis

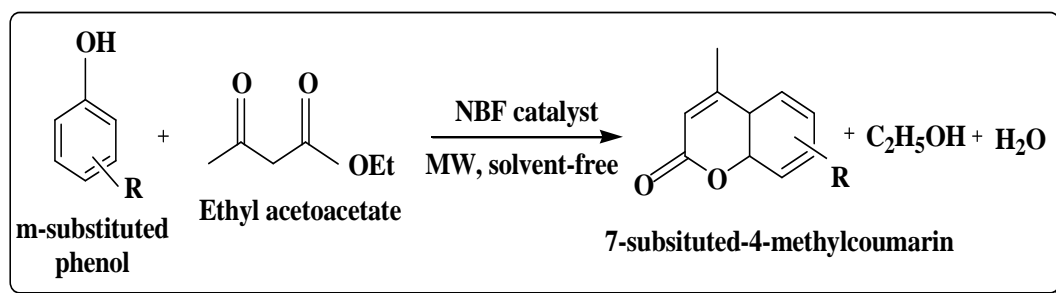
The steps involved in the synthesis of fly ash supported niobium catalyst are summarized in **Scheme 4.1**. Different niobium (Nb) containing milled fly ash samples were synthesized by incipient wetness impregnation method on 15 h mechanically activated fly ash (MFA-15) by the following procedure: As received fly ash was mechanically activated by milling in high energy planetary ball mill (Retsch PM-100, Germany) in an agate jar using agate balls with Ball to Powder ratio (BPR) of 10:1 for 15 h at 250 RPM rotation speed. MFA-15 possessing $17\text{ m}^2/\text{g}$ surface area was calcined at 800°C for 3 h and chosen as catalytic support material. Requisite amounts (0.6949 g for 2wt.%, 1.737 g for 5 wt.% and 3.474 g for 10 wt.%) of aqueous solution of niobium oxalate hydrate were added to 6 g of MFA-15 samples in 100 ml beaker and kept for 24 h stirring. After impregnation, samples were washed with distilled water till pH 7, dried in oven at 110°C for 24 h and calcined in air at 550°C for 6 h. These catalysts were denoted as NBF-x, where $x = 2, 5$ and 10 wt.% of the Nb content.

4.2.3 Catalyst characterization

Physico-chemical properties of the synthesized NBF catalysts were analyzed by using various techniques such as N_2 adsorption-desorption, X-ray diffraction, FTIR, pyridine FTIR, DR UV-Vis and SEM-EDS as illustrated in **Annexure I**.

4.2.4 Catalytic performance of NBF catalysts

Evaluation of the catalytic activity of the prepared NBF catalysts were performed by microwave assisted coumarins synthesis as shown in **Scheme 4.2**.



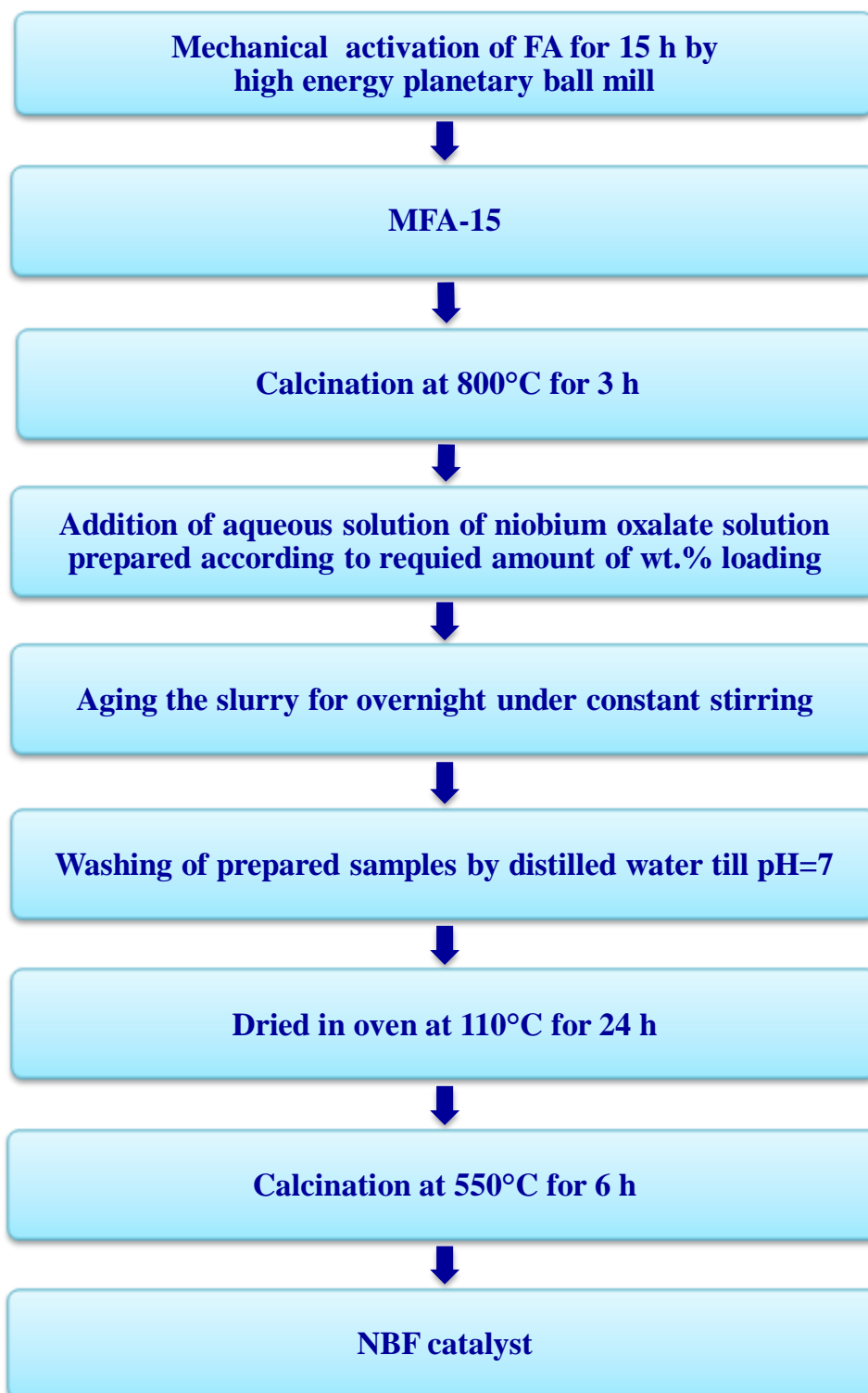
Scheme 4.2: Schematic representation of solvent-free, microwave assisted Pechmann condensation for synthesis of 7-substituted-4-methylcoumarin.

In the typical procedure protocol, resorcinol (10 mmol) and ethyl acetoacetate (20 mmol) in 1:2 molar ratio with NBF catalyst in resorcinol to NBF ratio=5:1 were filled in 10 ml pyrex glass vial. Before adding into reaction mixture, prepared STF catalyst was activated for 1 h at 450°C in muffle furnace. The reaction was carried out at 140°C, 50 psi pressure, 120W power with P_{\max} feature and medium stirring mode for 15 min in closed vessel system of CEM (model Discover) microwave synthesis system following the all stages of ramping, holding and cooling as described in **Chapter 2**. In the resulted mixture petroleum ether was added to remove unreacted reactant and filtered to separate out the catalyst. The crude product was recrystallized in ethanol to afford the corresponding pure product. To achieve maximum conversion and yield of the coumarins, reaction parameters were optimized. The analysis of benzaldehyde conversion was carried out by Gas chromatograph. The conversion of benzaldehyde and yield of coumarins was calculated as outlined below:

$$\text{Conversion (\%)} = \frac{(\text{Initial wt \%} - \text{Final wt \%})}{\text{Initial wt \%}}$$

$$\text{Yield (\%)} \text{ of salol obtained} = \frac{\text{g of coumarins obtained}}{\text{g of coumarins theoretically obtained}} \times 100$$

After extracted from fresh run, the obtained catalyst was washed thoroughly with acetone and dried in oven at 110°C for 12 h followed by activation at 450°C for 1 h in muffle furnace. Thus, the regenerated catalyst was used in next reaction cycle maintaining similar reaction conditions as earlier.



Scheme 4.1: Synthesis of fly ash supported niobia (NBF) catalyst

4.3 Results and discussions

Surface area is continuously decreased on increasing the niobium content from 2 to 10 wt% in the catalyst sample as shown in **Table 4.1** indicate the incorporation of impregnated niobium particles in MFA-15. **Table 4.2** summaries the atomic % of different elements in MFA-15 and NBF catalyst which are determined from EDS spectra as displayed in **Figure 4.1 & 4.2** respectively.

Table 4.1: Specific surface area of MFA-15 and NBF samples

Sample	Specific surface area (m ² /g)
MFA-15	17
NBF-2	16
NBF-5	14
NBF-10	11

Table 4.2: Atomic % of elements in MFA-15 and NBF-10 catalyst

Sample	Si (%)	O (%)	Al (%)	Nb (%)	Fe (%)	Ti (%)	K (%)
MFA-15	15.68	72.45	8.91	0.005	1.19	0.45	0.28
NBF-10	16.05	65.32	9.35	6.7	0.92	0.47	0.31

Figure 4.3 (a-d) displays the XRD patterns of MFA-15 and NBF catalysts with different niobium content at different 2θ angles ranging from 10° to 70° . MFA-15 displayed crystalline phases of mulite phases at $2\theta = 16.6^\circ$ and 26.3° along with strong peaks of quartz at 20.7° , 26.6° and 49.8° . The effect of 15 h milling resulted as increased amorphous content due to breaking of crystalline phases [29]. Similarity in XRD patterns MFA-15 and NBF catalysts indicates that incorporation of niobium has not altered the structural framework of fly ash. Although no appreciable Nb₂O₅ peaks were observed in all the NBF catalysts but on increasing Nb content, small reflections at $2\theta = 36.6^\circ$, 42.8° , 44.3° 46.4° and 50.2° corresponding to the presence of orthorhombic (T) phases of Nb₂O₅ (JCPDS no. 30-0873). [30].

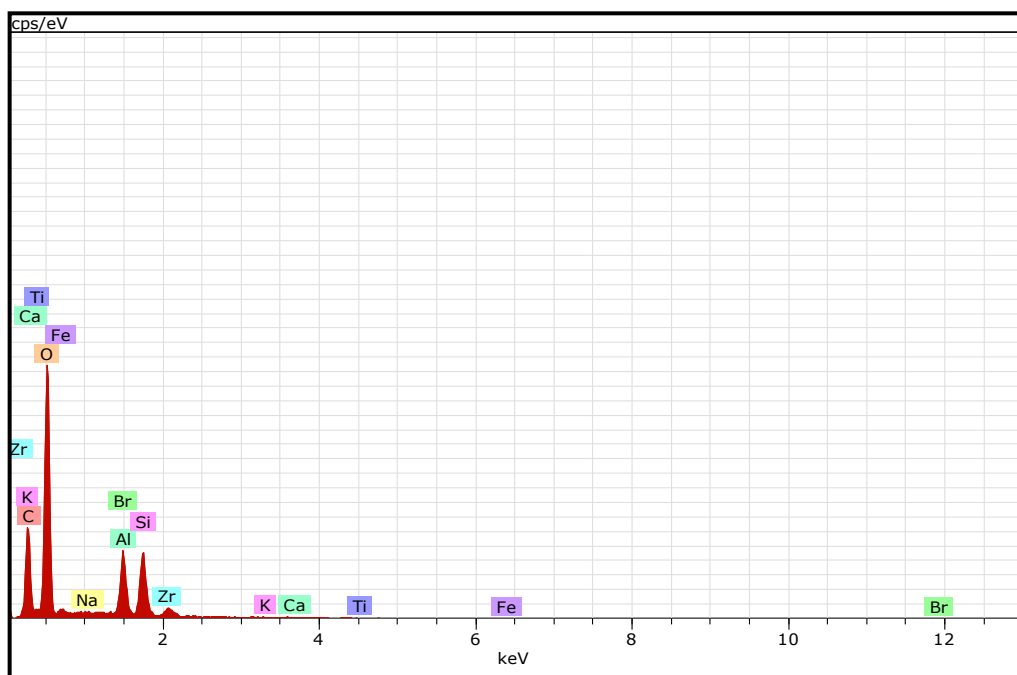


Figure 4.1: EDS spectrum of MFA-15 catalyst

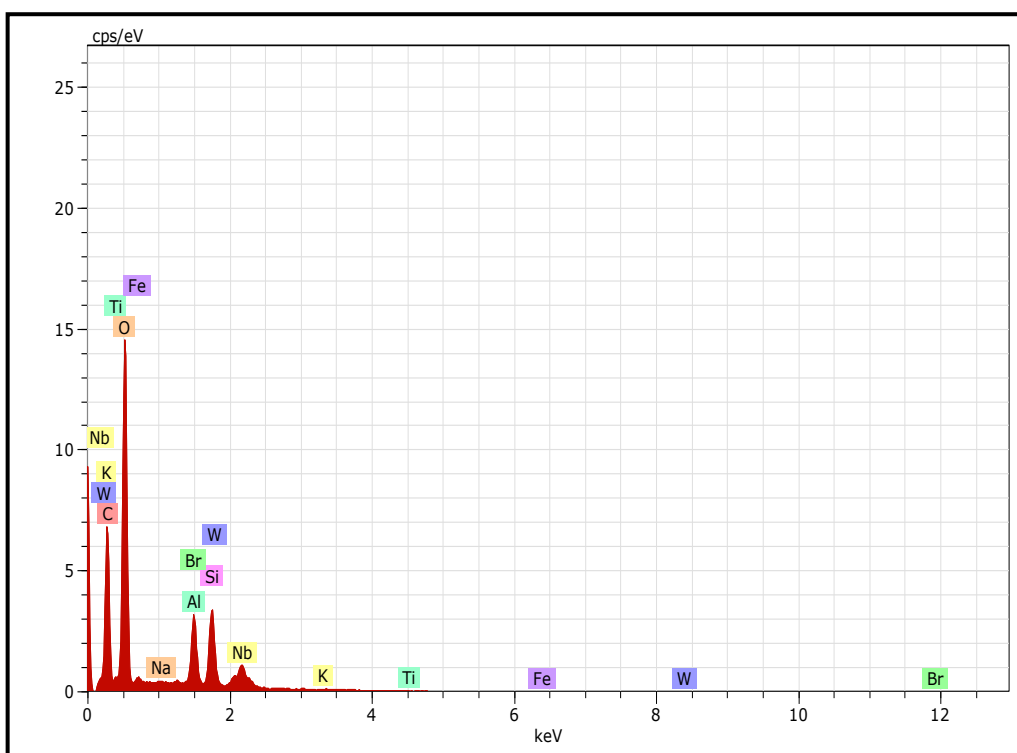


Figure 4.2: EDS spectrum of NBF-10 catalyst

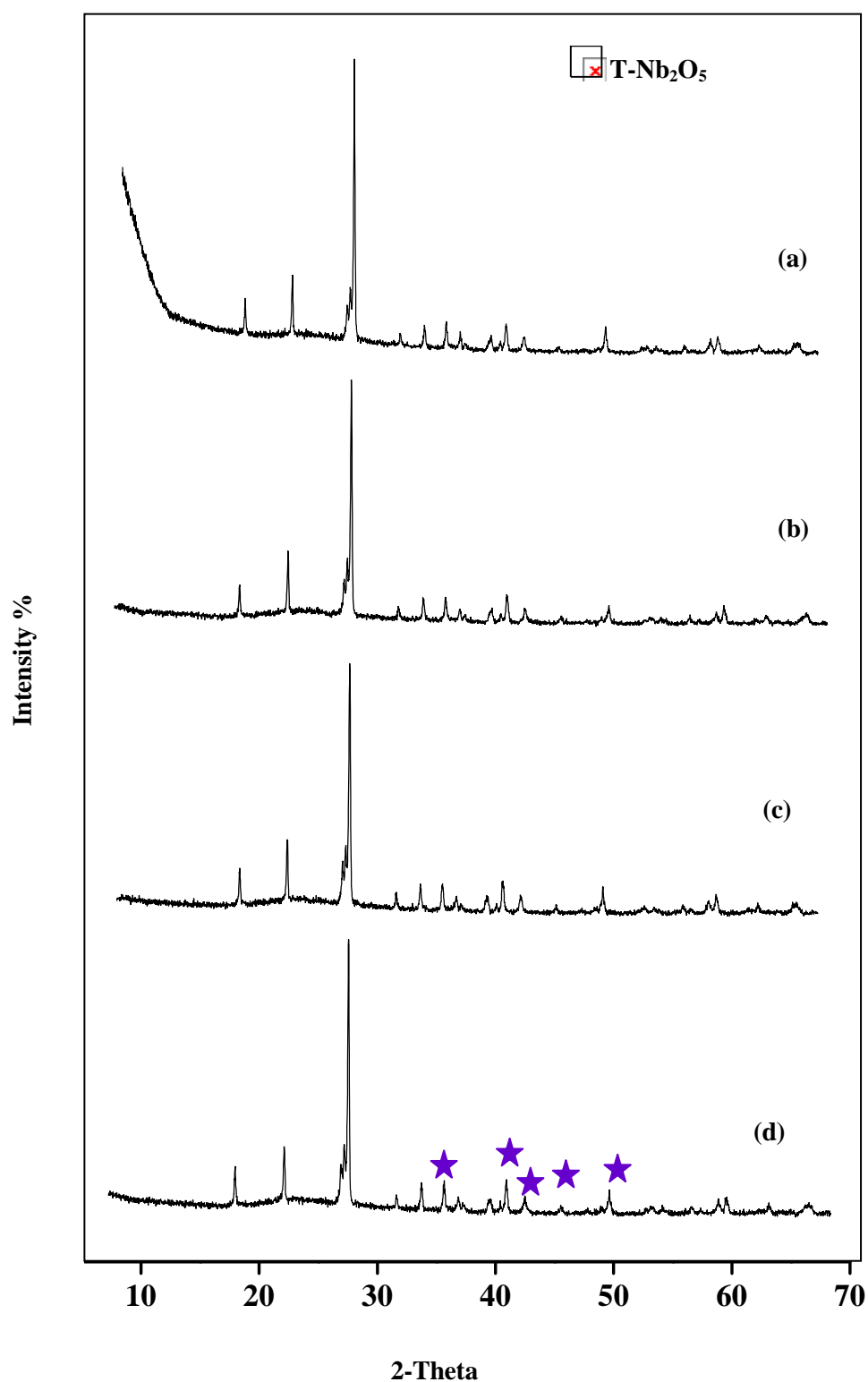


Figure 4.3: XRD patterns of (a) MFA-15 (b) NBF-2 (c) NBF-5 (d) NBF-10 catalysts

The FTIR spectra of MFA-15 and NBF catalysts are shown in **Figure 4.4 (a-d)**. In MFA-15, a broad band between 3500-3000 cm^{-1} is attributed to stretching vibrations of surface hydroxyl groups of Si-OH and adsorbed water molecules on the surface while peak at 1650 cm^{-1} assigned to bending mode ($\delta_{\text{O-H}}$) of water molecule. While broadening of band appeared in the range of 1000-1200 cm^{-1} is attributed to asymmetric stretching vibrations of Si-O-Si skeleton as characterized by the increased silica content due to 15 h milling [31]. In FTIR spectra of NBF catalysts displayed broad band is assigned to surface -OH groups while the peak at 3524 cm^{-1} is denoted to Nb-OH as appeared in NBF-10 and 5 samples [32]. Incorporation of Nb species in silica network of MFA-15 was evident by the red shift of the wave number of asymmetric mode of Si-O-Si from 1042 cm^{-1} to 1036, 1029 and 1022 cm^{-1} for NBF-2,5 and 10 respectively assigned to Nb-O-Si. The peaks appeared at 976 cm^{-1} in NBF-2 catalyst is ascribed to (Nb=O) stretching band which shifted to higher wave number to 981 cm^{-1} & 986 cm^{-1} for NBF-5 and NBF-10 respectively evidencing the presence of mono-oxo species. With increase in Nb loading to NBF- 10 samples appearance of peaks at 885 cm^{-1} and 620 cm^{-1} indicated the presence of $([\text{-O-Nb-O}]_n)$ stretching modes in Nb-O-Nb and Nb-O bondings corresponding to the presence of polymeric niobate species as shown in **Scheme 4.3**. While in case of NBF-5, lower wavenumber of these angular vibrations are observed indicating lesser polymerized niobyl forms over its surface [33]. NBF-2 has not shown both these peaks in FTIR spectrum indicating the presence of only monooxo niobium oxide species on the surface. The polymeric species formation possibly by restricted due to very low concentration of niobia on MFA-15 surface.

Pyridine adsorbed FTIR spectroscopy was used to determine the types of acid sites present in NBF samples. The relevant parts (1700-1400 cm^{-1}) of collected spectra are shown in **Figure 4.5 (a-c)**. All NBF samples possessed

intense bands 1450 cm^{-1} and 1615 cm^{-1} attributed to pyridine coordinated to Lewis acid centers. The bands at 1554 and 1648 cm^{-1} revealed the presence of pyridine ions bonded to Brönsted acid sites [34]. In NBF catalysts, NbO_4 tetrahedra units having +5 charge and polymeric NbO_6 moieties with highly distorted octahedra ($\text{Nb}=\text{O}$) generates Lewis acidity. While the Nb-OH bond as shown **Figure 4.4** in the form of Nb-(OH)-Si and/or slightly distorted octahedral forms with Nb-O-Nb bond are responsible for generation of Brönsted acid centers. The pyridine adsorbed spectrum of NBF-10 catalyst shows intense peaks at 1648 and 1450 cm^{-1} indicating the presence of higher amount of Brönsted and Lewis acid centers as compared to NBF-2 and NBF-5 which are attributed to increase in Nb content from 2 to 10 wt.%. Presence of band at 1498 cm^{-1} are associated to both Lewis and Brönsted sites present in all the samples [34].

Due to chemical interaction between Nb-O-Si, the generation of Brönsted acid site is expected as the protons are required to balance excess negative charge on O atom which is analog of Si or Al atom in the alumino-silicate cenospheres of fly ash [19]. The generation of Brönsted acid site is explained by Kung's assumptions [35,36] is explained by two modes: (1) electronic interaction between Nb_2O_5 and fly ash or alumino-silicate component (2) Nb-O bonds neighbouring the more covalent Si-O possess higher ionicity. Reduction of the electron density on OH bonds occurs due to inductive effect of nearly electronegative anions. As a consequence, OH bonds are weakened and Brönsted acid sites are generated.

At higher Nb loading, it is seen that increased amount of Lewis acidity is slightly lower than that of Brönsted acidity which indicates the presence of slightly distorted NbO_6 structures as evident by FTIR spectra (**Figure 4.5**). The interaction of niobia with support and formation of Nb-O-Si is also evident on FTIR spectra. Since, Nb is more electronegative than Si (Pauling scale 1.6 and 1.0) the niobia oxide ionic character and generation of Lewis acid sites in the NBF

samples can be a consequence of high ionicity of Nb-O bond. As reported earlier, the higher Lewis acidity could be generated on the first layer of the supported Nb₂O₅ on TS-1 [19].

As accordance to the earlier reported work [37], the IR peak observed in the range of 700-900 cm⁻¹ (Nb-O-Nb) are significantly broader than the band at 986 cm⁻¹ (Nb=O) due to the distribution of the bond and chain lengths found in polymerized metal-oxygen-metal (M-O-M) bonds. The structural distortions in monolayer type covered surface species generally cause shift (shortening of bond lengths) in metal-oxygen vibrational modes as increase in metal loading takes place. As shown in **Figure 4.4** shifts in the wave number assigned to ([-O-Nb-O]_n) stretching modes present in Nb-O-Nb polymerized forms shifted towards higher values i.e. 874 cm⁻¹ (NBF-5) to 885 cm⁻¹ (NBF-10) with increase in niobium content at monolayer coverage. However, in supported Nb₂O₅, the Nb=O stretching frequency generally remains unaffected or slight shift is observed due to the delocalization and concentration of NbOx vibrational potential energy in the Nb=O bond which can't be strongly influenced by less energetic Nb-O vibrations present in NbO₄ or NbO₆ units [37]. Therefore, on the basis of these bond length and bond strengths, the NBF-10 catalyst posses monolayer coverage as it possess band at 986 cm⁻¹ indicated that the Nb=O is vibrationally isolated due to negligible interaction with support.

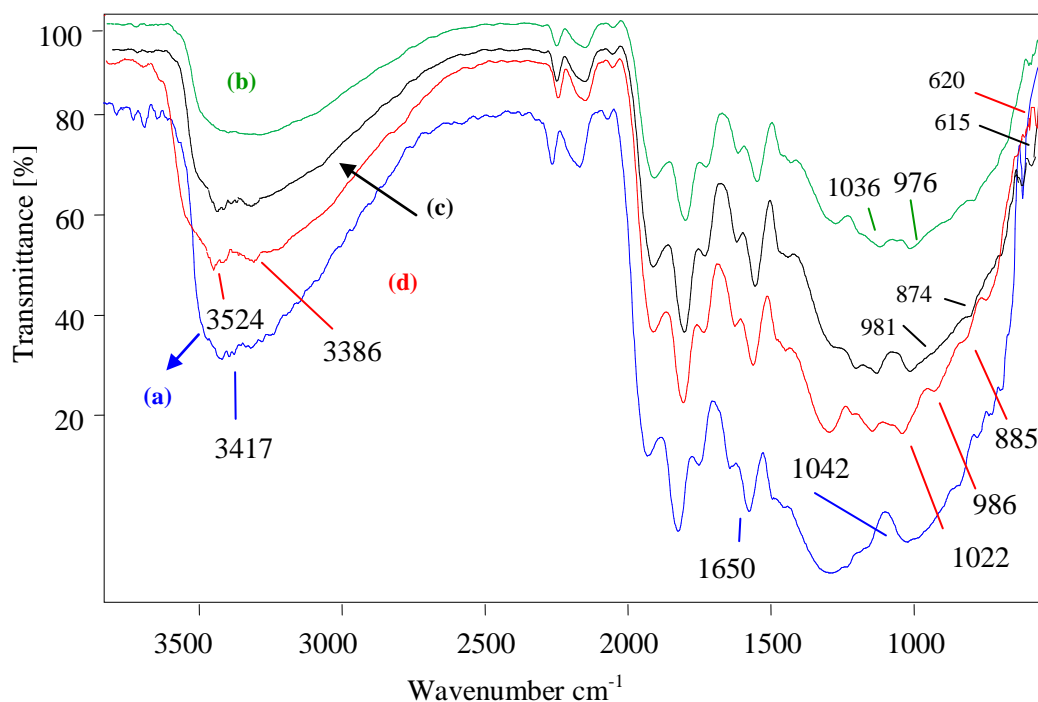


Figure 4.4: FTIR spectra of (a) MFA-15 (b) NBF-2 (c) NBF-5 and (d) NBF-10

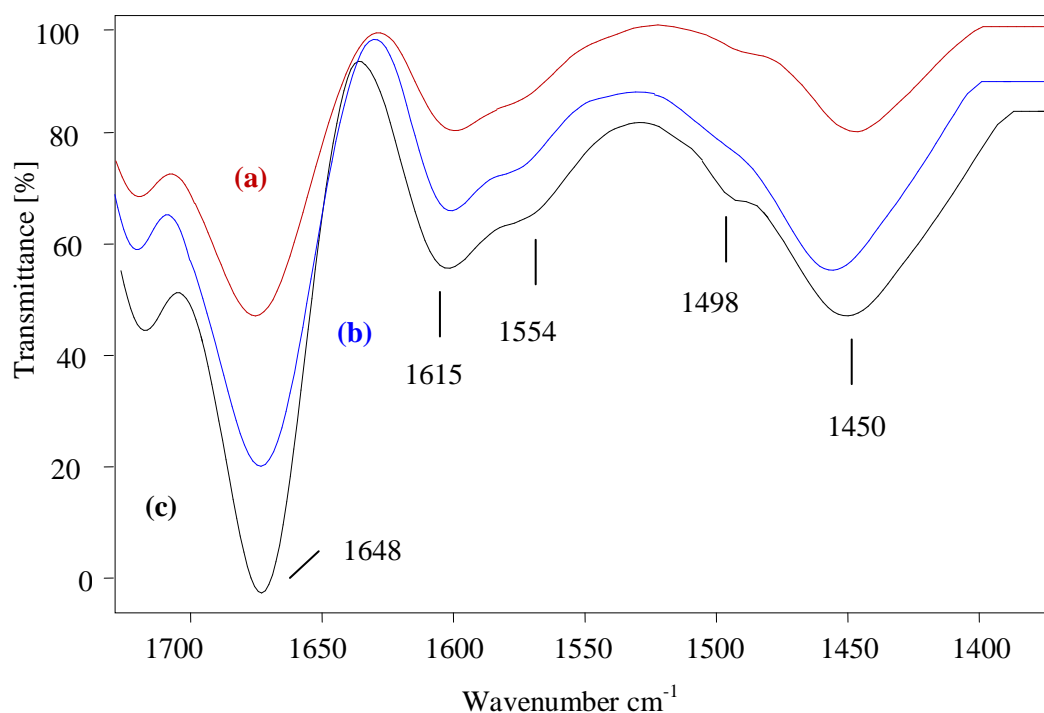


Figure 4.5: Pyridine FTIR spectra of (a) NBF-2 (b) NBF-5 and (c) NBF-10

The coordination geometry and chemical arrangement of the niobium species dispersed on MFA-15 support has been evaluated through DR UV-Vis spectroscopy which are displayed in **Figure 4.6(a-c)**. These absorption bands are attributed to ligand to metal charge transfer (O^{2-} to Nb^{5+}) which can be associated with the excitation of an oxygen 2p electron in the valence band to the empty orbital of the conduction band of 4d of Nb^{5+} ions surrounded by the oxygen [38]. The band observed around 210 nm is attributed to isolated mononuclear Nb(V) species with tetrahedral coordination present in the silica framework [39]. Another electronic band observed at 250 nm indicated the presence of NbO_6 species with octahedral coordination [40]. A weak band observed at 320 nm indicated that niobium oxide is visibly appeared at high Nb (10 wt.%) content loaded sample only with strong interaction with silico-aluminate phases of fly ash. Appearance of this band is usually noticed in the samples prepared by impregnation method, corresponding to the niobia species in form of nanodomains (polymerized species of NbO_6 octahedra clusters) [41]. In NBF-2 catalyst, presence of peaks at 220 nm and 250 nm indicated the presence monomeric isolated NbO_4 and NbO_6 species respectively while intensity of these peaks is increased in NBF-5 sample corresponding to NbO_4 units and with few polymerized NbO_6 species. In NBF-10 catalyst with high Nb content (10 wt.%) further bridging of Nb-O-Nb bonds led to the formation of Nb_2O_5 nanodomains along with polymerized NbO_6 and NbO_4 species.

SEM images of MFA-15 and Nb loaded samples are displayed in **Figure 4.7a**. Mechanical activation has transformed smooth, spherical cenospheres of FA into irregular shaped, agglomerated particles with rough surface due to structural break down [29] while SEM images of NBF-10 show increased agglomerated content due to loading of niobia species on surface of fly ash particles (**Figure 4.7b&c**).

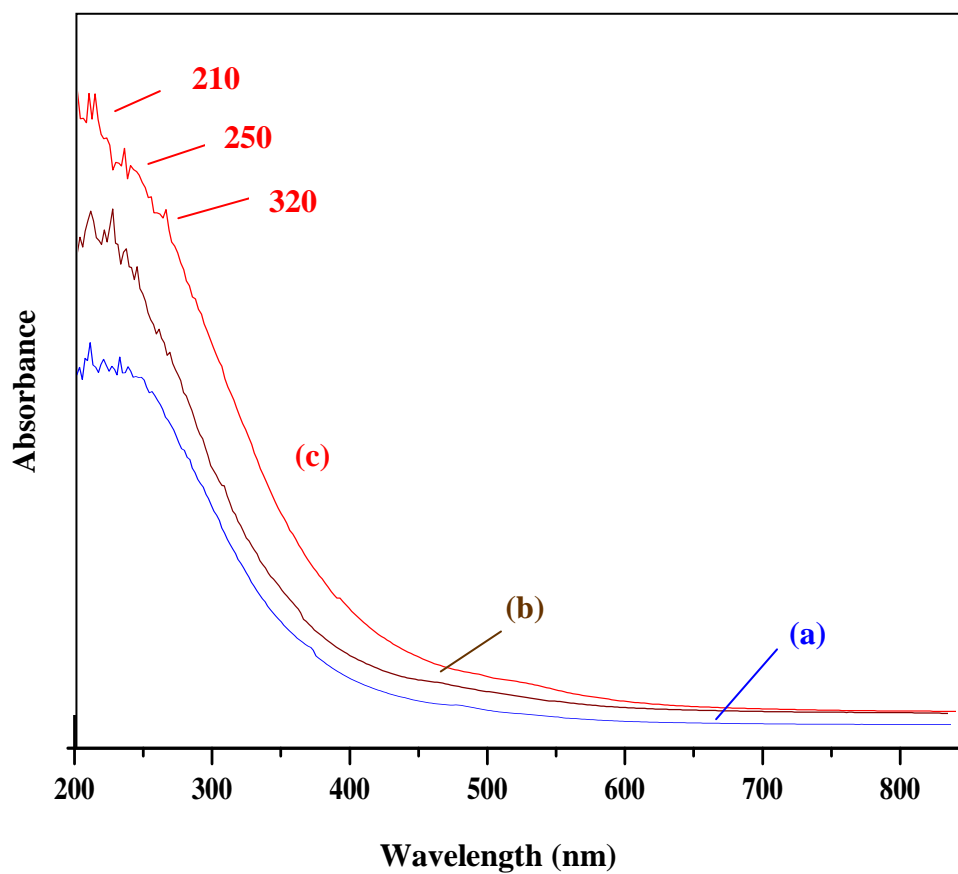
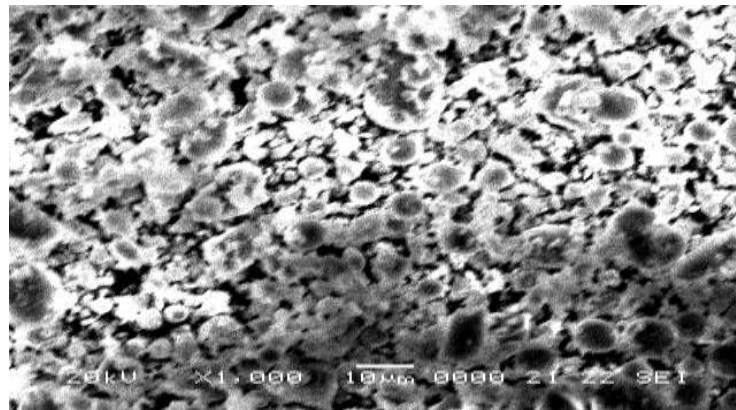
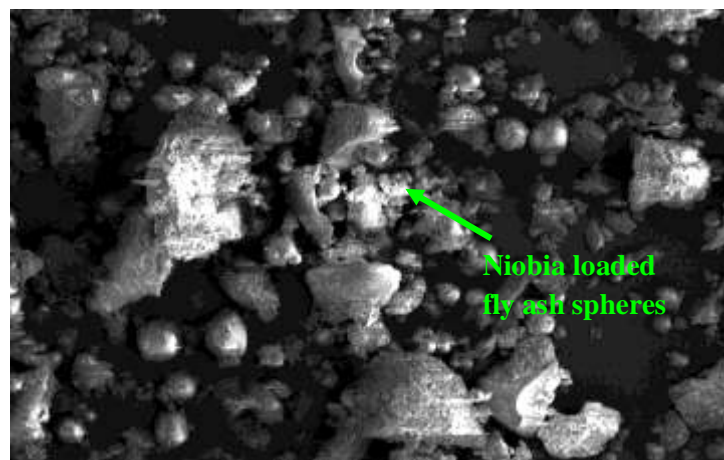


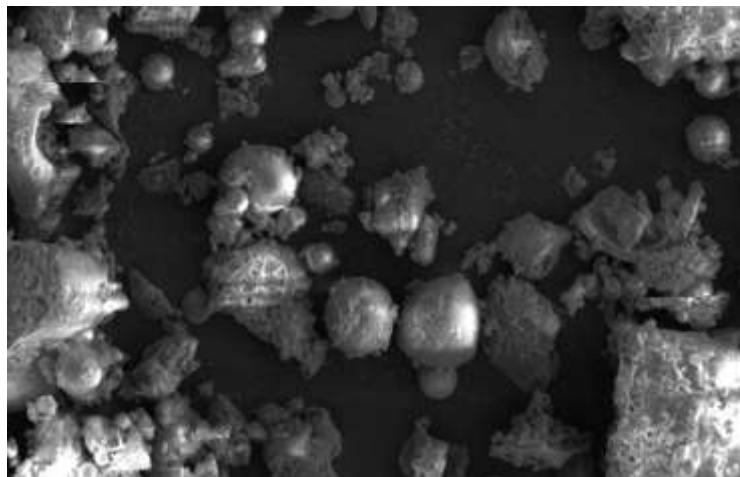
Figure 4.6: DR UV-Vis spectra (a) NBF-2 (b) NBF-5 and (c) NBF-10



(a)



(b)



(c)

Figure 4.7: SEM images of (a) MFA-15 (b) NBF-10 and (c) its magnified images

4.4 Catalytic performance of NBF catalysts

Catalytic efficiency of the prepared NBF samples was investigated by synthesis of 7-Hydroxy-4-methylcoumarin via. condensation reaction under microwave assisted conditions. Reaction was performed using resorcinol and ethyl acetoacetate (EAA) in molar ratio 1:2 along with resorcinol to NBF catalyst ratio 5:1, pressure (Pr) = 40 psi and 120 W power at 140°C for 15 min. Reaction was not preceded presence of microwaves while very less yield was obtained over MFA-15. On another hand, using NBF catalysts better conversion of resorcinol and yield of the product was obtained as shown in **Table 4.3**. Compared to NBF-2 and 5, NBF-10 catalyst with sufficient amount of Brönsted acid sites was able to produce better yield of 7-Hydroxy-4-methylcoumarin.

Table 4.3: Catalytic activity of MFA-15, NBF catalysts and catalyst-free conditions for microwave assisted 7-Hydroxy-4-methylcoumarin synthesis

Catalyst	Conversion% of resorcinol	Yield% of 7-Hydroxy-4-methyl coumarin
-	nil	nil
MFA-15	26	18
NBF-2	72	66
NBF-5	84	79
NBF-10	92	88

Reaction conditions under microwave irradiation: Temperature = 140°C; Time = 15 min; Pr = 40 psi; resorcinol / EAA = 1:2; resorcinol / NBF catalyst ratio = 5:1 and P = 120W with P_{max} = ON.

As evaluated by above results, NBF-10 was considered as main catalyst for optimization of reaction parameters to achieve maximum conversion and yield of 7-Hydroxy-4-methylcoumarin under microwave assisted solvent-free conditions. Along with this study, reusability and leachability performance of catalyst was also checked to determine its maximum efficiency and thermal stability of its acidic sites during course of the reaction.

4.4.1 Effect of reaction temperature

Effect of temperature on conversion and yield of product was monitored in the range of 100-150°C (**Figure 4.8**). On increasing reaction temperature, these factors were also increased upto 140°C giving maximum 92% conversion and 88% yield. While further increase in reaction temperature, conversion and yield% remained constant.

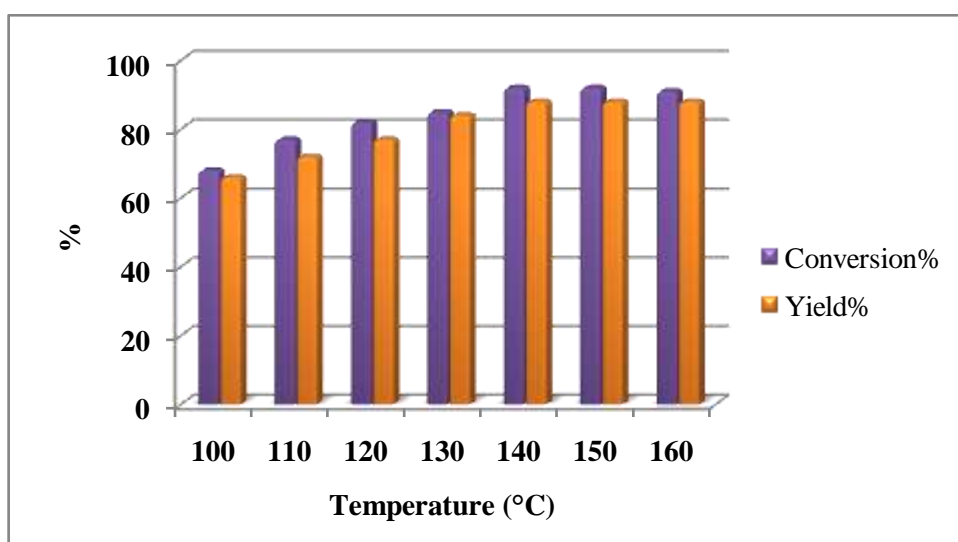


Figure 4.8: Variation of conversion% and yield% of microwave assisted 7-Hydroxy-4-methylcoumarin synthesis with temperature

Reaction conditions: Time = 15 min; Pr = 40 psi; resorcinol / EAA = 1:2; resorcinol / NBF catalyst ratio = 5:1 and P = 120W with P_{max} = ON.

4.4.2 Effect of reaction time

Reaction time was also varied from 3 to 18 min for determining optimum time to obtain maximum conversion% and yield% of 7-Hydroxy-4-methylcoumarin (**Figure 4.9**). Reaction time also showed a proportional relationship with these parameters. At 15 min reaction time, maximum conversion of 92% and 88% yield was achieved. Whereas extending the reaction time upto 18 min, constant values of conversion and yield were noticed. This may be due to less concentration of ethyl acetoacetate (EAA) left after consumed in the reaction and more time is required to generate carbocation from the EAA. In initial stage of reaction, desorption rate of product is high but as concentration of the product

increases in the reaction mixture, the reaction rate becomes sluggish or reaches a constant value [42].

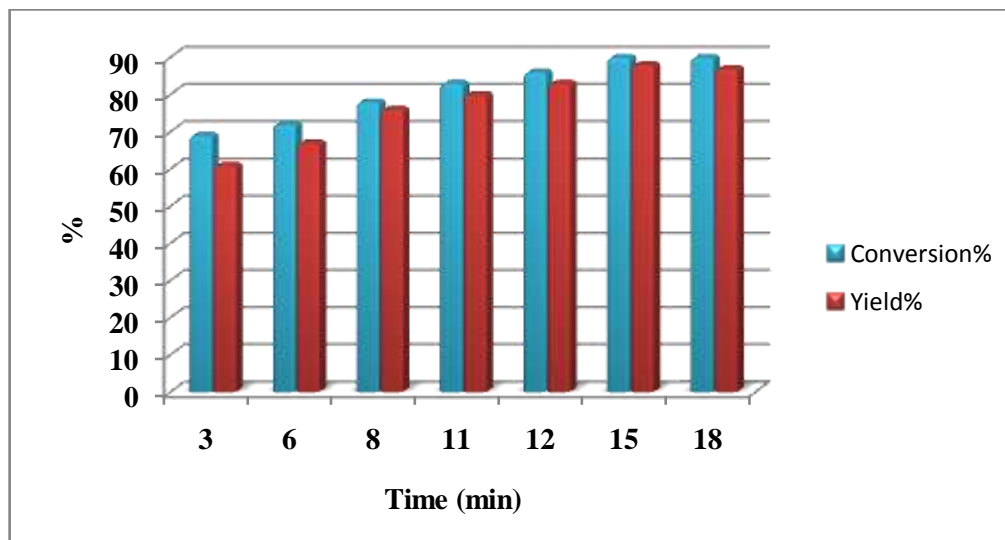


Figure 4.9: Variation of conversion% and yield% of microwave assisted 7-Hydroxy-4-methylcoumarin synthesis with reaction time

Reaction conditions: Temperature = 140°C; Pr = 40 psi; resorcinol / EAA = 1:2; resorcinol / NBF catalyst ratio = 5:1 and P = 120W with P_{max} = ON.

4.4.3 Effect of microwave power

To obtain maximum resorcinol conversion and 7-Hydroxy-4-methylcoumarin yield under minimum energy requirements, microwave power parameter was varied from 90 to 150W. As given in **Figure 4.10**, yield% showed directly proportional relationship with microwave power. At 120W, maximum 92% conversion and 88% yield was achieved while further increment in microwave power didn't improved yield% of the product.

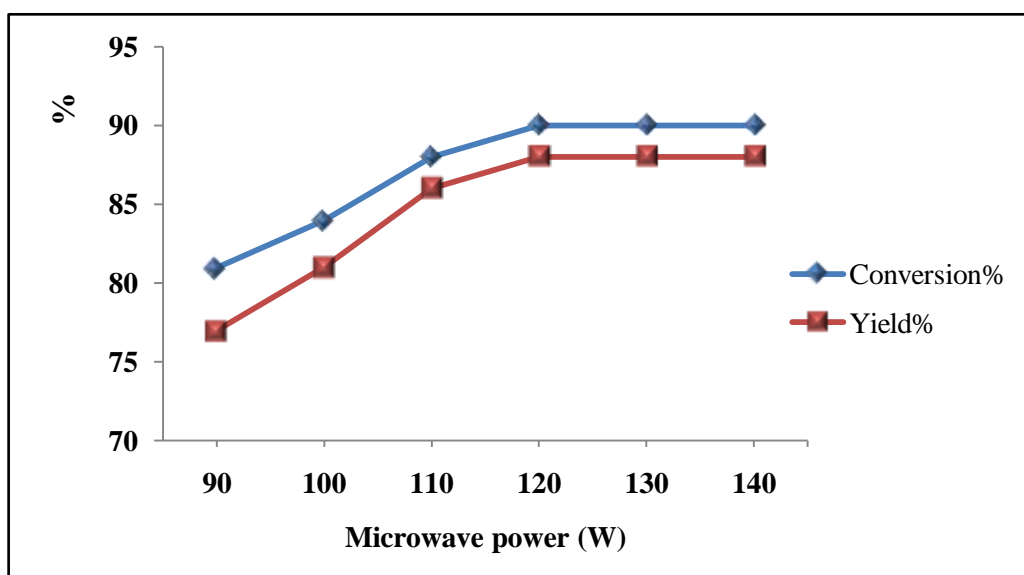


Figure 4.10: Variation of conversion% and yield% of microwave assisted 7-Hydroxy-4-methylcoumarin synthesis with microwave power

Reaction conditions: Temperature = 140°C; Time = 15 min; Pr = 40 psi; resorcinol / EAA = 1:2; resorcinol / NBF catalyst ratio = 5:1 and P = 120W with P_{max} = ON.

4.4.4 Effect of resorcinol to EAA molar ratio

Molar ratio of resorcinol to EAA molar ratio was varied from 2:1 to 1:3 given in **Table 4.4**. With resorcinol to EAA molar ratio of 2:1, better conversion and yield was not observed due to hindrance in stirring during course of reaction. With increase in molar ratio to 1:1, increment in conversion and yield was observed. Maximum 92% conversion was achieved with molar ratio of 1:2 having sufficient amount of reactants to get 88% yield of 7-Hydroxy-4-methylcoumarin as product. On using molar ratio of 1:3, observed decrease in product yield was noticed due to enhanced adsorption of EAA on active sites of the catalyst causing blockage of acid adsorption centers. Thus, competitive adsorption of EAA on acid sites with resorcinol reduced the efficiency of the catalyst [42].

Table 4.4: Effect of resorcinol to EAA molar ratio on conversion% of resorcinol and yield% of 7-Hydroxy-4-methylcoumarin

Resorcinol to EAA molar ratio	Conversion% of resorcinol	Yield% of 7-Hydroxy-4-methylcoumarin
2:1	49	42
1:1	87	76
1:2	92	88
1:3	39	35

Reaction conditions: Temperature = 140°C; Time = 15 min; Pr = 40 psi; resorcinol / NBF catalyst ratio = 5:1 and P = 120W with P_{max} = ON.

4.4.5 Effect of resorcinol to NBF-10 catalyst weight ratio

To determine the maximum efficiency of catalyst with adequate quantity, resorcinol to NBF-10 catalyst weight ratio was varied maintaining other reaction parameters same as earlier (**Table 4.5**). Yield of 7-Hydroxy-4-methylcoumarin was increased with catalyst weight ratio. Maximum 92% conversion and 88% yield of 7-Hydroxy-4-methylcoumarin was achieved at 5:1 due to availability of sufficient amount of Brönsted acid sites. Yield% of coumarins remained unaffected on further increase in resorcinol to NBF-10 catalyst weight ratio to 2.5:1.

Table 4.5: Effect of resorcinol to NBF-10 catalyst weight ratio on conversion% of resorcinol and yield% of 7-Hydroxy-4-methylcoumarin

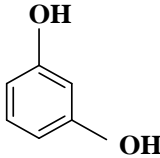
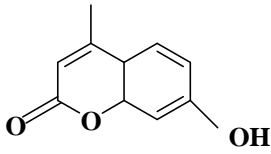
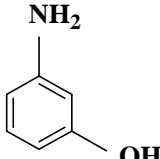
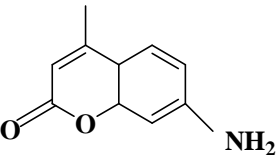
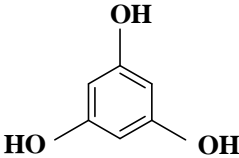
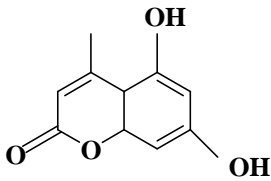
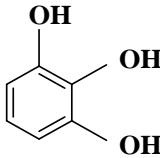
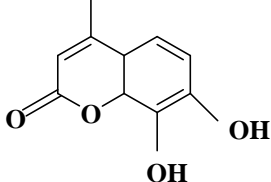
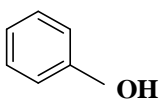
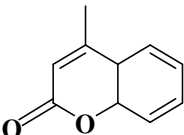
Resorcinol to NBF-10 catalyst weight ratio	Conversion% of resorcinol	Yield% of 7-Hydroxy-4-methylcoumarin
10:1	84	76
5:1	92	88
2.5:1	92	88

Reaction conditions: Temperature = 140°C; Time = 15 min; Pr = 40 psi; resorcinol / EAA = 1:2 and P = 120W with P_{max} = ON.

4.4.6 Effect of substituent groups on phenol substrate

Effect of substituent groups on the yield% of 7-Hydroxy-4-methylcoumarin synthesis under dielectric heating is displayed in **Table 4.6**.

Table 4.6: Synthesis of 4-methylcoumarin derivatives under microwave heating conditions catalyzed by NBF-10 catalyst

Entry	R-CHO	Product	Time (min)	Yield%
1			15	88
2			12	94
3			12	91
4			18	86
5			20	68

It is evident that the yield of corresponding coumarins is greatly affected by the presence of activated group and their position in phenol ring. m-amino phenol (**Entry 2**) gave the highest yield due to better activation of the aromatic ring. Pyrrogallol (**Entry 4**) gave lesser yield than that of phloroglucinol (**Entry 3**) even then both substrates have two electron donating hydroxyl groups but the activation of aromatic ring is better in phloroglucinol with two hydroxyl groups at meta-positions than that of one hydroxyl group at ortho-positions positions in pyrrogallol. The decrease in the strength of the ring activating group also affected activity of the substrate. Amongst substituted phenols studied here phenol was least reactive (**Entry 5**).

4.4.7 Comparison with other reported catalyst

As depicted from **Table 4.7**, fly ash supported niobia catalyst (NBF-10) has given better yield of xanthene compound than some earlier reported commercial catalysts.

Table 4.7: Comparative study of catalytic potential of STF-16 catalyst with other reported catalysts for the synthesis of 7-hydroxy-4-methylcoumain under microwave irradiation

Catalyst	Temperature (°C)	Time (min)	Yield %	Reference
12-TPA/TiO ₂	130	30	71.8	[43]
NBF-10	140	15	88	Present work

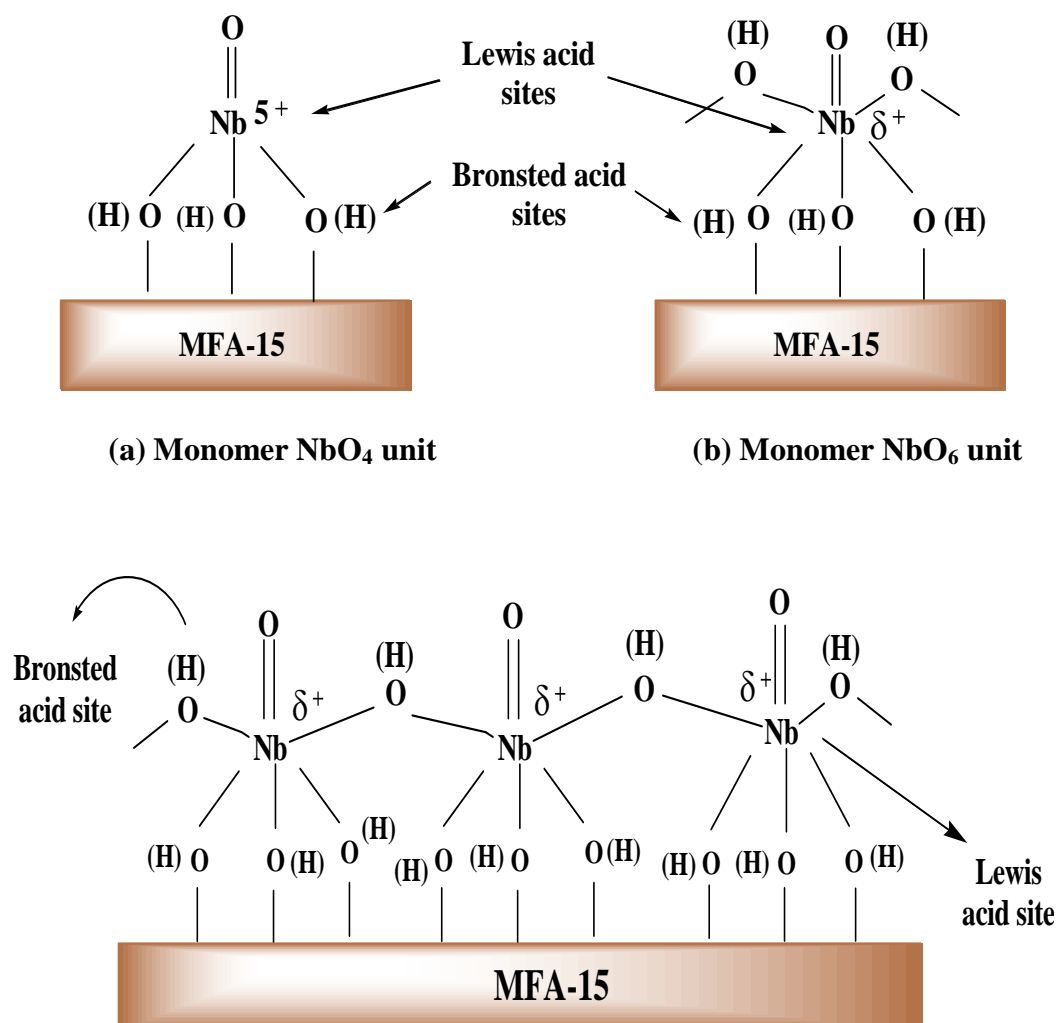
4.5 Mechanistic aspects

The proposed model structure of NBF catalysts are shown in **Scheme 4.3**. XRD, FTIR and DR UV-vis studies have revealed the formation of monomeric, polymeric and nanocrystalline niobia units over the MFA-15 surface with increase in Nb content. In NBF-2 catalyst, niobia species are dispersed on fly ash support through monomeric isolated species with NbO₄ units along with dispersed isolated NbO₆ units through Nb-O-Si linkages. With increase in Nb concentration to 5 wt.%, interaction of isolated niobia species with their nearest neighbours formed polymeric units of NbO₆ species through bridging Nb-O-Nb bonds by

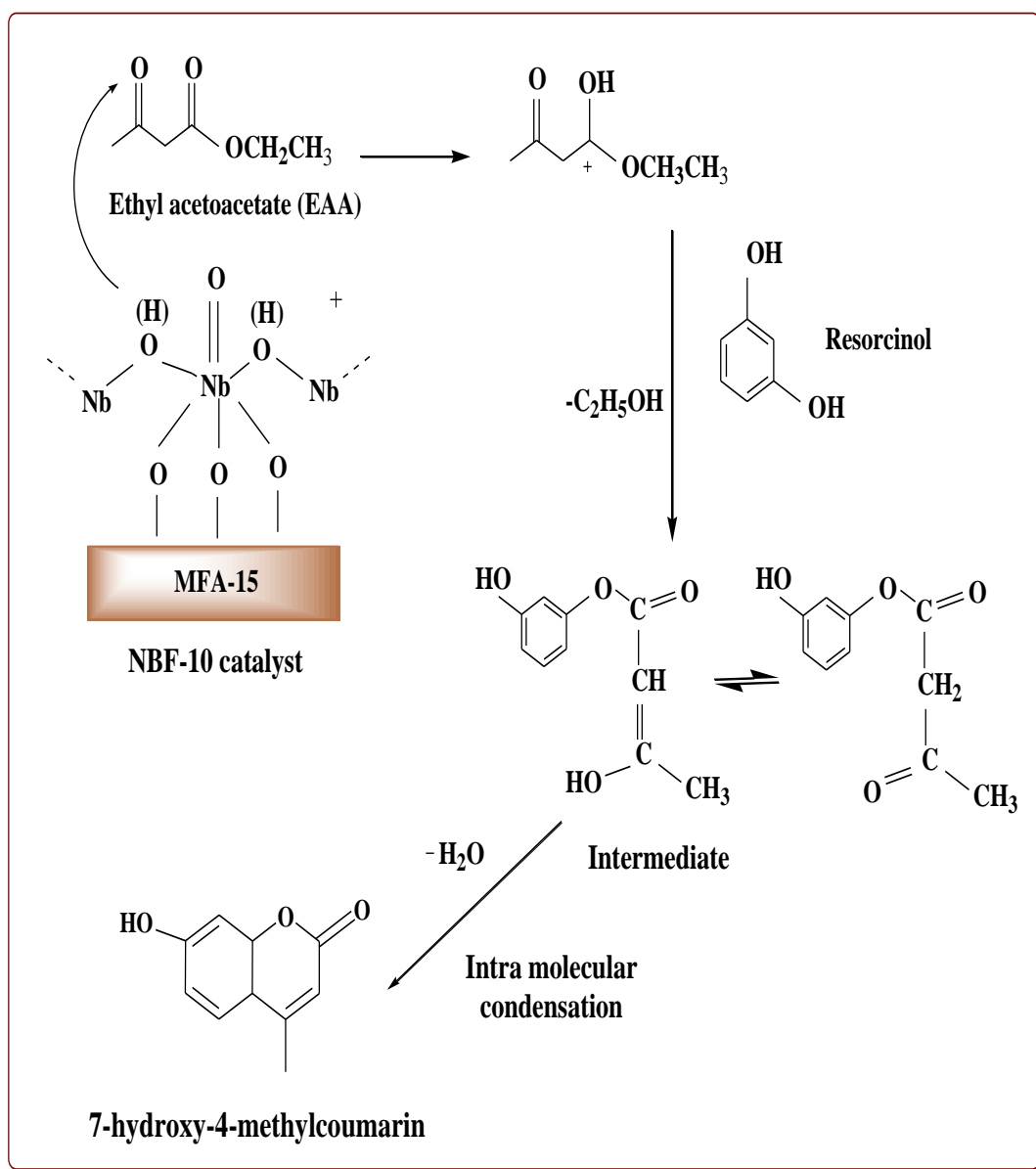
accumulating Nb-O-Si bond [44]. In NBF-10 catalyst, population of Nb-O-Nb bridge bonds increases well with increase in Nb content that led to the formation of nano crystalline Nb₂O₅ units. These nanocrystalline species along with polymeric NBO₆ and NBO₄ species have formed monolayer coverage over fly ash surface.

Presence of excess of effective positive charge (+5) on NbO₄ and NbO₆ (highly distorted octahedral) unit having Nb^{δ+} ion generates Lewis acid sites [40] while Brönsted acid sites are originated from Nb-OH-Nb (slightly distorted octahedral) and Nb-(OH)-Si bonds [45]. It is considered that Pechmann condensation reaction is very much depends upon the Brönsted acid sites of the catalyst [46], the bridged Nb-OH-Nb containing hydrogen produces better catalytic activity than Nb-OH-Si bonds which has also been confirmed by more yield% over NBF-10 catalyst compared to NBF-2 catalyst and finds good similarity with earlier reported work [44].

Pechmann condensation for synthesis of 7-hydroxy-4-methylcoumarin has been proposed by two mechanistic pathways. One is reported as on the Brönsted acid sites of NBF-10 catalyst chemisorption of ethyl acetoacetate (EAA) takes place and nucleophilic attack of resorcinol on it generates an intermediate and ethanol as side product. The formed intermediate rapidly undergoes cyclization via. intramolecular condensation and yielded 7-hydroxy-4-methylcoumarin with water as side product. Electrophilic reaction of chemisorbed EAA on resorcinol is ruled out due to not formation of chromones as side product and the mechanism proposed by Sudha et al. [47]. Use of microwave active reactants i.e. phenolic substrates and ethyl acetoacetate facilitated the reaction towards better product yield in less time. Possessing good microwave absorption capacity, the ethanol and water molecules generated as side products also helped to maintain Brönsted acid sites in NBF catalyst during the reaction (**Scheme 4.3**) to produce good yield of 7-hydroxy-4-methylcoumarin. Thus, use of microwaves as a heating source has made whole process energy, time and atom efficient. The plausible mechanism for the formation of 7-hydroxy-4-methylcoumarin has been illustrated in **Scheme 4.4**.



Scheme 4.3: Proposed structure of (a) monomeric tetrahedral NbO_4 units (b) isolated octahedral NbO_6 units (c) polymerized niobyl forms with Nb-O-Nb bridging bonds with Lewis (highly distorted) and Brönsted (slightly distorted) forms



Scheme 4.4: Proposed mechanistic pathway of microwave assisted synthesis of 7-hydroxy-4-methylcoumarin over NBF-10 catalyst

4.6 Regeneration and reusability of NBF-10 catalyst

The spent catalyst extracted from reaction cycle was filtered, washed and thermally regenerated by calcining at 450°C for 1 h. After regeneration NBF-10 catalyst was efficiently used upto four reaction cycles with conversion 87-77% and yield in the range of 85-72% respectively (**Figure 4.11**) under microwave assisted conditions signifying the stability of Brönsted acid sites during regeneration and during course of the reaction. After fourth reaction cycle, the observed decrease in conversion and yield of 7-Hydroxy-4-methylcoumarin was noticed due to physical adsorption of carbonaceous materials which blocked the active catalytic sites [48]. As shown in **Figure 4.12**, the resemblance in the FTIR spectrum of fresh NBF-10 and regenerated NBF-10 catalyst signifies the presence of niobyl species and with no change in chemical composition of catalyst surface. Sheldon hot filtration test was also performed by removal of NBF-10 catalyst during the course of reaction. This test was found negative as reaction didn't proceed further after catalyst removal, which confirmed the stability, heterogeneity and non-leaching ability of Nb species loaded on MFA-15 support [48]. Thus, NBF-10 catalyst possesses stable acidic sites which remained conserved and active during the microwave assisted synthesis of 7-Hydroxy-4-methylcoumarin under solvent-free conditions.

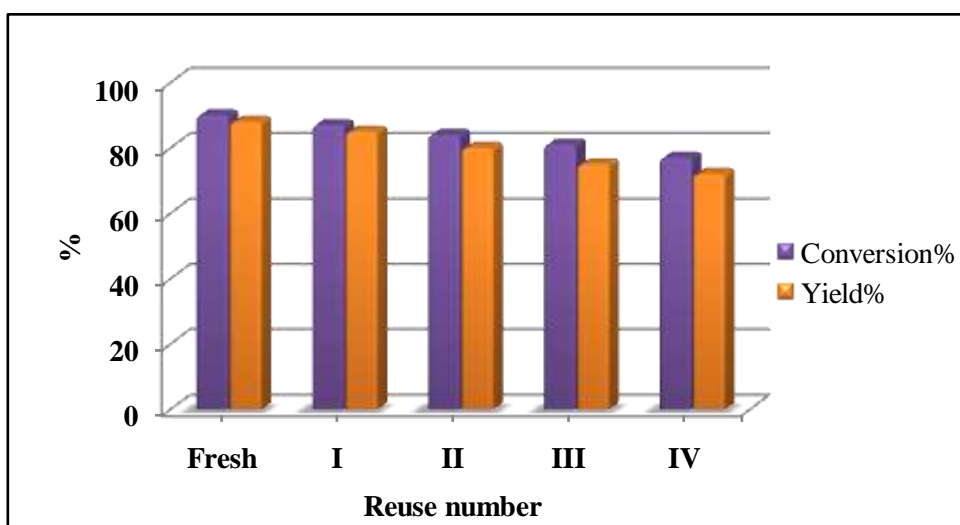


Figure 4.11: Reusability of NBF-10 catalyst for microwave assisted 7-Hydroxy-4-methylcoumarin synthesis

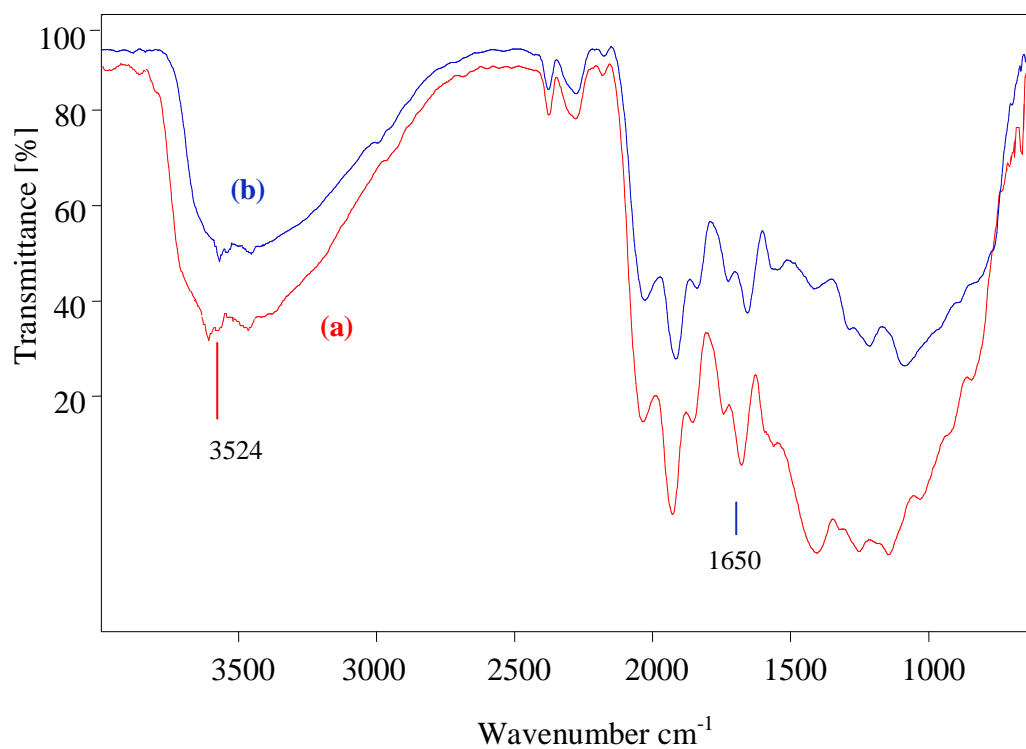


Figure 4.12: FTIR spectra (a) NBF-10 and (b) regenerated NBF-10 catalyst

4.7 Product identification

Product identification of 7-Hydroxy-4-methylcoumarin is done by melting point analysis, ^1H NMR and FTIR techniques:

m.p.: 185-187°C; **^1H NMR:** δ , 2.61 (s, 3H, CH_3) 6.18 (s, 1H), 6.68 (d, 1H), 6.76-6.81 (dd, 1H), 7.54 (d, 1H), 10.51 (s, 1H, -OH); **FTIR (cm^{-1}):** 3162, 2912, 1677, 1232, 1070, 786

4.8 Conclusion

Niobium is a minor constituent of fly ash present in trace amount. By enhancing the Nb content in fly ash an active, reusable and thermally stable solid acid catalyst has been synthesized via impregnation method. With increasing niobium amount to 10 wt.%, formation of nano-crystalline niobia species were noticed along with polymeric NBO_6 and NbO_4 units in the form of monolayer coverage over surface of milled fly ash. Increasing intensity of bands corresponding to Brönsted and Lewis acid sites in NBF samples confirmed the enhancement of acidity with increasing Nb wt.%. Possessing active acid centers, NBF-10 catalyst efficiently catalyzed microwave assisted, solvent-free synthesis of 7-hydroxy-4-methylcoumarin with 92% conversion and 88% yield. Catalyst was able to conserve acid sites after thermal activation and gave four reaction cycles with remarkable conversion and product yield. Thus, present work provides simple methodology to synthesize niobium oxide loaded fly ash as a new solid acid catalyst with stable acidic sites. Use of microwave heating and solvent-free conditions instead of using organic solvents makes the whole process in accordance with green chemistry principles.

4.9 References

- [1] D.M.young, J.J.C. Welker, K.M. Doxsee, *J. Chem. Edu.* 88 (2011) 319-321.
- [2] D. Bogdal, *J. Chem. Res.* (1988) 468-469.
- [3] M.M. Peng, P. Hemalatha, M. Ganesh, M. Palanichamy H.T. Jang, *J. Ind. Eng. Chem.* 20 (2014) 953-960.
- [4] S.M. Sethna, N.P. Kong, *Chem. Rev.* 36 (1945) 1.
- [5] B. Tyagi, M.K. Mishra, R.V. Jasra, *J. Mol. Catal. A: Chem.* 276 (2007) 47-56.
- [6] H. Von Pechmann, C. Duisberg, *Chem. Ber.* 17 (1884) 929.
- [7] G. Jones, *Org. React.* 15 (1967) 204-599.
- [8] J.R. Johnson, *Org. React.* 1 (1942) 210.
- [9] R.L. Shriner, *Org. React.* 1 (1942) 1.
- [10] N.S. Narasimahan, R.S. Mali, M.V. Barve, *Synthesis* (1979) 906.
- [11] N.Cairns, L.M. Harwood, D.P. Astles, *J. Chem. Soc. Perkin Trans.* 1 (1994) 3101.
- [12] H. von Pechmann, C. Duisberg, *Chem. Ber.* 16 (1883) 2119.
- [13] E.C. Horning, *Organic Synthesis III*, Wiley, New York, NY, 1955.
- [14] L.L. Woods, J. Sapp., *J. Org. Chem.* 27 (1962) 3703-3705.
- [15] H. Simmonis, P. Remmert, *Chem. Ber.* 47 (1914) 2229.
- [16] T.V. Nguyen, S. Debendetti, N. De Kimpe, *Tetrahedron Lett.* 44 (2003) 4199-4201.
- [17] M.K. Potdur, S.S. Mohile, M.M. Salunkhe, *Tetrahedron Lett.* 42 (2001) 9285.
- [18] A.D. Hoz, M. Andres, E. Vazquez, *Synlett.* (1999) 602-608.

- [19] D. Prasetyoko, Z. Ramil, S. Endud, H. Nur, *Adv. Mater. Sci. Eng.* Volume (2008) 1-12.
- [20] V.S. Braga, F.A.C. Gracia, J.A. Dias, S.C.L. Dias, *J. Catal.* 247 (2007) 68-77.
- [21] R.M. West, D.J. Braden, J.A. Dumesic, *J. Catal.* 262 (2009) 134-143.
- [22] M. Paulis, M. Martín, D.B. Soria, A. Díaz, J.A. Odriozola, M. Montes, *Appl. Catal. A: Gen.* 180 (1999) 411-420.
- [23] K. Srilatha, N. Lingaiah, P.S. Prasad, B.L.A. Prabhavati, R.B.N. Prasad, S. Venkateswar, *Ind. Eng. Chem. Res.* 48 (2009) 10816-10819.
- [24] L.C.A. Oliveira, M.F. Portilho, A.C. Silva, *Appl. Catal. B: Environ.* 117-118 (2012) 29-35.
- [25] C. García-sancho, R. Monero-Tost, J.M. Merída-Robles, J. Santanarúa-González, A. Jimenez-Lopez, P. Matres-Torres, *Appl. Catal. B: Environ.* 108-109 (2011) 161-167.
- [26] F. Hashenmzadeh, A. Gaffarinejad, R. Rahimi, *J. Hazard. Mater.* 285 (2015) 64-74.
- [27] J. M. Jehang, I.E. Wachs, *Catal. Today* 16 (1993) 49-58.
- [28] K. Tanabe, in: *Catal. Sci. Technol.* (Eds. J.R. Anderson, M. Boudart), *Springer, Berlin*, 1987, 232-271.
- [29] N. Shringi, K. Srivastava, A. Rani, *Chem. Sci. Rev. Lett.* 4 (2015) 561-570.
- [30] V.S. Braga, I.C.L. Barros, F.A.C. Gracia, S.C.L. Dias, J.A. Dias. *Catal. Today* 133-135 (2008) 106-112.
- [31] A. Sharma, K. Srivastava, V. Devra, A. Rani, *Ame. Chem. Sci. J.* 2 (2012) 177-187.
- [32] A.G.S. Prado, L.B. Bolzon, C.P. Pedroso, A.O. Moura, L.L. Costa, *Appl. Catal. B: Environ.* 82 (2008) 219–224.

- [33] L.J. Burcham, J. Datka, I.E. Wachs, *J. Phy. Chem. B* 103 (1999) 6015-6024.
- [34] D. Stošića, S. Bennicia, V. Rakićb, A. Aurouxa, *Catal. Today* 192 (2012) 160-168.
- [35] Y. gushikem, S.S. Rosatto, *J. Braz. Chem. Soc.* 12 (2011) 695-705.
- [36] S. Damyanova, L. Dimitrov, L. Petrov, P. Grange, *Appl. Surf. Sci.* 214 (2003) 68-74.
- [37] L.J. Burcham, J. Datka, I.E. Wachs, *J. Phys. Chem. B* 103 (1999) 6015-6024.
- [38] T. Armoli, G. Busca, C. Carlini, M. Giuttari, A.M. R. Galleti, G. Sbrana, *J. Mol. Catal. A* 151 (2000) 233-243.
- [39] C. Tiozzo, C. Palumbo, R. Psaro, C. Bisio, F. Carniato, A. Gervasini, P. Carniti, M. Guidotti, *Inorg. Chim. Acta* 431 (2015) 190-196.
- [40] R. Turco, A. Aronne, P. Carniti, A. Gervasini, L. Minieri, P. Pernice, R. Tesser, R. Vitiello, M. Di Serio, *Catal. Today* 254 (2015) 99-103.
- [41] M. Anilkumar, W.F. Hoelderich, *Catal. Today* 198 (2012) 289-299.
- [42] A.I. Ahmed, S.A. El-Hakam, M.A. Abd Elghany, W.S. Abo El-Yazeed *Appl. Catal. A: Gen.* 407 (2011) 40-48.
- [43] U. Chudasama, S. Ghodke, *Inter. J. Sci. Res.* 4 (2015) 1933-1939.
- [44] J. He, Q-J. Li, Y-N. Fan, *J. Solid State Chem.* 202 (2013) 121-127.
- [45] J. He, Y.N. Fan, *Acta Phys. Chim. Sin.* 27 (2011) 2416-2420.
- [46] B.M. Reddy, M.K. Patil, P. Laskshman, *J. Mol. Catal. A: Chem.* 256 (2006) 290-294.
- [47] B.M. Reddy, M.K. Patil, P. Laskshman, *J. Mol. Catal. A: Chem.* 256 (2006) 290-294.
- [48] A. Rani, C. Khatri, R. Hada, *Fuel Process. Technol.* 116 (2013) 366-373.



Chapter-5

*Synthesis and characterization of
chemically activated perlite supported
tungsten oxide solid acid catalyst for
microwave assisted synthesis of ethyl
levulinate used as fuel additive*

ABSTRACT

Synthesis of chemically activated perlite supported tungsten oxide (PTO) catalyst has been reported using impregnation method. Thermal activation followed by chemical treatment of perlite under microwave heating was carried out to increase silica content, active sites for anchoring active metal oxide moieties and specific surface area of the support material. By varying amount of tungsten content from 2 to 20 wt.%, formation of different tungstate forms and their dispersion on perlite support was studied. With increase in tungsten content (PTO), increased amount of WO_3 crystallites was noticed that blocked the interaction of active sites and reactant molecules which resulted as decrease in conversion% of levulinic acid. PTO-10 catalyst with sufficient amount of Brönsted acid sites was able to catalyze microwave assisted solvent-free esterification for levulinate ester synthesis using Levulinic acid and alcohols under microwave heating conditions. Catalyst was also regenerated and reused upto five reaction cycles with similar efficiency as fresh run. Use of perlite with silica as major constituent can become a suitable substitute of commercially available silica. Synthesis of cost-effective, efficient and reusable solid acid catalyst along with energy and time saving synthesis of fuel additive, levunilate ester makes good agreement with the protocols of green chemistry.

5.1 Introduction

The inevitable depletion of petroleum sources has driven global concern to use and promote natural resources based renewable biofuels and feedstock chemicals in recent years [1]. Amongst these chemicals, levulinic acid (LA) or gamma-ketovaleic acid has been considered as one of the top twelve building blocks to produce a spectrum of fuel additive and also in polymer and resins [2]. It is commercially produced from biomass such as cane sugar, starch, and lignocellulosic materials from agricultural wastes. Levulinate esters such as ethyl, methyl, n-butyl levulinates are produced by esterification of LA with fuel-grade alcohols [3]. In particular, ethyl levulinate (EL) has oxygen content 33% and possess similar properties to biodiesel fatty acid methyl esters (FAME). So it can be used upto 5 wt.% as the diesel miscible biofuel (DMB) which improves the fuel characteristics such as stability in flash point, reduction in sulfur content, viscosity and burning of fuel with high lubricity [4]. Traditionally, EL was synthesized by using inorganic liquid acids such as H_2SO_4 , HCl , H_3PO_4 etc. but environmental problems such disposal, handling, corrosive nature and non-reusability to substitute them with industrially greener solid acid catalysts. Recently, synthesis of EL was reported over UDCaT-5 catalyst [5], sulfonic mesostructured silicas [6], immobilized *Candida Antarctica* lipase B (Novozym 435) [7], dodecatungstophosphoric acid supported on desilicated H-ZSM-5 [3], sulfated mesoporous zirconosilicates [8], sulfated Si-doped ZrO_2 [9], sulfonated carbon nanotubes [10] etc. But poor reusability, use of expensive reagents and harsh conditions are still remaining area of further research. Recently, EL are also synthesized under microwave assisted conditions using $\text{Al}_2(\text{SO}_4)_3$ catalyst and have produced 99.4% yield within 10 min at 110°C [11].

In the field of heterogeneous catalysis, supported tungsten-oxo-species (tungstate) are best known for their catalytic activities for esterification [12], alkylation [13], Synthesis of 1,8-octahydroxanthene derivatives [14], furfural synthesis [15], oxidation reaction [16], petroleum and pollution control problems [17,18] etc. However, catalytic activity is strongly influenced by the interaction of tungsten oxides domains with support, WO_x precursor and content as well as

thermal history of these support materials [19]. At low tungsten content Lewis acid sites are found due to monomeric tetrahedral forms with low surface coverage while with increase in tungsten content, Brönsted acid sites are present due to predominance of polytungstate species with W-O-W modes. Further increment in tungsten amount formation of crystallites on the top of tungstate monolayer surface led to decrease in interaction of reactants and active sites [20].

This chapter describes the synthesis of activated perlite supported tungsten oxide (PTO) catalyst for the microwave assisted solvent-free esterification reaction. The tungsten amount was varied to determine the dispersion of tungstate domains over perlite support. Prior to use as a catalytic support, perlite was chemically activated under microwave heating to improve its silica amount and specific surface area. The tungsten amount was varied to determine the dispersion of tungstate domains over chemically activated perlite support. The prepared samples were characterized by various characterization techniques to determine their structural, textural and morphological characteristics. PTO catalysts efficiently catalyzed the esterification reaction under microwave assisted conditions and produced similar conversion performance as fresh run upto five reaction cycles. Thus, the present research work describes the novel use of perlite in field of heterogeneous catalysis for industrial important synthetic applications.

5.2 Experimental details

5.2.1 Materials and reagents

Perlite (volcanic ash) was supplied by Indica Chemical Industries Pvt. Ltd. Kotdwar, India. Ammonium metatungstate hydrate $((\text{NH}_4)_6\text{H}_2\text{W}_{12}\text{O}_{39} \cdot x\text{H}_2\text{O})$ was purchased from Alfa Aesar and HClO_4 , levulinic acid and ethanol were purchased from Loba Chemie.

5.2.2 Catalyst synthesis

Raw perlite (RP) was thermally activated at 800°C for 3 h and labeled as thermally activated perlite (TAP). 10 gm of TAP was chemically activated using 5N HClO_4 under open vessel system of microwave synthesis system CEM (model

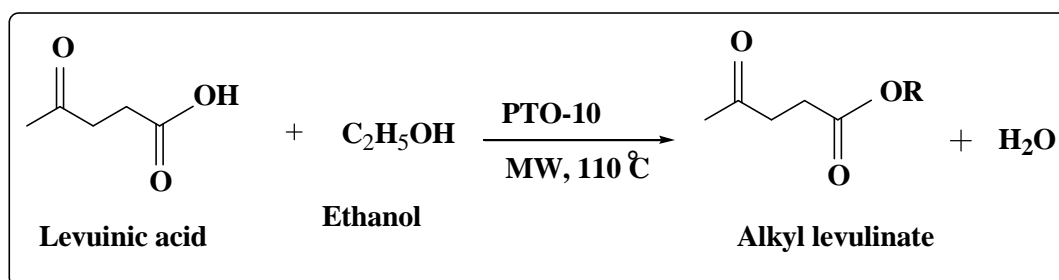
Discover) at 90°C for 60 min following the all stages as described in **Chapter 2**. The resulted slurry was filtered and washed with deionized water to remove perchlorate ion. Washed sample was dried in oven at 110°C for 24 h and calcined at 500°C for 4 h. Prepared sample was denoted as chemically activated perlite (CP) and used as support material for the synthesis of perlite supported tungsten oxide catalyst using incipient wetness impregnation method. Requisite amount of ammonium metatungstate (for 2 wt.%, 10 wt.% and for 20 wt.%) was dissolved in distilled water and added into 6 g of CP with constant stirring. This slurry was stirred for 24 h and then dried in oven at 110°C for 24 h. The resulted solid was calcined at 550°C for 6 h in a tubular muffle furnace under static conditions (**Scheme 5.1**) and denoted as perlite supported tungsten oxide (PTO-x, where represents 2, 10 and 20 wt.% content).

5.2.3 Catalyst characterization

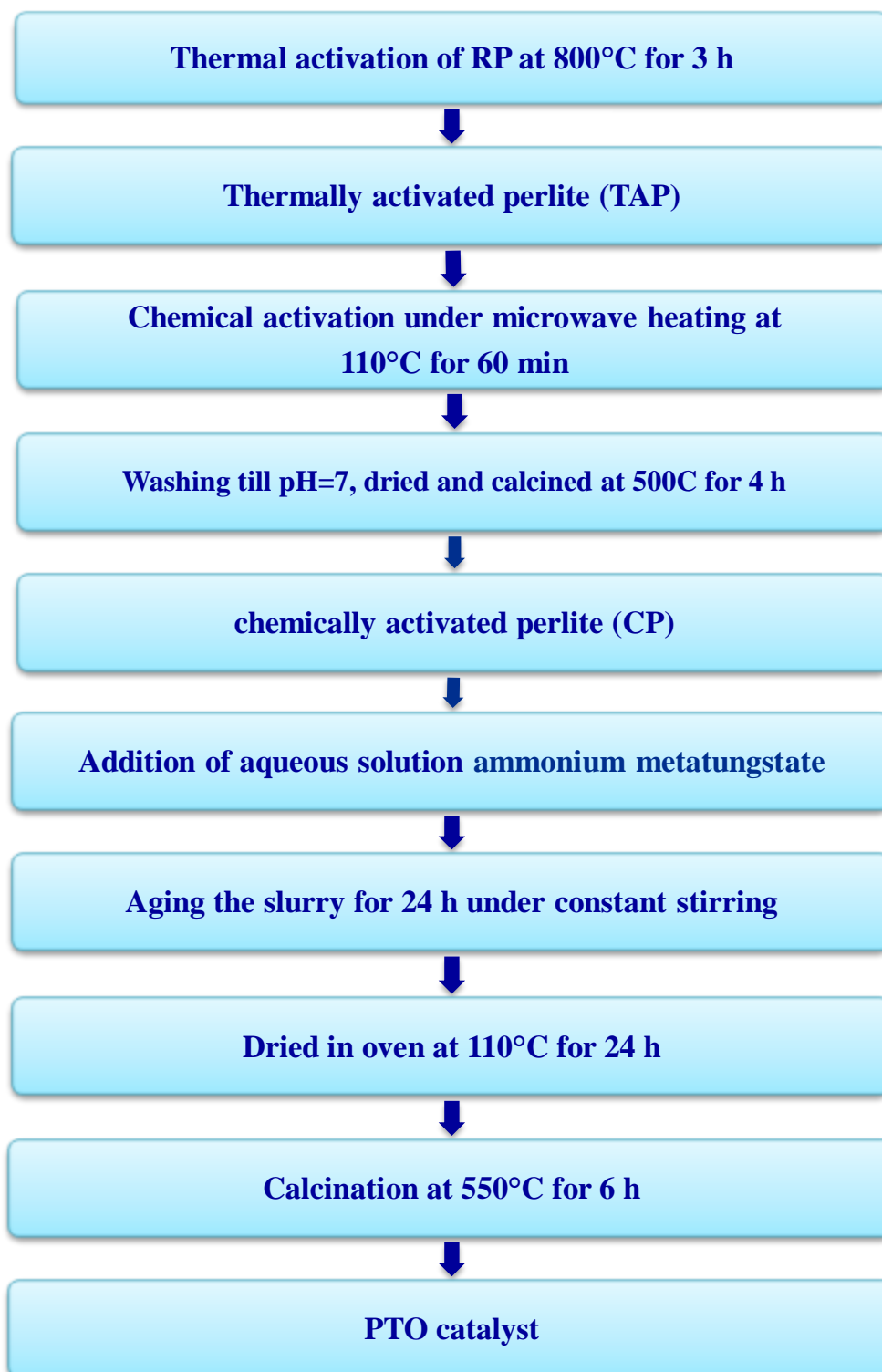
Physico-chemical properties of the synthesized PTO catalysts were analyzed various techniques such as N₂ adsorption-desorption, X-ray diffraction, FTIR, pyridine FTIR, DR UV-Vis, SEM-EDS and TGA as illustrated in **Annexure I**.

5.2.4 Catalytic performance of PTO catalysts

Evaluation of the catalytic activity of the prepared PTO catalysts was performed by microwave assisted esterification as shown in **Scheme 5.2**.



Scheme 5.2: Schematic representation of microwave assisted solvent-free esterification for synthesis of alkyl levulinate over PTO-10 catalyst



Scheme 5.1: Synthesis of activated perlite supported tungsten oxide (PTO) catalyst

In the typical procedure, levulinic acid (LA) (10 mmol) and ethanol (30 mmol) in 1:3 molar ratio with PTO catalyst in LA to PTO ratio=5:1 were filled in 10 ml pyrex glass vial. Before adding into reaction mixture, prepared PTO catalyst was activated for 1 h at 450°C in muffle furnace. The reaction was carried out at 110°C, 40 psi pressure, 100W power with P_{\max} feature at medium stirring mode for 15 min in closed vessel system of CEM (model Discover) microwave synthesis system following the all stages of ramping, holding and cooling as described in **Chapter 2**. In the resulted mixture petroleum ether was added to remove unreacted reactant and filtered to separate out the catalyst. To achieve maximum LA conversion and selectivity of the ethyl levulinate, reaction parameters were optimized. The analysis of LA conversion was carried out by Gas chromatograph. The conversion of LA and selectivity of ethyl levulinate was calculated as outlined below:

$$\text{Conversion (\%)} = \frac{(\text{Initial wt \%} - \text{Final wt \%})}{\text{Initial wt \%}}$$

$$\text{Selectivity (\%)} \text{ of ethyl levulinate} = \frac{(\text{GC peak area \% of alkyl levulinate product})}{\text{Sum of total peak area \% for all products}}$$

After extracted from fresh run, the obtained catalyst was washed thoroughly with acetone and dried in oven at 110°C for 12 h followed by activation at 450°C for 1 h in muffle furnace. Thus, the regenerated catalyst was ready to use for next reaction cycle maintaining the same reaction conditions as earlier.

5.3 Results and discussion

Table 5.1 summarizes the physico-chemical attributes of RP, TAP and CP before and after thermal and chemical activation. Raw perlite (RP) with 73.9% silica content and 5 m²/g surface area possess light grey colour due to the presence of carbon particles and small amount of other elements. On calcination at 800°C for 3 h, light grey colour of RP changed into light pink due to removal of moisture, few metals, sulfur impurities and other organic matter that led to

increase in silica and alumina percentage [21]. Surface area was also reduced to $4\text{m}^2/\text{g}$ after thermal activation. In chemically activated perlite (CP), the silica content and surface area was increased due to leaching of crystalline phases and metal impurities such as Fe, Zn and Ti etc [22]. On increasing tungsten loading from 2 to 20 wt.% reduction in surface area was noticed due to the blockage of the pores of support material after incorporation of tungstate species by impregnation method.

Table 5.1: The physico-chemical attributes of perlite before and after thermal, chemical activation and after tungsten loading

Samples	SiO ₂ (wt.%)	W content (wt.%)	Specific surface area (m ² /g)
RP	73.9	0.0	5
TAP	74.3	0.0	4
CP	82.6	0.0	9
PTO-2	82.6	1.4	8
PTO-10	82.6	7.3	7
PTO-20	82.6	15.6	5

The structural changes in perlite before and after thermal and microwave assisted chemical activation were illustrated by X-ray diffraction patterns as shown in **Figure 5.1 (a-c)**. Broad XRD pattern of raw perlite (RP) confirms the absence of any ordered crystalline structure [23] which is typical for amorphous solids. Amorphous substances show an atomic arrangement that is either random or short range order. Although TAP possess highly ordered structure with a single crystalline peak at $2\theta = 27.62^\circ$ due to presence of tridymite (polymorphs of quartz) phase (JCPDS No. 42-1401). A broad hump spread between $15-35^\circ$ is characteristic of amorphous nature of silica [24]. The presence of crystalline, amorphous or both the phases are related to the calcination temperature or the

method of sample attainment [25]. On chemical activation under microwave heating silica content was increased (**Figure 5.1c**) due to partial destruction of silico-aluminate components as reported earlier [26]. Resemblance in basic skeleton of raw perlite and chemically activated sample evidenced that microwave heating has not altered the basic silica framework.

The XRD patterns of PTO catalysts are given in **Figure 5.2 (b-d)**. The XRD pattern of PTO-20 has shown sharp peaks at $2\theta = 23.1^\circ, 27^\circ, 29^\circ, 33.29^\circ, 34.1^\circ, 42^\circ, 48^\circ$ corresponding to monoclinic WO_3 crystallites on fly ash surface [27]. The splitting of broad peak at 23.1° into $23.3, 23.5$ and 24.2° peaks also evidenced the crystalline formation [16]. In case of PTO-10 wt.% the intensity of these peaks was reduced while in PTO-2 dominance of amorphous content over crystalline form was observed. Appearance of amorphous content indicated that the tungsten species are homogeneously dispersed in silica framework of MFA-15 while with increase in tungsten content prominent WO_3 crystalline form was observed [13]. The structure of WO_3 is influenced by calcination temperature and NH_4^+ content. As prepared samples were calcined at high temperature i.e. 550°C , the possibility of formation of remaining various phases such as hexagonal tungsten bronze (HATB) and tetragonal hydrogen tungsten bronze (THTB) is ruled out due to removal of residual ammonium cations occluded in these intermediate crystalline forms [28].

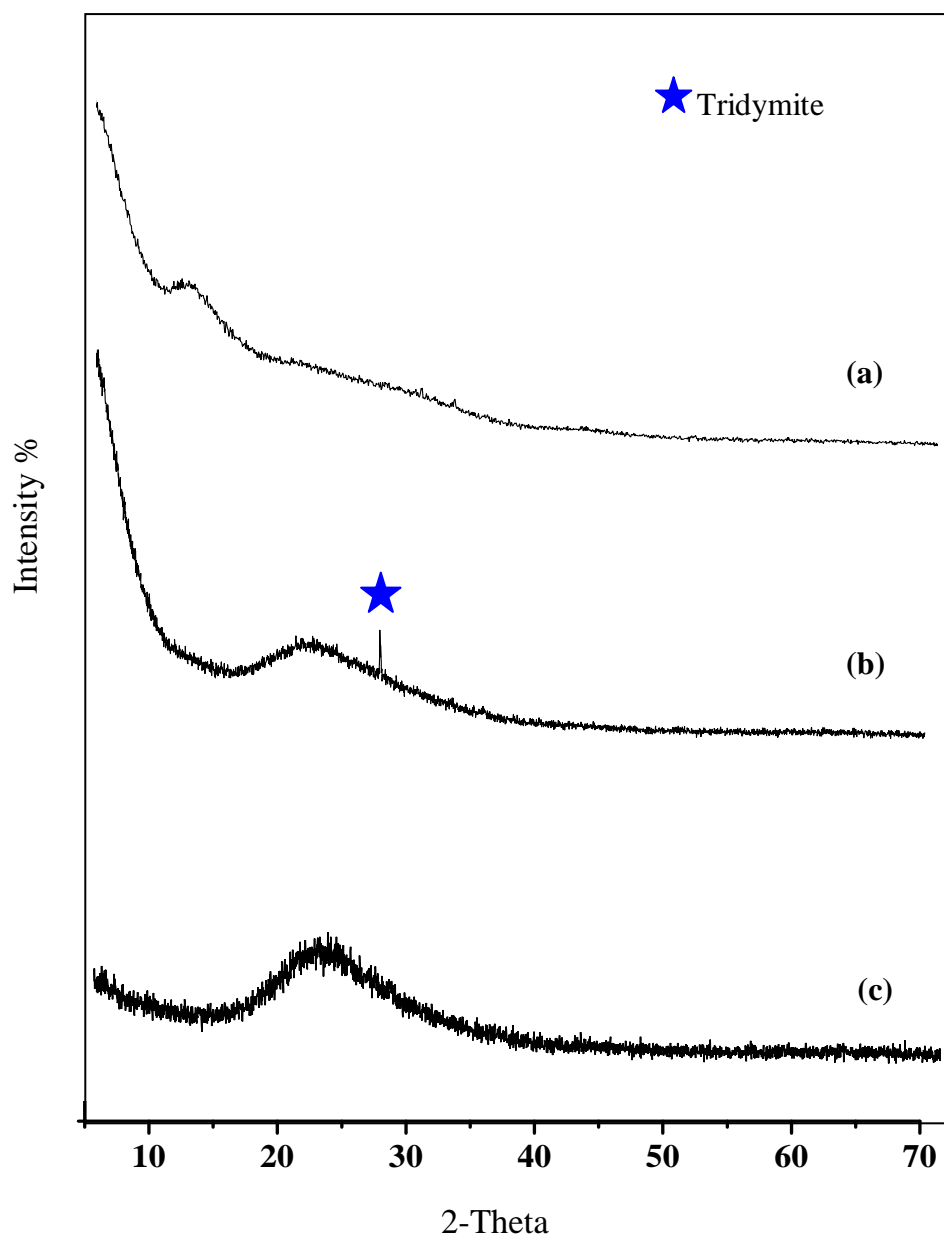


Figure 5.1: XRD patterns of (a) raw perlite (b) thermally activated perlite (TAP) and (c) chemically activated perlite (CP)

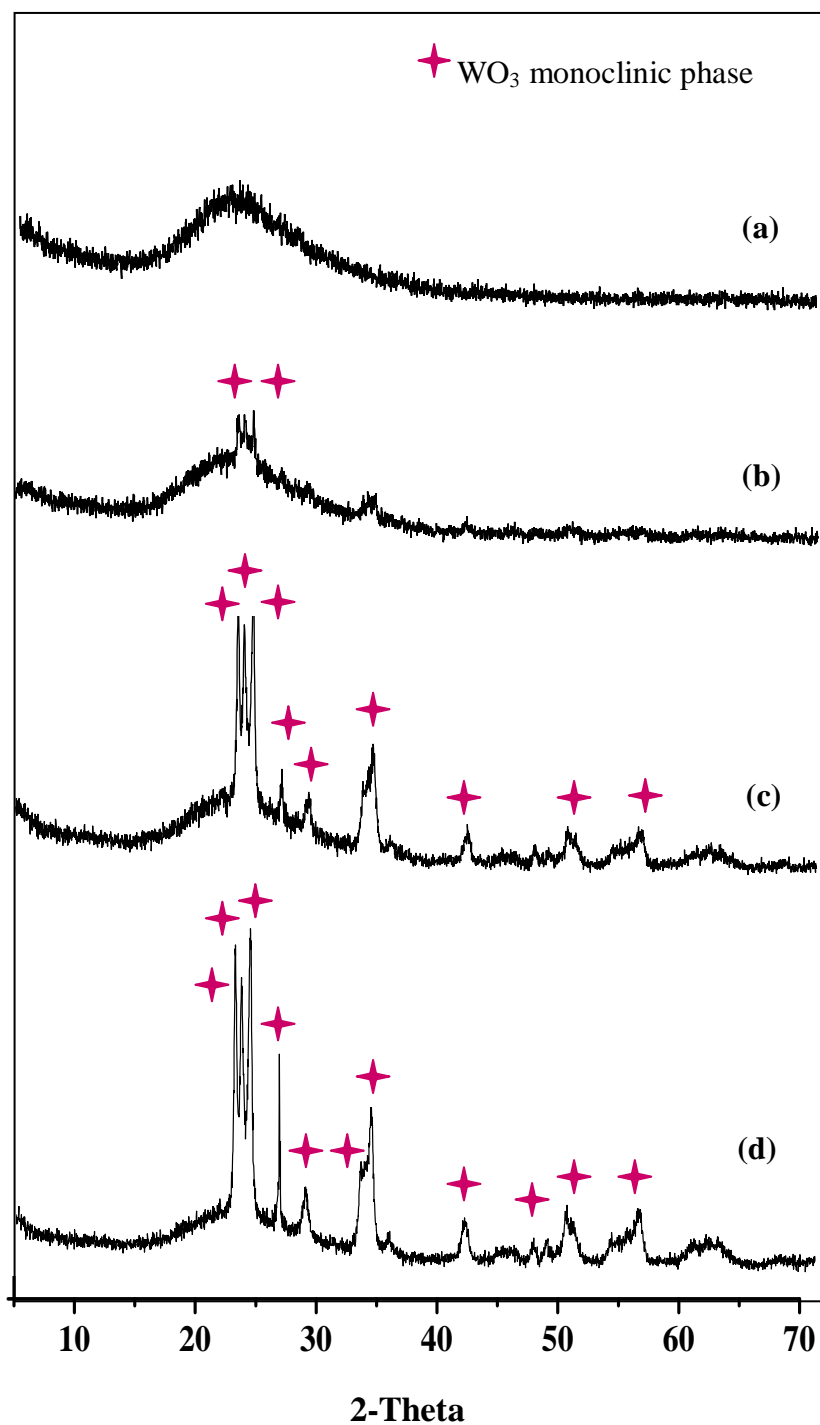


Figure 5.2: XRD patterns of (a) activated perlite (b) PTO-2 (c) PTO-10 and (d) PTO-20

The structural features of RP, TAP and CP are illustrated by FTIR spectra as given in **Figure 5.3**. A broad band observed between 3700 and 2800 cm^{-1} indicated stretching vibrations due to the presence of surface -OH groups and the adsorbed water molecules bound on silica surface. The bending mode of water molecule was shown by the peak observed at 1630 cm^{-1} [29]. After thermal treatment of RP at 800°C for 3 h, decreased the intensity of these peaks were observed. The peaks between 1200 and 1000 cm^{-1} are corresponding to asymmetric Si-O-Si stretching vibrations while band at 805 cm^{-1} ascribed to its symmetric stretching mode. In amorphous silica presence of a relatively strong peak at ~ 810 cm^{-1} distinguishes it from the band of crystalline silicate [30]. The intense peaks present in the range of 480-455 cm^{-1} are devoted to the Si-O asymmetric bending vibration of Si-O-Si bond. In FTIR of TAP, the intensity of these peaks have become more intense and moved towards higher wave number.

After chemical treatment, the broadness and intensity of the band at 3700-2800 cm^{-1} and 1630 cm^{-1} was observed indicating towards the increment in active surface Si-OH groups. Increment in the broadness in the band at 1200-1000 cm^{-1} also indicated towards increased amorphous silica content due partial dissolution of alumino-silicate structure under microwave heating. Hence, without affecting the basic skeleton of RP chemical activation under microwave heating has increased amorphous silica content and surface area which are essential requirements for the use of TAP as a catalytic support.

Figure 5.4 (a-d) shows the FTIR spectra of PTO catalysts with varying amounts of tungsten content. With increase in tungsten content from 2 to 20 wt.%, the broad band in the region 3700-2800 cm^{-1} was reduced due to consumption of surface -OH groups during tungstate-silica interactions. Complete removal of residual ammonium cations was evidenced by absence of the band at 1401 cm^{-1} [31]. The band observed at 3488 cm^{-1} and 3576 cm^{-1} indicated the presence of W-OH groups related to supported tungstate species and Si-OH groups respectively. The reduction in broadness of the band ascribed for Si-OH stretching vibrations

was noticed after inculcation of tungsten moieties due to consumption of hydroxyl groups in the tungstate-silica chemical interactions [32]. The band observed at 1168 cm^{-1} corresponding to Si-O-Si asymmetric vibrations in CP is shifted to lower wavenumber at 1162 , 1160 and 1156 cm^{-1} for PTO-2, 10 and 20 assigned to due to the formation of W-O-Si. In PTO-2 catalyst, the peak appeared at 1012 cm^{-1} corresponding to (W=O) stretching mode indicated the presence of mono-oxo-tungstates [33]. However, presence of small peaks appeared at 830 , 750 and 584 cm^{-1} ascribed to bridging W-O-W and W-O modes respectively indicated the presence of some polymeric forms along with few nanodomains of tungsten oxide which are uniformly dispersed over CP surface [34]. With increase in tungsten content to 10 wt.%, intense peaks appeared at 838 and 750 , 585 and 1016 cm^{-1} indicates the increasing quantity of polytungstates and some WO_3 crystallites, forming extra-framework structure over CP surface. While in PTO-20, presence of intense peaks 1020 , 844 , 755 and 588 cm^{-1} indicated the presence of polytungstates and bulk crystalline WO_3 species.

Insight study of nature of surface acid sites of CP and PTO catalysts was determined by pyridine probed FTIR technique. **Figure 5.5 (a-d)** have shown IR bands at 1450 , 1498 , 1550 , 1615 and 1650 cm^{-1} typical chemisorbed pyridine. The band at 1540 and 1650 cm^{-1} corresponds to pyridinium ion coordinated with Brönsted acid sites whereas 1445 cm^{-1} and 1615 cm^{-1} account for molecular pyridine coordinated to Lewis acid sites. Band at 1498 cm^{-1} is attributed to pyridine adsorbed over both Lewis and Brönsted acid sites. PTO catalysts have shown more intense bands as compared to CP signifying that tungstates have contributed to enhance surface acidity of perlite support. PTO catalysts possess Lewis acid sites due to W^{6+} (W=O) species while Brönsted acid sites due to W^{6+} -OH or W-O-W [35]. PTO-10 catalyst with predominance of polytungstates and WO_3 nano clusters possess OH groups associated with bridging W-O-W linkages are mainly responsible for generation of Brönsted acid sites whereas presence of W^{6+} species have contributed for Lewis acidity generation [31]. On increasing WO_x coverage over the CP surface to compensate the increasing charge density,

migration of ($H^{\delta+}$) protons takes place from W-O-W to neighbouring to WO_x domains which delocalizes electron charge density among several W^{6+} Lewis acid centres that leads to formation of $H^{\delta+}(WO_3)_n^{\delta-}$ active Brönsted site centers [36]. While in PTO-2 catalyst, lesser Brönsted acid sites are noticed possibly due to less charge delocalization over small amount of polymeric forms species having small domain size. In case of PTO-20 catalyst, decrease in Brönsted acid sites are observed due to increased amount of bulk WO_3 crystallites over other tungstate species. As reported earlier, increase in bulk WO_3 crystalline species forms $H^{\delta+}(WO_3)_n^{\delta-}$ or oxygen deficient WO_{3-x} species upon reduction by proton species. These species can't be reduced further to form O-H groups with Brönsted acid character. [35]. However, presence of Brönsted and Lewis acid character is still noticed in PTO-20 catalyst due to presence of polytungstates contributing in the formation of $H^{\delta+}(WO_3)_n^{\delta-}$ active Brönsted site centers and W^{6+} for Lewis acid sites over CP surface.

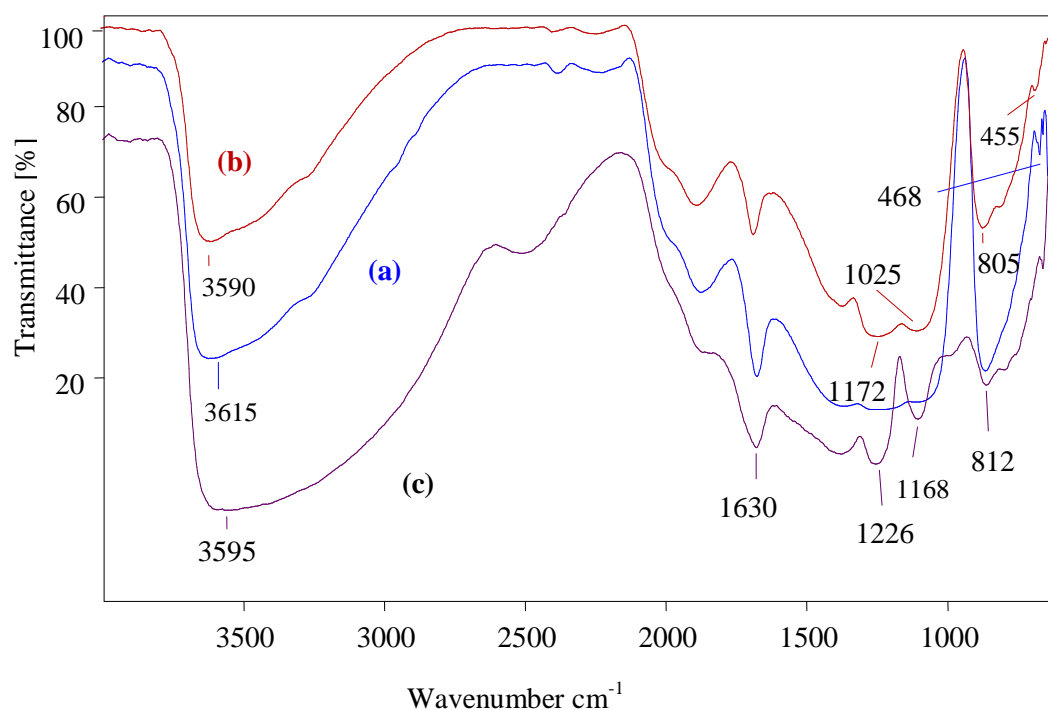


Figure 5.3: FTIR spectra of (a) RP (b) TAP and (c) CP

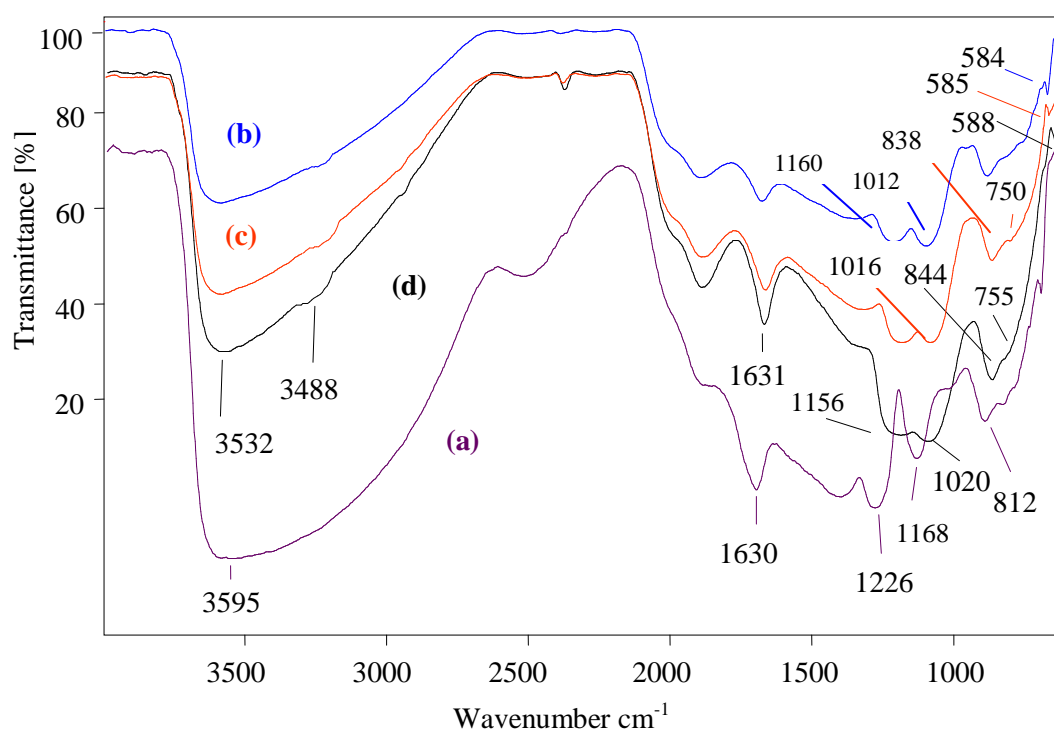


Figure 5.4: FTIR spectra of (a) CP (b) PTO-2 (c) PTO-10 and (d) PTO-20

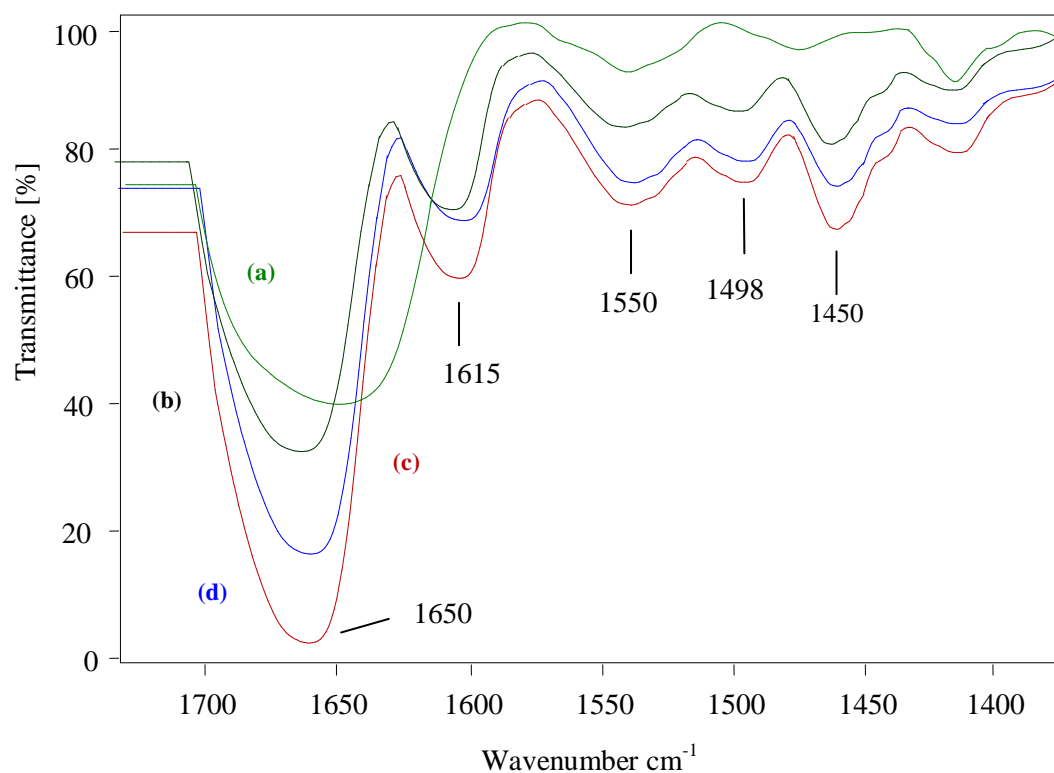


Figure 5.5: Pyridine FTIR of (a) CP (b) PTO-2 (c) PTO-10 and (d) PTO-20

UV-vis diffuse reflectance spectra of the PTO catalysts with different tungsten loading are shown in **Figure 5.6**. The observed bands are due to ligand to metal charge transfer (O 2p-W 5d) whose energy depends upon the metal loading [37]. Absorption band observed at 230 nm and 260 nm corresponding to W(VI) tetrahedral and W(VI) octahedral species respectively has shown to the presence of monomeric and polymeric tungstates [38]. On increasing tungsten content, a small band at 340 nm assigned to octahedral species in WO₃ or WO₃-like nanocrystallites is noticed [39] while peak observed at 370 nm is corresponding to bulk WO₃ crystallite formation [40]. In PTO-2 catalyst, presence of intense peaks at 220 nm and 260 nm indicated the presence of tetrahedral and octahedral monotungstates along with some polytungstates with octahedral coordination. A small band observed at 340 nm showed the indicated the presence of few nano domains of WO₃ crystallites. In PTO-10 catalyst in addition with these bands, appearance of a small band at 370 nm indicated the formation of WO₃ crystallites. On further increase in tungsten content to 20 wt.% in PTO-20 catalyst, increased intensity of the peaks at 340 and 370 nm corresponding to WO₃-like nanocrystallites and bulk WO₃ species respectively indicated the presence of increased amount these species over CP surface.

The morphological attributes of RP, TAP and CP were evaluated by SEM images as displayed in **Figure 5.7 (a-c)**. RP particles are irregular shaped, thin plate particles with broken or ragged edges (**Figure 5.7a**). As compared to RP, TAP has gained less irregular morphology due to evaporation of water and removal of carbonaceous material on calcining the RP at high temperature. This result implies that thermal activation does not affect the morphology of RP to any drastic extent [41]. After microwave assisted chemical activation, appearance of agglomerated particles evidenced by the increased silica content after acid leaching. SEM image of PTO-10 catalyst (**Figure 5.7d**) show dense agglomerated tungstate moieties dispersed on the support surface.

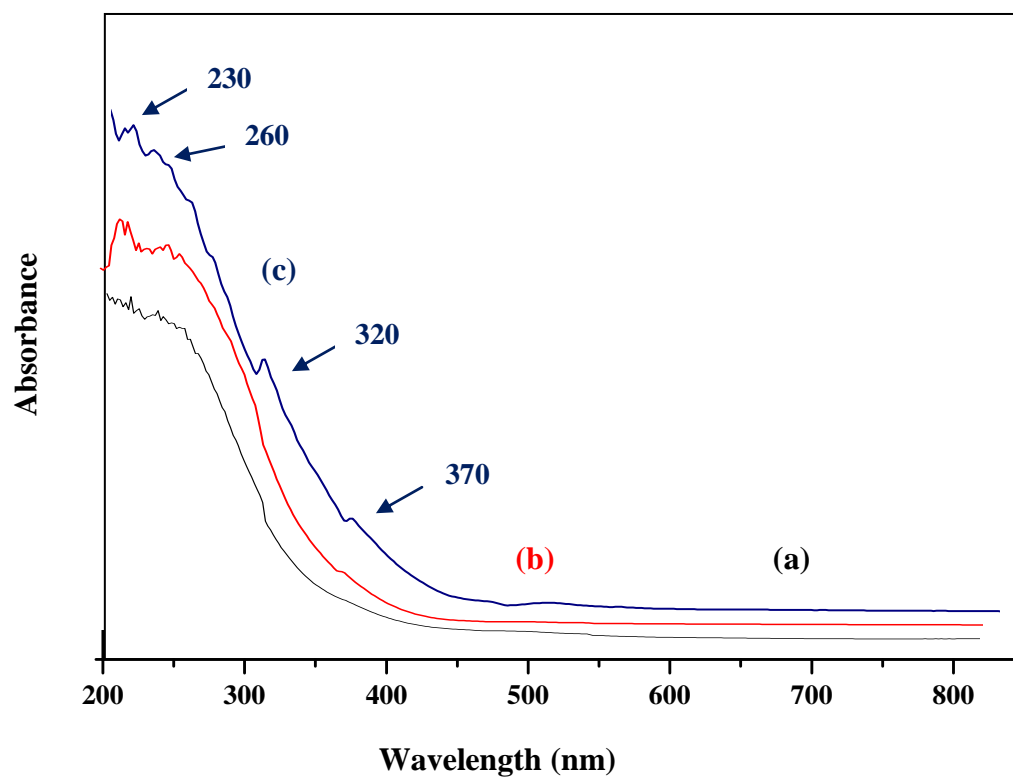
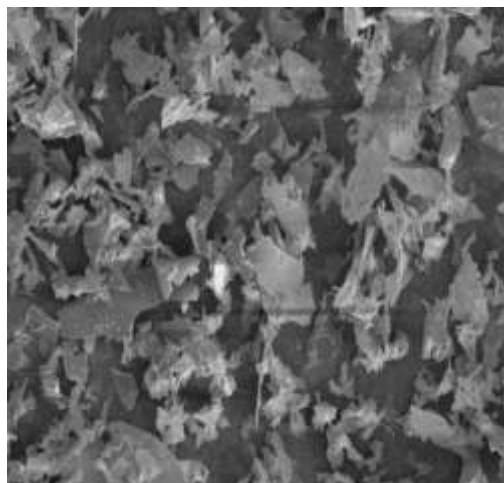
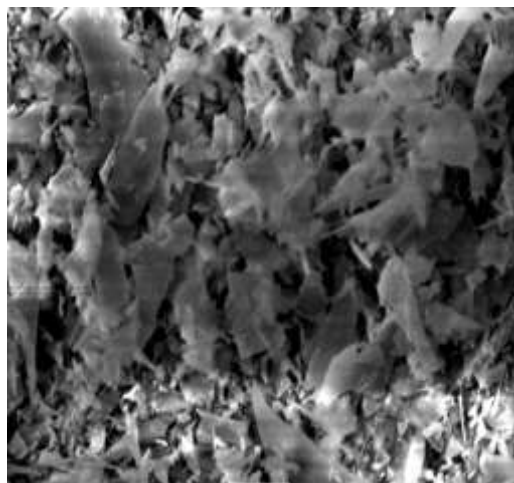


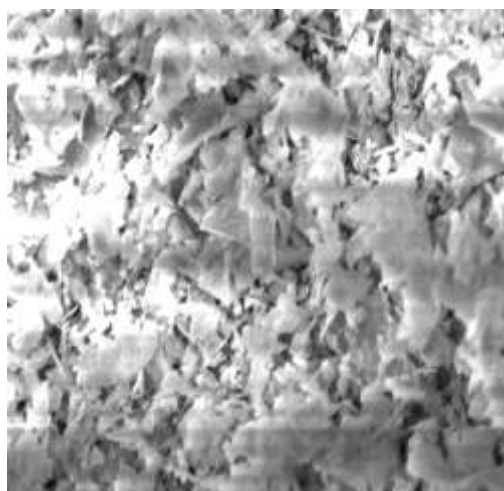
Figure 5.6: UV-vis DR spectra of (a) PTO-2 (b) PTO-10 and (c) PTO-20



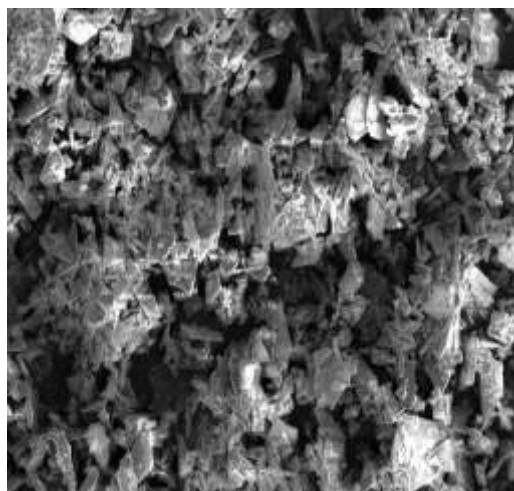
(a)



(b)



(c)



(d)

Figure 5.7: SEM micrographs of (a) RP (b) TAP (c) CP and (d) PTO-10

The TGA curve of raw perlite (RP) is shown in **Figure 5.8**. The continuous mass loss in temperature between 50 to 700°C can be attributed to removal of moisture content or physically adsorbed water molecules along with some volatile components. The total weight loss is 12.47%. The whole dehydration loss is divided into three parts: in first temperature range 50-250°C, molecular water either bounded loosely or trapped in pores is removed while in second range 250-550°C water molecules bound in inner pores of perlite are released. From the last temperature range > 500°C –OH groups associated to the oxygen atoms bound by strong hydrogen bonding are evacuated [42].

The TG curve of PTO-10 catalyst as shown in **Figure 5.9** show sharp initial weight loss upto 250°C is assigned to removal of large amount of physisorbed condensed water. The weight loss observed in the range of 250-400°C is due to desorption of ammonia and structural water followed by the weight loss between 400-600°C due to removal of ammonia and material restructures itself into monoclinic WO₃ phase [28]. No further was occurred from 600°C signifying the stability of tungstate forms on CP support.

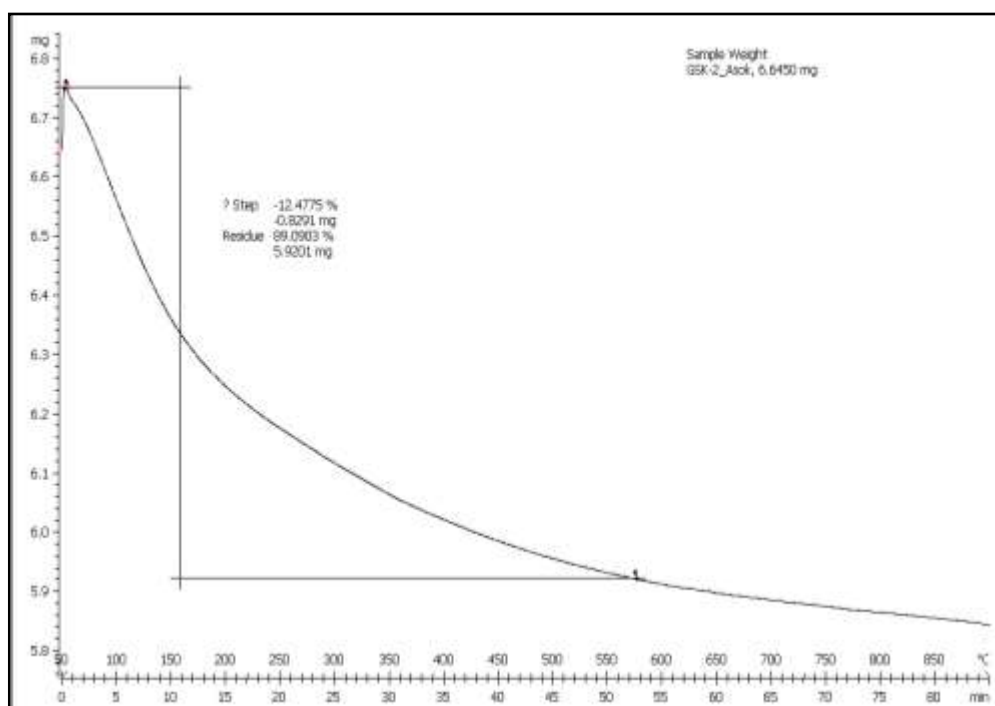


Figure 5.8: TGA curve of raw perlite (RP)

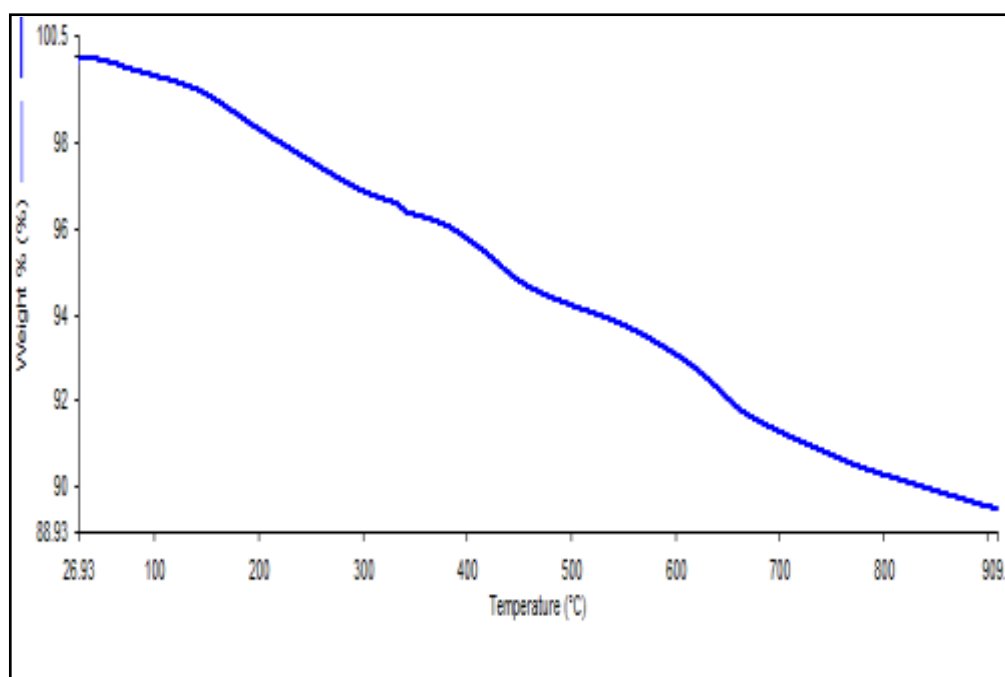


Figure 5.9: TGA curve of PTO-10 catalyst

5.4 Catalytic performance of PTO catalysts

The catalytic activity of prepared PTO catalysts were evaluated by microwave assisted solvent-free esterification of levulinic acid and alcohols to synthesize ethyl levulinate using reaction parameters as 110°C temperature, pressure (Pr) = 40 psi and power=100W with P_{\max} = ON feature within 15 min time period. Levulinic acid is able to auto catalyze the reaction [43] yet in the present reaction conditions, conversion and selectivity vary with PTO at fixed reaction conditions. CP was able to catalyze the reaction to some extent but PTO catalysts gave excellent conversion and selectivity% to alkyl levulinates. PTO-10 catalyst with sufficient amount of Brönsted acid sites gave highest 94% conversion and 98% selectivity (**Table 5.2**). The decrease in conversion and selectivity PTO-20 catalyst is observed due to predominance of non-acidic tungsten oxide crystallites at high tungstate loading which blocked the pores and hindered the approach of the reacting molecules to active sites [44].

Table 5.2: Catalytic activity of activated perlite, PTO catalysts and catalyst-free condition for esterification for synthesis of alkyl levulinates under microwave irradiation

Catalyst	Conversion% of levulinic acid (LA)	Selectivity% of ethyl levulinates
-	18	24
CP	21	29
PTO-2	68	74
PTO-10	94	98
PTO-20	82	86

Reaction conditions under microwave condition: Temp. = 110°C, pressure (Pr) = 40 psi, time = 15 min, molar ratio = LA/ethanol (1:3), LA/catalyst weight ratio = 5:1, Power = 100W and P_{\max} = ON

On the basis of above results, PTO-10 catalyst is chosen as prime catalyst to further optimize reaction conditions such as reaction time, temperature, power consumption, catalyst to substrate ratio and reactant molar ratio for obtaining maximum conversion with highest selectivity of the desired product under microwave assisted solvent-free conditions. The maximum efficiency of PTO-10 was determined by its reusability evaluation.

5.4.1 Effect of temperature

To study the effect of temperature on conversion and selectivity, studied reaction was performed at different temperatures ranging from 60-130°C as shown in **Figure 5.10**. The maximum conversion of 94% and 98% selectivity was achieved at 110°C within 15 min. While further increase in reaction temperature upto 130°C, declination in the conversion and selectivity was noticed because rise in temperature increased acid solubility and dissociation which decreased binding equilibrium that led to unfavourable esterification conditions [45].

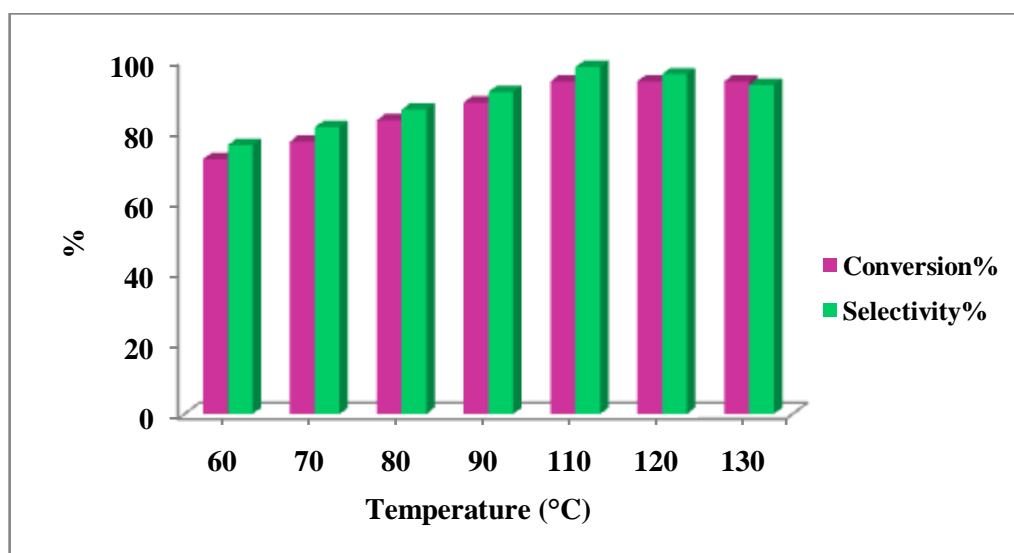


Figure 5.10: Variation of conversion% and selectivity% of ethyl levulinate over PTO-10 catalyst with temperature

Reaction conditions: Time = 15 min, LA/PTO-10 ratio = 5:1, LA/ethanol = 1:3, Pr = 40 psi, Power = 100W and P_{\max} = ON

5.4.2 Effect of reaction time

Reaction time parameter was also optimized from 5 to 25 min to achieve maximum conversion and selectivity at constant reaction conditions. On increasing reaction time from 5 to 15 min 94% conversion and 98% selectivity was achieved. Conversion and selectivity remained unaltered on further extending the reaction time upto 20 min (**Figure 5.11**).

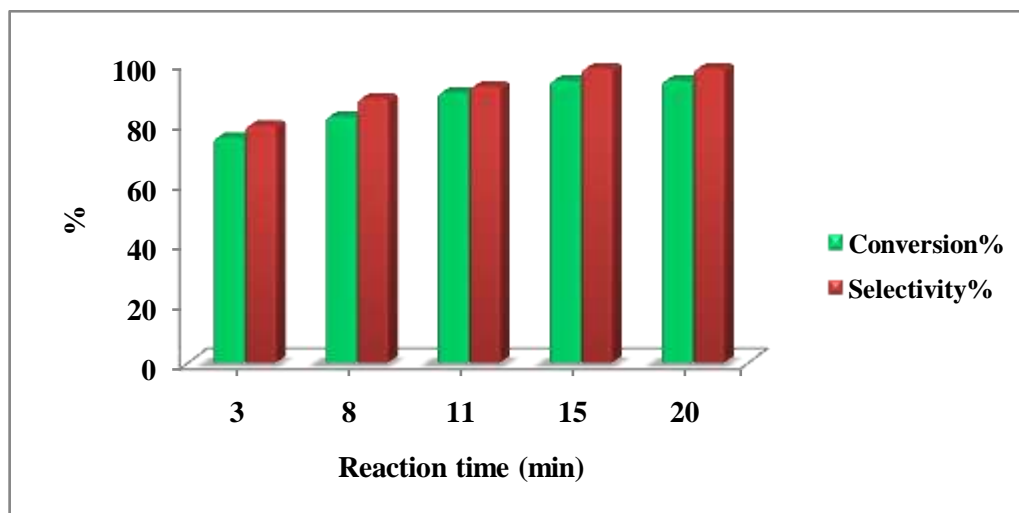


Figure 5.11: Variation of conversion% and selectivity% of ethyl levulinate over PTO-10 catalyst with time

Reaction conditions: Temperature = 110°C, LA/PTO-10 ratio = 5:1, LA/ethanol = 1:3, Pr = 40 psi, Power = 100W and P_{max} = ON

5.4.3 Effect of microwave power

To evaluate the effect of microwave power on conversion of LA and selectivity of ester under esterification reaction, microwave power was also varied from 60 to 110 W as displayed in **Figure 5.12**. Conversion was uniformly increased upto 94% upto 100W as displayed in **Figure 5.12**. With further increase in power, conversion and selectivity remained constant.

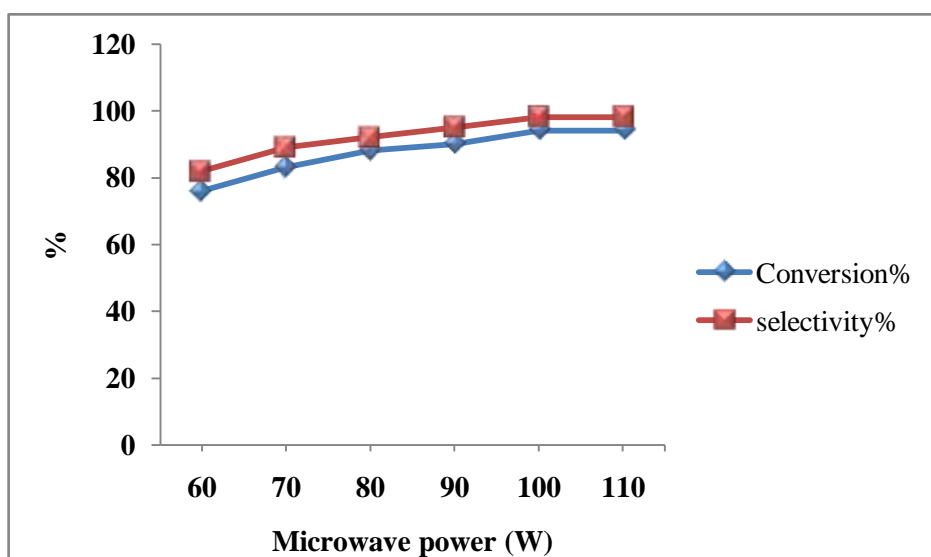


Figure 5.12: Variation of conversion% and selectivity% of ethyl levulinates over PTO-10 catalyst with microwave power (W)

Reaction conditions: Temperature = 110°C, Time = 15 min, LA/PTO-10 ratio = 5:1, LA/ethanol = 1:3, Pr = 40 psi, Power = 100W and P_{\max} = ON

5.4.4 Effect of levulinic acid and ethanol molar ratio

The esterification of LA with alcohol is a reversible reaction. By minimizing backward reaction high conversion could only be achieved. This can be possible by either removing the product water simultaneously or by using excess of ethanol. In present reaction system, it is not possible to remove water, as the boiling point of ethanol (351 K) is much lower than the boiling point of water (373 K). Hence, the ethanol was taken in excess to accelerate the reaction rate in forward direction. With increase in molar ratio from 1:1 to 1:4, conversion% of LA and ester selectivity% was increased as the excess amount of ethanol has favored the ester formation (**Table 5.3**). However, with further increase in ethanol amount to 1:5 molar ratio, dilution of reactants has lowered LA conversion, due to mass transfer limitation [4]

Table 5.3: Effect of levulinic acid and ethanol ratio on conversion% of levulinic acid

Levulinic acid and ethanol molar ratio	Conversion% of levulinic acid (LA)	Selectivity% of ethyl levulinate
1:1	82	91
1:2	89	94
1:3	94	98
1:4	90	96
1:5	83	89

Reaction conditions: Temperature = 110°C, Time = 15 min, LA/PTO-10 ratio = 5:1, Pr = 40 psi, Power = 100W and P_{max} = ON

5.4.5 LA to PTO-10 molar ratio

To achieve maximum conversion and selectivity of ethyl levulinate LA to PTO-10 catalyst ratio was varied as given in **Table 5.4**. With increase in ratio from 10:1 to 5:1 the LA conversion% increased uniformly, indicating towards the presence of sufficient amount of active acid sites. Further increase in LA to PTO-10 ratios didn't produce any significant change in conversion%.

Table 5.4: Effect of LA to PTO-10 catalyst weight ratio on conversion% of LA

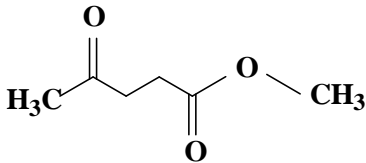
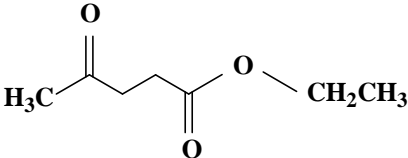
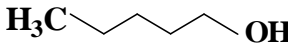
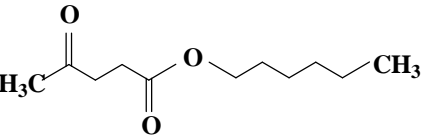
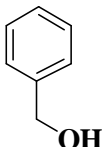
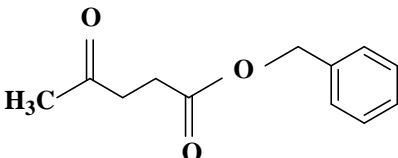
LA to PTO-10 catalyst weight ratio	Conversion% of LA	Selectivity% of ethyl levulinate
10:1	86	91
5:1	94	98
2.5:1	94	98

Reaction conditions: Temperature = 110°C, Time = 15 min, LA/ethanol = 1:3, Pr = 40 psi, Power = 100W and P_{max} = ON

5.4.6 Effect of substituted groups

To determine the effect of substituent on the conversion of the LA, different carbon chain containing alcohols were used and the resulted conversion% are shown in **Table 5.5**.

Table 5.5: Effect of various alcohols in microwave assisted solvent-free esterification of levulinic acid

Entry	R-CHO	Product	Time (min)
1	CH ₃ OH		15
2	CH ₃ CH ₂ OH		15
3			20
4			15

As suggested by the above results, lower carbon chain containing alcohols i.e. methanol and ethanol actively participated to produce esterification reaction (**Entry 1 & 2**). On the other hand, bulkier carbon chain containing pentanol (**Entry 3**) has taken longer time as compared to short carbon chain substrate due steric hindrance of carbon chains during the product formation. Due to resonating effect of benzene ring, benzyl alcohol also actively participated and produced desired levulinate ester.

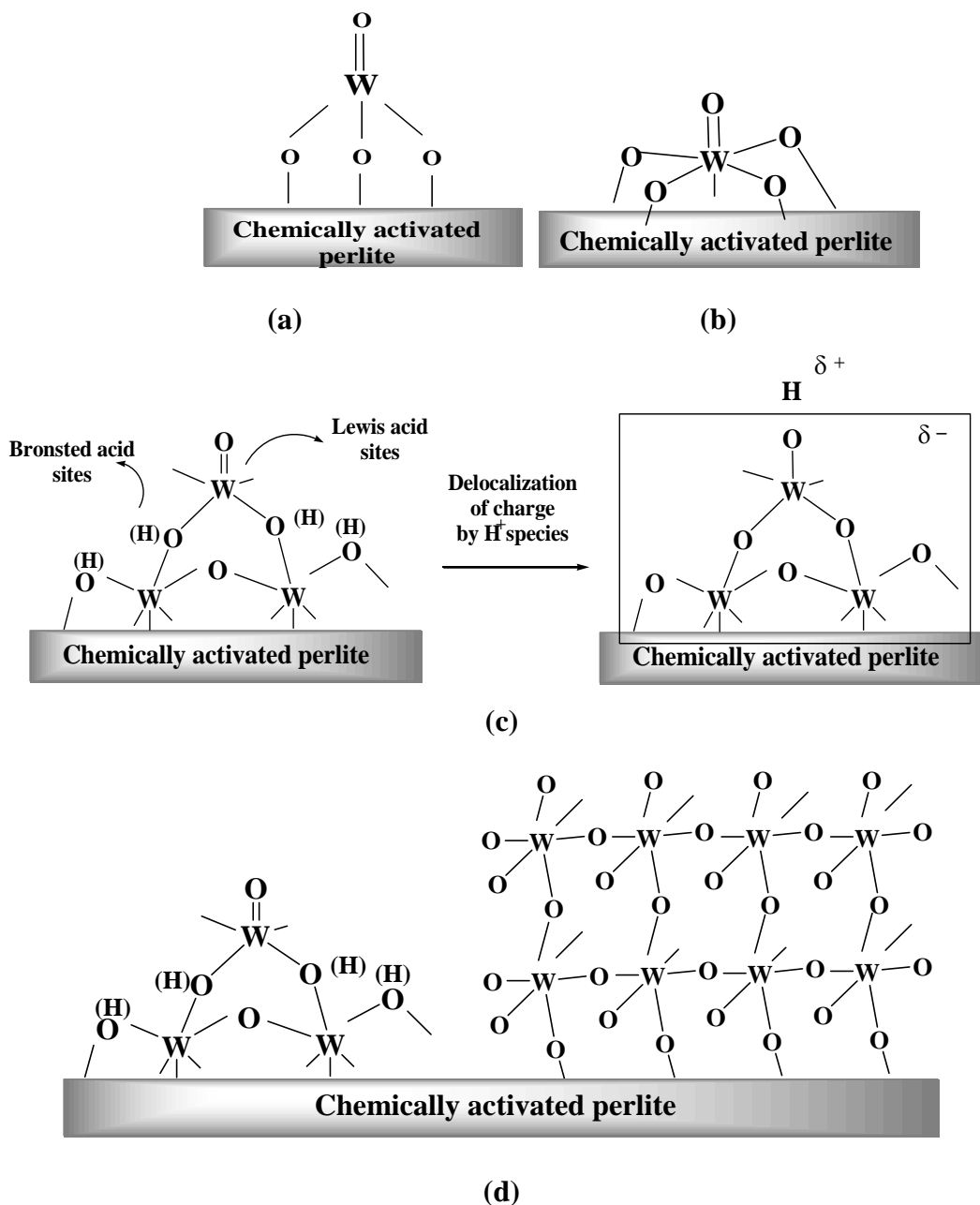
5.5 Mechanistic aspects

The structure of PTO catalysts were proposed and correlated to its catalytic activity as shown in **Scheme 5.3**. According to the detailed study of the results of XRD, FTIR, UV-vis DR, at PTO-2 catalyst contains of isolated mono-oxo tungstates with tetra and octahedral coordination and some polymerized tungstates as nano domains of WO_3 like structures which are homogeneously dispersed on CP structures. In PTO-10 catalyst polytungstates (octahedral coordination) becomes abundant with WO_3 nano-crystallites with bridging W-O-W while formation of some bulk WO_3 crystallites are observed as extra framework structures over CP support. Further increase in tungsten loading (PTO-20) led to increased amount of WO_3 crystallites over polytungstates is observed as shown in **Scheme 5.3** [46].

As discussed earlier, PTO-10 catalyst with polytungstates and with predominant nano and few WO_3 clusters caused charge compensation by protons present on neighbouring W-O-W by delocalization among W^{6+} Lewis acid sites generates active Brönsted acid sites (**Scheme 5.3**) whereas, as shown in pyridine FTIR spectra of PTO-20 catalyst, reduction in Brönsted acid sites was observed due to predominance of bulk WO_3 structures over polytungstates produced $\text{H}^{\delta+}(\text{WO}_3)_n^{\delta-}$ or oxygen deficient WO_{3-x} species which are unable to reduce further to form -OH Brönsted sites [35]. In PTO-2 catalyst less amount of acid sites were developed due to presence of monotungstates species and small amount of polytungstates and nano WO_3 crystallites that led to improper charge delocalization. However, presence W-O-W bridging bonds helped to generate Brönsted acid sites and W^{6+} species contributed to produce Lewis acidity.

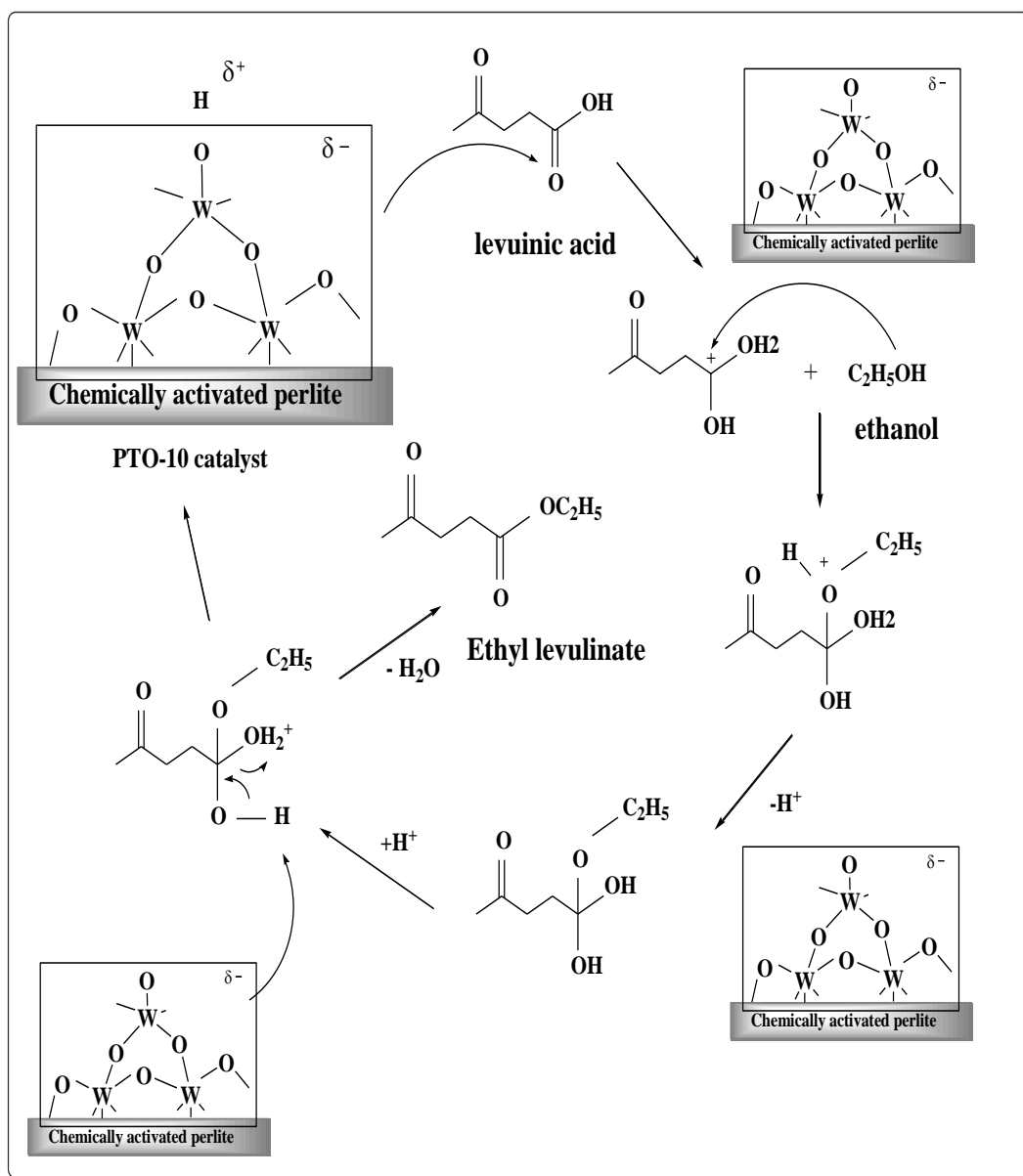
The studied esterification reaction follows single site Eley-Rideal mechanism as shown in **Scheme 5.4**. The reaction is initiated by chemisorption of the LA molecule on the Brönsted acid site on PTO-10 surface, forming a protonated LA intermediate and increases electrophilicity of carbonyl carbon. The formed carbocation was attacked by the nucleophile oxygen atom in the alcohol for the formation of corresponding oxonium ion. Finally, the proton transfer from this oxonium ion and the loss of water molecule produced ester as main product with simultaneous regeneration of the acid site of PTO-10 catalyst. Use of

microwave active LA and alcohols also accelerated the reaction rate as evident by reduction in reaction time at higher alcohol amount also acted as microwave supplier to the reaction medium homogeneously being microwave active.



Scheme 5.3: Possible molecular structures for WO_x surface species over chemically activated perlite (CP) (a) Monomeric tetrahedral and (b) octahedral tungstate species (c) Charge delocalization by H^+ amongst WO_x neighbours via bridging W-O-W bonds on polymeric tungstate species with nano clusters over CP (d)

WO₃ crystallite formation along with polytungstates on surface of CP



Scheme 5.4: Proposed reaction pathway for solvent-free microwave assisted esterification of levulinic acid and ethanol to produce ethyl levulinate over PTO-10 catalyst

5.6 Regeneration and reusability of PTO-10 catalyst

The spent PTO-10 catalyst was removed from reaction cycles, then filtered, washed and regenerated by calcining at 450°C for 1 h. After regeneration, PTO-10 catalyst was efficiently used upto five reaction cycles with conversion and selectivity upto 94-75% and 98-78% respectively as shown in **Figure 5.13**. Significant declination in conversion% was noticed after fifth reaction cycle due to the physical adsorption of carbonaceous materials that blocked the active catalytic sites and hindered the contact of reactant molecules with catalytic sites [47]. The FTIR spectra of regenerated PTO-10 catalyst shows similarity with fresh PTO-10 catalyst (**Figure 5.14**) indicating no change in chemical composition of catalyst surface. Hence, PTO-10 catalyst containing active Brönsted sites are responsible for microwave assisted esterification of levulinic acid and ethanol to give ethyl levulinates.

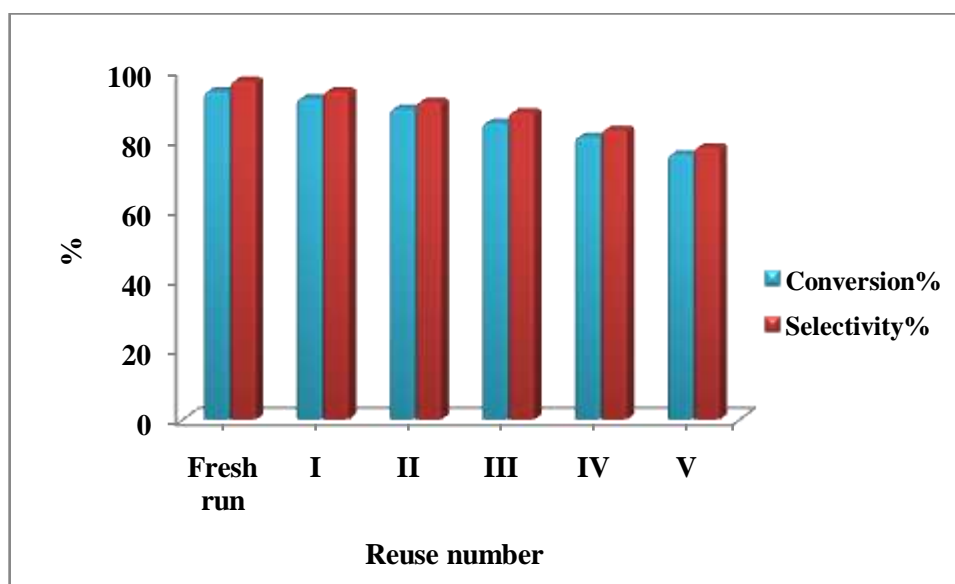


Figure 5.13: Reusability of PTO-10 catalyst for microwave assisted esterification of levulinic acid and ethanol

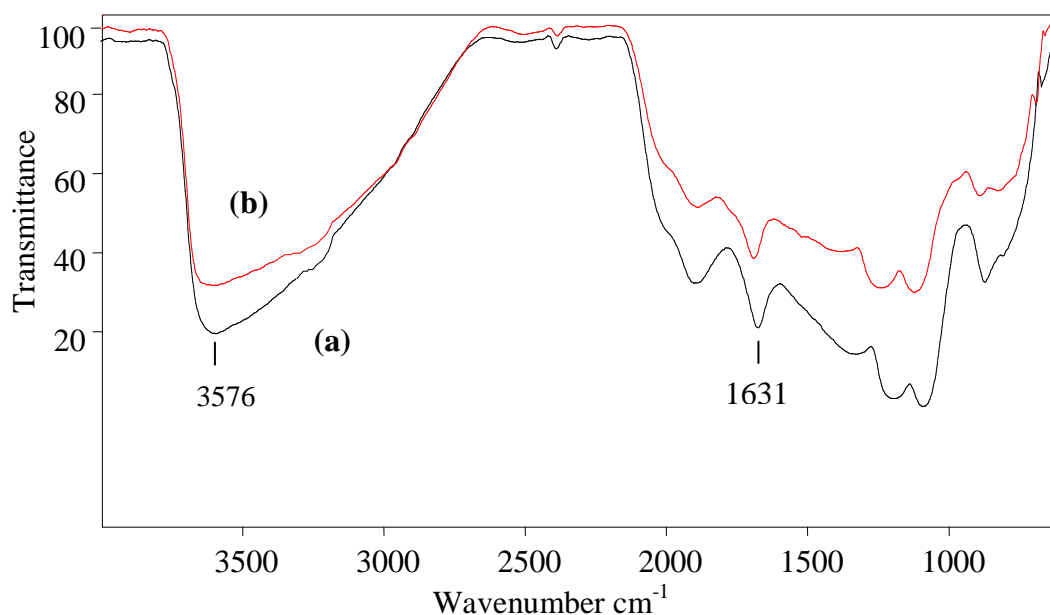


Figure 5.14: FTIR spectra of (a) Fresh PTO-10 (b) regenerated PTO-10 catalyst

5.7 Product identification

Ethyl levulinate: m.p.: 203-206°C, **FTIR (cm⁻¹):** 2962, 2874, 1728, 1210

5.8 Conclusion

Highly active perlite supported tungsten oxide catalysts with varying tungsten content has been synthesized by incipient wetness impregnation of ammonium meta tungstate over chemically activated perlite. Before tungsten loading, surface modification of perlite was carried out by thermal activation followed by microwave assisted chemical treatment. On increasing tungsten amount and calcination at 550°C temperature formation of monoclinic WO₃ crystallites were observed which was highest in PTO-20 compared to PTO-10 and 2 wt.% as revealed by XRD patterns. PTO-20 with predominance of crystallite form was not able to catalyze the reaction efficiently due to blockage of active acid sites whereas PTO-10 catalyst with mono polytungstates and few WO₃ crystallites gave excellent 94% conversion and 98% selectivity towards ethyl levulinate formation. The catalyst was regenerated and reused upto five reaction cycles with equivalent efficiency as fresh run. Thus, the present research provides novel use of perlite as a cost effective, recyclable solid acid catalyst which can become suitable substitute of commercially available costly solid catalysts used in industrially important organic transformations.

5.9 References

- [1] J. Zakaeski, P.C.A. Bruijinincx, A.L. Jongerious, B.M. Weckhuysen, *Chem. Rev.* 110 (2010) 3552-3599.
- [2] B. Kamm, M. Kamm, P.R. Gruber, S. Kromus (Eds.), *Biorefinery Systems- An Overview Biorefineries-Industrial Processes and Products: Status Quo and Future Directions*, Vol. 1, Wiley-VCH, Weinheim, 2006.
- [3] S. Wetzel, L.C. Duchesne, M.F. Laporte, *Bioproducts from Canada's Forests: New Partnerships in the Bioeconomy*, 1st Edn. **Springer**, the Netherlands, 2006.
- [4] K.Y. Nandiwale, S.K. Sonara, P.S. Niphadkara, P. N. Joshi, S.S. Deshpande, V.S. Patil, V.V. Bokade, *Appl. Catal. A: Gen.* 460-461 (2013) 90-98.
- [5] G.D. Yadav, A.R. Yadav, *Chem. Eng. J.* 243 (2014) 556-563.
- [6] J.A. Meleroa, G. Moralesa, J. Iglesias, M. Paniaguaa, B. Hernández, S. Penedo, *Appl. Catal. A: Gen.* 466 (2013) 116– 122.
- [7] A. Leea, N. Chaibakhsha, Mohd B. A. Rahmana, M. Basria, B.A. Tejoa, *Indus. Crop Prod.* 32 (2010) 246–251.
- [8] Y. Kuwaharaa, T. Fujitania, H. Yamashita, *Catal. Today* 237 (2014) 18-28.
- [9] Y. Kuwahara, W Kaburagi, K. Nemoto, T. Fujitani, *Appl. Catal. A: Gen.* 476 (2014) 186–196.
- [10] B.L. Oliveria, V. Teixeira da Silva, *Catal. Today* 234 (2014) 257–263.
- [11] Y.B. Huang, T. Yang, B. Cai, X. Changa, H. Pan, *RSC Adv.* 6 (2016) 2106-2111.
- [12] G. Mitran, T. Yuzhakova, I. Popescu, I.C. Marcu, *J. Mol. Catal. A: Chem.* 396 (2015) 275-281.
- [13] S. Sarish, B.M. Devassy, W. Bohringer, J. Fletcher, S.B. Halligudi, *J. Mol. Catal. A: Chem.* 240 (2005) 123-131.
- [14] A. Amoozadeh, S. Rahmani, *J. Mol. Catal. A: Chem.* 396 (2015) 96-107.

-
- [15] P. Bhaumik, T. Kane, P.L. Dhepe, *Catal. Sci. Technol.* 4 (2014), 2904-2907.
- [16] F. Adam, A. Iqbal, *Chem. Eng. J.* 171 (2011) 1379-1386.
- [17] C.L. Thomas, *Heterogeneous catalysis in practice*, McGraw-Hill, New York, 1980.
- [18] L.L. Murrell, C.J. Kim, D.C. Grenoble, U.S. Patent no. 4,233, 139 (1980).
- [19] J. E. Herrera, J.H. Kwak, J.Z. Hu, Y. Wang, C.H.F. Peden, J. Macht, E. Iglesia, *J. Catal.* 239 (2006) 200-211.
- [20] I.E Wachs, T. Kim, E.I. Ross, *Catal. Today* 116 (2006) 162-168.
- [21] K. Sodeyama, Y. Sakka, Y. Kamino, *J. Mater. Sci.* 34 (1999) 2461-2468.
- [22] M.A. Vicente, J.D.L. Gonzalez, M.A.B. Munoz, *Clay Miner.* 29 (1994) 361-367.
- [23] U. Kalapathy, A. Proctor, J. Shultz, *Bioresour. Technol.* 73 (2000) 257-262.
- [24] K. Amutha, R. Ravibakar, G. Sivakumar, *Int. J. Nanotechnol. Appl.* 4 (2010) 6.
- [25] S.R. Kamath, A. Proctor, *Cereal. Chem.* 75 (1998) 484-487.
- [26] N. Shringi, K. Srivastava, A. Rani, *Chem. Sci. Rev. Lett.* 4 (2015) 561-570.
- [27] M. Visa, C. Bogatu, A. Duta, *J. Hazard. Mater.* 289 (2015) 244-256.
- [28] C. Yuea, X. Zhua, M. Rigutto, E. Hensena, *Appl. Catal. B: Environ.* 163 (2015) 370-381.
- [29] J.P. Nayak, J. Bera, *Trans. Ind. Ceram. Soc.* 68 (2009) 1-4.
- [30] J. Ojima, *J. Occup. Health* 45 (2003) 94-103.
- [31] C. Martin, P. Malet, G. Solana, V. Rives, *J. Phys. Chem. B* 102 (1998) 2759-2768.
- [32] M.A. Zaki, G.A.H. Mekhemer, N.E. Fouad, A.I.M. Rabee, *Appl. Surf. Sci.* 308 (2014) 380-387.

-
- [33] T. Onfroy, V. Lebarbier, G. Clet, M. Houalla, *J. Mol. Catal. A: Chem.* 318 (2010) 1-7.
- [34] M.A. Cortés-Jácome, C. Angeles-Chavez, E. López-Salina, J. Navarrete, P. Toribio, J.A. Toledo, *Appl. Catal. A: Gen.* 318 (2007) 178-189.
- [35] J. Macht, C.D. Baertsch, M. May-Lozano, S. L. Soled, Y. Wang, E. Iglesia, *J. Catal.* 227 (2004) 479-491.
- [36] D.C. Barton, S.L. Soled, E. Iglesia, *Topics in Catalysis* 6 (1998) 87-99.
- [37] V. Cristina dos Santos, K. Wilson, A.F. Lee, S. Nakagaki, *Appl. Catal. B: Environ.* 162 (2015) 75-84.
- [38] B. Hu, H. Liu, K. Tao, C. Xiong, S. Zhou, *J. Phys. Chem. C* 117 (2013) 26385–26395.
- [39] S. Huang, F. Chen, S. Liu, Q. Zhu, X. Zhu, W. Xin, Z. Feng, C. Li, Q. Wang, L. Xu, *J. Mol. Catal. A: Chem.* 267 (2007) 224–233.
- [40] M.J. Zaki, N.E. Fouad, S.A.A. Mansour, A.I.M. Rabee, *Appl. Surf. Sci.* 282 (2013) 898-907.
- [41] S. Kabra, S. Katara, A. Rani, *Inter. J. Innov. Res. Sci. Eng. Technol.* 2 (2013) 4319-4326.
- [42] A.G. Celik, A.M. Kilic, G.O. Cakal, *Physicochem. Probl. Miner. Process.* 49 (2013) 689-700.
- [43] D.R. Frenandes, A.S. Rocha, E.F. Mai, C.J.A. Mota, V. Teixeira, da Silva, *Appl. Catal. A: Gen.* 425-426 (2012) 199-204.
- [44] K.M Parida, P.K. Pattnayak, P. Mohapatra, *J. Mol. Catal. A: Chem.* 260 (2006) 35-42.
- [45] A. Lee, N. Chaibakhsha, Mohd B. A. Rahman, M. Basria, B.A. Tejo, *Ind. Crops Prod.* 32 (2010) 246–251.
- [46] C.D. Baertsch, S.L. Soled, E. Iglesia, *J. Phys. Chem. B* 105 (2001) 1320-1330.
- [47] A. Rani, C. Khatri, R. Hada, *Fuel Process. Technol.* 116 (2013) 366–373.

Annexure I

CHARACTERIZATION TECHNIQUES

Physicochemical properties of the prepared catalytic materials were characterized by N₂ adsorption-desorption, XRD, FTIR and pyridine FTIR, SEM-EDS, TGA, UV-Vis DRS. The reaction products are analyzed by ¹H NMR, ¹³C NMR, FTIR and gas chromatography.

1. X-ray fluorescence spectrometer (XRF)

The chemical components of the prepared samples were analyzed from by X-ray fluorescence spectrometer (Philips PW 1606).

2. N₂ adsorption-desorption analysis

The specific surface area, pore size and pore volume of the prepared samples were measured by N₂ adsorption-desorption isotherms study at liquid nitrogen temperature by BET and BJH approaches using 77K by NOVA 1000e surface area and pore size analyzer. The samples were degassed under vacuum at 120°C for 4 h, before adsorption measurement to evacuate the physisorbed moisture.

3. X-ray diffractometer (XRD)

Powder X-ray diffraction studies were carried out by using (Bruker D8 Advance diffractometer, using Ni-filter and Cu K α radiation (E=8047.8 eV, λ =1.5406 Å). The samples were scanned in 2 θ range of 5-75° at a scanning rate of 0.04 s⁻¹. The crystalline size of phases was determined from the peak of maximum intensity (2 θ = 26.57) by using Scherrer formula as Eq. (1) with a shape factor (K) of 0.9.

$$\text{Crystallite size} = K \cdot \lambda / W \cdot \cos\theta \quad (1)$$

Where, $W = W_b - W_s$; W_b is the broadened profile width of experimental sample and W_s is the standard profile width of reference silicon sample.

4. Fourier transform infrared spectrophotometer (FTIR)

Fourier transform infrared (FTIR) study of the synthesized samples was performed by FTIR spectrophotometer (Tensor-27, Bruker, Germany) in DRS (Diffuse Reflectance Spectroscopy) system by mixing the sample with KBr (spectroscopic grade) in 1:20 weight ratio in the range of 550-4000 cm^{-1} with resolution of 4 cm^{-1} . FTIR spectrophotometer (Alpha-T model, Bruker, Germany) is also used to record FTIR spectra in range of 400-4000 cm^{-1} with resolution of 4 cm^{-1} by mixing the sample with with KBr (spectroscopic grade) in 1:20 weight ratio.

5. Pyridine FTIR

The acid sites in prepared catalysts were determined by Pyridine adsorbed FTIR. The sample (0.2 g) was activated at 450°C for 2 h and then exposed to pyridine (25 ml) for 24 h. The FTIR spectra of the adsorbed samples were recorded by FTIR spectrophotometer (Tensor-27, Bruker, Germany) in DRS (Diffuse Reflectance Spectroscopy) system in the range of 550-4000 cm^{-1} with resolution of 4 cm^{-1} .

6. Diffuse reflectance UV-Visible spectrophotometer (DR UV-Vis)

The UV-Vis DRS spectra of the prepared catalysts were recorded on Perkin Elmer Lambda 950 UV-Vis spectrophotometer equipped with Harrick DRS assembly in the range of 200-800 nm at ambient temperature.

7. SEM-EDX

The detailed imaging information and morphological features of the samples were provided by SEM (Model-JEOL JSM 5600). The % elemental analysis was performed by using EDX studies.

8. Thermogravimetric analysis (TGA)

The TGA analysis of the samples was done with STA 6000 (Perkin Elmeris) thermal analyzer by heating the sample in the range of 25-900°C with the heating rate of 10°C/min under nitrogen flow (20 ml/min).

9. ^1H and ^{13}C NMR

^1H and ^{13}C NMR analysis of the reaction products was done with ECS 400 MHz (JEOL) NMR spectrometer.

10. Gas Chromatograph

The products were analyzed by Gas Chromatograph (Agilent Technologies 7820A) with FID detector and Agilent J&W Advanced Capillary HP 5 GC Columns of 30 m length and 0.320 mm diameter, programmed oven temperature of 60-325°C and N_2 (1.5 ml/min) as a carrier gas.

11. Melting point apparatus

Melting points of the synthesized products were determined by using Xd-6 microscope melting point apparatus.

Annexure II

List of papers published: 4

1. “Pure silica extraction from perlite: Its characterization and affecting factors”, Khushboo Srivastava, *Niharika Shringi*, Vijay Devra, Ashu Rani, International Journal of Innovative Research in Science, Engineering and Technology 2 (2013) 2936-2942.
2. “Environmental benign route for the utilization of fly ash as heterogeneous acid catalyst for various organic transformations,” Khushboo Srivastava, *Niharika Shringi*, Vijay Devra, Ashu Rani, International Journal of Inventions in Research, Engineering Science, and Technology 1 (2014) 74-75.
3. “A facile method for production of Amorphous Silica from Perlite under Microwave Irradiation”, Khushboo Srivastava, *Niharika Shringi*, Vijay Devra and Ashu Rani, International Journal of IT, Engineering, Applied Sciences Research, 4 (2015) 18-24.
4. “Microwave Assisted Acid Activation of Fly Ash: A Green Process for Enhancing its Physico-Chemical Attributes for Esterification under Dielectric Heating”, *Niharika Shringi*, Khushboo Srivastava and Ashu Rani, Chemical Science Review and Letters 4 (2015) 561-570.

Annexure III

Papers and posters presented/ participated in International Conferences

1. *Participated* in **Indo-Swedish Symposium on strategic Knowledge on Climate Change**, held on 9 Oct. 2012 at Department of Pure & Applied Chemistry, University of Kota, Kota,.
2. *Participated* in **International Workshop on Green Initiatives in Energy, Environment and Health**, held on 2nd and 3rd Dec. 2013 Gautam Buddha University, New Delhi.
3. *Accepted research paper* in **International Conference on Emerging Trends in Engineering and Applied Sciences-2013 (ICATEAS-2013)** held on 27th and 28th Dec. 2013 organized by IEEE and CSI at Rajasthan College of Engineering for Women, Jaipur, Rajasthan.
4. *Presented research paper* in **International Conference on Advance Trends in Engineering and Technology (ICATET) 2013**, during 19th to 20th Dec, 2013 at Arya College of Engineering and IT, Jaipur, Rajasthan.
5. *Participated in* 4th **International Conference on Solid Waste Management and exhibition on Municipal Services, Clean technology and Machineries, ICONSWM 2014**, held on 28th and 30th Jan. 2014 at Acharya Agriculture University, Hyderabad, Andhra Pradesh, India.
6. *Presented research paper* in **International Conference on Advance Trends in Engineering and Technology (ICATET) 2013**, held on 18th and 19th April 2014 at Arya College of Engineering and IT, Jaipur, Rajasthan.

Papers and posters presented/ participated in National Conferences/

Workshops

1. *Accepted abstract* in National Conference on Innovative use of Fly Ash at Jindal Steel Works (JSW) Energy's Barmer Plant, 21th June 2013.

2. *Oral and Paper presentation* in National Seminar on **“Socio-Legal Issues and Challenges of Female Feticide and Infanticide in India”** held on 4th and 5th Oct. 2013 organised by Women cell, sponsored by National Commission for Women, New Delhi: UGC, New Delhi & University of Kota, Kota.
3. *Participated* in National Conference on **Frontiers in Physical, Chemical and Biological Sciences** held on 4th to 6th Oct. 2013 at Department of Chemistry, University of Pune, Pune Maharashtra, India.
4. *Presented poster* in **National Conference on Global Environmental Changes and Disaster Management for Sustainable Life on Earth- A Burning Issue** held on 21th Oct. 2013 at Maharshi Arvind College of Engineering and Technology, Ranpur, Kota, Rajasthan.
5. *Participated* in **5th National Academic Workshop on Organic Mechanisms & Analytical Techniques used in Chemical Sciences**, during 21th Oct. to 25th Oct. 2013 at Department of Pure & Applied Chemistry, University of Kota, Kota, Rajasthan.
6. *Actively participated* in **National Symposium on E-Resources**, held on 16th to 17th Dec. 2013 at Department of Library and Information Science, University of Kota, Kota, Rajasthan.
7. *Presented oral* in **National Seminar on Environmental issues and Social Sciences**, held on 21th to 22th March 2014 at Department of Social Sciences, University of Kota, Kota, Rajasthan.
8. *Presented poster* in **National Seminar on Recent Advancements in Protection of Environment and its Management Issues (NSRAPEM-2015)** held on 27th to 28th Feb. 2015 at Maharishi Arvind College of Engineering and Technology, Ranpur, Kota, Rajasthan.

Annexure IV

1. Industrial tour visit at Jindal Steel Works (JSW) Energy's Barmer Thermal Power Plant, Barmer, Rajasthan, 21st June 2013.
2. Industrial tour visit at Pesticide India Pvt. Ltd. Udaipur, 29th Nov. 2014.



Pure Silica Extraction from Perlite: Its Characterization and Affecting factors

Khushboo Seivastava¹, Niharika Shringi², Vijay Devra³, Ashu Rani^{4*}

¹Research Scholar, Department of Pure and Applied Chemistry, University of Kota, Kota, Rajasthan, India

²Research Scholar, Department of Pure and Applied Chemistry, University of Kota, Kota, Rajasthan, India

³Lecturer, Department of Chemistry, Govt. J.D.B. Girls P.G. College, Kota, Rajasthan, India

⁴Head, Department of Pure and Applied Chemistry, University of Kota, Kota, Rajasthan, India

Abstract: A simple method based on alkaline extraction followed by acid precipitation and acid dissolution has been developed to produce pure amorphous silica from perlite. The reaction parameters such as molar ratio of NaOH/SiO₂, reaction time and reaction temperature are varied for obtaining maximum silica conversion. About 70.6 % pure precipitated silica from perlite has been achieved in closed system at 120 °C within 60 min. XRF, BET surface area, XRD, FTIR and SEM techniques are used to characterize the physico-chemical attributes of materials. The present research includes a cost benefit process under optimized conditions for produce wealth out of waste.

Keywords: Perlite, Silica conversion, Silica gel, Affecting factors.

1. INTRODUCTION

Technologies related to production method and applications of pure precipitated silica have been studied and developed throughout the world in great variety of ways. Commercially available precipitated silica is manufactured by the fusion of high purity caustic soda and silica sand in furnaces at temperatures of 1300-1500 °C and higher to produce solid glass [1]. Tetraethylorthosilicate (TEOS) is also widely used for production of commercial silica. But these processes are very expensive and energy intensive [2]. Recently, a large amount of precipitated silica has been extracted from various types of bio waste such as rice husk ash [3], rice hull ash [4] and bagasse ash [5] etc. Several techniques such as acid leaching or by gasification of rice hull with a pilot flame in a modified fluidized bed as well as by burning the rice hull ash at high temperature have been reported for the extraction of silica [6, 7].

The global market and demand for specially silicas (silica gel, precipitated, fumed and colloidal silica) reached and estimated value of \$1.7 million. Through the year 2002, the global market for specially silicas is expected to grow at a rate of roughly 4.0 % a year exceeding \$2 billion in that year [3]. Highly purified precipitated silica has been widely used in many applications including production of nanomaterials, in reinforcement of rubbers and plastics, in thickening and thixotropy of coatings and paints, printed inks, plastics and cosmetics, as desiccants, stabilizer, adsorbent, food rheology modifier and as carrier of pesticides and catalysts [8].

The present study has been undertaken to evaluate systematically and quantitatively the influence of various physical and chemical factors on the extraction of pure precipitated amorphous silica from perlite, an abundant solid waste. Perlite containing high silica and alumina content can be an economically viable raw material for production of pure precipitated silica. It is an acheric, siliceous, and volcanic glass lava containing crystal water, falling into the category of igneous rock [9]. China has the third largest in reserves of perlite in the world. The available world production of perlite in 2010 in respect of principal countries has estimated at 3.32 million tonnes [10]. The results permit a rational approach to the development and production of highly purified precipitated silica to satisfy individual requirements. This study employs a report on the manufacture, affecting factors and characterization of silica made from perlite using alkali solubilisation followed by subsequent precipitation and dissolution with different acids at lab scale.

II. EXPERIMENTAL

Perlite was obtained from Indian Chemical Pvt. Ltd., Kothwar. All chemicals were purchased from S. D. Fine Chem. Ltd., India.

A. Preparation of highly purified precipitated amorphous silica from perlite

Fig.1 represents the flow diagram for production of precipitated amorphous high purity silica from perlite. Perlite was thoroughly washed with distilled water to remove adhering soil and dust and then dried at 110 °C for 12 h. After that, it was calcined at 800 °C for 3 h. For producing sodium silicate solution, the reaction mixture of perlite (10 g) and NaOH solution was stirred in two types of systems: (i) open (ii) closed system. In the first one, the reaction was carried out in open borosil beaker under atmospheric pressure while in closed system, the reaction mixture was placed in an air tight

Erlenmeyer flask under stirring at 600 rpm. The solution was filtered through Whatman No. 41 filter paper and the residue was washed with 20 ml boiled distilled water. The filtrate and washings were allowed to cool to room temperature and titrated with 5 N H_2SO_4 with constant stirring. The pH of the solution was monitored and titration stopped at pH 7. A soft white gel was formed and aged for 6 h. After aging, the slurry was washed by vacuum filtration using distilled water to remove sodium sulphate and then dried at 110 °C for 12 h, weighed. For removing other mineral contents such as Al, Na etc. the dried material was refluxed with 1 N HCl at 120 °C for 2 h and then washed repeatedly using deionised water to make it acid free. Now, the obtained pure precipitated amorphous silica was dried at 110 °C for 12 h. The solid residue obtained during filtration was washed with distilled water and dried at 110 °C for 12 h.

B. Quantification of silica conversion pct. %

The silica conversion with lesser amount of Al, Na content (wt. %) was determined by mass balance (Fig. 1) using following formula:-

$$SiO_2 \text{ conversion (wt. \%)} = \frac{P - R}{P} \times 100$$

Where P = total wt. of perlite, R = wt. of solid residue consisting water insoluble unreacted silica. The reaction parameters such as reaction time (0 to 60 min), molar ratio of NaOH:SiO₂ (0.6 to 2.4) and reaction temperature (60-120 °C) were optimized during silica extraction.



Fig. 1 Flow diagram for production of highly purified precipitated amorphous silica from perlite

C. Regeneration

Regeneration is the step where calcium hydroxide reacts with sodium sulphate to form calcium sulphate and sodium hydroxide. As per the reported procedure, NaOH is regenerated upto 90 %. The regenerated NaOH solution is used for digestion of the fresh perlite [11]. The obtained calcium sulphate can be used for other laboratory work.

D. Characterization Techniques

The chemical components of the samples were analyzed by X-ray fluorescence spectrometer (Philips PW1606). The BET surface area was measured by N₂ adsorption-desorption isotherm study at liquid nitrogen temperature (77 K) using

Quantachrome NOVA 1000e surface area analyzer. Powder X-ray diffraction studies were carried out by using (Philips X'pert) analytical diffractometer with monochromatic $\text{CuK}\alpha$ radiation ($\lambda = 1.54056 \text{ \AA}$) in a 2θ range of $0-50^\circ$. The particle size of the samples was determined from the X-ray diffraction data using Debye-Scherrer formula.

$$C_s = 0.9 \lambda / \beta \cos \theta$$

Where C_s is the particle size, λ is the wavelength of the incident X-ray beam, β is the full width at half maximum (FWHM) of the X-ray diffraction peaks and θ is half of the angle 2θ corresponding to the peak [12]. The FTIR study of the samples was done using FTIR spectrometer (Alpha-T model, Bruker, Germany) by mixing the sample with KBr pellet mode (in 1:20 wt. ratio) in the range of $4000-400 \text{ cm}^{-1}$. The detailed imaging information about the morphology and surface texture of the sample was provided by SEM (Philips XL30 ESEM TMP).

III. RESULT AND DISCUSSION

A. The physico-chemical characteristics of perlite

The chemical composition of raw perlite was as determined by XRF (in wt. %): SiO_2 (74.9%), Al_2O_3 (12.6%), Fe_2O_3 (0.8%), CaO (0.6%), MgO (0.1%), TiO_2 (0.1%), Na_2O (4.6%), K_2O (4.7%) and trace elements (4.0%). The L.O.I. (loss on ignition) was 2 wt. %. It can be evidenced that the perlite contains 73.9 wt. % silica with light grey color due to presence of carbon particles and small amount of other elements considered as impurities which turns into white-pink color with 74.3 wt. % silica content after calcination at 800°C for 3h. Thermal treatment at high temperature leads to the removal of water and the organic matter [13]. The surface area and average particle diameter of raw perlite were $5 \text{ m}^2/\text{g}$ and $3.20 \mu\text{m}$.

B. Effect of reaction parameters

Fig. 2 presents the influence of molar ratio of NaOH/SiO_2 variation from 0.6 to 2.4 on silica extraction which indicates that the concentration of NaOH solution positively affects the silica dissolution since silica extraction is increased on increasing NaOH concentration. The dissolution process of silica in aqueous solutions is mainly due to hydrolysis of Si-O-Si bonds, therefore silica configuration has strong influence on this process. As a comparison, quartz silica is the most stable form while amorphous silica is the most soluble [14, 15]. Extraction with more concentrated NaOH does not improve the silica yield.

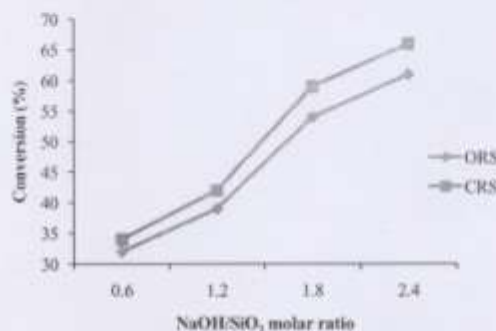


Fig. 2 Silica conversion as function of NaOH/SiO_2 molar ratio for open (ORS) and closed (CRS) reaction system ($T = 100^\circ\text{C}$, time = 90 min).

Fig. 3 exhibits that silica conversion into sodium silicate in closed vessel results better than open system on increasing reaction time (0 to 90 min) at 100°C temperature. The time of "0 minute" corresponds to the time necessary for reaction system to reach the desired temperature.

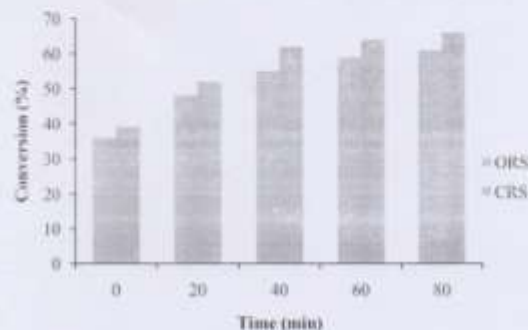


Fig. 3 Silica conversion as function of reaction time for open (ORS) and closed (CRS) reaction system ($T = 100\text{ }^{\circ}\text{C}$, $\text{NaOH/SiO}_2 = 2.4$).

The influence of reaction temperature on silica extraction is shown in Fig. 4. It is observed that the silica conversion increases with rising temperature, reaching 71.4 % at $120\text{ }^{\circ}\text{C}$ in 60 min. Further increasing the reaction temperature, the conversion reaches at constant value in lesser time.

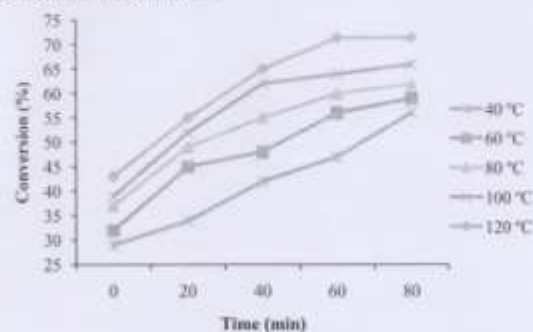


Fig. 4 Silica conversion as function of reaction time for different temperatures (time = 80 min, closed reaction system)

C. Characterization of pure extracted silica from perlite

The XRF analysis shows that the obtained precipitated silica from perlite is found to be white fine solid with 70.6 % pure silica content having $\sim 98\text{ m}^2/\text{g}$ specific surface area in the range of $0.3\text{--}1\text{ }\mu\text{m}$ particle size.

As shown in Fig. 5, the X-ray diffractogram of extracted silica confirm amorphous characteristic along with broad humps centred between $10\text{--}35^{\circ}$ (2 θ). Amorphous substances display an atomic arrangement that is either random or has very short-range order [4, 7].

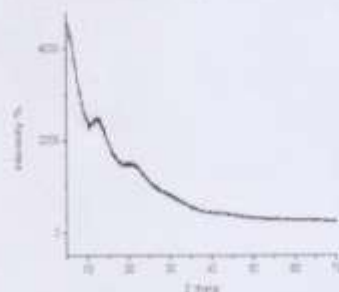


Fig. 3 XRD pattern of precipitated silica

The major chemical groups present in extracted silica are identified by the FT-IR spectra shown in Fig. 4. The broad band between 3645-3400 cm^{-1} indicates the presence of isolated and surface Si-OH groups. The predominant absorbance peak at 1085 cm^{-1} is due to asymmetric stretching vibration of siloxane bonds (Si-O-Si) and the corresponding symmetric stretch at 795 cm^{-1} . The peaks at 1085, 795 and 450 cm^{-1} are attributed to the vibration modes amorphous silica gel network [16, 17].

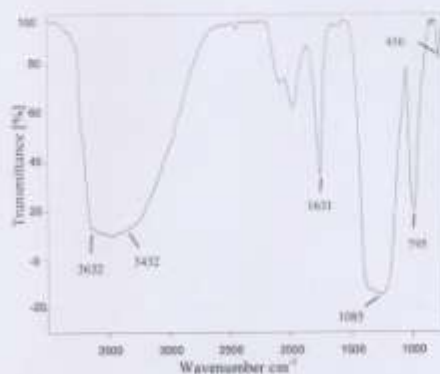


Fig. 4 FTIR spectrum of pure precipitated silica

In Fig. 7 (a & b), the SEM image of raw perlite indicates irregular shaped crumbled particles whereas the SEM micrograph of extracted pure silica demonstrates globular shaped highly porous particles of different shapes and sizes in agglomerated form. Such type of large gelatinous mass is due to the presence of amorphous silica gel skeleton.



Fig. 7 SEM images of (a) raw perlite (b) pure precipitated silica

IV. CONCLUSION

This study reveals a simple low energy chemical process for the generation of high purity amorphous silica from perlite without using any organic additive. The yield of extracted silica from perlite was 70.6 % with $\sim 98 \text{ m}^2/\text{g}$ surface area in closed reaction system using $\text{NaOH}:\text{SiO}_2 = 2.4$ molar ratio at 120°C within 60 min. The acid chemicals can be regenerated making it an environmentally benign, cost effective and atom efficient process and thus finds a novel route to utilize abundant waste perlite in future.

ACKNOWLEDGEMENT

The authors are thankful to Dr. D.D. Phadke and Dr. V.K. Ahire for SEM analysis and Mr. Mukul Gupta for XRD conducted at UGC DAE-CSR Lab Indore. XRF analysis was conducted at Poojibh University, Channarayana. The financial support was provided by Department of Science and Technology, Rajarathn, India, project sanction no. P-7/DST/R&D/11433-38.

REFERENCES

- [1] M. Stephens et al., "Precipitated silica, silica gels with and free of deposited carbon from caustic biomass ash solutions and processes," U.S. Patent 6,438,754 B2, Oct. 28, 2003.
- [2] Nakamura, "Method for production of novel nano silica particle and use of the nano silica particle," U.S. Patent 2010/0330342 A1, Dec. 30, 2010.
- [3] Mahapatra et al., "A novel process and apparatus for the manufacture of precipitated silica from Rice Husk Ash," International Application Published under the Patent Cooperation Treaty (PCT) WO 2004/075409 A2, Sep. 2, 2004.
- [4] Krishnamoorthy, U., Panchan, A., and Shetty, J., "A simple method for production of pure silica from rice husk ash," Biomass Technology, Vol. 73, pp. 237-242, 2000.
- [5] Haridass, V., and Sivakumar, G., "Studies on synthesized nanosilica obtained from Pigeonite ash," International Journal ChemTech Research, Vol. 5, pp. 1263-1266, 2013.
- [6] Chakraverty, A. and Kalamirajulu, S., "Conversion of Rice husk into amorphous silica and combustible gas," Energy Conversion and Management, Vol. 32, pp. 365-370, 1991.
- [7] Kamath, S. R., and Phadke, A., "Silica gel from Rice husk ash: Preparation and Characterization," Ceram Chemistry, Vol. 75, pp. 444-447, 1998.
- [8] http://www.pptchem.com/pdf/Silica/Silica_Fumed_Web.pdf
- [9] Rajwade, A., "A selective preparation of phillipsite and sodalite from perlite," Materials Letters, Vol. 58, pp. 2012-2015, 2004.
- [10] <http://www.researchgate.net/publication/25004238180/Perlite.pdf>
- [11] Subramanian, D. N., Suresh, K. C., Paul, P. J., Dasgupta, S., and Rajan, H. K. S., "Precipitated silica from Rice husk ash by BSA process," 15th European Biomass Conference and Exhibition, Berlin, Germany, pp. 2091-2097, May 2007.
- [12] Mahapatra, L., and Narasimhan, S. K., "Synthesis and characterization of nanosilica," International Conference on Advances in Polymer Technology, India, pp. 278-284, Feb. 2010.
- [13] Soderqvist, K., Saka, Y., and Kuroki, Y., "Preparation of fine expanded perlite," Journal of Material Science, Vol. 34, pp. 2461-2468, 1999.
- [14] Falcato, E. L., Gattieri, E., Oliveira, L. H. D., Jato, S. L., "Conversion of Rice husk into soluble sodium silicate," Materials Research Bulletin, Vol. 9, pp. 335-338, 2006.
- [15] Sousa, A. M. D., Vicente, L., Mendes, C., and Fardade, C., "Silica gel obtained from rice husk ash," Chemistry and Chemical Technology, Vol. 3, pp. 321-326, 2009.
- [16] Thanday, N., and Nairayana, A., "Preparation of nanosilica powder from Rice husk ash by precipitation method," Chung Mei Journal of Science, Vol. 35, pp. 208-211, 2008.
- [17] Nayak, J. P., and Datta, J., "Preparation of silica aerogel by ambient pressure drying process using rice husk ash as raw material," Transactions of the Indian Ceramic Society, Vol. 88, pp. 1-4, 2009.

Biography



Ms. Khushboo Srivastava is pursuing Ph. D. from University of Kota, Kota [Rajasthan]. She got 4th rank in M. Sc. (Pure & Applied Chemistry) and 6th rank in M. Phil (Environmental Chemistry) at University of Kota. Her research interests are Solid Waste Management, Nanotechnology and Heterogeneous kinetics and Chemical Engineering. Besides being a scholar, she is associated with a Junior Research Fellow Project funded by Department of Science and Technology, Rajasthan, India.



Ms. Niharika Shringi is pursuing Ph. D. from University of Kota, Kota [Rajasthan]. She got 3rd rank in M. Sc. (Industrial Chemistry) at University of Kota. She has also qualified National Eligibility Test Examination. She is working in the field of Waste Management and Green Chemistry specially associated with microwave organic transformations.



Dr. Vijay Devi is a Lecturer in Department of Chemistry at Govt. J.D.B. Girls P.G. College, Kota, Rajasthan, India. She is working in the field of Homogeneous Catalysis. Several research scholars are doing Ph. D. under the supervision of her.



Prof. Ashu Rani is currently working as Head, Department of Pure and Applied Chemistry and Dean of post graduate departments at University of Kota, Kota [Rajasthan]. Several research scholars are doing M. Phil and Ph. D. under the supervision of her. Her research interests are Heterogeneous Catalysis, Waste management, Climate change and Nanotechnology. She is associated with several National and International Collaborations from the Industries and Universities.

Environmental Benign Route for the Utilization of Fly Ash as Heterogeneous Acid Catalyst for Various Organic Transformations

Kishore Srivastava¹, Nishita Shringi², Vijay Devn¹, Jyoti Kaul²

¹Department of Pure and Applied Chemistry, University of Kota, Kota-324005, Rajasthan, India

²PG Department of Chemistry, Govt. J.J.H. PG Girls College, Kota, Rajasthan, India

Abstract - Heterogeneous acid catalysts are active in a wide range of applications. In this review, an overview is given of the current knowledge available about the fly ash supported solid acid catalysts and their catalytic activity in various organic transformations. Atom effective, cost effective, recyclable and environmentally benign like attributes makes fly ash as solid acid catalyst a good alternative over hazardous homogeneous acid catalyst.

Keywords: Fly ash, Heterogeneous acid catalyst, Organic transformations.

I. INTRODUCTION

Catalytic technologies play a key role in the economic development and growth of the chemicals industry and contribute to around 20% of world GNP (gross national product). Development of heterogeneous catalysts has been a relatively recent area of research in the organic synthesis. A major emerging and challenging area of heterogeneous catalysis is that of environmental pollution control, with tightening legislation on the release of waste and toxic emissions having serious implications for the chemical industry [1]. The need for development of heterogeneous catalysts has arisen from the fact that homogeneous catalysts used for organic synthesis pose a few drawbacks. Heterogeneous catalysts offer several intrinsic advantages over their homogeneous counterparts: ease of product separation and catalyst reuse; bifunctional phenomena involving reactant activation/spillover between support and active phases; and process advantages through reactor operation in continuous flow versus batch configuration [2]. Heterogeneous catalysts are categorized as solid acid and solid base. A solid acid catalyst should possess high stability, numerous strong acid sites, large pores, a hydrophobic surface providing a favorable condition for reaction, and should also be economically viable [3]. This review focuses exclusively on fly ash supported solid acid catalysts as potential heterogeneous catalysts and their role in various organic transformations.

II. MATERIALS OF HETEROGENEOUS ACID CATALYSTS

Some materials which catalyze acid-catalyzed reactions are listed in Table 1.

Table 1: Materials for solid acid catalysts

Supports	Heterogeneous acid catalysts	catalyzed reactions are
Silica supported metal oxides	$\text{HClO}_4/\text{SiO}_2$, CoBr_2/S	[10], [11]
Alumina supported metal oxides	Polyphosphoric acid/ Al_2O_3	[12]

Heterogeneous acid materials	$\text{Al}_2\text{SiO}_5/\text{H}$	[13]
Solid super acids	Tungstic acid/mica-clay/mica	[14]
Pure metal oxides	TaCl ₅ , WO_3 , ZrO_2	[15], [16]

Heterogeneous acid catalysts can be prepared via several methods. Such as impregnation, precipitation, co-precipitation, chemical vapor deposition etc. Various characterization techniques like FTIR, pyridine FTIR, XRF, SEM-EDX, ESR, XPS and XRD can provide the detailed information of acidic sites on the catalytic surface.

III. GENERATION OF ACIDIC SITES

Heterogeneous acid catalysts are generally categorized by their Brønsted and/or Lewis acidity, the strength and number of these sites, and the morphology of the support (e.g. surface area, pore size, pore volume). The synthesis of pure Brønsted and pure Lewis acid catalysts attracts a great degree of academic interest, although the latter is harder to achieve because Brønsted acidity often arises from Lewis acid-base complexation, as illustrated in Scheme 1.



Scheme 1: Brønsted acidity arising from inductive effect of Lewis acid center coordinated to a silica support

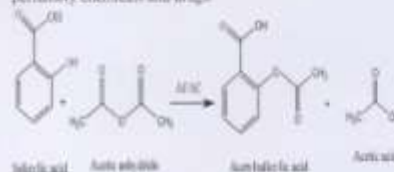
IV. FLY ASH SUPPORTED SOLID ACID CATALYSTS

FA contains high silica and alumina content, high degree of fineness, larger surface area, higher surface energy and more active faces which make it suitable to be used as solid catalyst and catalytic support for acid catalyzed reactions under solvent free condition. To improve surface activity of fly ash, several activation techniques such as mechanical [17], thermal [18] and chemical treatments [17] have been discussed in the literature which enhances the reactivity of fly ash from the combined effects of increased surface area and physicochemical changes induced in the bulk as well as on the surface.

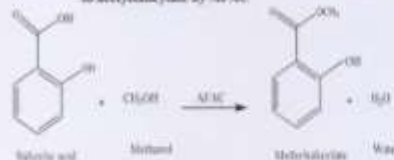
Homogeneous acids such as H_2SO_4 , H_3PO_4 [19] and heteropolyacids [20] represent the most commonly used catalysts for most of the important esterification reactions. But these acids are corrosive, hazardous, used in more than stoichiometric amounts, difficult to recover from reaction mixture, cannot be reused and leads to low selectivity of desired product with production of large volume of environmentally hazardous acidic waste. New environmental legislations calls for the reduction of waste production and use of more environmentally friendly alternative catalysts makes the current homogeneous system environmentally unacceptable. The substitution of traditional homogeneous Lewis and Brønsted acid catalysts by heterogeneous ones, e.g. solid acid catalysts such as sulfated zirconia, zeolites, acidified silica [21] constitutes a more environmentally friendly alternative to the organic reactions.

Acid activation of FA has been widely used for developing acidic sites for catalytic applications as solid acid. HCl treated fly ash catalyst was prepared by Anita et al [22] to examine their catalytic activity in esterification acetic acid with *n*-butanol which gave high selectivity (99.6%) and high yield of *n*-butyl acetate.

Khatti et al. [23] reported H_2SO_4 treated fly ash as nano-crystalline solid acid catalyst (AFAC) for esterification of salicylic acid with acetic anhydride and methanol to produce acetylsalicylic acid (aspirin) and methyl salicylate (oil of wintergreen) respectively in a single step, liquid phase and solvent free reaction condition with high yield >90% and purity (Scheme - 2 & 3). Acetylsalicylic acid is commonly known by its trade name aspirin is an effective non-steroidal analgesic, antipyretic and anti-inflammatory drug. Esterification products have wide applications in flavors, perfumery chemicals and drugs.



Scheme 2. Esterification of salicylic acid with acetic anhydride to acetylsalicylate by AFAC



Scheme 3. Esterification of salicylic acid with methanol to methylsalicylate by AFAC

Friedel-Craft acylation of 3,4-dimethoxyacetophenone using veratrole and acetic anhydride was investigated over cesium triflate loaded fly ash as a solid acid catalyst by Khatri et al.

[24]. The catalytic activity of the catalyst was efficiently reported upto 4 reaction cycles.

Recently, Coal fly ash supported Cr_2O_3 catalysts were synthesized using impregnation method by Muhammad et al. [25]. These catalysts were tested in peroxymonosulfate activation for sulfate radical generation and phenol degradation in aqueous solution. Kinetic study showed that phenol degradation followed first order kinetics. Resource recovery is one of the most effective strategies in waste management. Using solid waste for other application provides a route for solid waste recycling and a reduction waste disposal to landfills, bringing in environmental benefits and economic profits.

Sulfated zirconia supported fly ash catalyst was investigated by Khatri et al. [26] which found to be effective in solvent-free liquid phase benzylation of benzene, or toluene with benzyl alcohol.

V. CONCLUSION

This article deals with application of fly ash supported solid acid catalysts for various organic synthesis applied in recent publications. The process adopted for their preparation, their textural properties, thermal treatment, reuse, and leaching aspect have been discussed. The solid acid catalyst should be active, selective and stable under the reaction conditions.

ACKNOWLEDGMENT

The financial support was provided by Department of Science and Technology, Rajasthan, India, project sanction no. P-7/DST/R&D/11435-38.

REFERENCES

- [1] K. Wilson and J.H. Clark, "Solid acids and their use as environmentally friendly catalysts in organic synthesis," *Prog. Appl. Chem.*, vol. 72, pp. 1313-1319, 2000.
- [2] Y.C. Sharma and B. Singh, "Advancements in solid acid catalysts for eco-friendly and economically viable synthesis of biofuel," *Biomass, Bioproc. Biorefin.*, vol. 3, pp. 69-82, 2011.
- [3] <http://en.scribd.com/doc/45414444/Acid-catalysis>
- [4] M.R.E. Nugge, E. Kamath, E. Desrosky and A.K. Ghansai, "Two step method for preparation of TiO₂-X zeolite blend from fly ash for removal of cesium ions," *J. Hazard Mater.*, vol. 154, pp. 963-972, 2008.
- [5] M. Fan and R.C. Brown, "Comparison of the loss on ignition and thermogravimetric analysis techniques in measuring unburned carbon in coal fly ash," *Energy Fuel*, vol. 15, pp. 1414-1417, 2001.
- [6] I.K.A. Sear, "UK. Practice - a review of fly ash for use in concrete proceedings of the international workshop on novel products of combustion residue: opportunities and limitations," *Morilla, Spain, June 6-8, 2001*, pp. 45-52.
- [7] F. Blanes, M.P. Garcia and J. Ayala, "The effect of mechanically and chemically activated fly ash on mortar properties," *Fuel*, vol. 85, pp. 2018-2026, 2006.
- [8] T.C. Hu, "Adsorption of an acid dye onto coal fly ash," *Fuel*, vol. 87, pp. 3040-3045, 2008.
- [9] S. Shabchi and C.Y. Chia, "PM Processing and Characterization of New ZrO₂-Fly Ash Composites," *Frontier Metallurgy*, vol. 50, pp. 60-65, 2007.
- [10] A.T. Khan, T. Preiss and L.H. Choudhary, "Green Chemistry Approach to Fast and Highly Efficient One-Pot Synthesis of Bis-Imazopyl-1,2,5,6-Tetrahydropyridine-3-Carboxylate/Pyridine," *Synthesis*, vol. 15, pp. 2497-2502, 2006.

- [11] H.K. Fancey, "Zirconium(IV) Chloride-Silica Catalyzed Thioacetalization of Carbonyl Compounds," *Tetrahedron Lett.*, vol. 37, pp. 4621-4622, 1996.
- [12] H. Nomura, A. Terasaka and M. Nakagishi, "Preparation, Characterization and First Application of Alumina Supported Polyphosphoric Acid (PPA / Al₂O₃ - 20 - 3) as a Reusable Catalyst for the Synthesis of 14-Aryl-14H-dioxane [a, j] naphthalene," *Bull. Korean Chem. Soc.*, vol. 32, pp. 2311-2313, 2011.
- [13] Y. Li, W. Zhang, L. Zhang, Q. Yang, Z. Wei and Z. Feng, "Direct Synthesis of Al-SBA-15 Mesoporous Materials via Hydrolysis,"
- [14] Cunniffed, Approach," *J. Phys. Chem. B.*, vol. 108, pp. 9736-9744, 2004.
- [15] D.G. Barton, S.L. Sefid and E. Iglecia, "Solid acid catalysts based on supported tungsten oxides," *Topics in Catal.*, vol. 6, pp. 87-99, 1998.
- [16] M. H. Sarvari and H. Sharghi, "Zinc Oxide (ZnO) as a New, Highly Efficient, and Reusable Catalyst for Acylation of Alcohols, Phenols and Anilines under Solvent Free Conditions," *Tetrahedron*, vol. 61, pp. 10903-10907, 2005.
- [17] S. Ramu, N. Lingiah, B. Devi and I. Sanyasirama, "Esterification of palmitic acid with methanol over tungsten oxide supported on zirconia solid acid catalyst: effect of method of preparation of the catalyst on its structural stability and reactivity," *Appl. Catal. A Gen.*, vol. 276, pp. 163-168, 2004.
- [18] A. Sharma, K. Srivastava, V. Devra and A. Rani, "Modification in properties of fly ash through mechanical and chemical activation," *American Chem. Soc. J.*, vol. 2, pp. 177-187, 2012.
- [19] S. Kataria, S. Kabra, A. Sharma, R. Hada and A. Rani, "Surface modification of fly ash by thermal activation: A DR/FTIR Study," *Int. Res. J. Pure & Applied Chemistry*, vol. 3, pp. 299-307, 2013.
- [20] K. L. Williamson, *Macroscale and microscale organic experiments*, 2nd ed, Boston: Houghton Mifflin, 1994.
- [21] Y. Peng and G. Song, "Heteropoly acid catalyzed synthesis of aspiro," *J. Chem. Educ.*, vol. 3, pp. 144, 2000.
- [22] G. Eamukon, N. Nagaraja, "Selective synthesis of phenyl salicylate (salol) by esterification reaction over solid acid catalyst," *J. Mol. Cat. A Chem.*, vol. 223, pp. 155-159, 2004.
- [23] A. Sharma, S. Kataria, S. Kabra, R. Hada and A. Rani, "Acid Activated Fly Ash, as a Novel Solid Acid Catalyst for Esterification of Acetic Acid," *Indian J. Appl. Res.*, vol. 3, pp. 37-39, 2013.
- [24] C. Khatri and A. Rani, "Synthesis of nano-crystalline solid acid catalyst from fly ash and its catalytic performance," *Fuel*, vol. 87, pp. 2886-2892, 2008.
- [25] C. Khatri, D. Jain and A. Rani, "Fly ash supported cerium triflate as an active recyclable solid acid catalyst for Friedel-Crafts acylation reaction," *Fuel*, vol. 89, pp. 3853-3859, 2010.
- [26] S. Muhammad, E. Saputra, H. Sun, J.D.C. Ardero, D.A. Fungaro, H.M. Ang, M.O. Yade and S. Wang, "Coal fly ash supported Ce/Co catalysts for phenol degradation using peroxymonosulfate," *RSC Advances*, vol. 2, pp. 5645-5650, 2012.
- [27] C. Khatri, M. Mishra and A. Rani, "Synthesis and characterization of fly ash supported sulfated zirconia catalyst for benzoylation reaction," *Fuel Process. Technol.*, vol. 91, pp. 1288-1295, 2010.

BIOGRAPHY



First author Dr. Khushbu Srivastava is pursuing Ph. D. from University of Kota, Kota (Rajasthan). She got M.Phil. in M. Sc. (Pure & Applied Chemistry) and M.Tech. in M. Phil. (Environmental Chemistry) at University of Kota. Her research interests are Solid

Waste Management, Nanotechnology and Heterogeneous Catalysis and Chemical Engineering. Besides being a scholar, she is associated with a Junior Research Fellow Project funded by Department of Science and Technology, Rajasthan, India.



Ms. Shreelika Shringi is pursuing Ph. D. from University of Kota, Kota (Rajasthan). She got 3rd rank in M. Sc. (Industrial Chemistry) at University of Kota. She has also qualified National Eligibility Test Examination. She is working in the field of Waste Management and Green Chemistry specially associated with microwave organic transformations.



Dr. Vijay Devra is a Lecturer in Department of Chemistry at Govt. J.D.B. Girls P.G. College, Kota, Rajasthan, India. She is working in the field of Heterogeneous Catalysis. Several research scholars are doing Ph. D. under the supervision of her.



Correspondence author Prof. Asha Rani is currently working as Head, Department of Pure and Applied Chemistry and Dean of post graduate departments at University of Kota, Kota (Rajasthan). Several research scholars are doing M. Phil. and Ph. D. under the supervision of her. Her research interests are Heterogeneous Catalysis, Waste management, Climate change and Nanotechnology. She is associated with several National and International

Collaborations

the Industries and Universities.

A Facile Method for Production of Amorphous Silica from Perlite under Microwave Irradiation

Khushboo Selvastava, Research Scholar, Department of Pure and Applied Chemistry, University of Kota, Kota, Rajasthan

Niharika Shringi, Research Scholar, Department of Pure and Applied Chemistry, University of Kota, Kota, Rajasthan

Vijay Devra, Department of Chemistry, JDB Girls College, Kota, Rajasthan

Ashu Rani, Professor & Head, Department of Pure and Applied Chemistry, University of Kota, Kota, Rajasthan

ABSTRACT

The objective of this study was to develop a method to produce amorphous silica from perlite under microwave irradiation and to determine the influence of different NaOH concentration, microwave irradiation time and temperature on the percentage yield of SiO_2 content in the obtained amorphous silica. The whole process was divided into three steps: (i) alkali solubilisation of perlite, (ii) subsequent gel formation and (iii) acid dissolution. The synthesized materials were characterized by XRF, BET surface area, XRD, FTIR and SEM-EDS techniques. The maximum percentage yield of SiO_2 (94.48%) content was extracted by 4 N NaOH at 90 °C for 15 min. The specific surface area of synthesized AS was found to be ~194 m²/g. EDS analysis indicated that silicon was the most abundant element present in AS. The XRD pattern and FTIR data supported the involvement in amorphous nature and hydrogen bonded silanol and siloxane groups in AS respectively as compared with raw perlite. The results show that this novel preparation procedure provides an easy pathway to produce amorphous silica with high SiO_2 content from perlite, solid waste, according to specification.

Keywords

Amorphous silica, Affecting factors, Microwave irradiation, Perlite

1. INTRODUCTION

Perlite is a naturally occurring amorphous, hydrated volcanic glass formed through the secondary alteration of obsidian by the incorporation of water into the glass silica structure and can be an economically viable for production of silica gels and powders. The estimated worldwide reserves of perlite are estimated about 700 million tonnes [1]. The use of silica from the perlite is a major concern of research interest. Their approach may be classified into two categories: (a) purification or modification of perlite to produce highly pure silicon and (b) silica compounds utilization as an economic source of silica for the cement

industry, lightweight construction products, abrasives and absorbents [2].

Perlite is rich in silica that is a cost effective raw material for dried silica gel (SG) and amorphous silica (AS) production. SG is the amorphous (non-crystalline) form of SiO_2 which contains three-dimensional network or aggregated silica particles of colloidal dimension and is classified as aerogel (pores filled with water), xerogel (aqueous phase in the pores is removed by evaporation) or aerogel (solvent is removed by supercritical extraction) while AS is a fine powder form with high surface area obtained by coagulation of particles from aqueous solution under the influence of appropriate electrolyte concentration [3]. Both materials have many potential applications, such as reinforced filler, an adsorbent, a catalyst host, for chromatograph packing columns, in cosmetics, in vegetable oil refining, in pharmaceuticals, in paint and coating etc. Commercially, SG and AS are produced from tetraethoxyorthosilicate through sol-gel process [4] or from the fusion of quartz sand with soda ash in a furnace at high temperature (>1300 °C) [5]. But these techniques are very expensive and energy intensive. Recently, SG and AS have been synthesized from various types of biomass such as rice husk ash [6], rice hull ash [7] and corn cobs ash [8] etc. Critical economic and environmental situations of the current days encourage companies and researchers to develop and improve technologies intended to reduce or minimize solid wastes. As a consequence, much effort has been expended in different areas. Therefore, it would be advantageous to develop a simple, economic, time and energy efficient method for the production SG and AS from perlite under microwave heating, thereby utilizing solid waste for an economically value-added product.

Microwave irradiation (MW), a non-classical heating technique has now become an indispensable part of all fields of synthetic chemistry. Green, economic, efficient heating, drastic reduction in reaction time, providing phase purity with high yields under milder reaction condition and high reproducibility like characteristics has made it a promising tool for the synthesis various organic transformations. MW irradiation causes internal heating (in core volumetric heating) by directly coupling with the

molecules of the substrate of reaction, leading to rapid increase in temperature for consuming time and energy [9]. In recent years, synthesis of various types of silica materials such as SBA-15, MCM-41, organosilica and metal modified MCM-41 under microwave heating has also attracted attention due to fast response rate, low energy consumption and the product of uniform size [10]. MW can heat up substances even in Teflon plastic containers which avoid corrosion of reactors due to leaching of strong base. The MW equipment offers an immediate incline to desired temperature and distributes heat homogeneously giving rise to high quality materials [11].

In this context, the use of MW heating for preparation of AS from perlite is proposed. The effects of various parameters such as different concentrations of NaOH solutions, microwave irradiation time and reaction temperature are investigated. AS production from perlite alleviates the solid waste disposal problem and creates a commercially viable value-added product.

2. EXPERIMENTAL

A. Materials and Apparatus

Perlite ($\text{SiO}_2 + \text{Al}_2\text{O}_3 > 70\%$) was collected from Indica Chemical Industries Pvt. Ltd., Kothwar, India. All chemicals such as NaOH (99%), H_2SO_4 (98%) were purchased from S.D. Fine Chem. Ltd., India. The SG and AS preparation are carried out in MW synthesis system made by CEM, USA (Model - Discover) which can adjust its power within the range of 0-700 W (Figure 1).



Figure 1. Microwave Synthesis System

B. Preparation of AS from Perlite

The whole process as indicated in Scheme-1 is divided into three steps:

(i) Alkali solubilisation of perlite

Raw perlite (RP) was thoroughly washed with distilled water to remove adhering soil, dust and then dried at 110°C for 12 h. After that, it was calcined at 800°C for 3 h and name is thermally activated perlite (TAP). 5 g of TAP was added to various concentrations of NaOH solution (1, 2, 3 and 4 N) in open vessel system of CEM MW reactor using round bottomed flask made of Pyrex glass attached with air condenser to produce sodium silicate solution. Then mixture was heated under MW irradiation at 150 W for different time and alkali concentration with high stirring mode to obtain best results. The solution was filtered through Whatman No. 41 filter paper and was washed with 15 ml of de-ionized water. Later the filtrate and washing were allowed to cool to room temperature.

(ii) Preparation of silica gel

In the gelation process, the sodium silicate solution was titrated with 5 N H_2SO_4 under constant stirring. The pH of the solution was monitored and the titration was stopped at pH 7 to produce SG. The soft gel was aged for 5 h. After aging, the gel was gently broken by adding 30 ml of deionized water to make slurry. Now, the slurry was washed by vacuum filtration using distilled water to remove sodium sulfate followed by drying in a vacuum oven at 80°C for 12 h and ground into dried SG.

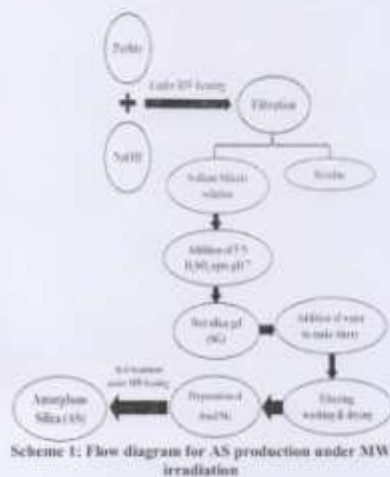
(iii) Synthesis of amorphous silica (AS)

For producing AS, the dried SG was heated with 15 ml of 1 N HCl solution by MW heating at 90°C for 10 min at 150 W and then washed repeatedly using deionized water to make it acid free. Now, the obtained AS was dried at 110°C for 12 h.

In order to compare the effect of heating methods same experiment was performed in oil bath under conventional heating maintaining similar reaction conditions as kept under MW heating.

C. Regeneration

Regeneration is the step where calcium hydroxide reacts with sodium sulphate to form calcium sulphate and sodium hydroxide. As per the reported procedure, NaOH is regenerated up to 90 %. The regenerated NaOH solution is used for digestion of the fresh perlite [12]. The obtained calcium sulphate can be used for other laboratory work.



Scheme 1: Flow diagram for AS production under MW irradiation

D. Characterization Techniques

The chemical components of the samples were analyzed by XRF spectrometer (Philips PW1606). The BET surface area was measured by N_2 adsorption-desorption isotherm study at liquid nitrogen temperature (77 K) using Quantachrome NOVA 1000c surface area analyzer. Powder XRD studies were carried out by using (Philips X'pert) analytical diffractometer with monochromatic $CuK\alpha$ radiation ($\lambda = 1.54056 \text{ \AA}$) in a range of $0 - 60^\circ$. The particle size of the samples was determined from Mastersizer 3000 laser diffraction particle size analyzer manufactured by Malvern Instruments Ltd. FTIR study of the samples was done using FTIR spectrometer (Alpha-T model, Bruker, Germany) by mixing the sample with KBr pellet mode (in 1:20 wt. ratio) in the range of $4000-400 \text{ cm}^{-1}$. The detailed imaging information about the morphology and surface texture of the sample was provided by SEM (Model - JEOL JSM 5600).

3. RESULT AND DISCUSSION

A. COMPARISON BETWEEN CONVENTIONAL VS MW HEATING AND EFFECT OF NaOH CONCENTRATION

Table-1 presents the yield percentage of silica obtained from MW heating in MW reactor and conventional heating in oil bath at various concentrations of NaOH solution (1, 2, 3 and 4 N) which indicates that the concentration of NaOH solution positively affects the % yield of SiO_2 in AS. It has been found that for 4 N NaOH concentration, MW heating for 15 min at 90°C yielded

more SiO_2 in AS (94.48%) whereas at same conditions, the effect of conventional heating showed a quite low yield (87.61%) of product. It has been found that for every NaOH concentration, due to in core volumetric MW heating of materials it produced more silica than conventional heating [13].

Table 1. Effect of concentration of NaOH solution on the % yield of silica in AS

Concentrations of NaOH solution (N)	Yield of SiO_2 (%)	
	under microwave heating	under conventional heating
1 N	59.08	47.37
2 N	73.76	64.06
3 N	88.06	79.13
4 N	94.48	87.61

Optimized conditions: Temperature = 90°C , time = 15 min, power = 150 W

(i) Effect of MW Irradiation Time

Exposure time to MW is one of determining factors of AS production. Figure 2 represents a directly proportional relationship of % yield of SiO_2 in AS obtained with MW irradiation time. Increase in MW irradiation time from 5 to 15 min along with concentration of NaOH (1 N to 4 N) solution produced better results. MW irradiation for 15 min using concentration of 4 N NaOH solution produced 94.48% yield of silica which the highest amongst all combinations. On further increasing MW irradiation time and alkali concentration no change in AS amount was observed.

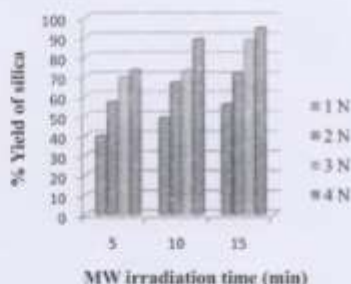


Figure 2. % Yield of silica in AS obtained as function of concentration of NaOH solution and MW irradiation time

(iii) Effect of Temperature

Figure 3 clearly shows effect of temperature on the % yield of SiO_2 in AS. On increasing temperature from 50 to 90 °C, the yield is continuously increased from 40.64 to 94.48%. MW irradiation for 15 min at 90 °C generated maximum yield percentage of silica content.

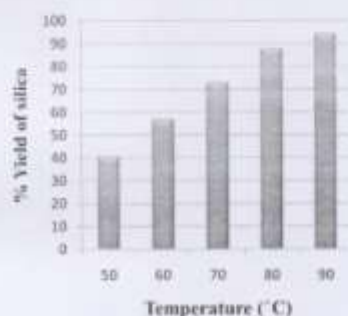


Figure 3. Effect of temperature on % yield of silica in AS

B. Characterization of AS

Prior to its use as a raw material, the components of perlite were characterized by XRF (in wt%): SiO_2 (73.9%), Al_2O_3 (12.8%), Na_2O (4.7%), K_2O (4.6%), ZnO (0.8%), Fe_2O_3 (0.6%), TiO_2 (0.1%), and trace elements (2.7%).

RP contains 73.9 wt.% silica with 5 m^2/g surface area and 3.20 μm average particle diameter while TAP poses 74.3 wt.% silica content with 4 m^2/g surface area. Quantitative analysis of the components indicates the obtained AS contains white fine solid with 94.48% yield of SiO_2 having ~104 m^2/g specific surface area in the range of 500 nm - 0.6 μm particle size. EDS spectra of RP and AS are also shown in Figure 4 indicating the presence of high amount of Si content in AS as compared with RP. Loss on ignition (LOI) is determined by heating a certain weighed quantity of perlite in muffle furnace at 800°C for 3 h. The LOI amount was 4.1 wt. % which corresponds to the removal of moisture and coexisting unburned carbon from sample [14].



Figure 4. EDS spectra of (a) RP (b) AS

The images of wet SG and AS obtained from perlite are shown in Figure 5.

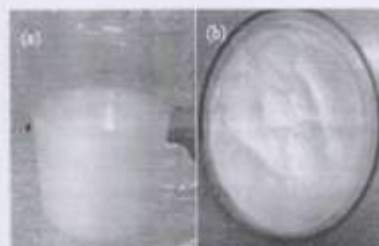


Figure 5. Images of (a) Wet SG (b) AS

XRD patterns of RP, TAP and prepared AS are shown in Figure 6 (a-c) which indicates the hump in the 2θ ranging from 10 to 25° indicating disordered structure, due to AS.

particles [15]. A lack of sharp, defined peaks in RP and AS exhibits non-crystalline or amorphous material while TAP exhibits more highly ordered structure along with single crystalline peak at $2\theta = 27.39^\circ$ due to the presence of tridymite (polymorphs of quartz) phase (ICPDS No.: 42-1401) [16]. The presence of strong broad peaks in AS suggests more characteristics of amorphous SiO_2 , as compared with RP.

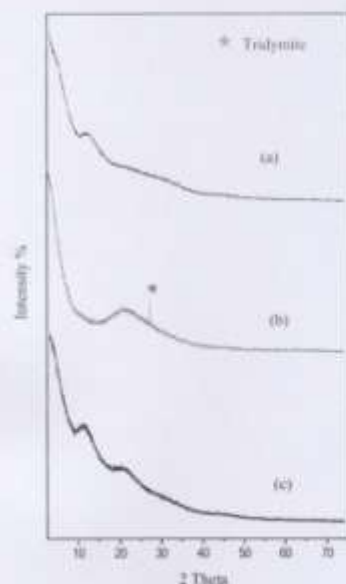


Figure 6. XRD diffraction patterns of (a) RP (b) TAP (c) AS

FTIR spectroscopic tool is used to identify the key functional groups indicating structural changes in the samples (Figure 7.a-c). A broad band in the range of 3670-3000 cm^{-1} responsible for the isolated and surface -OH groups of -Si-OH whereas the band at 1630 cm^{-1} assigned to the bending mode (ν_{bend}) of coordinated water [17]. The results indicates that the intensity of these peaks is decreased after calcination whereas is increased after silica extraction. The predominant absorbance peak between 1200 and 1050 cm^{-1} is associated with the Si-O-Si asymmetric band stretching vibration and the

corresponding symmetric stretch at $\sim 802 \text{ cm}^{-1}$ [18]. The intense peak in the range of 470-450 cm^{-1} is attributed to the Si-O asymmetric bending vibration of Si-O-Si bond. After thermal activation and silica extraction, the intensity of all these peaks is shifted towards higher wave number [19]. AS is exhibited a relatively strong peak at about 817 cm^{-1} and it can be distinguished from the band of crystalline silicate [20]. The presence of more pronounced Si-O-Si bending vibrations at 473 cm^{-1} confirms the highly condensed silica network in AS spectra (Figure 7c) [21].

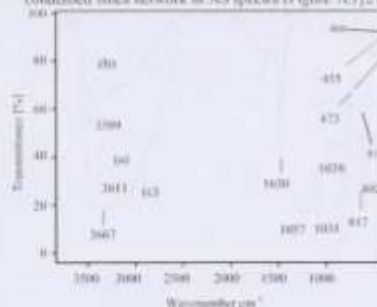


Figure 7. FTIR spectra of (a) RP (b) TAP (c) AS

In Figure 8 (a-d), the SEM image of RP (Figure 8a & b) indicates irregular shaped crumbled porous particles with broken or ragged edges [22]. The morphology of TAP (Figure 8c) is less irregular due to evaporation of water from the perlite whereas the SEM micrograph of AS (Figure 8d) demonstrates globular shaped highly porous gelatinous particles of different shapes and sizes in agglomerated form. Such type of large gelatinous mass is due to the presence of amorphous silica gel skeleton [23].

C. Surface chemistry of AS

The surface properties of AS, which is considered to be an oxide adsorbent, in many cases depend on the presence of different types of silanol groups. Surface OH groups are subdivided as following groups and are presents on the surface of AS in Figure 9 (a-d): (a) isolated free (single silanols), SiOH (b) geminal free (geminal silanols or silanediols), Si(OH)_2 (c) vicinal, or bridged, or OH groups bound through the hydrogen bond (H-bonded single silanols, H-bonded geminals, and their H bonded combinations) (d) surface siloxane groups Si-O-Si bridges with oxygen atoms on the surface. At last, there is structurally bound water inside the silica skeleton and very fine ultra micropores, $d < 1 \text{ nm}$ (d is the pore diameter), i.e. internal silanol groups [24].

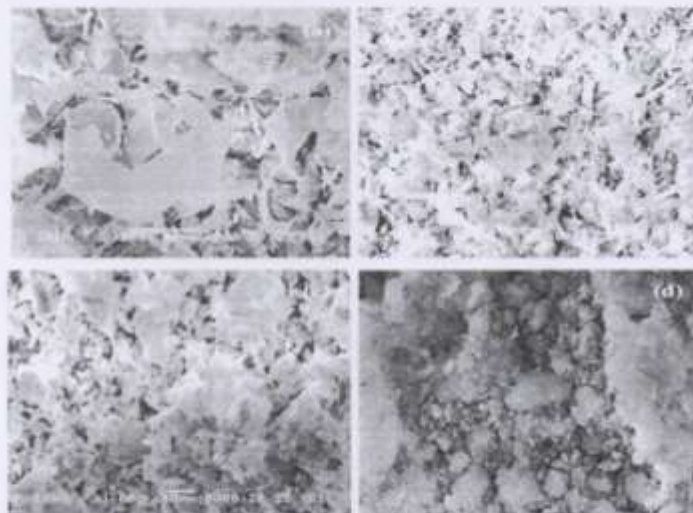


Figure 8. SEM micrographs of (a) RP at low magnification (b) RP at high magnification (c) TAP (d) AS

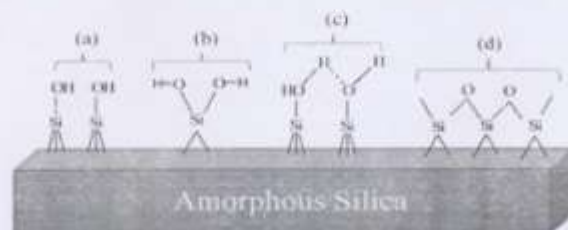


Figure 9. Types of silanol groups and siloxane bridges on the surface of AS

4. CONCLUSIONS

A rapid, simple and energy efficient method has been developed to produce AS from perlite using microwave heating by alkali solubilisation and subsequent acid treatment. Compared with conventional heating method at the same reaction time and temperature, MW heating at 90 °C for 15 min gave a higher percentage yield of AS (94.48%) using 4 N NaOH solution. The study revealed that the obtained AS was found in agglomerated form with $\sim 104 \text{ m}^2/\text{g}$ specific surface area. The used chemicals can be regenerated making it an environmentally benign, cost

effective and atom efficient process and finds a novel route to utilize abundant waste perlite in future.

5. ACKNOWLEDGEMENT

The authors are thankful to Dr. D.D. Phuse and Er. V.K. Abhis for SEM-EDS analysis and Mr. Mukul Gupta for XRD conducted at UGC DAE-CSR Lab Indore. XRF analysis was conducted at Punjab University, Chandigarh. The financial support was provided by Department of Science and Technology, New Delhi, India, project sanction no. FAU/UST/ 600 (56) /C/2013-14.

6. REFERENCES

- [1] A. G. Celik, A. M. Kiliç and G. O. Cakal, "Expanded perlite aggregate characterization for use as a lightweight construction raw material," *Physicochemical Problems of Mineral Processing*, vol. 49, no. 2, pp. 689-700, 2013.
- [2] S. Kabra, S. Kataria and A. Rani, "Characterization and study of narkesh perlite," *Inter. J. Innovative Res. Sci. Eng. and Technol.*, vol. 2, no. 9, pp. 4319-4326, 2013.
- [3] U. Kalapathy, A. Proctor and J. Shultz, "A simple method for production of pure silica from rice hull ash," *Bioresour. Technol.*, vol. 73, pp. 257-262, 2000.
- [4] Nakamura, Method for production of novel nano silica particle and use of the nano silica particle, U.S. Patent 2010/030582 A1, Dec. 30, 2010.
- [5] M. Stephens et al., Precipitated silicas, silica gels with and free of deposited carbon from caustic biomass ash solutions and processes, U.S. Patent 6 638 354 B2, Oct. 28, 2003.
- [6] R. Prasad and M. Pandey, "Rice husk ash as a renewable source for the production of value added silica gel and its application: an overview," *Bulletin Chemical Reaction Eng. & Cat.*, vol. 7, no. 1, pp. 1-25, 2012.
- [7] S.R. Kamath and A. Proctor, "Silica gel from Rice hull ash: Preparation and Characterization," *Cereal Chemistry*, vol. 75, pp. 484-487, 1998.
- [8] E.A. Okunribido, P.E. Inuishi and S.O.O. Olusunkan, "Extraction and characterization of Amorphous Silica from Corn Cob Ash by Sol-Gel Method," *Chemistry and Mater. Res.*, vol. 3, no. 4, pp. 68-72, 2013.
- [9] C. Oliver Kappe, "Controlled Microwave Heating in Modern Organic Synthesis," *Angewandte Chemie Inter. Ed.*, vol. 43, pp. 6250-6264, 2004.
- [10] C. Yuan, W. Hong-jun and X. Zhi-nan, "Advances in Microwave Assisted Synthesis of Ordered Mesoporous Materials," *Trans. Nonferrous Metals Soc. China*, vol. 19, pp. s656-s664, 2009.
- [11] I. Bilecka and M. Niederberger, "Microwave Chemistry for Inorganic Nanomaterials Synthesis," *Nanoscale*, vol. 2, pp. 1358-1374, 2010.
- [12] D.N. Subbukrishna, K.C. Suresh, P.J. Paul, S. Dasappa and N.K.S. Rajan, "Precipitated silica from Rice husk ash by IPSIT process," *15th European Biomass Conference and Exhibition, Berlin, Germany*, pp. 2091-2093, 2007.
- [13] S. Rangrodmunichai, W. Phokkhamui and N. Sangkhao, "Preparation of Silica Gel from Rice Husk Ash Using Microwave Heating," *J. Metals, Materials and Minerals*, vol. 19, no. 2, pp. 45-50, 2009.
- [14] K. Kordatos, S. Gavala, A. Ntzouni, K.N. Pitsiolos, A. Kyritsi and V. Kanelouri-Rigopoulou, "Synthesis of Highly Siliceous ZSM-5 Zeolite using Silica from Rice Husk Ash," *Microporous and Mesoporous Mater.*, vol. 115, no. 1-2, pp. 189-196, 2008.
- [15] K. Anantha, R. Ravibhaskar and G. Sivakumar, "Extraction, Synthesis and Characterization of Nanosilica from Rice Husk Ash," *Inter. J. Nanotech. and Applications*, vol. 4, no. 1, pp. 61-66, 2010.
- [16] Z. Ghossein and H. Younesi, "Preparation and Characterization of Nanosilica NAA from Rice Husk at room temperature without Organic Additives," *J. Nanomaterials*, vol. 2011, pp. 1-8, 2010.
- [17] R.M. Silverstein and F.X. Webster, *Spectrometric Identification of Organic Compounds*, 6th ed., Wiley India Pvt. Ltd., John Wiley Publication, 2006.
- [18] K. Srivastava, V. Devra and A. Rani, "Fly ash supported vanadia catalyst: An efficient catalyst for vapor phase partial oxidation of toluene in a micro-reactor," *Fuel Process Technol.*, vol. 121, pp. 1-8, 2014.
- [19] N. Thindilij, and A. Namiya, "Preparation of nanosilica powder from Rice husk ash by precipitation method," *Chiang Mai J. Sci.*, vol. 35, pp. 206-211, 2008.
- [20] J. Oyama, "Determining of Crystalline Silica in Respirable Dust Samples by Infrared Spectrophotometry in the Presence of Interferences," *J. Occup. Health*, vol. 45, pp. 94-103, 2003.
- [21] J.P. Nayak and J. Bera, "Preparation of Silica Aerogel by Ambient Pressure Drying Process using Rice Husk Ash as Raw Material," *Trans. Ind. Ceramic Soc.*, vol. 68, pp. 1-4, 2009.
- [22] K. Srivastava, N. Shringi, V. Devra and A. Rani, "Pure Silica Extraction from Perlite: Its Characterization and Affecting factors," *Inter. J. Innovative Res. Sci. Eng. Technol.*, vol. 2, no. 7, pp. 2936-2942, 2013.
- [23] J. Nayak and J. Bera, "A Simple Method for Production of Humidity Indicating Silica Gel from Rice Husk Ash," *J. Metals, Materials and Minerals*, vol. 19, no. 2, pp. 15-19, 2009.
- [24] Colloidal Silica: Fundamentals and Applications, edited by Horacio E. Bergna and William O. Roberts, CRC Press, Taylor & Francis Group, 2006.

Research Article

Microwave Assisted Acid Activation of Fly Ash: A Green Process for Enhancing its Physico-Chemical Attributes for Esterification under Dielectric Heating

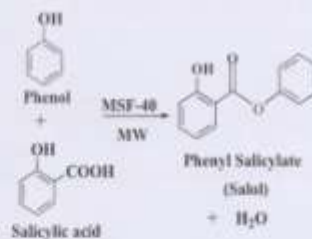
Niharika Shringi, Khushboo Srivastava and Ashu Rani*

Department of Pure and Applied Chemistry, University of Kota, Kota, Rajasthan, India

Abstract

In the present investigation, acid activation of ball milled fly ash was performed under microwave heating. The samples were initially ball milled and then treated with 5N H₂SO₄ under microwave irradiation for 20 to 40 min. To determine the physico-chemical attributes of samples, various techniques i.e. XRF, N₂ adsorption-desorption, XRD, FTIR, pyridine FTIR and SEM were used. Mechanical activation broke large particles and acid treatment under microwave heating provided in-core volumetric heating of sample to increase surface area and acidity. The prepared MSF-40 catalyst with crystalline size 14 nm and 22 m²/g surface area was observed as an efficient solid acid catalyst for solvent-free esterification of phenol and salicylic acid under dielectric heating.

Keywords: Fly ash, Ball milling, Microwaves, Chemical activation, Esterification.



*Correspondence

Author: Ashu Rani

Email: ashu.uok@gmail.com

Introduction

Approaches to address the environmental concerns by application of non-traditional methods such as microwave (μ W) irradiation and catalysis has emerged as major tools in green synthesis and engineering. The use of ' μ W flash heating' in synthetic chemistry has emerged as an energy efficient heating source as it reduces processing time by several orders of magnitude by in-core volumetric heating, suppresses side reactions and improves yield, product purity and reproducibility compared to traditional processes [1]. Along with this, encouragement of heterogeneous catalysis in organic synthesis has facilitated greener, safer and non-corrosive route by reduction in waste and easy handling allows the design of continuous flow processes that are economically very attractive at the industrial scale compared to their homogeneous counterparts [2]. Involvement of μ W irradiation with activated catalysts (AC) during reaction offer several advantages. AC not only provide active surface for the reaction but also acts as direct selective heating source by absorbing μ W. The AC is also capable to serve as medium for reactions, promotes dry or solvent-free synthesis. Use of different phase catalyst other than reaction substrate provides easy recovery from reaction mixture and reusability of catalyst after simple activation [3].

Acid activation of inorganic materials such as silica, clays and activated carbon etc. with hot mineral acids under reflux condition is one of the widely used techniques to improve surface acidity thus catalytic efficiency of the material. In recent years, μ W assisted acid treatment of clays has produced equivalent or better results compared to traditional refluxing methodologies. Among μ W activation parameters, μ W power plays a crucial role in specific surface area (SSA) enhancement and can affect the basic skeleton during acid treatment. Smectite clay treated with 2M HCl upto 500 W showed increased SSA but didn't change the component structure to any perceptible extent while the samples activated at 650 W showed partial destruction in structure as evident by XRD and also showed

reduction in SSA [4, 5]. Up to 600 W, Brazilian bentonite activated with H_2SO_4 (6N) didn't show any significant alterations and SSA also followed a proportional relationship. Activation above 800 W power gave more drastic reduction and 1000 W showed complete destruction in structure while in SSA sharp declination was observed [6]. μW assisted 4N H_2SO_4 treated Amazon flint kaolin served as an efficient solid acid catalyst for the biodiesel production with 96.4 % conversion rate for esterification confirming sufficient active catalytic sites compared to catalyst prepared under reflux conditions [7].

Recently, fly ash (FA) has been explored as active solid support in synthesis of different heterogeneous Brønsted and Lewis acid catalysts such as FA supported scandium triflate [8], sulphated zirconia [9] and cerium triflate [10] for industrial important organic transformations. All such studies although resulted with increased active acid sites on FA surface, conventional hydrothermal acid digestion and high temperature exposure for a longer time encouraged to find a faster technique for FA supported catalyst preparation. μW irradiation heating has been reported earlier in FA sintering [11], zeolite synthesis [12] and curing of FA filled epoxy composites [13]. During the present work, H_2SO_4 activated FA is prepared in microwave reactor possessing stable Brønsted active sites catalyzing μW assisted solvent free synthesis of phenyl salicylate, commercially known as 'salol', widely used as an antiseptic, anodyne analgesic [14] and ultraviolet radiation filters [15].

Experimental

Materials and Apparatus

Coal fly ash (Class F type with $SiO_2+Al_2O_3 > 70\%$) was collected from Jamshedpur Thermal Power Station (Jamshedpur, Jharkhand, India). Concentrated sulphuric acid (98 %), salicylic acid and phenol were purchased from S. D. fine Chem. Ltd., India and were used as such. Mechanical activation of FA was performed in high energy planetary ball mill Retsch PM-100, Germany. The prepared catalysts were calcined in CEM microwave furnace (Model- Phoenix). The acid activation of milled FA and its catalytic evaluation for esterification reaction was carried out in Microwave synthesis system CEM, USA (Model-Discover) single mode type, using following modes:

Open vessel system

Acid treatment of milled FA was carried out under this mode in atmospheric pressure condition. The operating parameters were controlled by software that enables on-line control during the activation. The reaction temperature during the run was monitored with infrared sensor placed aligned just below the reaction vessel and was stirred with the help of built-in automatic magnetic stirrer. Variable power was supplied by microprocessor-controlled single-magnetron system. The maximum μW irradiation power was utilized during 'ramping time' to attain desired temperature and then, lower power was used to maintain reaction temperature during the 'holding time'. The reaction mixture was cooled to 50 °C within the instrument in 'cooling time'.

Closed vessel system

Evaluation of catalytic activity of prepared FA samples were performed in closed vessel system using closed Pyrex glass tubes (ca. 10 mL) with teflon-coated septa and teflon stirring bar. The reaction was carried out at desired temperature in solvent-free condition using power maximum (P_{max}) feature, responsible for maintaining temperature throughout the reaction by simultaneous μW heating and cooling by compressed air. The reaction run was accomplished through the same stages of ramping, holding and cooling time as mentioned in open vessel system.

Preparation of catalyst

For preparation of MSF catalysts, raw FA was mechanically activated in ball mill for 15 h to synthesize MFA-15 having specific surface area ($17\text{ m}^2/\text{g}$) according to earlier procedure [16]. For the removal of carbon, sulfur and other impurities, MFA-15 was calcined at 800 °C for 3 h in muffle furnace. Then MFA-15 was refluxed in 5N H_2SO_4 at 1:2 molar ratio in an open vessel system at 90 °C and 100 W power for 20 and 40 min. Thus prepared slurry was cooled,

filtered and washed thoroughly with hot distilled water to achieve pH 7 and make it free from sulphate ions (tested by BaCl_2 solution). The activated samples were dried at 110°C for 24 h followed by calcining at 450°C for 1 h under static condition in microwave furnace. The prepared samples MSF-20 and MSF-40 are designated according to their microwave irradiation time. Figure 1 represents the temperature and power monitoring profile for acid activation of MSF-40 catalyst.

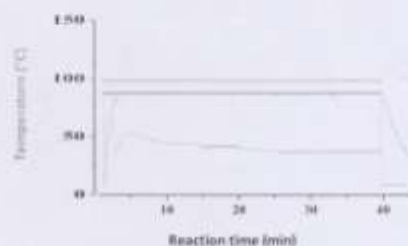


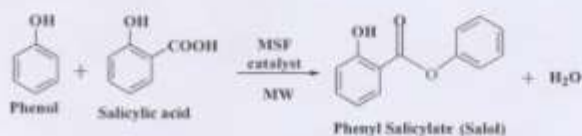
Figure 1 Temperature and Power profile of MSF-40 catalyst.

Characterization Techniques

The physico-chemical and morphological attributes of EA, MFA-15 and MSF samples were analyzed by XRF (Philips PW 1606), Quamachrome NOVA 1000e surface area analyzer (N_2 adsorption-desorption isotherm study), Powder XRD (Bruker diffractometer D8 Advance), FTIR DR5 spectrophotometer (Bruker Tensor-27) and SEM (JEOL JEM 5600). The crystalline size of phases and surface acidity measurement by FTIR experiment were determined by the previously reported procedure [17].

Catalytic activity: microwave assisted solvent-free synthesis of salol

The microwave assisted solvent-free esterification reaction using salicylic acid and phenol was carried by MSF catalyst as shown in Scheme 1.



Scheme 1 Microwave-assisted solvent-free synthesis of salol over MSF catalyst

In a typical reaction procedure, 20 mmol of phenol, 10 mmol of salicylic acid and catalyst (salicylic acid/MSF catalyst weight ratio = 3:1) were filled in Pyrex glass vial. Prior to the reaction, catalyst was activated at 450°C for 1 h in microwave furnace. After the reaction, acetone was added in the reaction mixture to dissolve the unreacted salicylic acid and filtered to separate out the catalyst. The reaction conditions were varied to obtain maximum yield and conversion into salol. The analysis of salicylic acid conversion was carried out by Gas Chromatograph (Agilent 7820 A) having a flame ionization detector and HP-5 capillary column of 30 m length and 0.25 mm diameter, programmed oven temperature of 70 – 240°C and N_2 (25 ml/min) as a carrier gas. The conversion of salicylic acid and yield of salol was calculated by using weight percent method as follows:

$$\text{Conversion (\%)} = 100 \times (\text{Initial wt \%} - \text{Final wt \%}) / \text{Initial wt \%}$$

$$\% \text{Yield of Salol obtained} = \frac{\text{g of Salol obtained}}{\text{g of Salol theoretically obtained}} \times 100$$

Catalyst regeneration

After the initial run, the used catalyst was filtered, washed thoroughly with acetone and dried in oven at 110 °C for 12 h followed by activation at 450 °C for 1 h in microwave furnace. Thus, the regenerated catalyst was used in next reaction cycles under the same reaction conditions.

Results and Discussion

The changes in structural and textural properties of FA after mechanical and chemical activation are summarized in Table 1. Increment in specific surface area from 17 m²/g (MFA-15) to 22 m²/g (MSF-40) was observed due to increased finely dispersed silica components by dissolution of mineral structure. However, further increase in μ W activation time didn't produce significant results [18].

Table 1 Characterization of fly ash before and after mechanical and chemical activation

Sample	Silica (wt, %)	Crystalline size (nm)	Specific surface area (m ² /g)
FA	61.90	33	9
MFA-15	64.27	29	17
MSF-20	65.12	15	21
MSF-40	65.79	14	22

FA: Raw fly ash, MFA-15: 15 h mechanically activated fly ash, MSF-20: Chemically activated fly ash under microwave heating for 20 min, MSF-40: Chemically activated fly ash under microwave heating for 40 min

The powder XRD of the raw, MFA-15 and MSF samples have shown mullite (3Al₂O₃·2SiO₂) phases at 16.4°, 25.8° and 26.2° while 20.73°, 26.55°, 40.68° and 49.95° confirms the presence of quartz (SiO₂) phases as represented in Figure 2 (a-d). The effect of 15 h ball milling of FA has reduced crystalline size from 33 to 29 nm [16] while acid activation under dielectric heating from 20 to 40 min has increased amorphous content and reduced crystalline size to 15 nm (MSF-20) and 14 nm (MSF-40) due to dissolution of some crystalline phases during acid treatment. Dielectric heating at low (100 W) μ W power has not altered the basic skeleton of FA which is evident by the resembling XRD patterns of FA and MSF samples. Nevertheless, the surficial structural changes were noticed due to partial destruction of aluminosilicate components evident by the increased silica content as shown in Table 1. Similar results were also reported in the literature signifying the effectiveness of μ W heating with low power supply [4, 5].

The FTIR spectra of raw FA and MFA-15 in Figure 3a shows a broad band with a maximum centered at 3500-3000 cm⁻¹ attributed to surface silanol -OH groups due to physisorbed water. The peak at 1650 cm⁻¹ attributed to the bending vibration ($\delta_{\text{H}_2\text{O}}$) of coordinated water molecule. Ball milling for 15 h broke the quartz structure and formation of more Si-OH groups took place which is evident by broadness in region of 1000-1200 cm⁻¹ range corresponding to the valence asymmetric stretching vibrations of the silicate oxygen skeleton [19].

In Figure 3b, FTIR spectra of MSF samples show noticeable increment in broadness at 3500-3000 cm⁻¹ compared to FA due to increased silanol groups and adsorbed water molecules on the surface. Instead of remaining isolated these surficial hydroxyl groups shows extensive hydrogen bonding with their neighbouring hydroxyl groups resulting in broadness of band. The increased amorphous silica in milled and acid activated samples can be characterized by an intense band in the range of 1000-1300 cm⁻¹ observed due to asymmetric Si-O-Si stretching which represents a higher shift from 1042 cm⁻¹ (MFA-15) towards 1048 cm⁻¹ (MSF-20) and 1061 cm⁻¹ (MSF-40). The promotion in amorphous silica percentage in MSF catalysts enhanced surface area and increased population of surface hydroxyl groups responsible for the improved surface reactivity of the samples.

The nature of acidic sites of the prepared catalysts was investigated by the presence of the adsorption bands of pyridine in the magnified range of 1650-1400 cm^{-1} as shown in Figure 4a & b. The IR peaks at 1598 cm^{-1} and 1540 cm^{-1} in MSF catalysts confirms the presence of sufficient Brønsted acidity due to formation of coordinated pyridine and hydrogen bonded pyridine respectively with surface -OH groups while band at 1490 cm^{-1} shows the pyridine associated with all acidic sites. Another peak at 1450 cm^{-1} assigned for Lewis acid sites as coordinately bound pyridine [20]. The pyridine adsorbed spectrum of MSF-40 catalyst shows more intense peak at 1540 cm^{-1} and 1448 cm^{-1} confirming the presence of higher amount of acidic sites as compared to MSF-20. Microwave heating efficiently facilitates the surface acidity of the materials along with its textural and structural properties in less time under controlled heating [7].

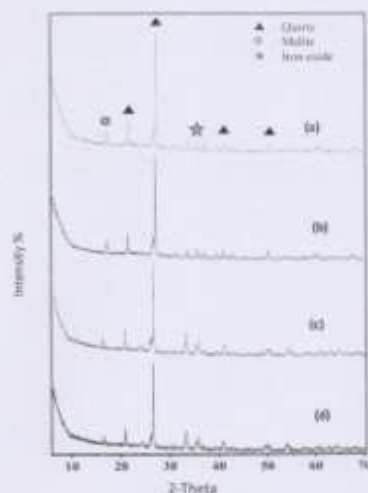
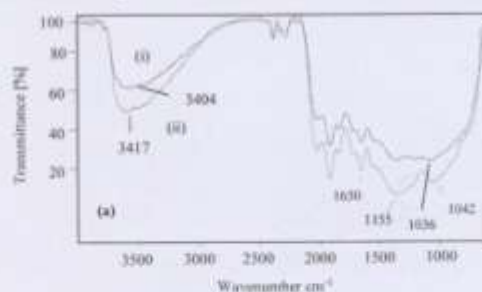


Figure 2 Powder XRD patterns of (a) Raw FA (b) MFA-15 (c) MSF-20 (d) MSF-40.



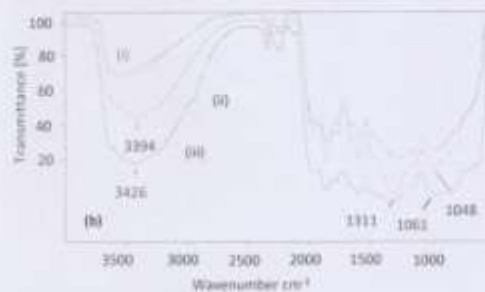


Figure 3 (a) FTIR spectra of (i) FA (ii) MFA-15 (b) FTIR spectra of (i) MFA-15 (ii) MSF-20 (iii) MSF-40.

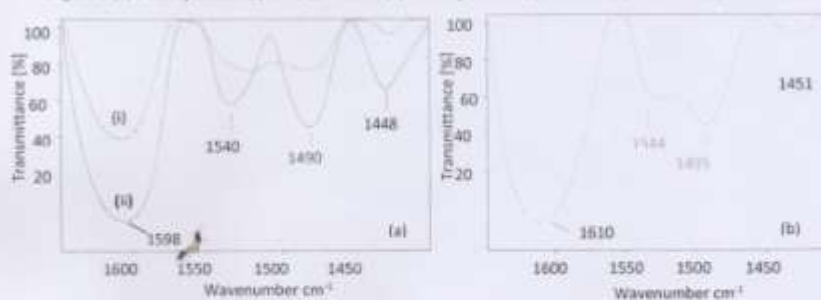


Figure 4 (a) Pyridine adsorbed FTIR spectra of (i) MSF-20 (ii) MSF-40 and (b) Regenerated MSF-40 catalyst.

SEM micrographs of raw FA in Figure 5A revealed different shaped, relatively smooth surface hollow cenospheres [21], whereas SEM image of MFA-15 (Figure 5B) shows structural break down of large particles and increased surface roughness due to ball milling. SEM images of MSF-40 revealed increased large gelatinous mass due to partial dissolution of aluminosilicate phases during acid treatment as shown in Figure 5C.



Figure 5 SEM micrographs of (A) FA (B) MFA-15 (C) MSF-40.

Catalytic activity- μ W assisted solvent-free synthesis of salol

μ W assisted solvent-free synthesis of phenyl salicylate (salol) using phenol and salicylic acid was chosen as test reaction to check the catalytic activity of MSF catalysts. The reaction was also preceded only in presence of μ W and using MFA-15 as catalyst but conversion of salicylic acid was negligible. Higher conversion (88 %) and yield (90 %) of salicylic acid was obtained by MSF-40 as compared to MSF-20 with 78 % conversion and 82 % yield. Hence, optimization of the following reaction parameters was carried out using MSF-40 catalyst followed by its reusability evaluation.

Effect of reaction temperature

On increasing reaction temperature, conversion % of salicylic acid showed a linear increase upto 120 °C with maximum 88 % conversion and after which remained almost constant upto 140 °C (Figure 6).

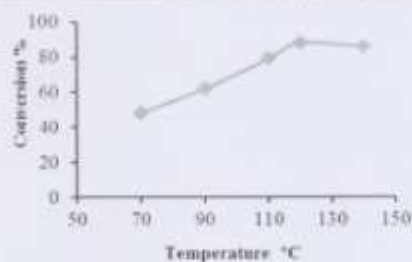


Figure 6 Variation of conversion (%) of salicylic acid over MSF-40 catalyst with temperature.

Effect of reaction period

Optimization of reaction time period was carried to achieve maximum conversion of salicylic acid to salol ranging from 2 to 20 min as shown in Figure 7 maintaining rest of the reaction parameters same. In the first 10 min, the conversion of salicylic acid increased linearly upto 88 % which remained constant upto 20 min.

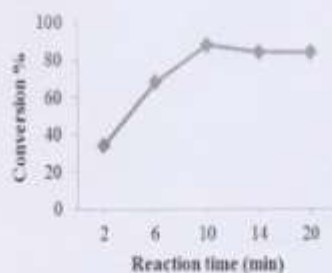


Figure 7 Variation of conversion (%) of salicylic acid over MSF-40 catalyst with reaction time

Effect of reactant molar ratio

The influence of molar ratio of salicylic acid and phenol on conversion % of salicylic acid was monitored at different molar ratios from 1:1 to 1:3 by increasing the amount of phenol only. However, due to solubility restrictions higher concentration studies with salicylic acid could not be conducted [22]. As shown in **Table 2**, on increasing molar ratio of salicylic acid to phenol from 1:1 to 1:2, maximum conversion (88 %) and 90 % yield of salol was obtained. The above results show that the yield of product increased with increasing the molar ratio of salicylic acid to phenol. This is mainly due to the reversible nature of the esterification reaction, with the increase in molar ratio salicylic acid to phenol leads to a shift of the equilibrium to the direction of salol ester production. However, further increasing molar ratio to 1:3, decrease in yield % of the salol was observed due diphenyl ether (by-product) formation favored by excess of phenol [14].

Table 2 Effect of molar ratio of salicylic acid/phenol on conversion (%) of salicylic acid to salol over MSF-40 catalyst

Molar ratio (salicylic acid : phenol)	Conversion (%)	Yield (%)
1:1	35	42
1:1.5	64	72
1:2	88	90
1:3	79	82

Reaction conditions under microwave irradiation: Temperature = 120 °C; Time = 10 min; salicylic acid/MSF-40 catalyst weight ratio=5:1; Power = 100W; P_{max} = ON

Effect of Salicylic acid to MSF-40 weight ratio

The salicylic acid to MSF-40 weight ratio on conversion of salicylic acid was monitored by varying the amount of catalyst under optimized reaction conditions as shown in **Table 3**. Weight ratio of 5:1 gave maximum conversion of 88 % of salicylic acid attributed to availability of sufficient amount of catalytic active sites. On further increase in the amount of catalyst no further change in conversion % was observed.

Table 3 Effect of Salicylic acid to MSF-40 weight ratio on conversion (%) of salicylic acid to salol with MSF-40 catalyst

Salicylic acid to MSF-40 weight ratio	Conversion (%)	Yield (%)
10:1	74	76
5:1	88	90
2:1	88	90

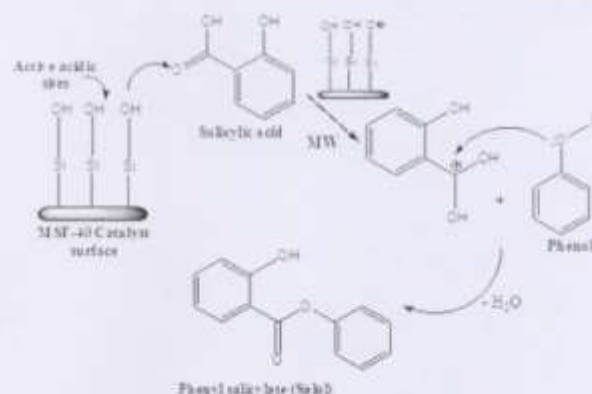
Reaction conditions under microwave irradiation: Temperature = 120 °C; Time = 10 min; molar ratio (Salicylic acid: Phenol) = 1:2; Power = 100W; P_{max} = ON

Proposed mechanism of salol formation over an acidic site

In proposed mechanism of salol synthesis, the salicylic acid gets adsorbed on acidic sites of MSF-40 catalyst and transforms into an electrophile by borrowing a proton from its surface hydroxyl groups. In microwaves, the electric component is responsible for generating heating effects, as it interacts with the polar or charged species (generated electrophile) and in response of this interaction these species start to move or rotate which further resulted as additional polarization of the polar species in the vicinity. When phenol (dipolar species) interacts with the electric field component of microwave it starts oscillating, following the oscillation of the electric field. During such

oscillation, the polar species collide with neighboring charged particles i.e. carbonium ion, results as intermolecular friction. This friction generates intense internal heat responsible for the formation of intermediate species which further leads to formation of salol with subsequent removal of water as a byproduct. Microwaves heat only the reactants which avoid the overheating of the reaction walls and help to increase the yield of the product and minimize the side product formation as shown in Scheme 2.

The spent MSF-40 catalyst was regenerated by simple microwave regeneration method and retained its activity upto 4th reaction cycle giving conversion 84 % of salicylic acid. The pyridine adsorbed FTIR of the reused catalyst after fourth reaction cycle as given in Figure 4b shows similar acidic sites with that of fresh catalyst signifies that active sites remained unaffected by microwaves during the reaction. The significant decrease in conversion was reduced after fourth reaction cycle due to blockage of active sites of the catalyst by the deposition of carbonaceous material [23].



Scheme 2 Proposed mechanistic pathway of microwave-assisted esterification of salicylic acid with phenol over MSF-40 catalyst

Conclusion

The present research work provides an energy efficient microwave methodology over traditional thermal refluxing for acid activation of FA under less processing time. Mechanical activation of FA increased surface area by breaking down larger particles while acid treatment under microwave heating further increased surface area, silica content and surface hydroxyl groups resulted as increased surface activity without alternating the basic skeleton of FA to any noticeable extent. Prepared MSF-40 catalyst gave 88 % conversion of salicylic acid and yield 90 % for solvent-free esterification reaction under dielectric heating. This investigation concludes that microwave in-core heating is a clean, fast and innovative source for improving the surficial properties of FA and provides cost effective pathway for organic transformations with high conversion and better selectivity.

Acknowledgements

The authors are thankful to Dr. D.D. Phane and Er. V.K. Ahire for SEM-EDX analysis and Dr. Mukul Gupta for XRD conducted at UGC DAE-CSR Lab Indore. XRF analysis was conducted at Punjab University, Chandigarh. The financial support was provided by Department of Science and Technology, New Delhi, India, project sanction no. FAU/DST/600(56)/C/2013-14.

References

- [1] Bilecka I, Niederberger M, *Nanoscale* 2010; 2, 1358-1374.
- [2] Wilson K, Clark JH, *Pure Appl Chem* 2000; 72, 1313-1319.
- [3] Dastan A, Kulkarni A, T're'ok B, *Green Chem* 2012; 14, 17-37.
- [4] Korichi S, Elias A, Mefti A, *Appl Clay Sci* 2009; 42, 432-438.
- [5] Korichi S, Elias A, Mefti A, Bensmaili A, *Appl Clay Sci* 2012; 59-60, 76-83.
- [6] Foleno EL, Paz DS, Gündel A, *Appl Clay Sci* 2013; 83-84, 63-67.
- [7] Oliveira AN, Silva Costa LR, Oliveira Pires LH, S Nascimetto LA, S Angélica R, Costa Carlos EF, Zamian JR, Rocha Filho GN, *Fuel* 2013; 103, 626-631.
- [8] Rami A, Khatri C, Hada R, *Fuel Process Technol* 2013; 116, 366-373.
- [9] Khatri C, Mishra M, Rami A, *Fuel Process Technol* 2010; 91, 288-295.
- [10] Khatri C, Jain D, Rami A, *Fuel* 2010; 89, 3853-3859.
- [11] Chou SY, Lo SL, Hsieh CH, Chen CL, *J Hazardous Mater* 2009; 163, 357-362.
- [12] Querol X, Alastuey A, López-Soler A, Plana F, Andrés JM, Juan R, Ferrer P, Ruiz CR, *Environ Sci Technol* 1997; 31, 2527-2533.
- [13] Chaowasakoo T, Sombatsomporn N, *Composites Sci Technol* 2007; 67, 2282-2291.
- [14] Mohamed SSZ, Nagaraju N, *J Chem Sci* 2010; 122, 193-201.
- [15] Hoyos CD, Vicente MA, Rives V, *Clay Minerals* 1998; 33, 467-474.
- [16] Sharma A, Srivastava K, Devra V, Rami A, *Am Chem Sci J* 2012; 2, 177-187.
- [17] Srivastava K, Devra V, Rami A, *Fuel Process Technol* 2014; 121, 1-8.
- [18] Rožić Ljiljana S, Petrović Srdan P, Vuković Zorica M, Novaković Tatjana B, Stanišavljević Dragomir R, *Hem Ind* 2011; 65, 489-495.
- [19] Paul GA, Anandhan S, *Inter J Energy Eng* 2012; 2, 57-62.
- [20] Du Y, Du X, George MS, *J Phys Chem C* 2007; 111, 219-226.
- [21] Jain D, Khatri C, Rami A, *Fuel Process Technol* 2010; 91, 1015-1021.
- [22] Kuziakose G, Nagaraju N, *J Molecular Catal A: Chem* 2004; 223, 153-159.
- [23] Khatri C, Rami A, *Fuel* 2007; 87, 2886-2892.

© 2015, by the Authors. The articles published from this journal are distributed to the public under "Creative Commons Attribution License" (<http://creativecommons.org/licenses/by/3.0/>). Therefore, upon proper citation of the original work, all the articles can be used without any restriction or can be distributed in any medium in any form.

Publication History

Received 01st May 2015
Revised 06th May 2015
Accepted 12th May 2015
Online 30th May 2015